NASA CR- 66196

[redacted]

GPO PRICE $ _____

CFSTI PRICE(S) $ _____

Hard copy (HC) $2.75

Microfiche (MF) .50

#653 July 65

Lockheed

MISSILES & SPACE COMPANY

A GROUP DIVISION OF LOCKHEED AIRCRAFT CORPORATION

SUNNYVALE, CALIFORNIA

LMSC-A824787
17 August 1966

LOCKHEED MISSILES & SPACE COMPANY
A GROUP DIVISION OF LOCKHEED AIRCRAFT CORPORATION
SUNNYVALE, CALIFORNIA

"STUDY TO DEFINE AGENA VIBRATION AND ACOUSTIC ENVIRONMENT"

Submitted Under
Contract NAS 1-5150

Prepared By Allan D. Houston
A. D. Houston

Checked By W. Henricks
W. Henricks
Environmental Analysis

Approved By T. R. Calvert
T. R. Calvert
Supervisor, Dynamics

Approved By T. J. Harvey
T. J. Harvey, Manager
Loads & Structural
Dynamics Engineering

ABSTRACT

This report summarizes the acoustic, random vibration, and quasi-periodic environments encountered by the Agena vehicle and associated payloads for various commonly used mission configurations. The booster systems for which the environments are described are the Atlas, Thor and Thrust-Augmented-Thor Systems, with consideration being given to the type of launch pad used and the geometry of the payload shroud employed. The various environments are described in a form which permits preparation of a test specification for future payload and hardware applications of the Agena. Specific examples are also provided to illustrate recommended LMSC procedures for formulation of these specifications. The analysis and report were prepared in fulfillment of the contract NAS 1-5150.

SUMMARY

The analyses described in the NAS 1-5150 Contract (LMSC-A648296, NASA Specification L-5631) have been performed and have yielded comprehensive definitions of the acoustic, random vibration and quasi-sinusoidal vibration environments encountered during Agena flight from launch through orbital boost. The environments have been described in a form which enables test specifications for the Agena and new Agena payload applications to be devised. A discussion of the recommended qualification test procedures, based upon an examination of the established environment, is also included.

CONTENTS

GLOSSARY OF TERMS

Schematic Drawing of Agena Vehicle:

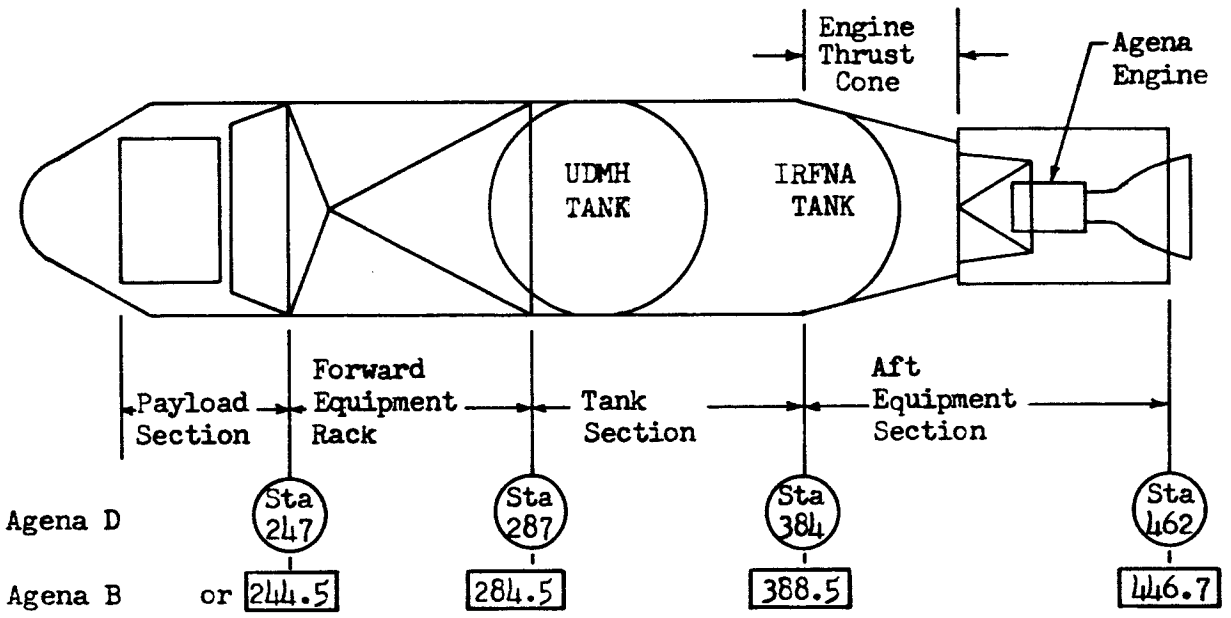

GLOSSARY OF TERMS (continued)

Term	Description
PS	PAYLOAD SECTION
FER	FORWARD EQUIPMENT RACK – This consists of an outer cylindrical shell structure, which is reinforced by three rings, and longerons, and an internal tubular structure to which primary Agena equipment is mounted.
AER	AFT EQUIPMENT RACK – This consists of a conical engine thrust cone (having skin, longeron and ring construction) and a portion extending aft of the cone having longerons and shear transmitting structure which can be in the form of either webs or tubular diagonal members. This aft portion carries primary Agena equipment and secondary payload equipment.
PRIMARY STRUCTURE	This refers to the basic airframe of the Agena vehicle consisting of rings and longerons and other primary load carrying structures
SECONDARY STRUCTURE	Structure whose primary purpose is to support equipment.
BOOSTER	Satellite launch vehicle, including the Atlas, Thor, Thrust-Augmented-Thor and Agena.
TAT	Thrust-Augmented-Thor
MECO	Main Engine Cutoff
SECO	Sustainer Engine Cutoff

Term	Description
"POGO" PROPULSION – STRUCTURE INSTABILITY	This refers to a phenomenon that occurs approximately at burnout on TAT and Thor boosters. It takes the form of a longitudinal oscillation that gradually appears during the last 30 to 40 seconds of boosted flight, diminishes again before booster burnout and exhibits a frequency of approximately 20 cps.
"WET" LAUNCH PAD	The term "wet," as applied to a launch pad, refers the type in which water is introduced into the exhaust stream deflection tunnel or vane.
"DRY" LAUNCH PAD	This term refers to the type of launch pads which do not have provision for water cooling of the deflection vanes.

ILLUSTRATIONS

TABLES

INTRODUCTION

The Agena vehicle has been the subject of many acoustic and vibration measurement programs during the past few years which have been designed to monitor various facets of the vehicle flight and ground environments.

There now exists the need to analyze all of this data so that a comprehensive definition of the various flight environments encountered by the Agena vehicle and associated payload, can be made. The intent in so doing is; (1) to provide information which will enable dynamic qualification test specifications to be devised for new payload applications of the Agena, and (2) to present qualification test procedures in light of the newly analyzed data.

The topics discussed are:

(1) The launch and transonic acoustic excitations for various boosters, launch pads and shroud profiles (Section 1).

(2) Acoustically induced random vibration environments for the booster, launch pad and shroud profiles considered in the analysis of the acoustic environments, and also vibration occurring during Agena steady burn (Section 2).

(3) Quasi-periodic transients such as those encountered during engine ignition and shutdown and during atmospheric flight, when wind gust and buffeting occur. The periodic longitudinal "POGO" oscillation occuring on Thor and TAT-boosted vehicles is also discussed (Section 3).

(4) Before analyzing the structural vibration data, consideration was given to the effect of the added mass and change in stiffness introduced by the transducer mounting brackets (Section 4).

(5) A discussion of how the environments, in the form provided, can be used to generate qualification test specifications is presented (Section 5).

In estimating the launch acoustic environments, data obtained from umbilical mast measurements were used in conjunction with internal vehicle measurements and noise reduction data obtained from captive ground test firings.

The effective transonic acoustic environments, for the various configurations analyzed, were estimated from transonic vibration data. The method of analysis consisted of establishing correlations between external launch acoustic environments and launch vibration response and applying these correlations to measured transonic vibration data to arrive at "effective" external acoustic environments. This method of analysis was used because, (1) there was a lack of direct acoustic measurements in local areas of high excitation for many configurations and, (2) it was considered desirable to obtain "effective" external transonic acoustic levels in terms of launch type acoustic environments since acoustic tests are usually conducted using an environment similar to that which exists at launch.

The random vibration environments defined for vehicle inner and outer structures were established from data obtained from in-flight measurements attached to various types of vehicle structure such as rings, longerons, stringers and frames (as opposed to skin or web panel structures). In order to estimate equipment random vibration environments, data obtained from measurements attached to equipment mounting points during Agena captive ground firings was used. In some cases, when data was not available, it was necessary to extrapolate vibration data as a function of sound pressure levels. In such cases, a linear relationship between sound pressure level and random vibration level was assumed. The random vibration data was evaluated statistically and is presented in terms of 95 percent probability values and maximum values.

The quasi-periodic environments for primary structure are based upon flight measurements made on this type of structure and are presented in terms of transient peak acceleration values, shock spectra analysis of transients, and decay characteristics of transients. Due to the lack of flight data, it was decided to use data obtained from laboratory simulation of Agena engine ignition and shutdown transients to estimate equipment transient responses.

The author wishes to acknowledge the valuable assistance of V. Overstreet, a Research Engineer in the LMSC organization, for her efforts in connection with the analysis of the data upon which this report is based.

Section 1

ACOUSTIC ENVIRONMENTS

The most significant acoustic environments occur at launch and during periods of transonic flight and high aerodynamic pressure. The acoustics during launch results from energy radiated directly from the turbulent engine exhaust streams and from energy reflected from the ground and pad facilities. The severe acoustic environments which occur during transonic (and also during certain periods of supersonic flight when high aerodynamic pressures exist) are a result of random-sized eddies being convected along the vehicle surface at less than the free stream velocity. The eddies are the result of either viscous interactions between the vehicle surface or turbulent flow separation caused by abrupt changes in vehicle geometry. Unstable or oscillatory shock waves cause short time, large pressure fluctuations on the vehicle surface during transonic flight.

The discussion of the vehicle acoustic environment will be divided into two parts; the first deals with acoustics generated during the launch phase; the second is concerned with the periods of flight associated with transonic Mach numbers. The acoustic environment during maximum aerodynamic pressure, which occurs during supersonic flight, has been investigated and the data available indicated that the transonic condition was more severe.

The environment is defined in terms of the sound-pressure level in one octave bands. In all cases the sound-pressure level is expressed in db referenced to 0.000 2 dynes/cm^2.

Launch Environment

The acoustic environment encountered by the Agena vehicle during launch is affected principally by the following factors:

(1) The power output of the booster engines

(2) The launch pad configuration and the manner in which the engine exhaust streams are diverted.

(3) The differential temperature between the booster engine exhaust stream and the surrounding atmosphere which is influenced by whether or not cooling water is introduced into the streams.

(4) The position of the Agena vehicle with respect to the source of the acoustic environment.

Therefore, in describing the various Agena launch environments, consideration was given to the above factors so that a logical grouping of the available data could be made. The Agena acoustic environments will be specified separately for Atlas launch from "dry" pad, Thor launch from "dry" pad, Thor launch from "wet" pad, TAT launch from "wet" pad and TAT launch from "dry" pad. Based on the limited measurements available, the Agena-Atlas wet and dry pad environments were assumed to be the same.

The external launch environments corresponding to the above boosters and launch pad configurations were estimated from microphone measurements attached at various locations to the umbilical mast servicing the Agena vehicle. Data from these sources were obtained from measurements having frequency response capability of ten kilocycles.

In some instances, it was necessary to extrapolate the available external data between measurement locations to obtain estimates of the environment at the significant regions of the vehicle.

The launch environment existing within the outer shells of the vehicle was estimated from measurements located in this region and also from ground data which provided estimates of the attenuation of the external environment imposed by various types of shell structure.

Figure 2 shows the distribution of acoustic environment at launch as function of time for each booster and launch pad considered. This is specified in terms of the length of time for which a given percentage of the maximum level is equalled or exceeded.

Atlas Launch From "Dry" Pad

Figure 3 shows the facility arrangement of Atlas launch from a "dry" launch pad. Figure 6 shows the estimate of the external acoustic environment for the Atlas launch from a "dry" pad which was based upon data obtained during launch of vehicles 2203 and 2204. The locations of the measurements made during these launchings are summarized in Table 1.

Table 1

MEASUREMENTS CONSIDERED IN ESTIMATE OF ATLAS EXTERNAL ACOUSTIC ENVIRONMENT AT LAUNCH

Vehicle	Microphone Station Number (LMSC)
2203	138.5 153.5 462.5 474.5
2204	138.5 462.5 474.5

The forward section internal acoustic environments for vehicles having magnesium skins having nominal thickness of 0.090 inch were estimated from the measurements summarized in Table 2. The internal acoustic environment for the Agena forward section having the beryllium shells with 0.060 inch nominal thickness was estimated from the ground test data contained in Reference (1).

The internal aft section environment was estimated by applying booster adapter attenuation data obtained from the Reference (2) adapter acoustic test to the established external levels.

Table 2

MEASUREMENTS CONSIDERED IN ESTIMATE OF ATLAS LAUNCH INTERNAL ACOUSTIC ENVIRONMENT (MAGNESIUM SHELLS)

Vehicle	Microphone Station Number (LMSC)
2102	306
6008	189
6009	189
1007	325

Thor Launch From "Wet" Pad

The "wet" launch pad facility commonly used at PMR is shown in Figure 4. LMSC has no valid external acoustic data for launch of the Thor booster from a "wet" pad. However an internal measurement obtained during launch of vehicle 6101 at station 238 shows spectrum distributions and overall levels very similar to the corresponding Atlas launch data from the "dry" type pad. It will therefore be assumed that both the internal and external acoustic environment for Thor launch from a "wet" pad is the same as that presented in Figure 6 for Atlas launch.

Thor Launch From "Dry" Pad

The external acoustic environment for launch of the Thor booster from a "dry" pad, shown in Figure 5, was derived from data obtained during launch of vehicles 1116 and 1119. The estimated spectrums for the forward and aft sections are shown in Figure 7. LMSC has no internal acoustic measurement data for launch of the Thor booster from a dry pad. Therefore, shell attenuation data established from Atlas and TAT launch measurements was applied to the measured external levels to estimate the internal environment for vehicles having magnesium shells. The attenuation data for the forward rack beryllium skins, which was used to estimate internal environment

during Atlas launch, was also applied in estimating the internal levels for the Thor "dry" pad launch for vehicle having beryllium skins. The previously used booster adapter attenuation data was applied to obtain levels internal to the booster adapter.

TAT Launch From "Wet" Pad

The "wet" pad configuration used during launch of the TAT booster is shown in Figure 4. Umbilical mast measurements obtained during launch of vehicle 1166 from a wet pad were used to estimate the external acoustic environment for this booster and launch pad configuration. They were located at Stations 200, 300, 400, and 770. The corresponding forward section internal levels for vehicles having magnesium skins was determined from data obtained during launch of vehicle 1168 from this type of pad. The external and internal acoustic environments are shown in Figure 8.

TAT Launch From "Dry" Pad

The "dry" pad configuration for TAT launch is described in Figure 5. Of all the launch pad configurations and boosters considered in this analysis, this combination of booster and pad exposes the Agena to the most severe launch environment, which is shown in Figure 9. Table 3 summarizes the umbilical mast measurements which were considered in arriving at the estimate of the external acoustic environment for the forward and aft regions of the vehicle.

Table 3

MEASUREMENTS CONSIDERED IN ESTIMATE OF EXTERNAL ACOUSTIC ENVIRONMENT FOR TAT "DRY" PAD LAUNCH

Vehicle	Station (LMSC)
1159	200 300
1164	770
1165	200 300 460 770

The levels for these regions of the vehicle were linearly extrapolated from Table 3 data. The forward section internal acoustic environment for vehicles having magnesium shells was established from an envelope of measurements obtained during launch of vehicles 1159, 1165, 2314, 2315, 2316, and 2317. The internal environments for other regions of the vehicle were estimated from the previously mentioned ground test data.

Transonic Acoustic Environment

The acoustic environment encountered by the Agena vehicle and associated payload during periods of transonic and supersonic flight is dependent upon the following factors:

(1) The magnitude of the free-stream aerodynamic pressure existing during transonic flight and the magnitude of the maximum free-stream aerodynamic pressure.
(2) The angle of attack assumed by the vehicle during transonic and supersonic flight.
(3) The profile of the vehicle, particularly the nose shroud, which governs the aerodynamic flow characteristics around it.
(4) The location of the area of interest relative to discontinuities of geometry.

In arranging the available data into appropriate groups, consideration was given to the above factors.

Since the Atlas and Thor-boosted vehicles experience similar maximum and transonic values of free-stream aerodynamic pressure, 900−1000 pounds per square foot and 600−700 pounds per square foot, respectively, data obtained during flight of vehicles utilizing these boosters have been combined. Transonic acoustic environments for TAT-boosted vehicles, which encounter significantly higher maximum value and transonic aerodynamic pressures of 1300−1400 pounds per square foot and 900−1000 pounds per square foot, respectively, are presented separately.

Angle of attack monitors are seldom installed on Agena vehicles and therefore no information was available which would directly describe the attitude of the various

vehicles analyzed during the critical flight periods. Insufficient information exists, therefore, to make a comprehensive evaluation of angle of attack. However, the Ranger vehicle 6007 experienced an angle of attack of between 6 and 7 degrees during transonic flight, according to angle of attack monitors. It is therefore assumed that the environment described for the Ranger configuration corresponds to that for angle of attack up to 7 degrees. A review of winds aloft and theoretical six-degree-of-freedom flight simulations reveals that angles of attack of 5 degrees is representative for the other configurations.

Environments have been described for the four shroud profiles shown in Figure 1, which are the most commonly used on the Agena vehicle. Rather than specifying environments for specific zones of the vehicle (e.g., the forward equipment rack and aft equipment rack) the environments have been described for significant regions of the shroud profile such as changes in slope or rapid changes in diameter. The zones for which environments are described are as shown in Figure 1. Zone 1, influenced by the detached flow, extends aft a distance equal to 1.5 diameters from the intersection of the conical and cylindrical portions of the shroud [Figure 1 (A)] . Zone 2 refers to profile regions having rapid diameter changes, such as in the case of so called "hammerhead" configurations [Figure 1 (B)] . Extending aft of Zones 1 and 2, there is known to be a region of re-attached flow with a turbulent boundary layer. This latter region is referred to as Zone 3. The remaining Zone 4 [Figure 1 (C) and 1(D)] refers to the forward portions of the Mariner and Ranger type shrouds, the environments for which are later shown to be similar (see Figure 12). To establish these significant zones of fluctuating pressure, a qualitative evaluation was made of Ames Research Center wind tunnel data obtained from tests conducted on similar configurations.

To establish the external acoustic environments for the various zones of the vehicle described above, it was decided to use transonic vibration data in conjunction with launch acoustic and vibration data. The method of analysis consisted of establishing correlation of the random vibration response of the vehicle structure at launch with the external acoustic field existing during launch phase. These correlations were then

applied to the corresponding transonic random vibration data to arrive at an "effective" external transonic acoustic excitation. The correlation factors were established from launch vibration data by normalizing the mean square value of the fluctuating pressure existing external to the vehicle in terms of the power spectral density value of random vibration present in each 50 cps bandwidth.

Therefore the required mean square fluctuating pressure value in any given 50 cps bandwidth for transonic flight $\left(p_T^2\right)$ is given by the formula:

$$\left(p_T\right)^2 = \frac{\left(p_L\right)^2}{S_L}\left(S_T\right)$$

where

$\left(p_L\right)^2$ = mean square fluctuating pressure at launch (in any 50 cps bandwidth)

S_L = power spectral density (in any 50 cps bandwidth) of vibration response at launch in g^2/cps

S_T = power spectral density (in any 50 cps bandwidth) of vibration response during transonic in g^2/cps

This method of analysis was selected for two reasons:

(1) The acoustic data available was sparse and there are shroud configurations and important local regions of high fluctuating pressure for which the environment could not be comprehensively defined.

(2) The structural responses induced by a launch type acoustic field are, in general, quite different from that caused by the acoustic field generated during transonic flight, since there are differences in spatial correlations between the launch and transonic fluctuating pressure fields. Therefore, it was thought appropriate to specify "effective" external transonic acoustic environments, since acoustic testing is normally conducted using excitation similar to that existing at launch.

The data utilized in establishing the transonic acoustic environments for Atlas and Thor-boosted vehicles is summarized in Table 4. The corresponding environments for TAT-boosted vehicles were obtained by increasing the levels established for Atlas and Thor-boosted vehicles in the ratio of aerodynamic pressures. This approach was used because in the TAT data, narrow band "spikes" having very high PSD values resulted in poor resolution of the data in frequency ranges of the spectrum other than where the "spikes" occurred.

The shell attenuation factors used in estimating the internal launch acoustics were also used in the case of transonic environments.

The "effective" acoustic environments for transonic and supersonic periods of flight are shown in Figures 10 through 15 for the various configurations described above.

Figure 16 shows the variation of excitation levels as a function of time; this is specified in terms of the length of time for which a given percentage of maximum level is equalled or exceeded.

Table 4

DATA USED TO ESTABLISH EFFECTIVE EXTERNAL TRANSONIC ACOUSTIC ENVIRONMENTS

Zone	Vehicle	Measurement	Station
1	2303	A452	228
	2312	A4	244
	2312	A9	244
	2351	A192	247
	2351	A452	247
	1155	A451	260
	1155	A452	260
	1155	A453	260
	1160	A536	247

Table 4 (Cont.)

Zone	Vehicle	Measurement	Station
2	6101	AA024	
	6101	AA22	240
	6101	AD5	240
	6101	AD2	240
	6101	AD8	240
	6001	RA5	232
	6003	RA6	232
	6004	RA6	232
	6006	A10	227
	2202	A10	227
3	2312	A11	408
	1127	A10	408
	1133	A10	408
	1127	A4	408
	1133	A3	408
	1119	D6	408
	2204	A9	412
	2204	A4	412
	2204	A3	412
	4701	P2	247
	4701	P1	247
	4702	P1	247
4	6932	Ch 171	222
	6932	Ch 181	Adapter
	6006	RA8	Spacecraft

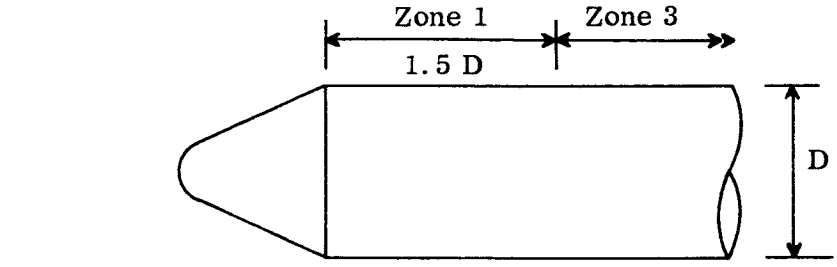

(A)

Configuration "A"

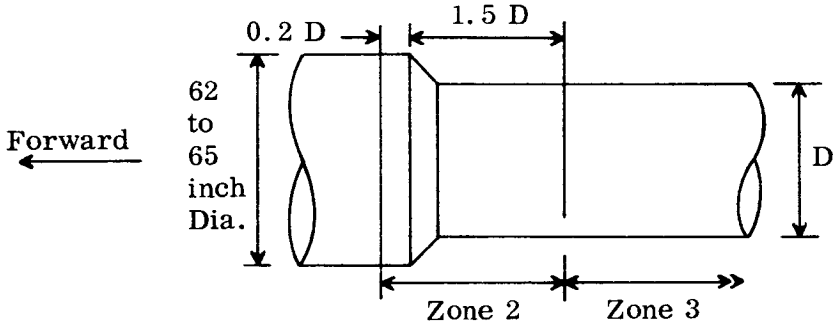

(B)

Configuration "B"

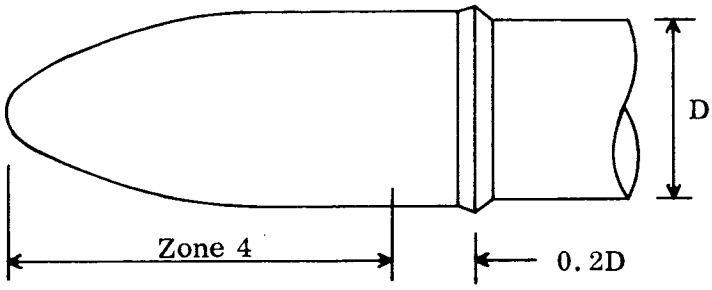

(C)

Configuration C (Mariner)

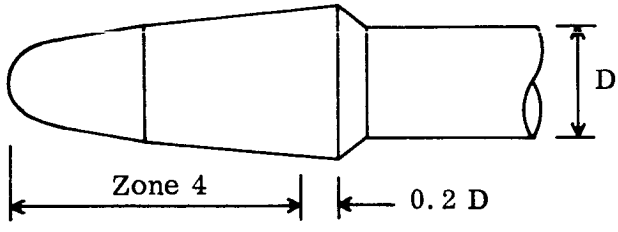

(D)

Configuration D (Ranger)

Fig. 1 Shroud Configurations for Which Transonic Environments Have Been Established

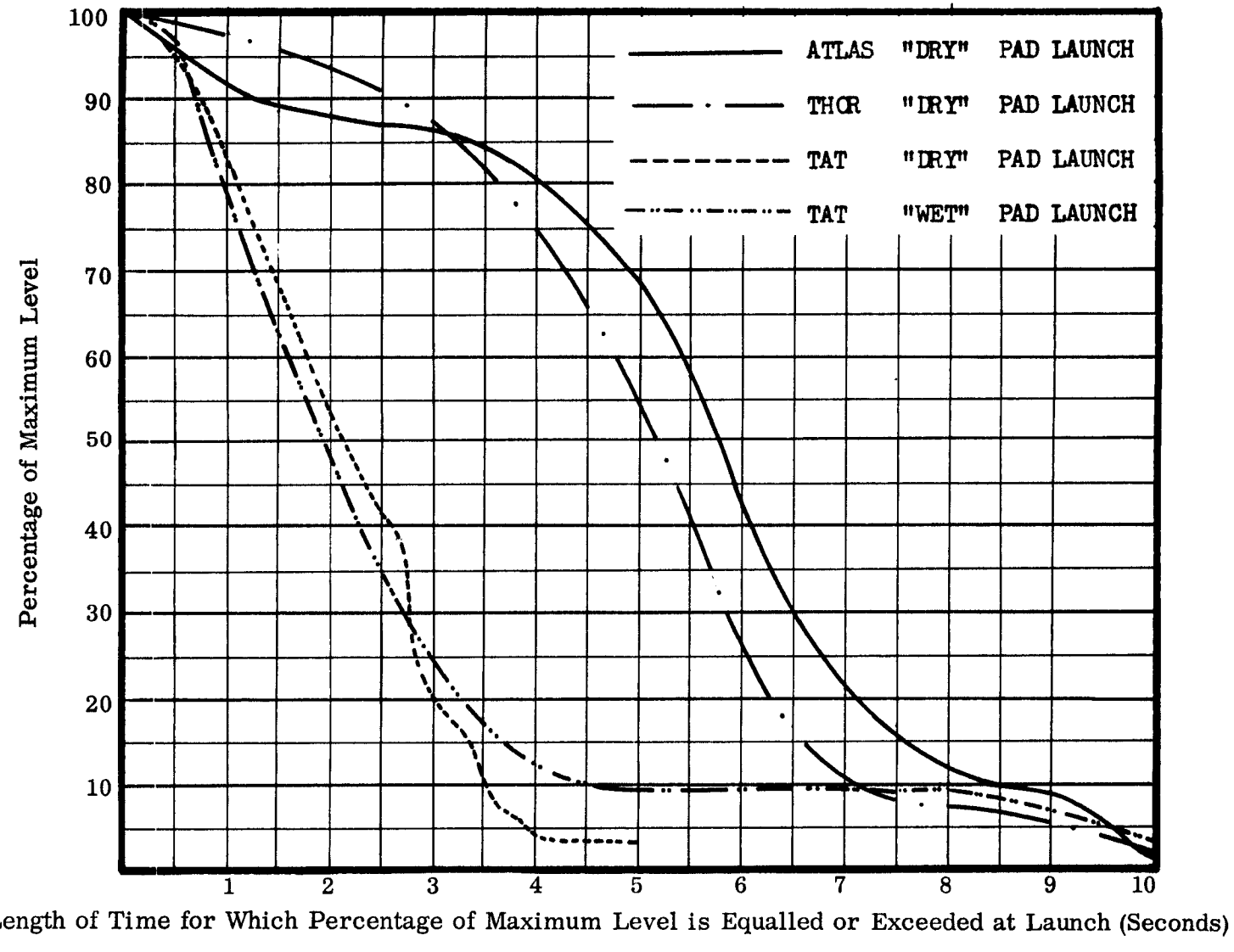

Fig. 2 Distribution of Acoustic and Random Vibration Excitation at Launch

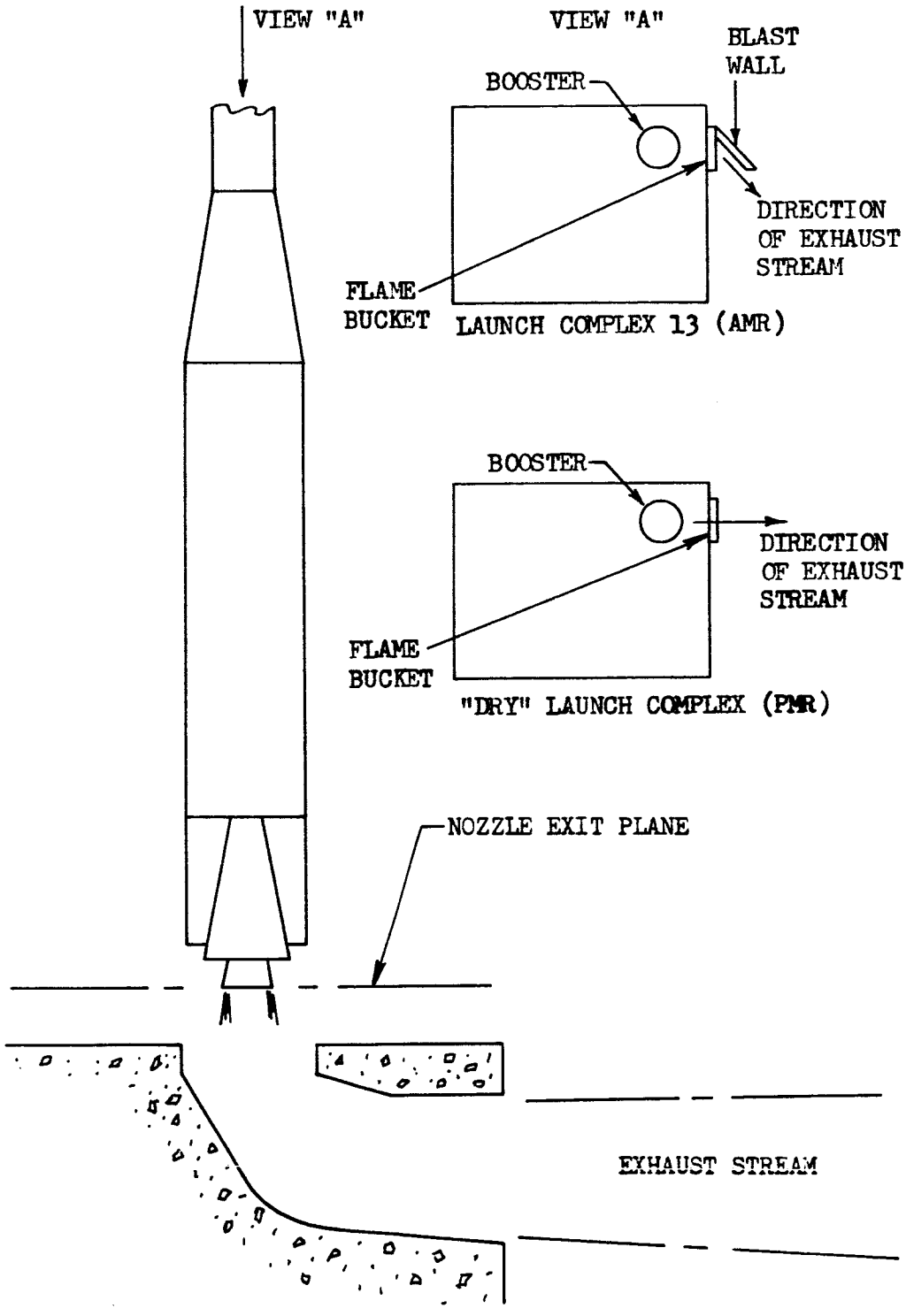

Fig. 3 "Dry" Pad Configuration for Atlas Launch

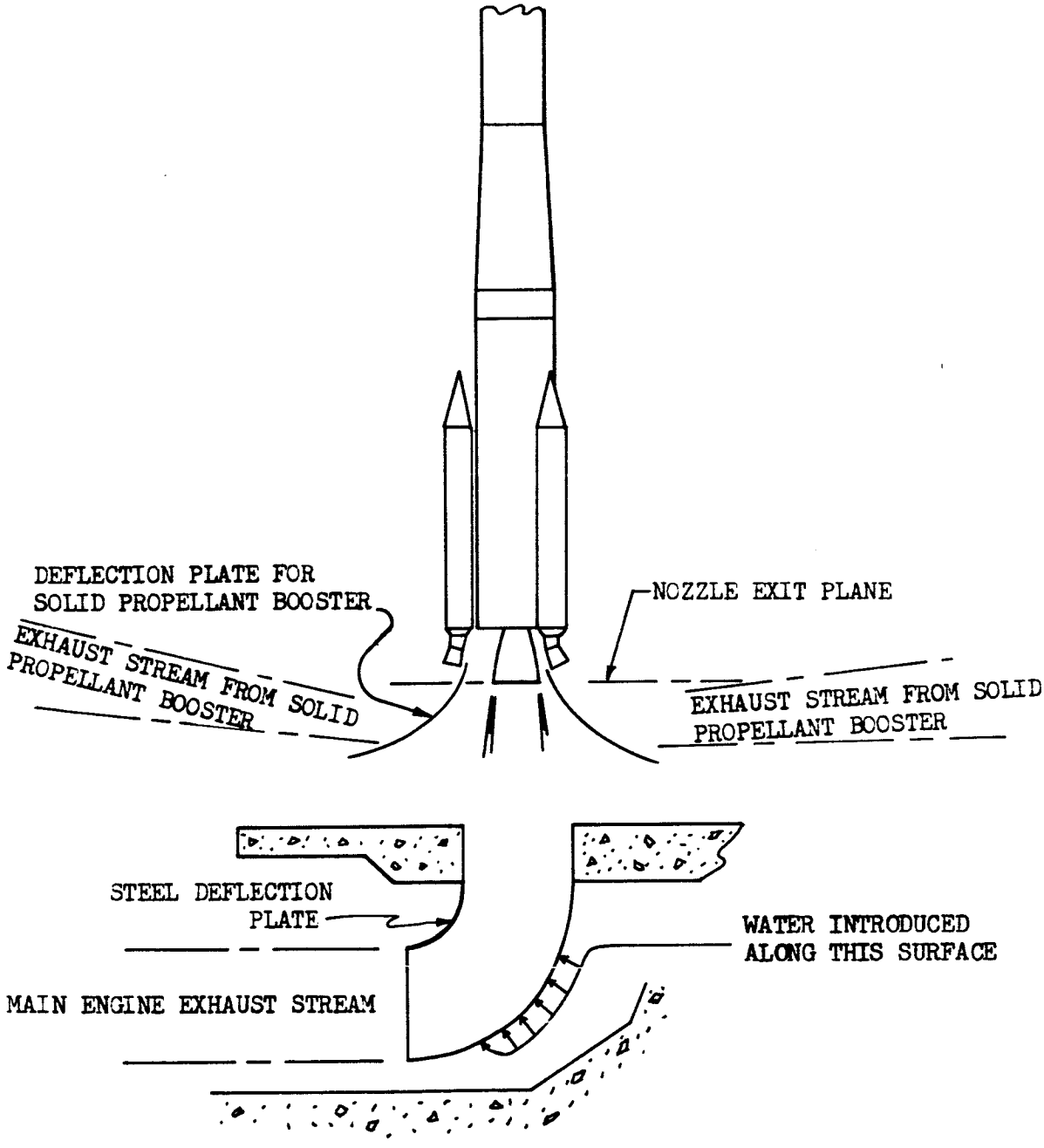

Fig. 4 "Wet" Pad Configuration for Thor or TAT Launch

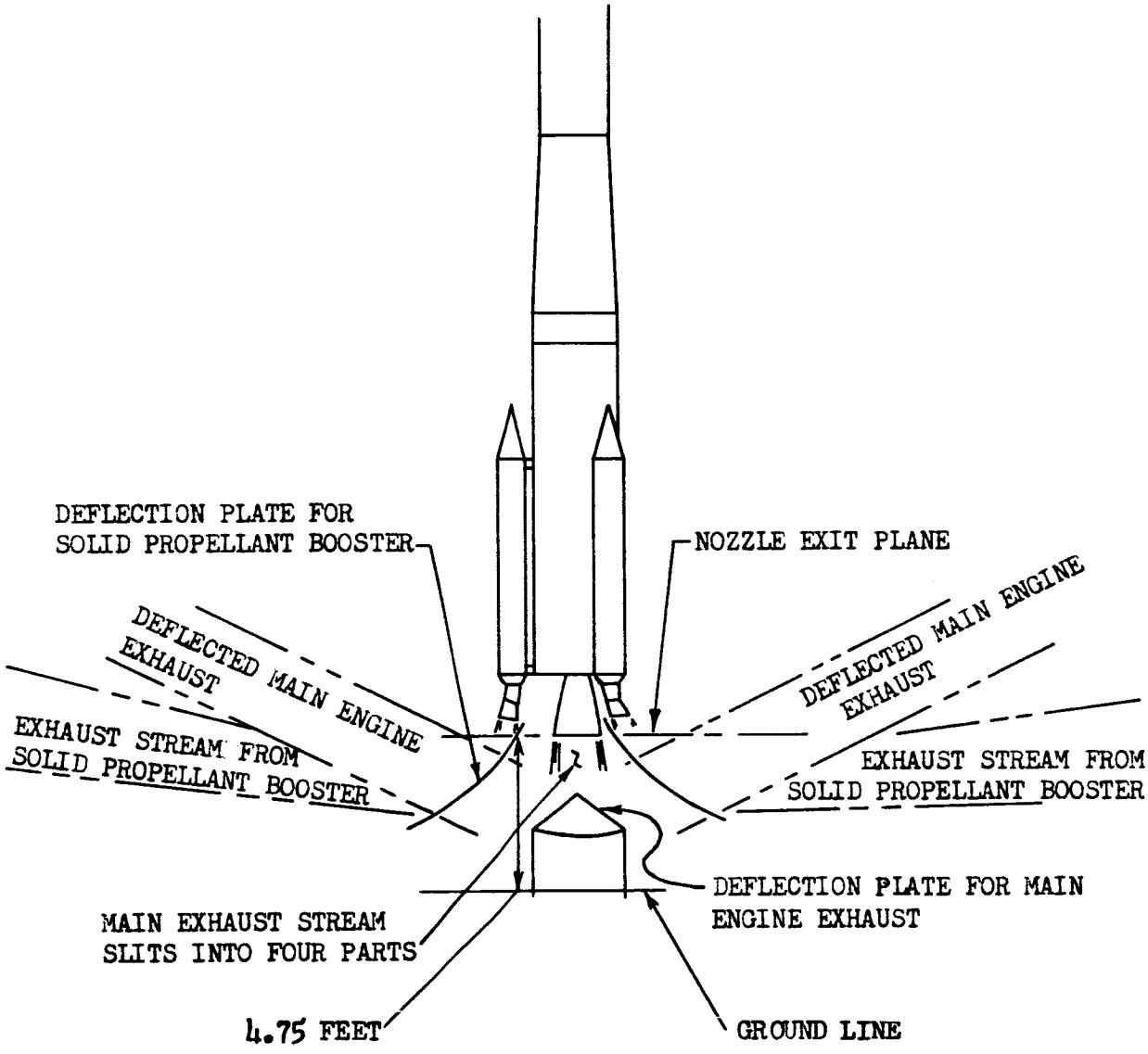

Fig. 5 "Dry" Pad Configuration for Thor or TAT Launch

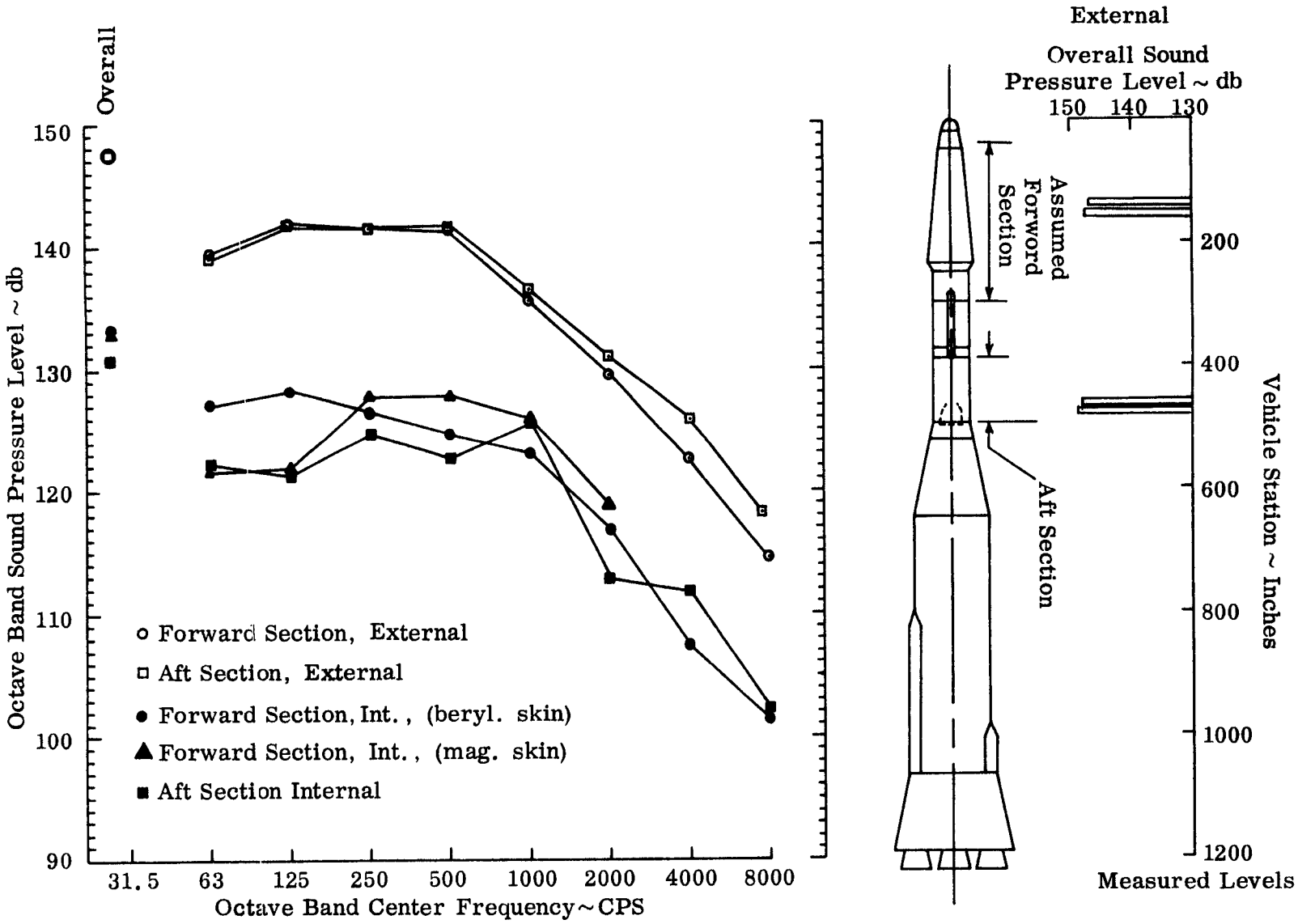

Fig. 6 Acoustic Environments During Atlas Launch from "Dry" Pad and Thor Launch from "Wet" Pad

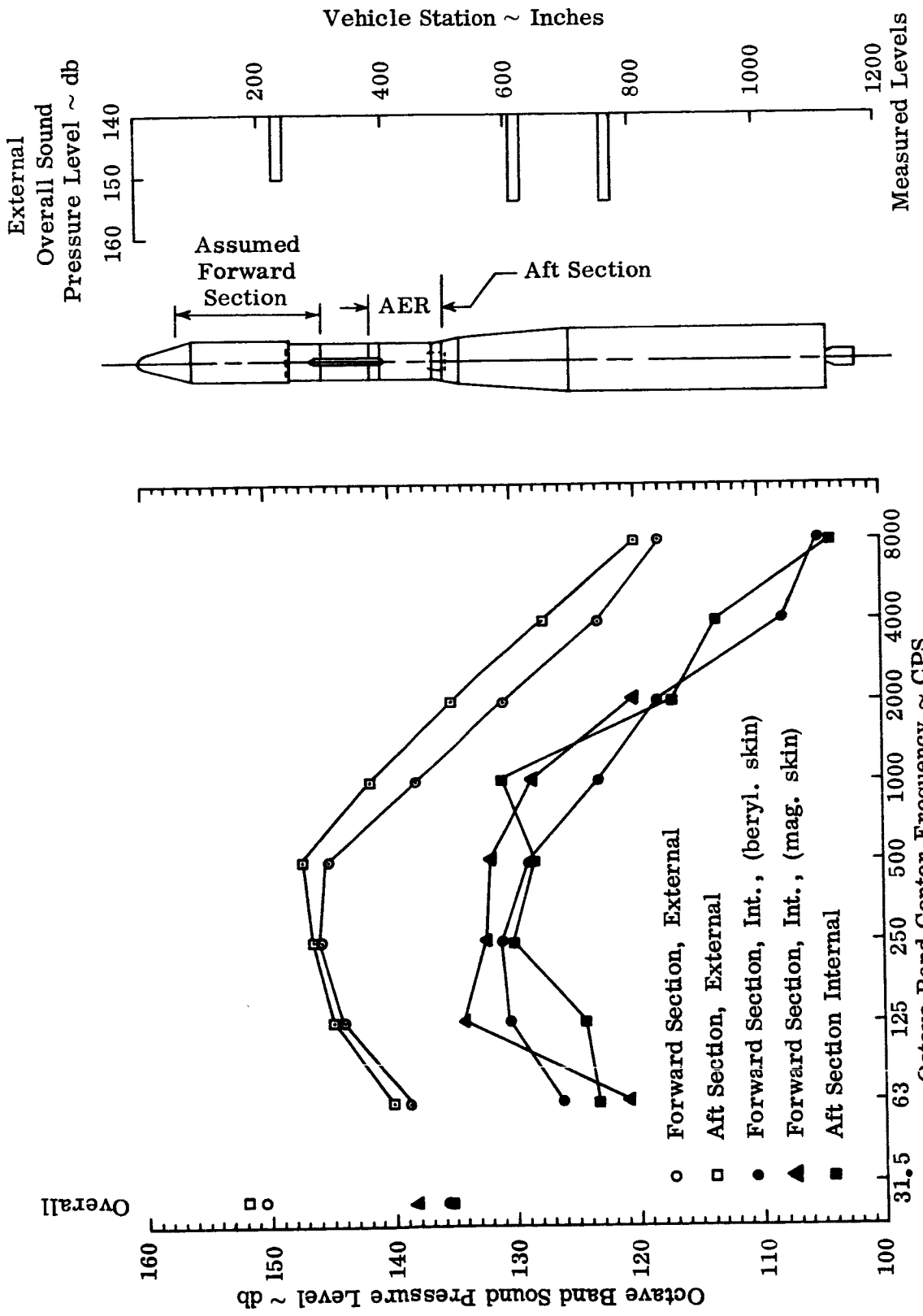

Fig. 7 Acoustic Environment During Thor Launch from "Dry" Pad

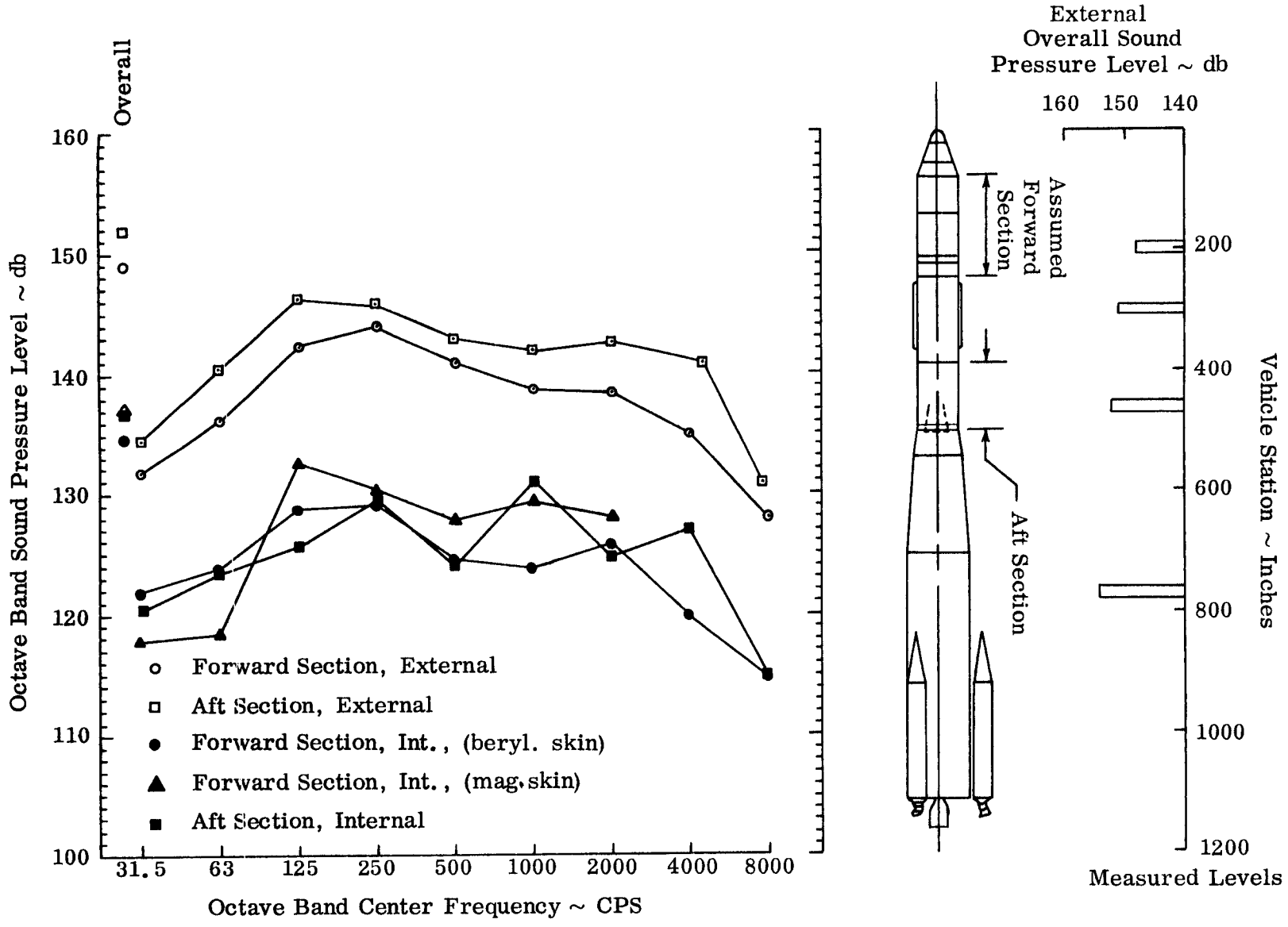

Fig. 8 Acoustic Environment During TAT Launch from "Wet" Pad

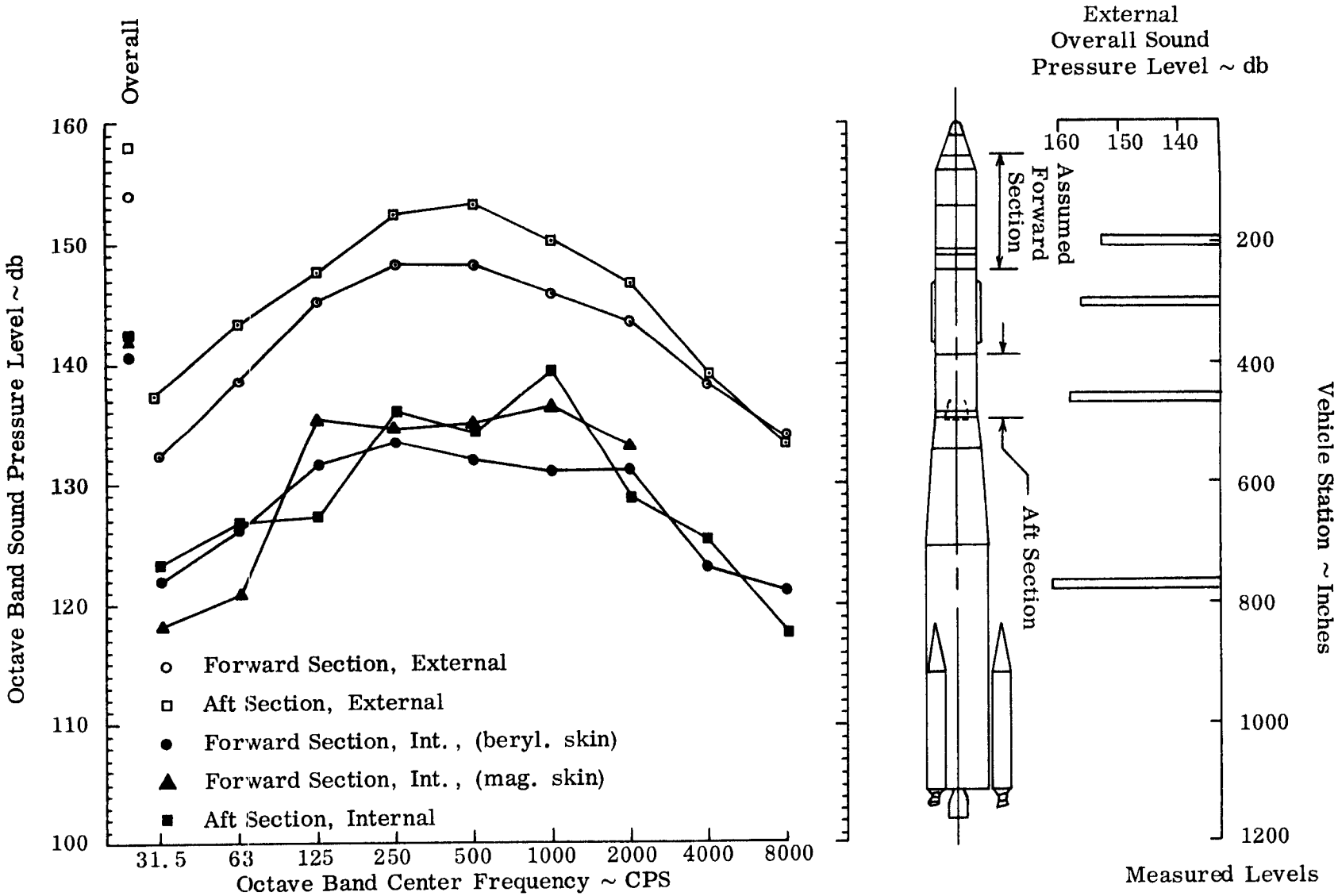

Fig. 9 Acoustic Environment During TAT Launch from "Dry" Pad

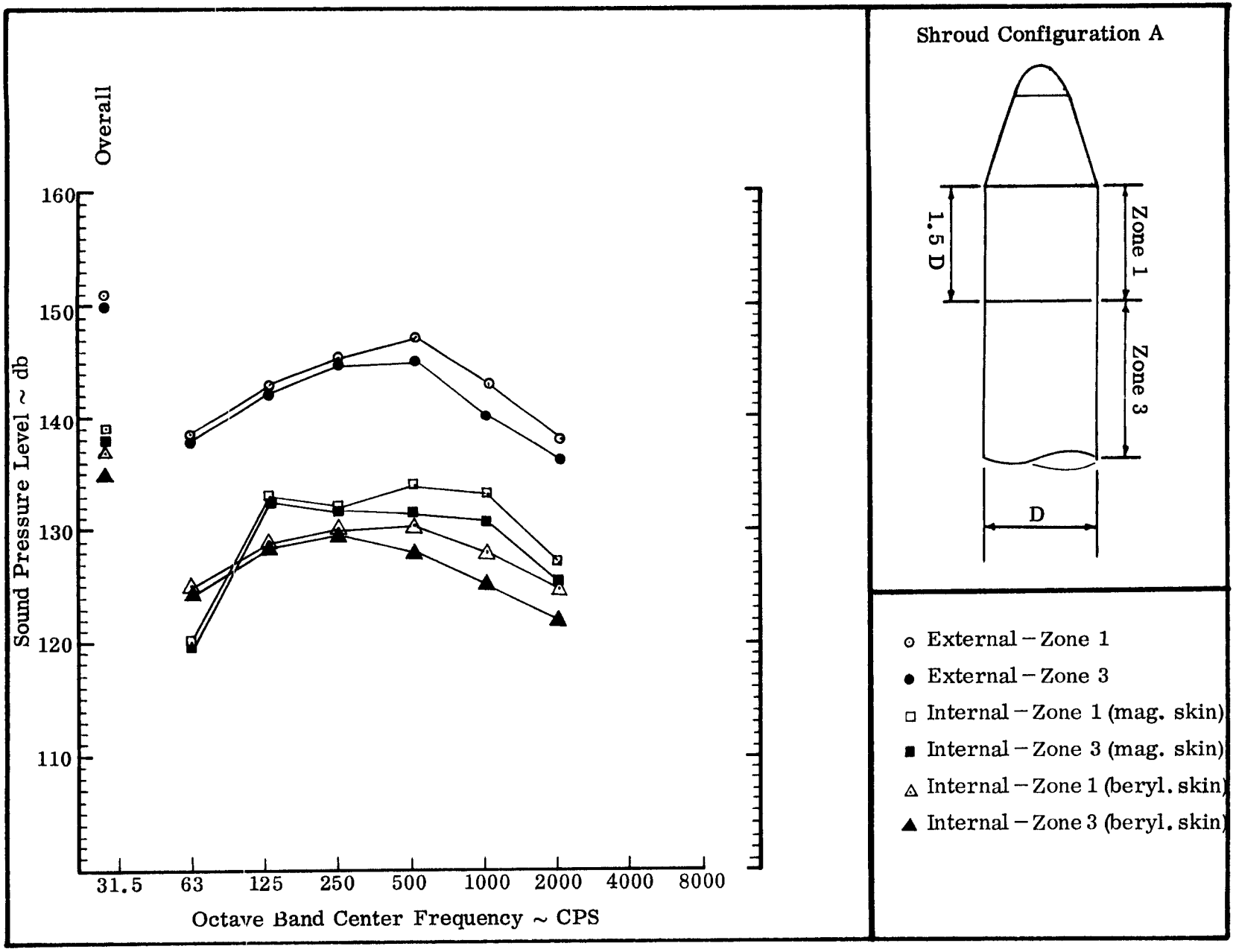

Fig. 10 Acoustic Environment During Thor and Atlas Transonic Flight, Configuration A, Zones 1 and 3

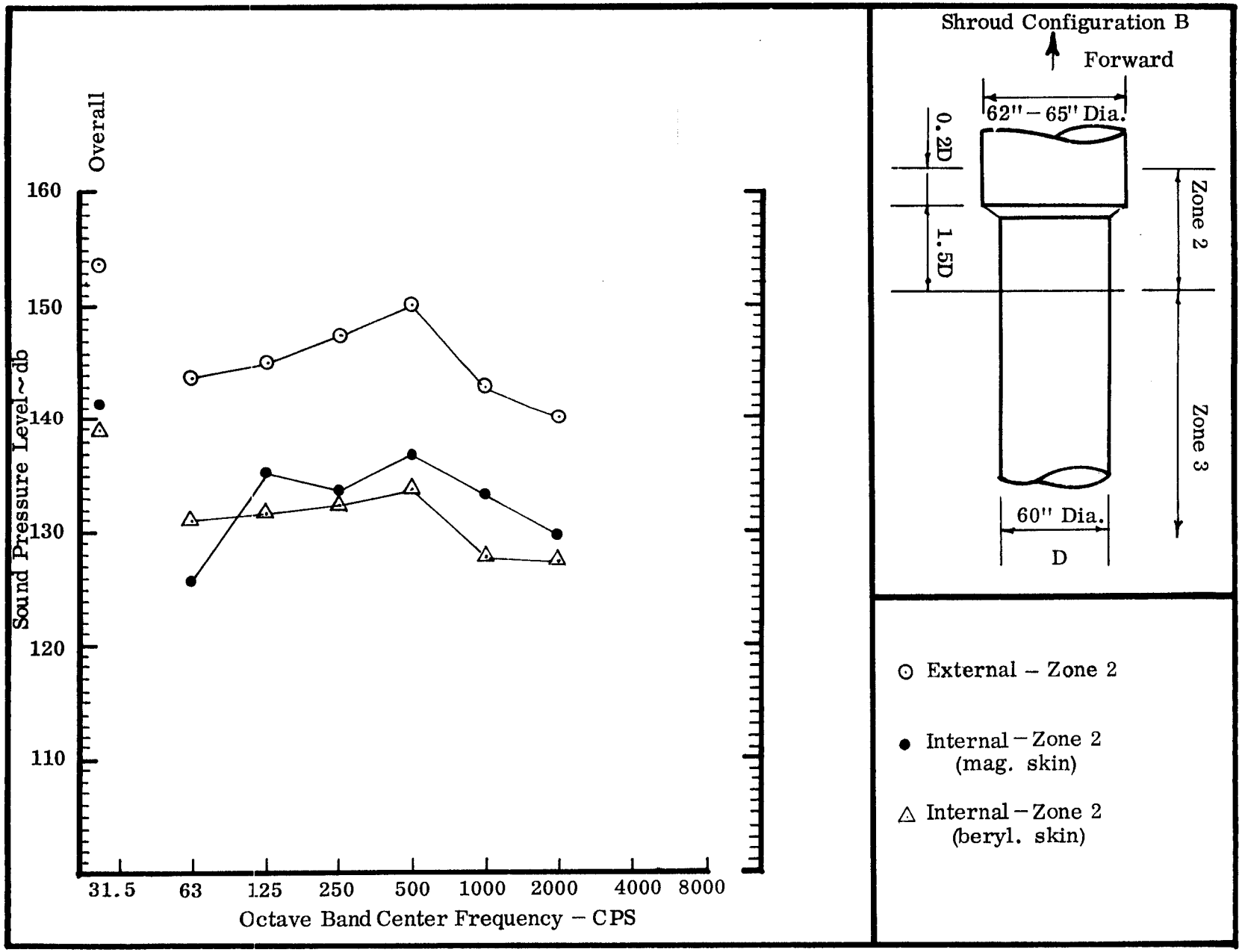

Fig. 11 Acoustic Environment During Thor and Atlas Transonic Flight, Configuration B, Zone 2

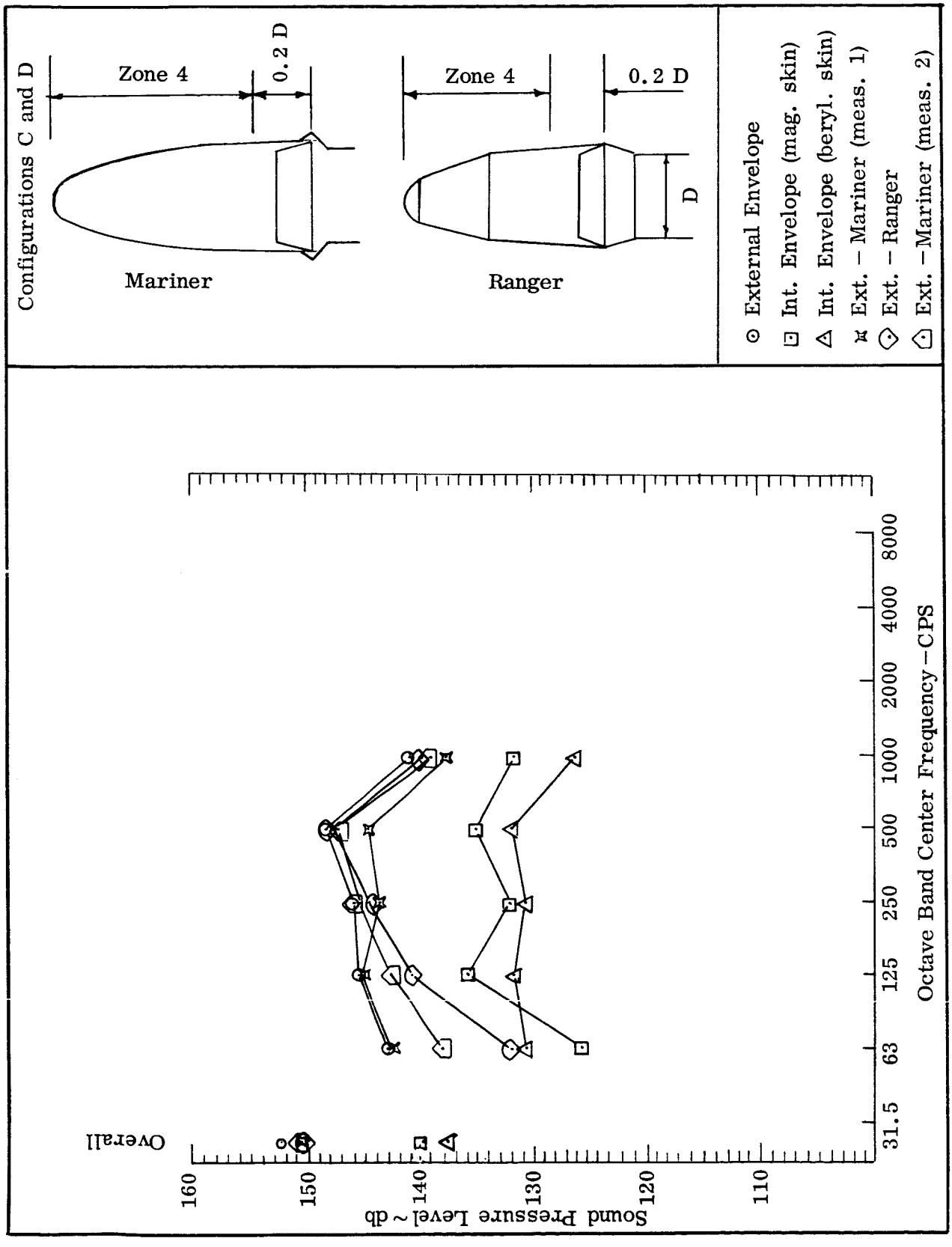

Fig. 12 Acoustic Environment During Thor and Atlas Transonic Flight, Configurations C and D, Zone 4

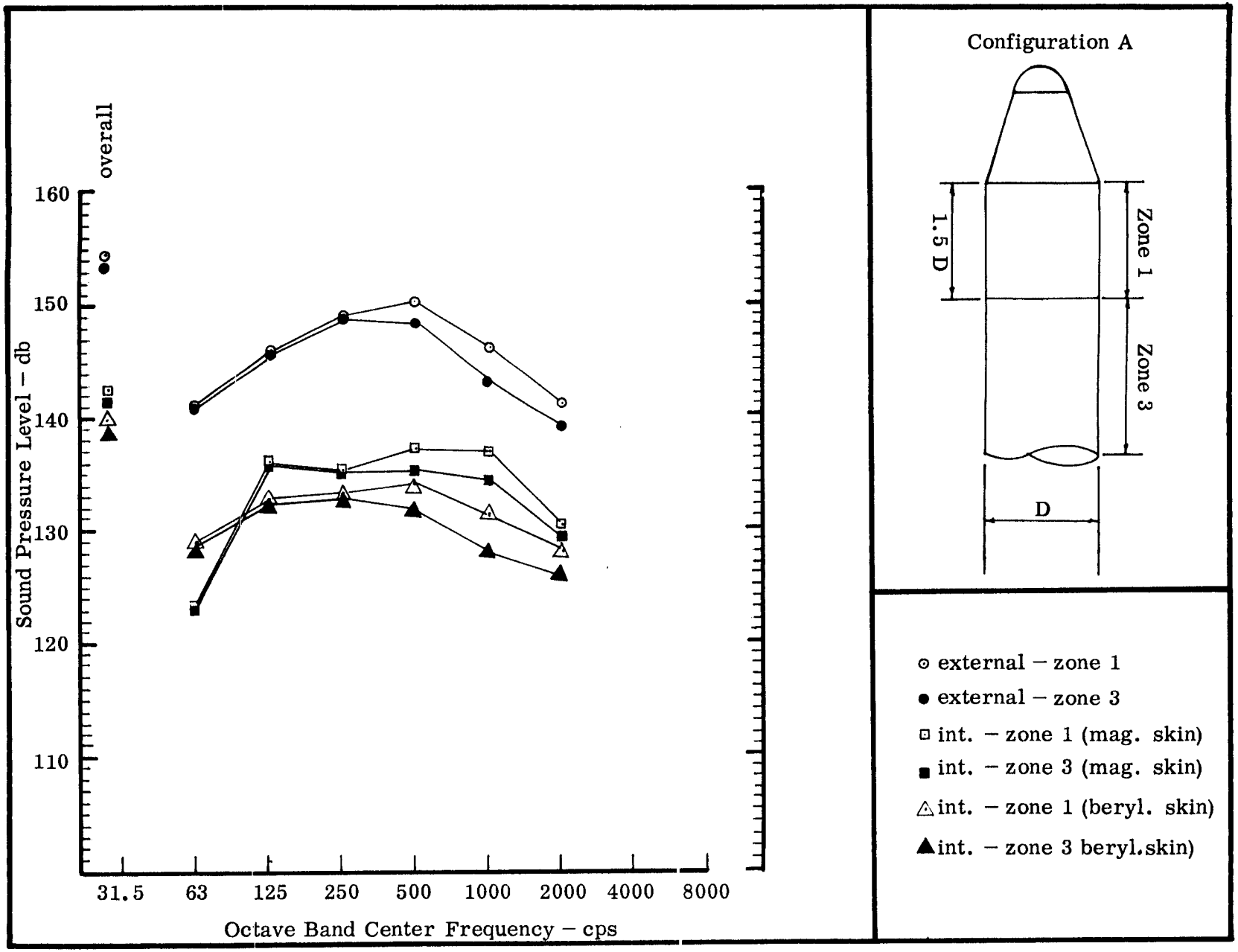

Figure 13 Acoustic Environment During TAT Transonic Flight Configuration A, Zones 1 and 3.

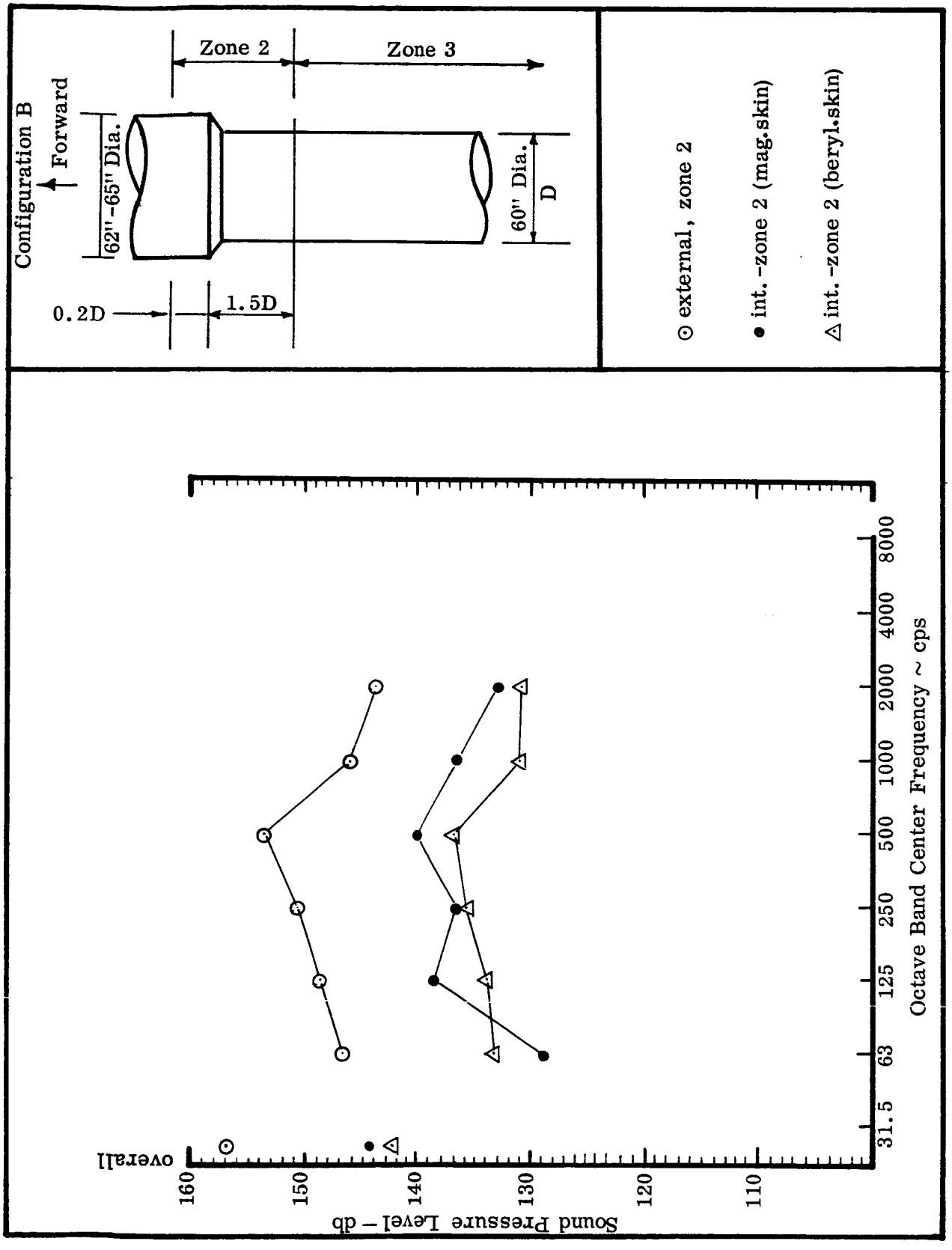

Figure 14 Acoustic Environment during TAT Transonic Flight Configuration B, Zone 2

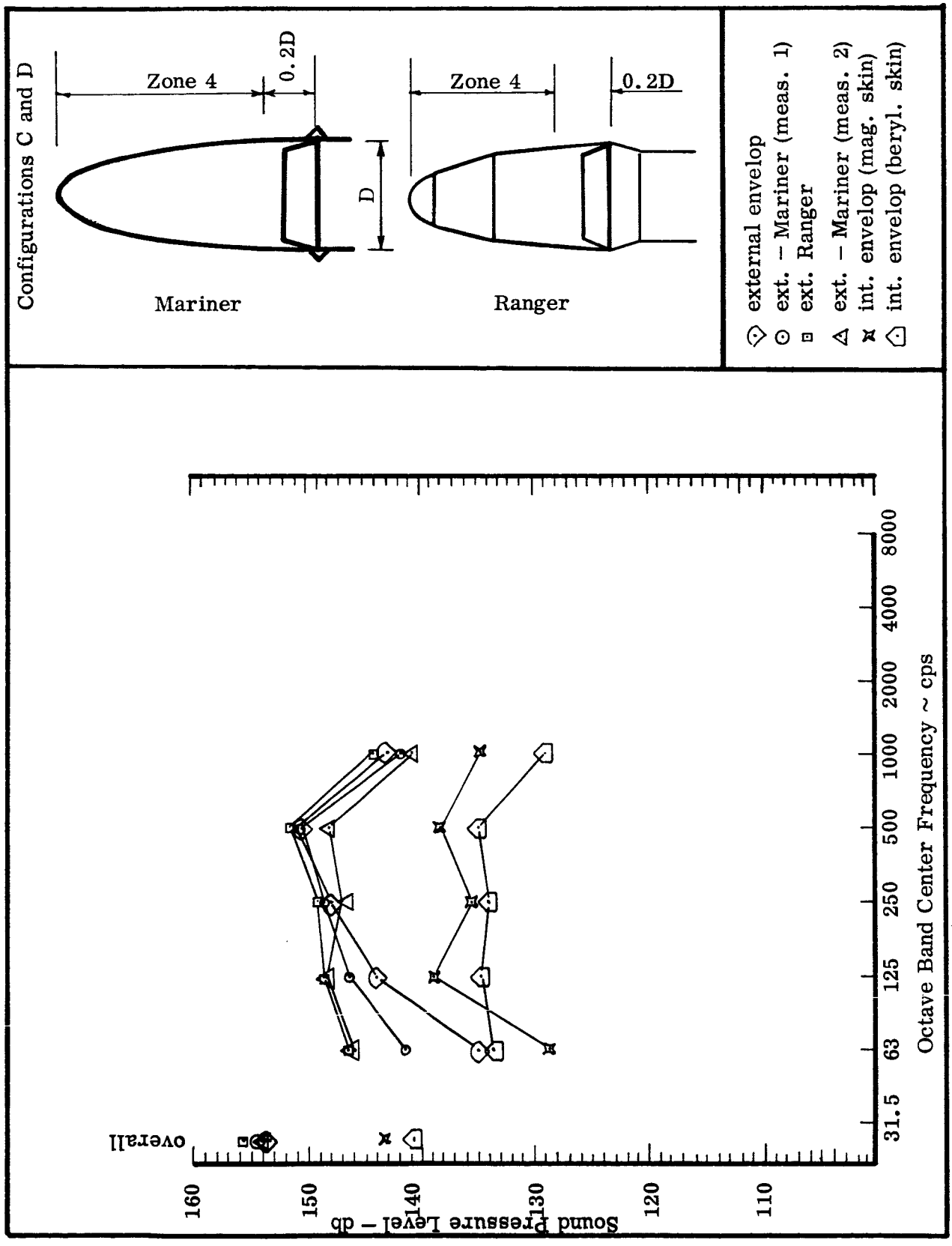

Figure 15 Acoustic Environment During TAT Transonic Flight, Configurations C and D, Zone 4

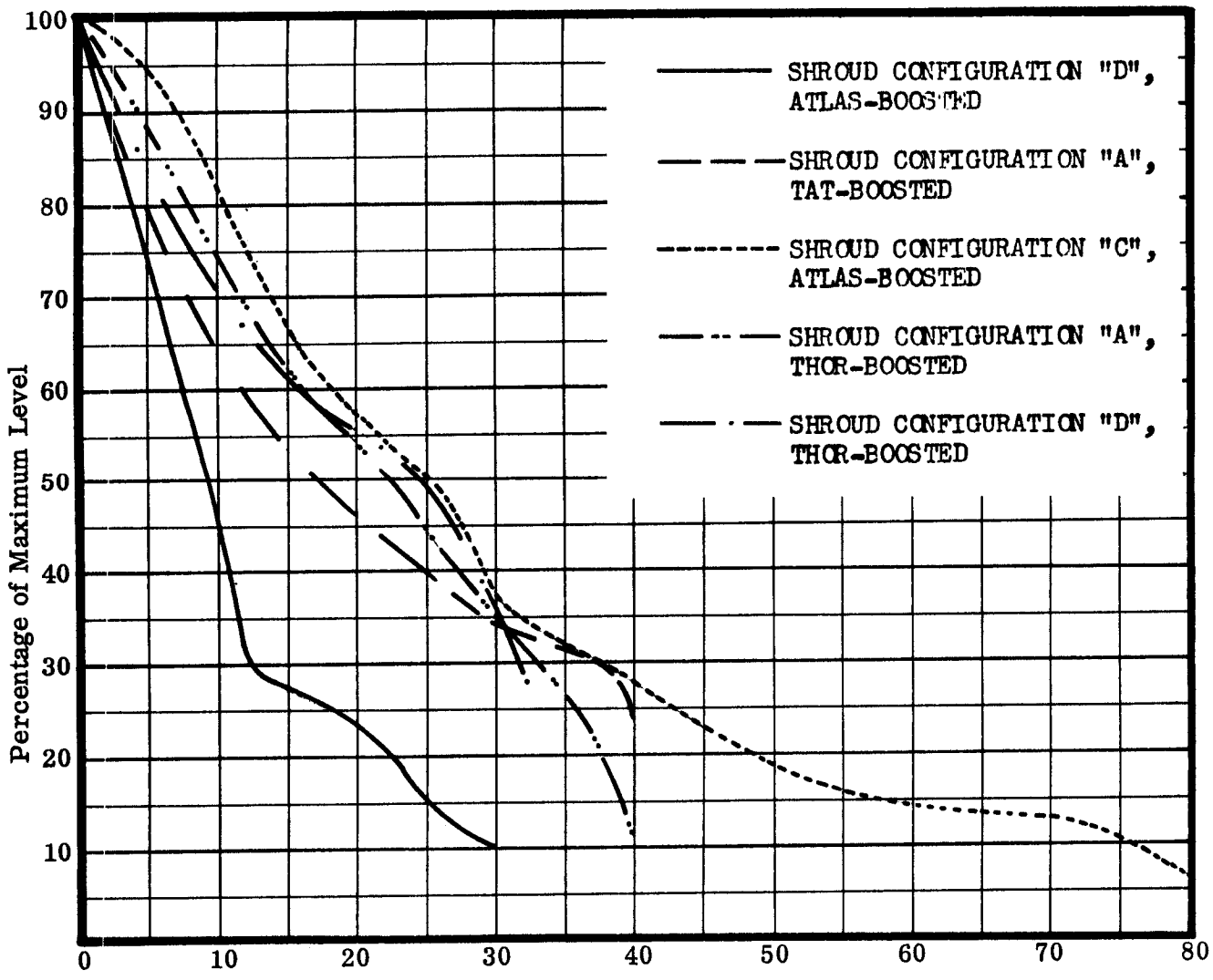

Figure 16 Distribution of Acoustic and Random Vibration Excitation During Transonic Flight

Section 2
RANDOM VIBRATION

Significant random vibration environments in the Agena vehicle occur during the flight phases when the acoustic environment is most severe (i.e., at launch and during periods of transonic flight). Vibration excitations are also evident during Agena steady burn but, except for the aft equipment rack, these are much less severe than during the periods of high acoustic levels.

Launch and Transonic Environments

Since the severe random vibration environment is dependent upon the degree of acoustic excitation present, the random vibration data available was organized and grouped in the same manner as the acoustic data. Random vibration levels are specified for the launch pads and booster combinations considered in the analysis of the launch acoustics; Atlas launch from "dry" pad, Thor launch from "wet" pad, Thor launch from "dry" pad, TAT launch from "wet" pad and TAT launch from "dry" pad. In the case of transonic flight, random vibration levels are described for the same four shroud profiles for which transonic acoustic levels were described.

The acoustically induced random vibration data was further catagorized with respect to the type and location of the structure for which the environment was being described. These catagories are as follows:

(1) Outer structure (excluding skin panels) such as rings and longerons associated with the outer shell of the vehicle, unloaded by equipment.
(2) Inner structure such as longerons, frames and rings which is not exposed directly to the acoustic environment existing external to the vehicle.
(3) Equipment attached to the inner structure described in Item 2, above.

A review of power spectral density (PSD) data generally indicated the presence of a relatively low background random vibration, extending from low frequencies up to 2000 cps, with superimposed concentrations ("spikes") of energy having high PSD values. These "spikes," approximately 50 cps wide at their base, accounted for 80 to 90 percent of the overall G_{RMS} levels of the vibration monitored; the remaining 10 to 20 percent being identifiable with the background random vibration.

The measurements upon which the random vibration environments for outer and inner structures were based, are summarized in Table 5. All of this data was obtained during the lift-off phase of flight and from ground acoustic test.

So that statistical evaluation of the vibration data could be made, it was necessary to combine all of the data, within any of the above three structural groups, into single populations. This was done by normalizing the power spectral densities of each measurement in terms of the mean square fluctuating pressure value of acoustic excitation present when the measurement was made. Power spectral density values in each 25 cps bandwidth up to 400 cps, and each 50 cps bandwidth from 400 up to 2000 cps, were normalized in terms of unit mean square fluctuating pressure present in these bands. Thus, the PSD value in a given narrow band was divided by the corresponding mean square fluctuating pressure value existing within the local one-third octave band. The units of the normalized data are therefore those of PSD divided by (pound per square inch)^2, or:

$$\left(\frac{g^2}{cps}\right)\left(\frac{inch^4}{pounds^2}\right)$$

Transonic vibration data was not used in this normalization process since the transonic acoustic environment which induced the measured structural response was not comprehensively defined, whereas the launch acoustic environment was known.

Table 5

MEASUREMENTS USED TO ESTABLISH RANDOM VIBRATION ENVIRONMENTS FOR STRUCTURE

Type of Structure	Measurement Number	Data Reference
Outer Structure	V12 V13	Booster Adapter, Acoustic Test (Ref. 2)
	P1 P2	4701 vehicle at launch
	P1	4702 vehicle at launch
	P1 P2	4703 vehicle at launch
	CH 18	2351 vehicle at launch
	CH 17 CH 18	1801 vehicle at launch
	CH 162 AD022 AA025	6101 vehicle at launch
Inner Structure	A536	1160 vehicle at launch
	A011	2313 vehicle at launch
	A452	2303 vehicle at launch
	A10	2202 vehicle at launch
	RA005	6001 vehicle at launch
	RA006	6003 vehicle at launch
	RA006	6004 vehicle at launch
	PL23	6006 vehicle at launch
	PL20	6007 vehicle at launch
	PL23	6008 vehicle at launch
	CH 17	6101 vehicle at launch
	AD005	6101 vehicle at launch
	A536	1164 vehicle at launch
	A536	1165 vehicle at launch
	A536	1168 vehicle at launch

Vibration data for equipment was also converted to a normalized form and was obtained from measurements made during the referenced ground tests. Seven measurements from the Reference (3) test and fifteen measurements from the Reference (4) test were combined into a single population.

The normalized data in each of the three groups (13 samples for outer structure, 15 samples for inner structure, and 22 samples for equipment) were then evaluated statistically. Assuming a log-normal distribution of data, 95 percent and 50 percent probability PSD values were obtained for each group, in each narrow band.

The maximum values, 95 percent probability values and the 50 percent (mean) values of PSD for each group are shown in normalized form in Figures 17 through 22. Data in this form in useful since it can be de-normalized in terms of any acoustic environment for which the spectrum is known.

The overall G_{RMS} values for all measurements in the three groups were also recorded and normalized in terms of the appropriate overall fluctuating pressure values. These normalized values were then evaluated statistically and the 95 percent probability values computed on the basis of a log-normal distribution of samples. These normalized values of overall G_{RMS} are shown in Figures 18, 20, and 22 for the outer structure, the inner structure, and the equipment groups, respectively.

It should be noted that all outer and inner structure data was normalized in terms of mean square fluctuating pressure values existing external to the vehicle shells. The equipment data, however, was normalized in terms of mean square fluctuating pressure values existing internal to the outer shells. The reason for the latter method of computation was that for the ground static firings, from which all of the equipment data was obtained, the internal acoustic excitation was very similar in magnitude to the external environment because large holes were cut in the outer doors. Equipment vibration is composed of two components; vibration transmitted from the outer shell, which is responsive to external acoustic environment,and vibration induced in internal

structures by the internal acoustic environment. Since the internal acoustic environment in the case of the static firings was approximately 10 to 15 db higher than it would normally be with complete doors, it would be too conservative to normalize equipment data in terms of external acoustic environment.

The maximum and 95 percent probability values of vibration PSD, corresponding to the various launch and transonic acoustic environments, were then obtained by multiplying the normalized values by the appropriate mean square fluctuating pressure values present in each narrow band considered (25 cps from 50 to 400 cps, and 50 cps from 450 cps to 2000 cps). The outer structure and inner structure environmental groups were de-normalized in terms of acoustic environment existing external to the vehicle skins; the equipment group in terms of internal acoustic environment. The maximum value and 95 percent probability value data obtained in this form provides an indication of how peak PSD values are distributed with respect to frequency, however are not descriptive of the overall G_{RMS} levels measured during flight.

The 50 percent (mean) probability values were de-normalized in the same fashion as were the 95 percent values. This data was assumed to be indicative of the PSD shape of the background random vibration environment. The mean value PSD plots were then adjusted (with original shapes maintained) such that their overall mean square acceleration values coincided with the 95 percent overall values of acceleration established for the various launch and transonic acoustic environments. These 95 percent overall acceleration values were obtained by multiplying the 95 percent normalized overall vibration data by the overall acoustic level present during the flight event considered. The mean vibration data for outer structure and inner structure were de-normalized in terms of overall external acoustic level; the equipment data in terms of overall internal acoustic level.

In estimating the random vibration environment corresponding to high values of acoustic excitation it was necessary to conservatively assume proportionality between mean square fluctuating pressure and resulting random vibration response of structure in order to project up to the high levels. It was observed from the data obtained in

Reference (2) that this proportionality existed for acoustic excitations from 140 db up to 153 db, whereas linearity up to 157 db has been assumed. Until further data corresponding to these higher acoustic levels become available, this assumption will be used.

The random vibration environments are shown in Figure 23 through 54 for each launch pad and booster combination considered in the section dealing with launch acoustics.

Transonic and Supersonic flight random vibration levels are specified in Figures 55 through 96 for each shroud configuration considered in the discussion of the transonic acoustic environment.

Figures 2 and 16 describe the durations for which the above random vibration environments are sustained during the launch and transonic flight phases of flight. These are described in terms of the periods of time for which maximum levels are exceeded, and are based upon G_{RMS} histories obtained during transonic flight.

Agena Steady Burn Environments

The Agena steady burn environment is mechanically transmitted throughout the vehicle structure due to absence of atmosphere during this period of flight. The environment for the forward section, established by forming an envelope of the measurements for that region of the vehicle shown in Table 6, is presented in Figure 97.

The environment in the aft section, based on two measurements at Station 408, consists of low level background noise, with superimposed narrow frequency band having high power spectral density values. The high narrow band excitations are thought to originate from periodic disturbances related to the Bell engine turbo-machinery. The envelope of the two measurements is shown in Figure 98. Until further data becomes available which shows the distribution of vibration throughout the aft section, the environment for the aft section will be assumed to be as described in Figure 98.

Table 6

MEASUREMENTS USED TO ESTABLISH AGENA STEADY BURN VIBRATION ENVIRONMENT

Region	Vehicle	Measurement Number	Station
Forward Equipment Rack and Payload	6101	AA020	244.5
	6101	AA022	244.5
	6101	AA024	244.5
	6101	AD002	238.5
	6101	AD005	238.5
	2351	A452	247
	1164	A536	231
	1165	A536	231
Aft Section	2312	All	408
	1203		408

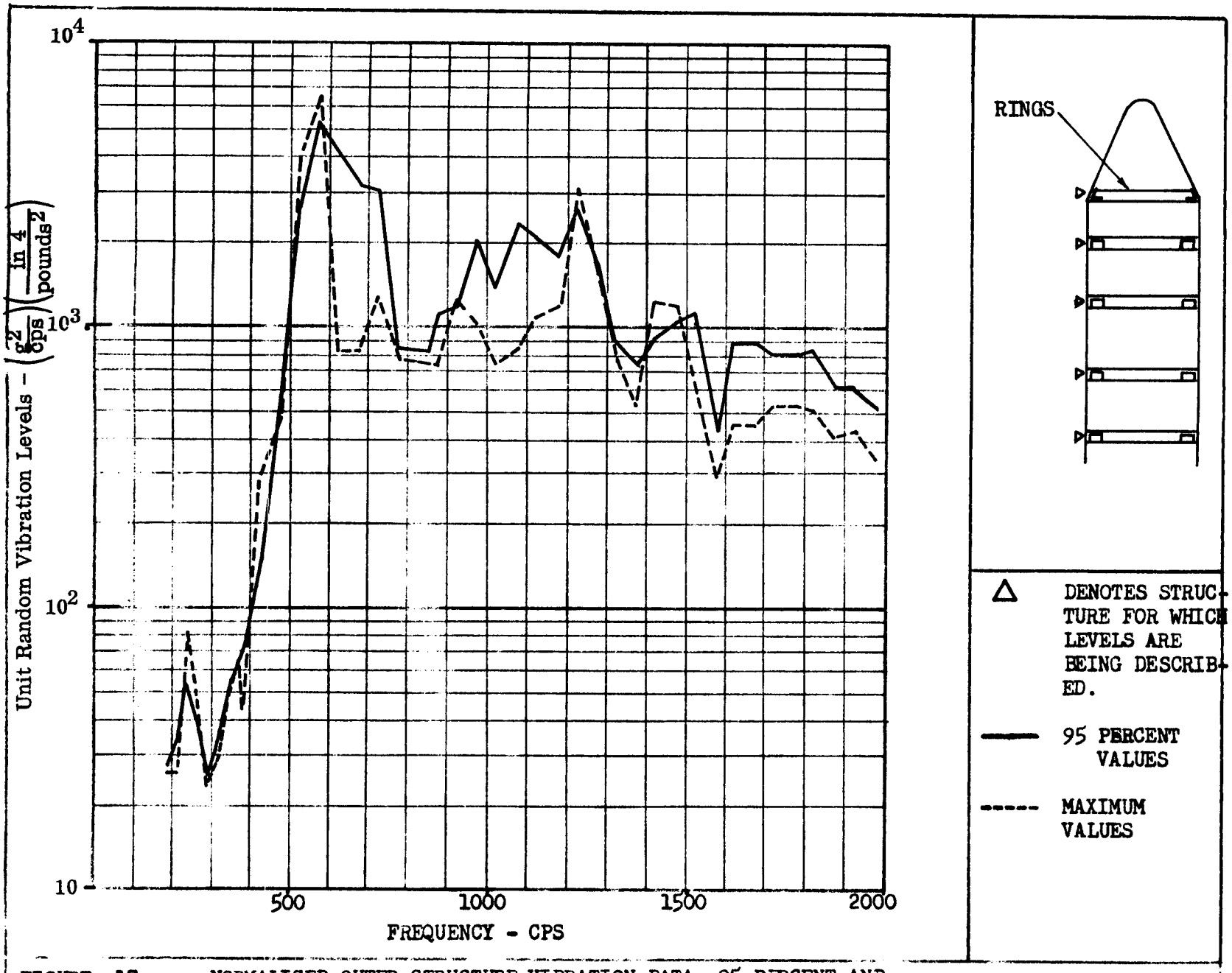

FIGURE 17 NORMALIZED OUTER STRUCTURE VIBRATION DATA, 95 PERCENT AND MAXIMUM VALUES

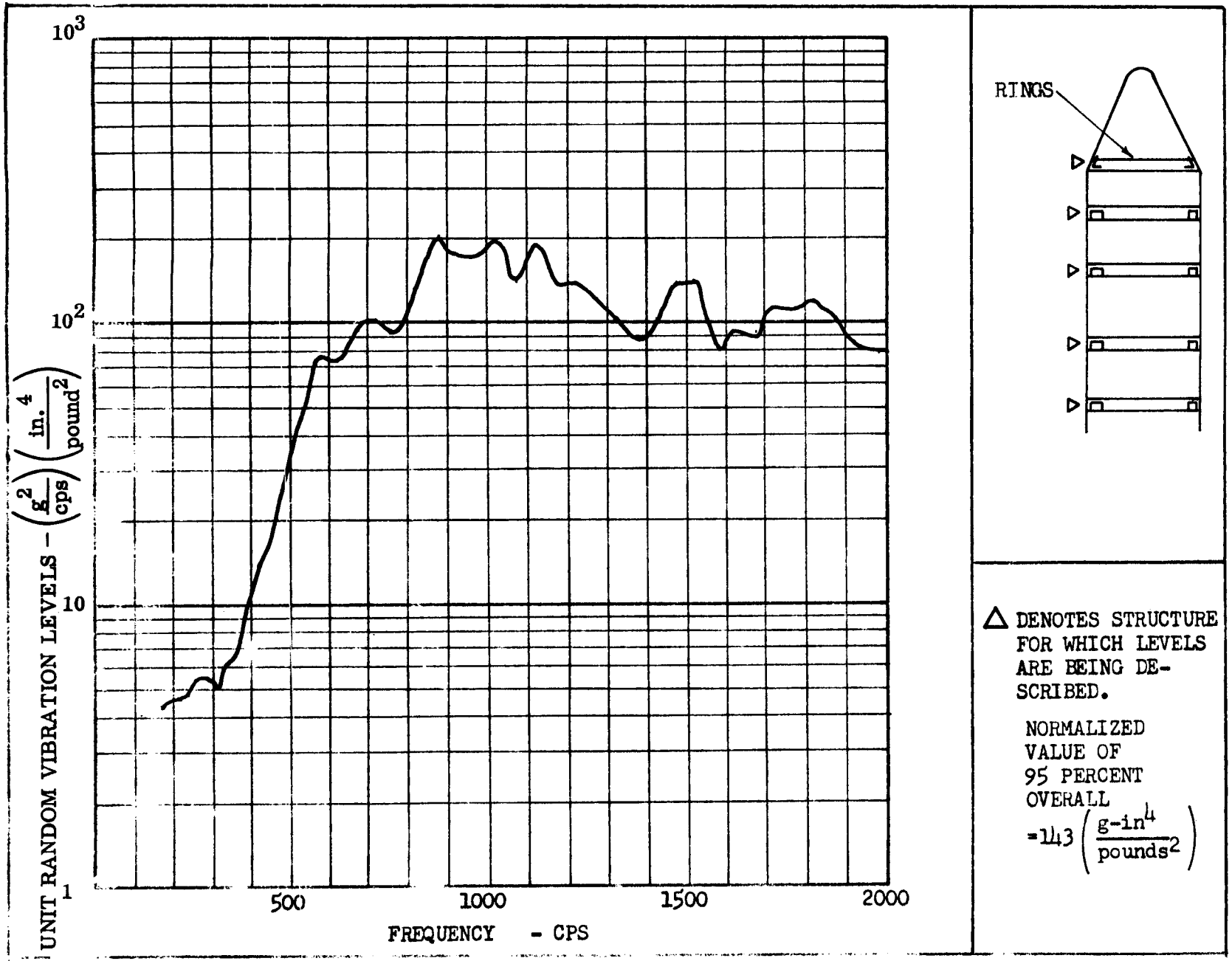

FIGURE 18 NORMALIZED OUTER STRUCTURE VIBRATION DATA, MEAN VALUES

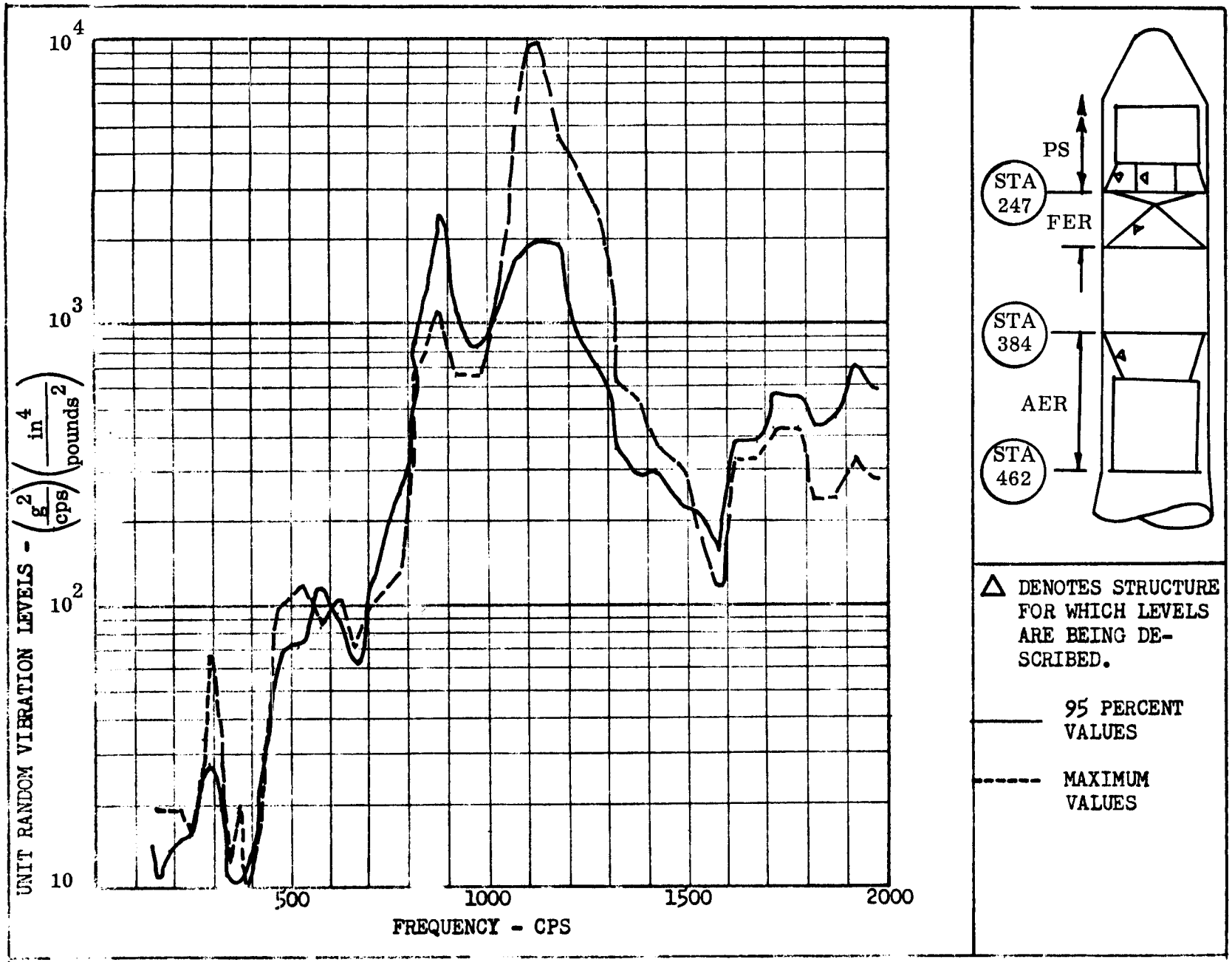

FIGURE 19 NORMALIZED INNER STRUCTURE VIBRATION DATA - 95 PERCENT AND MAXIMUM VALUES

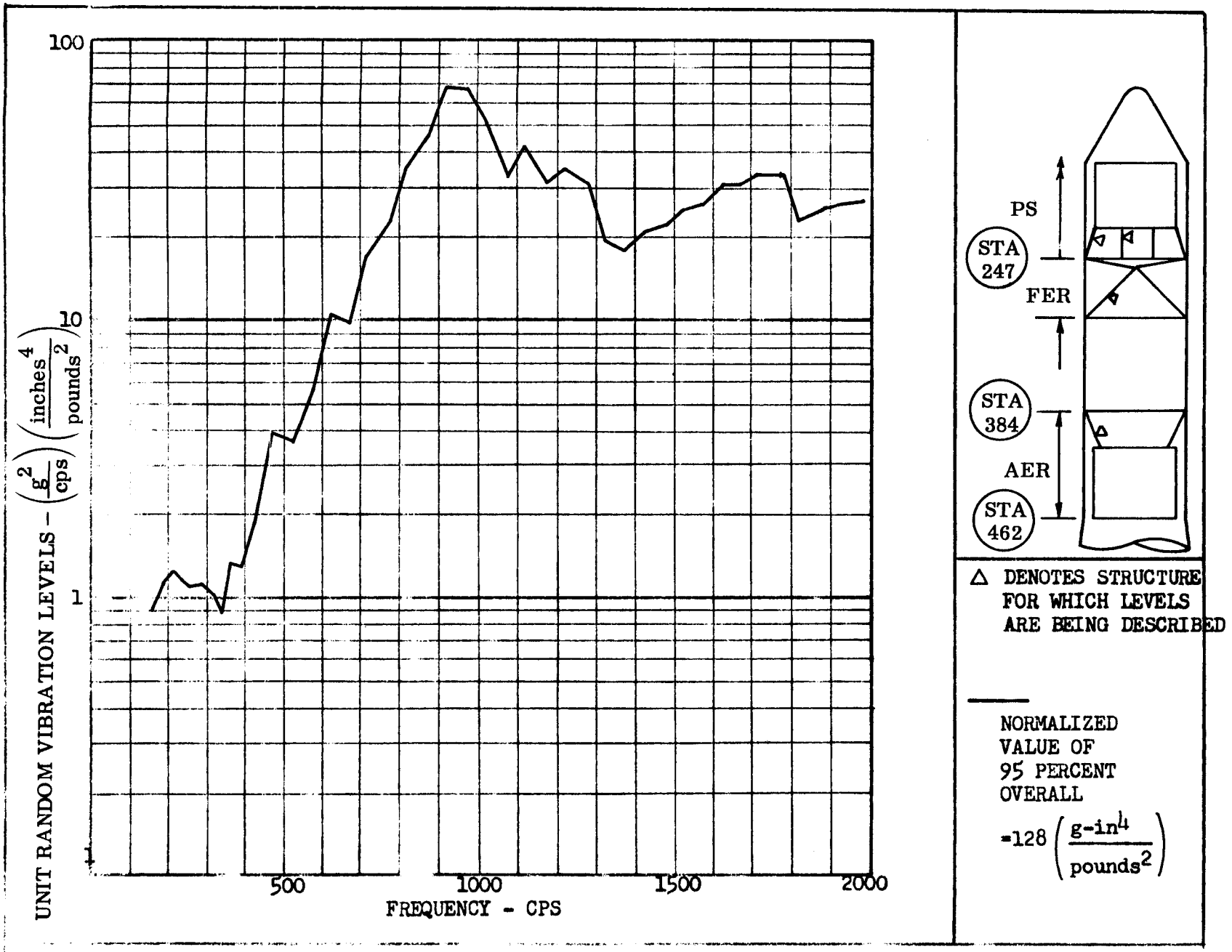

FIGURE 20 NORMALIZED INNER STRUCTURAL VIBRATION DATA, MEAN VALUES

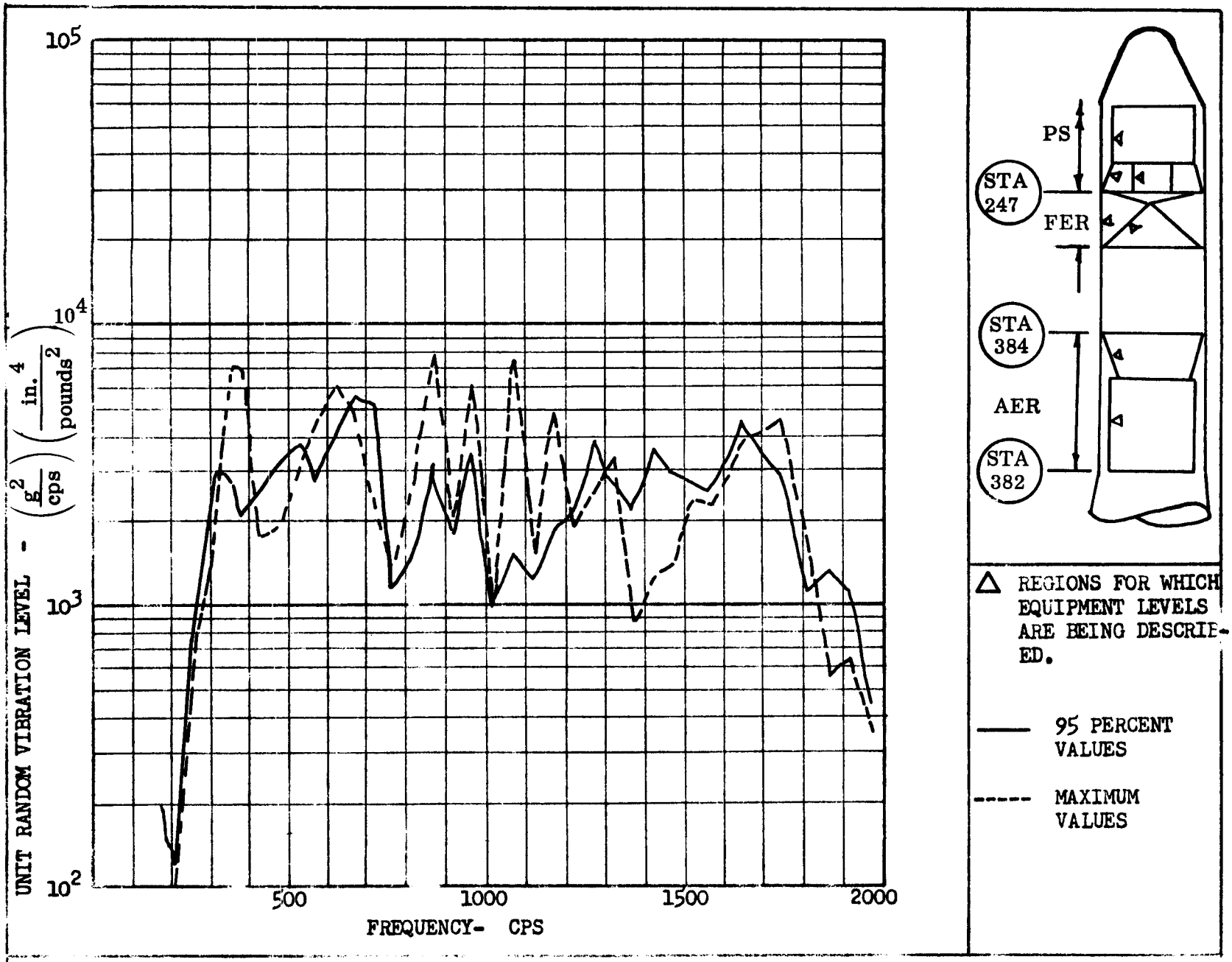

FIGURE 21 NORMALIZED EQUIPMENT VIBRATION DATA, 95 PERCENT AND MAXIMUM VALUES

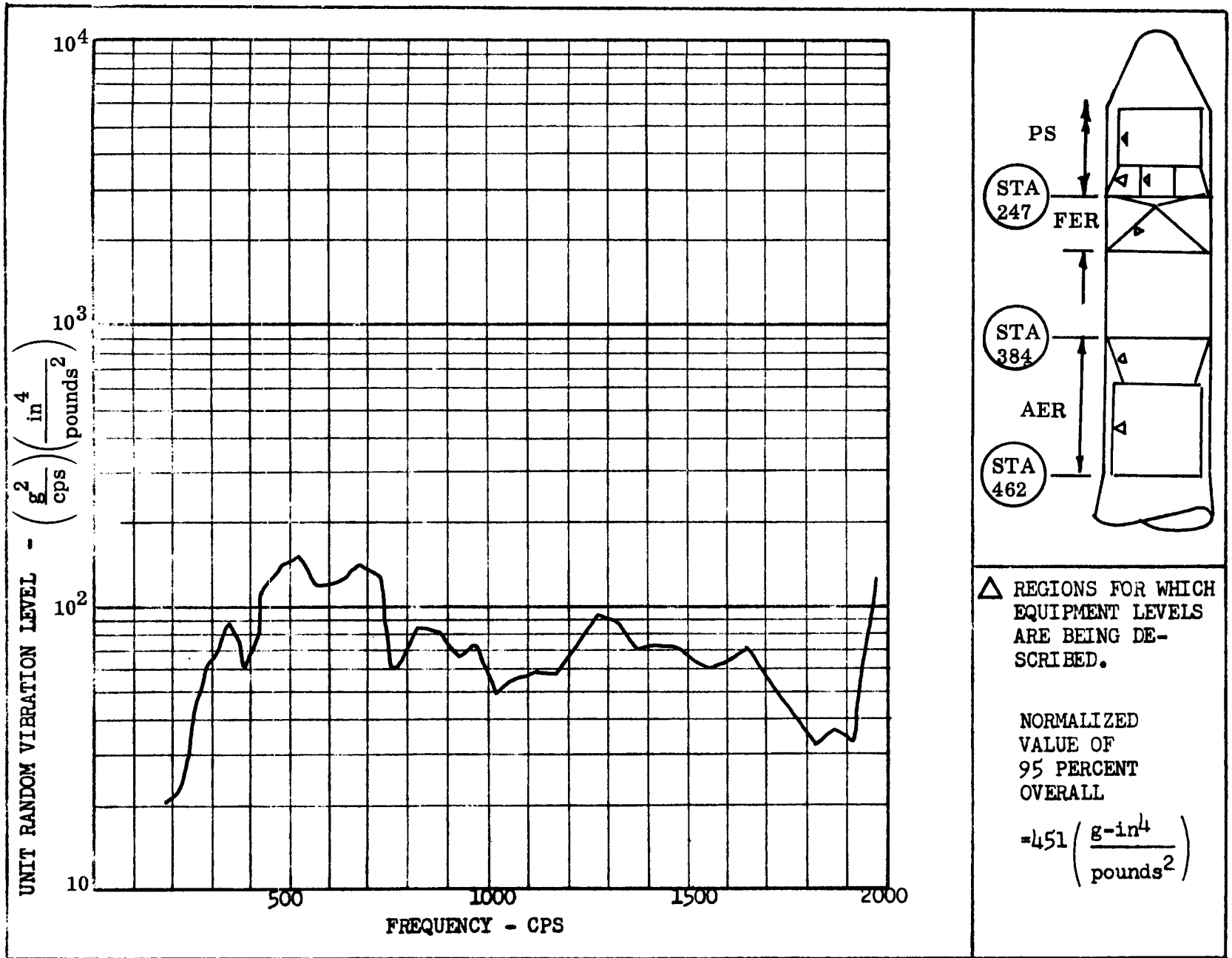

FIGURE 22 NORMALIZED EQUIPMENT VIBRATION DATA, MEAN VALUES

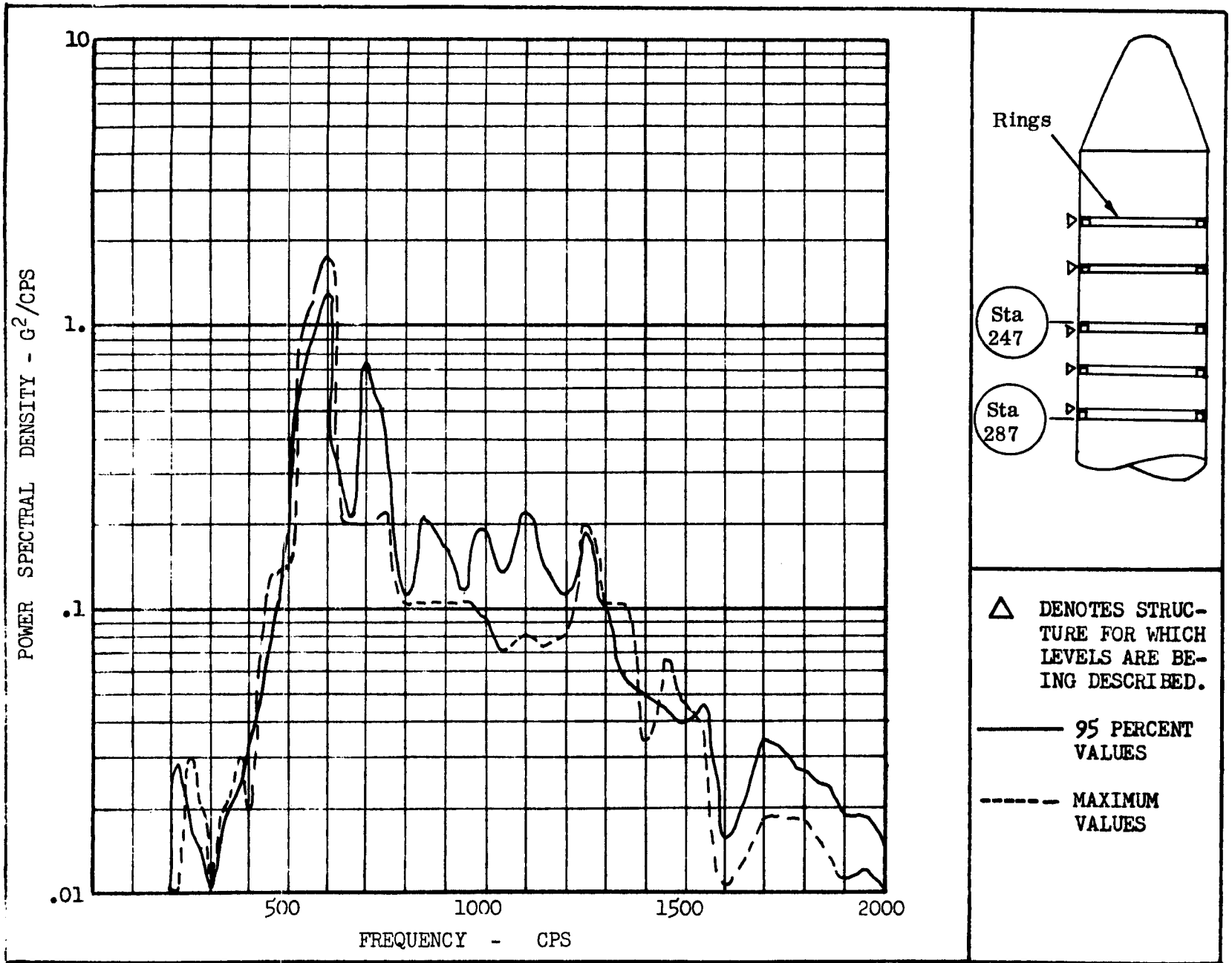

FIG. 23 95 PERCENT AND MAXIMUM PSD VALUES FOR PS AND FER OUTER STRUCTURE, ATLAS "DRY" PAD, AND THOR "WET" PAD LAUNCH

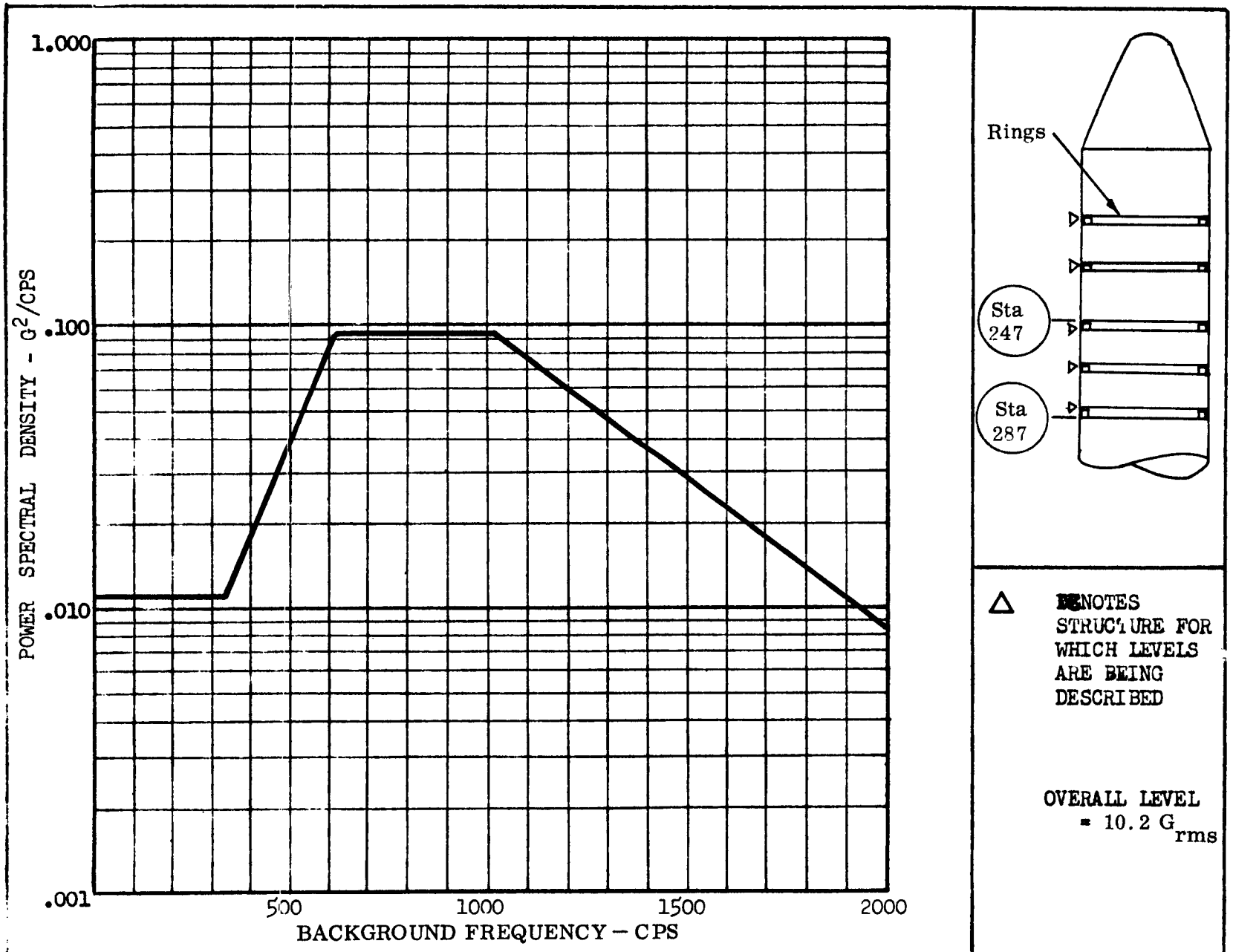

FIG. 24 BACKGROUND VIBRATION FOR PS AND FER OUTER STRUCTURE, ATLAS "DRY" PAD AND THOR "WET" PAD LAUNCH

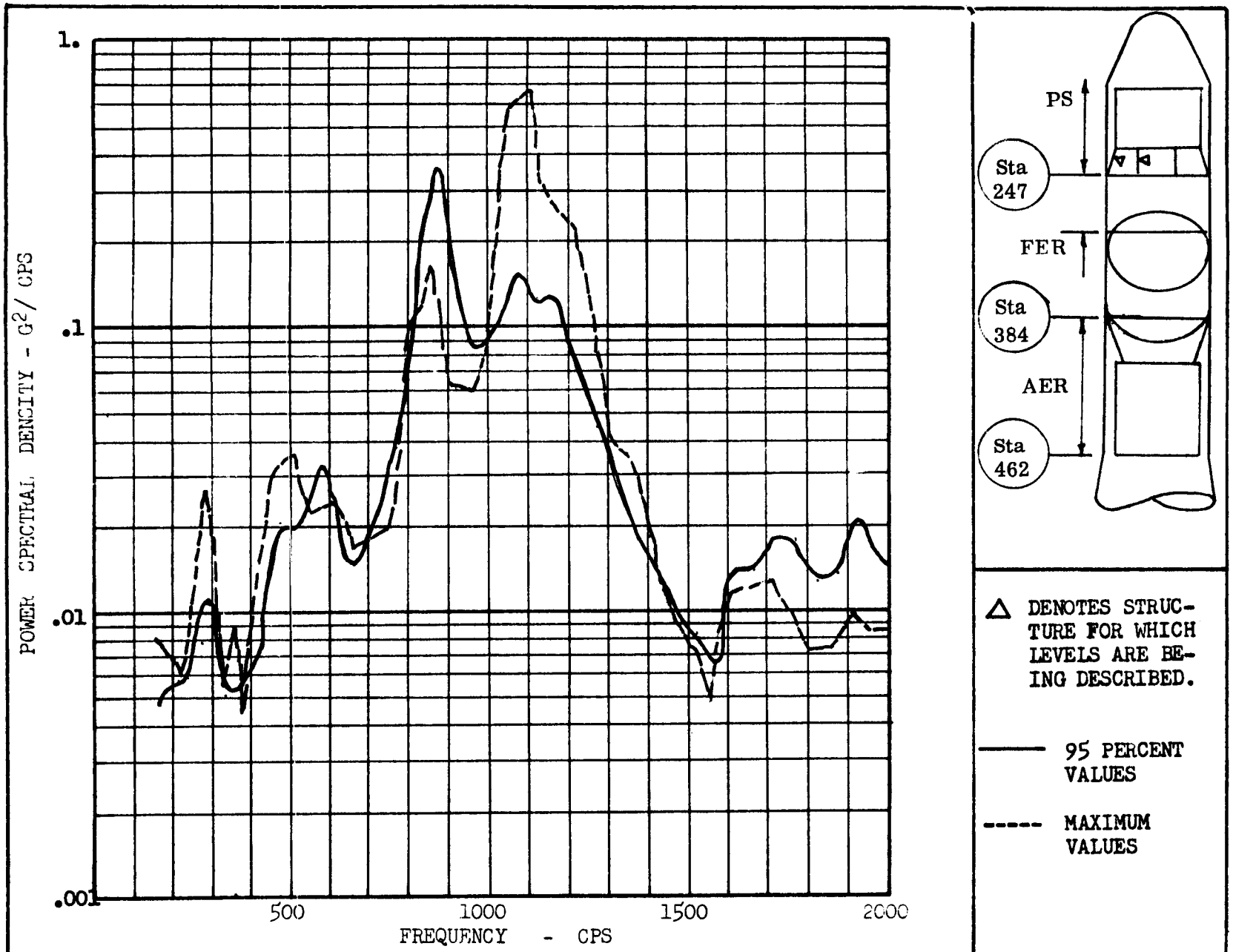

FIG. 25 95 PERCENT AND MAXIMUM PSD VALUES FOR PS AND FER INNER STRUCTURE, ATLAS "DRY" PAD, AND THOR "WET" PAD LAUNCH

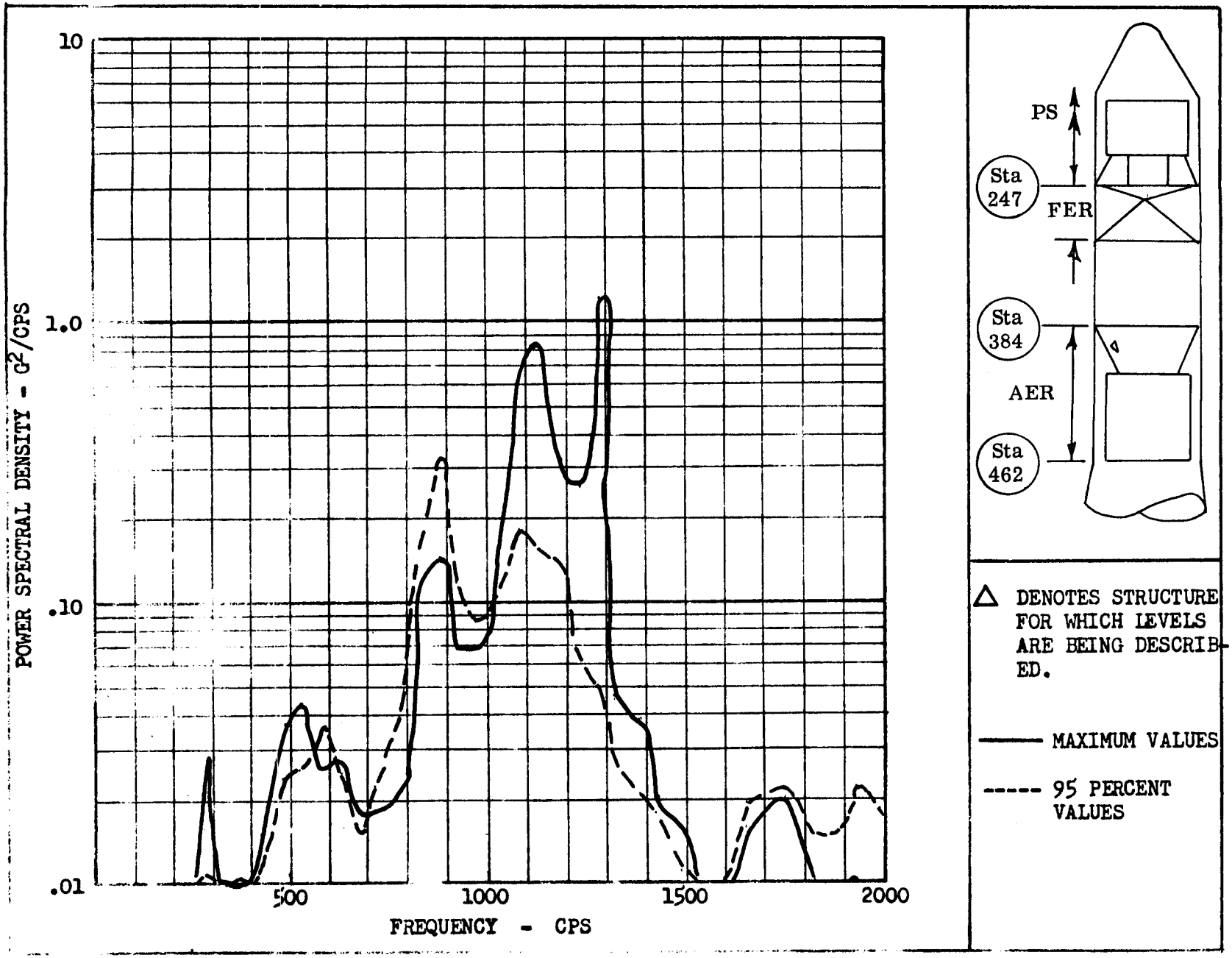

FIG. 26 95 PERCENT AND MAXIMUM PSD VALUES FOR AER INNER STRUCTURE, ATLAS "DRY" PAD, AND THOR "WET" PAD LAUNCH

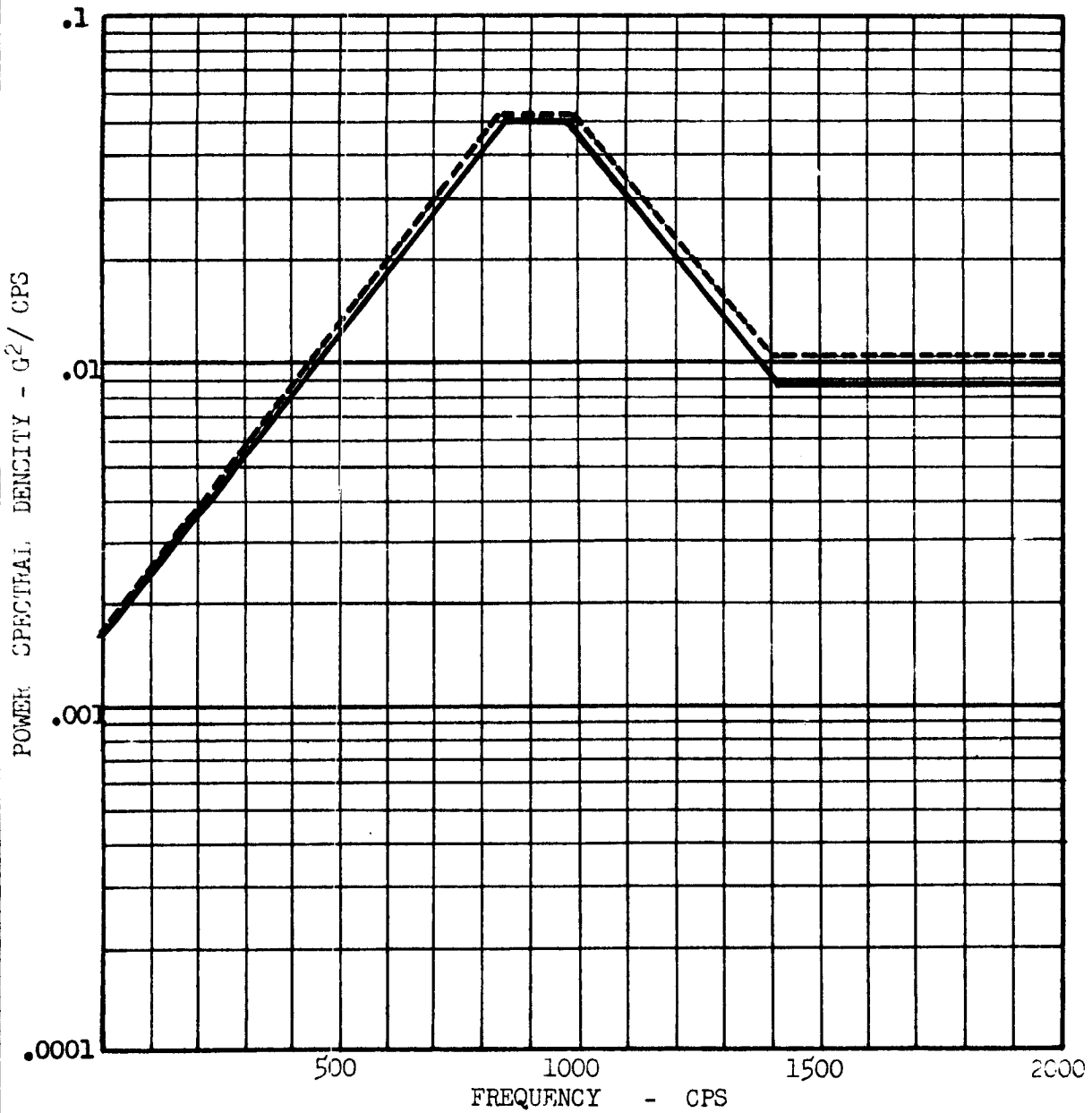

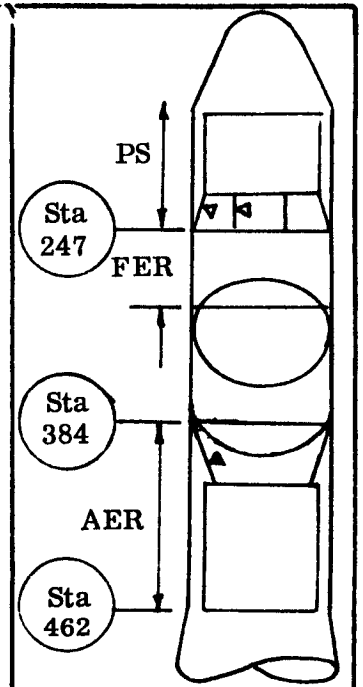

△ DENOTES STRUCTURES FOR WHICH LEVELS ARE BEING DESCRIBED.

----- AFT SECTION (6.75 G_{rms})

——— FORWARD SECT. (6.72 G_{rms})

FIG. 27 BACKGROUND VIBRATIONS FOR PS, FER AND AER INNER STRUCTURE, ATLAS "DRY" PAD, AND THOR "WET" PAD LAUNCH

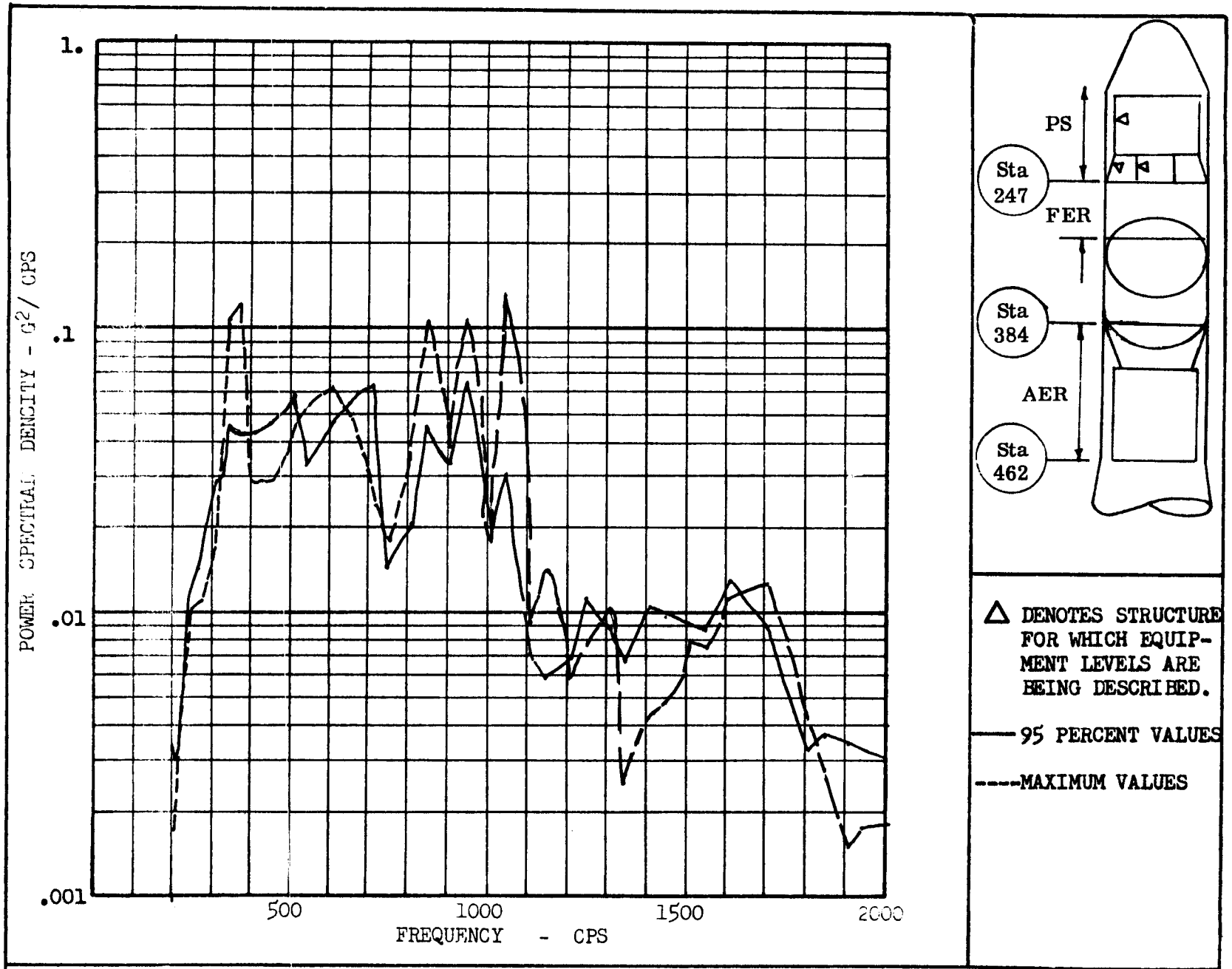

FIG. 28 95 PERCENT AND MAXIMUM PSD VALUES FOR PS AND FER EQUIPMENT, ATLAS "DRY" PAD, AND THOR "WET" PAD LAUNCH

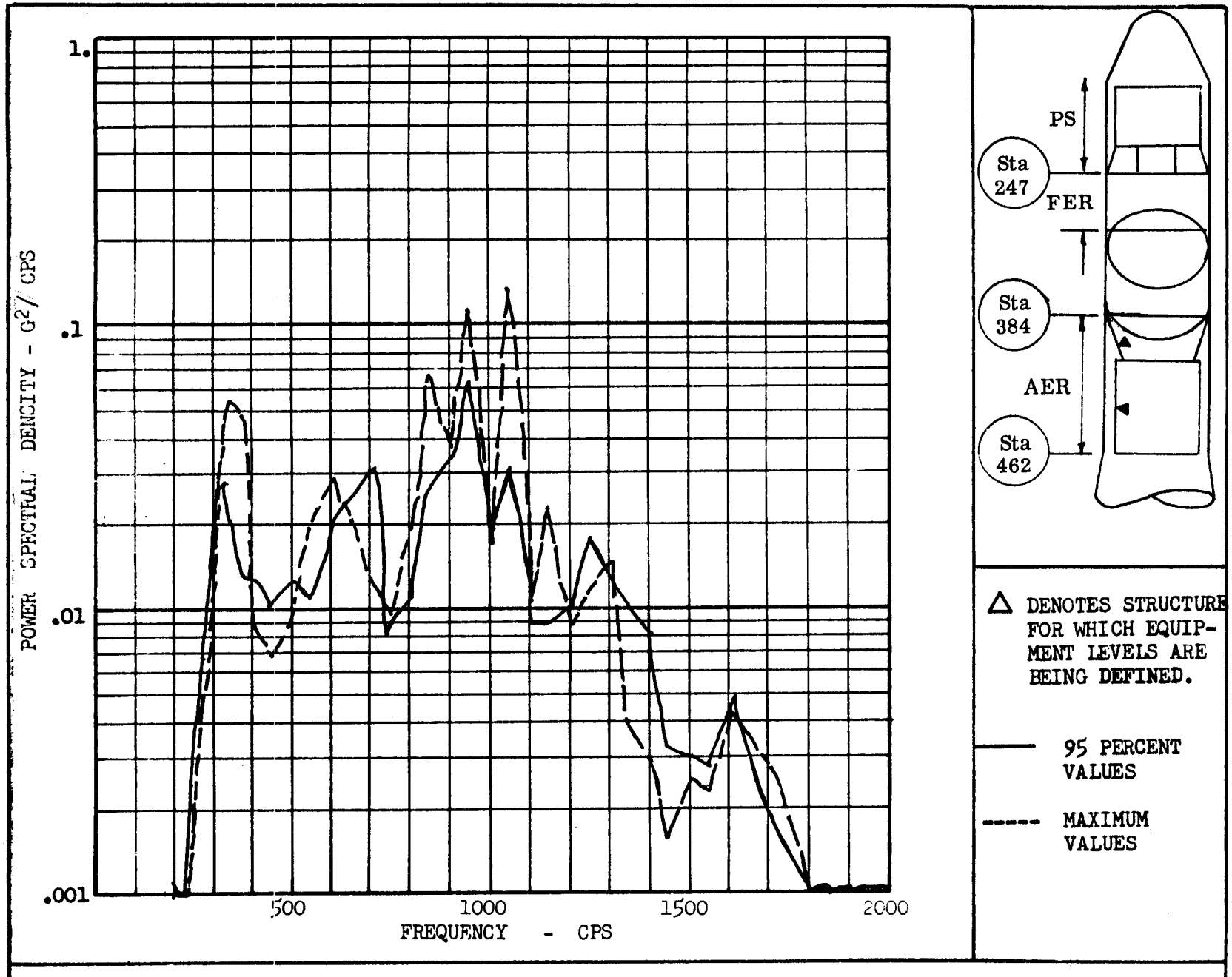

FIG. 29 PERCENT AND MAXIMUM PSD VALUES FOR AER EQUIPMENT, ATLAS "DRY" PAD AND THOR "WET" PAD LAUNCH

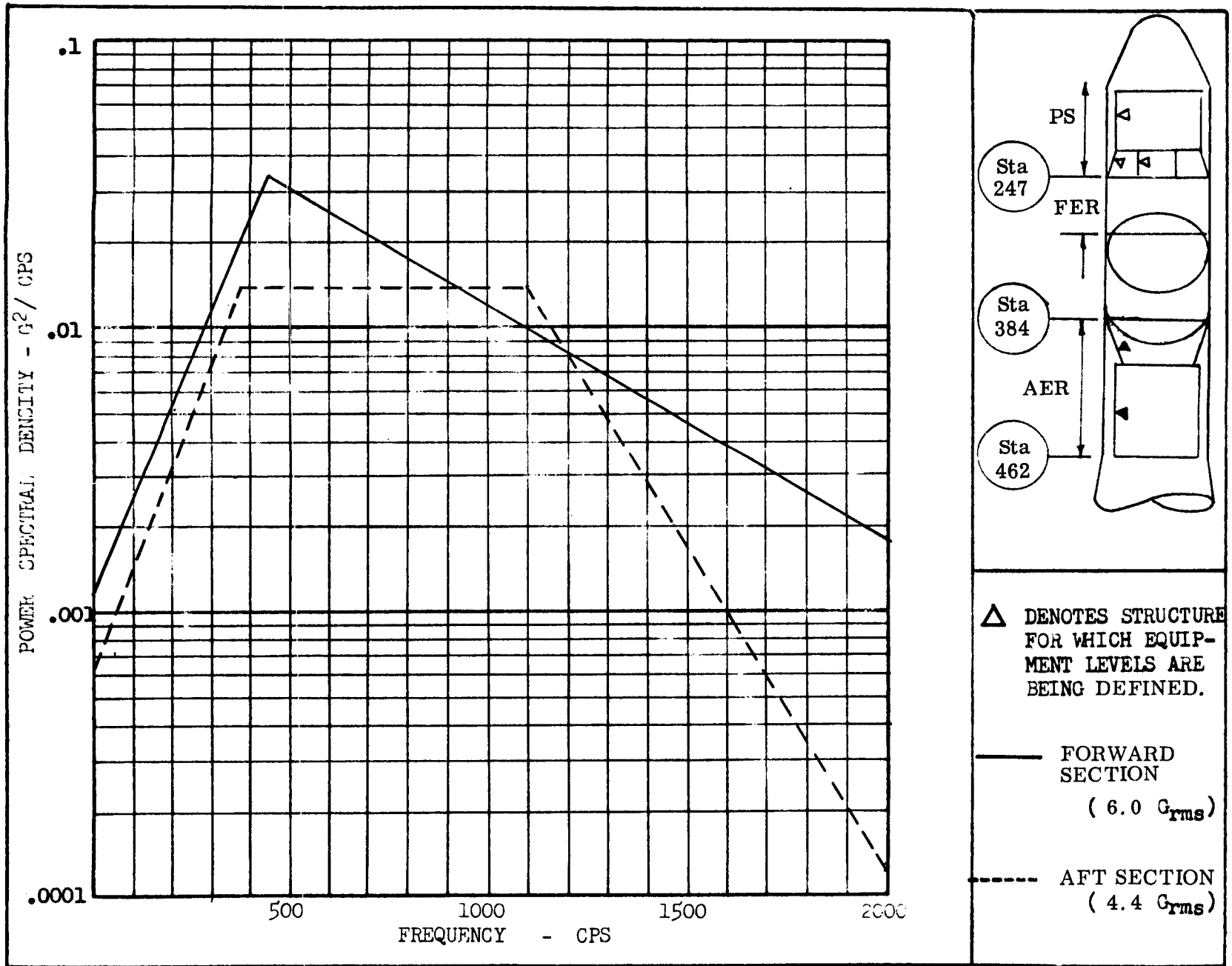

FIG. 30 BACKGROUND VIBRATION FOR PS, FER AND AER EQUIPMENT, ATLAS "DRY" PAD, AND THOR "WET" PAD LAUNCH

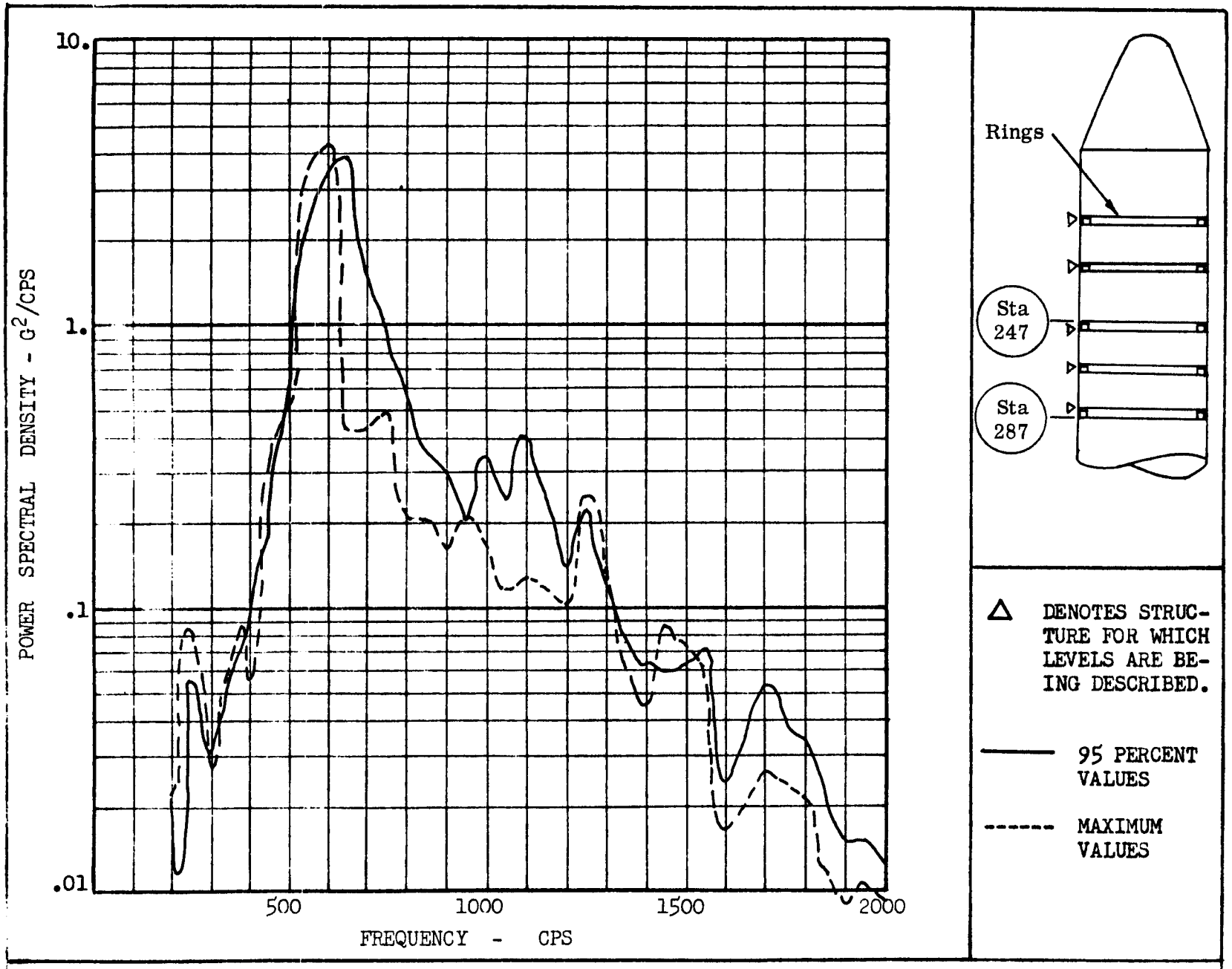

FIG. 31 95 PERCENT AND MAXIMUM PSD VALUES FOR PS AND FER OUTER STRUCTURE, THOR LAUNCH FROM "DRY" PAD

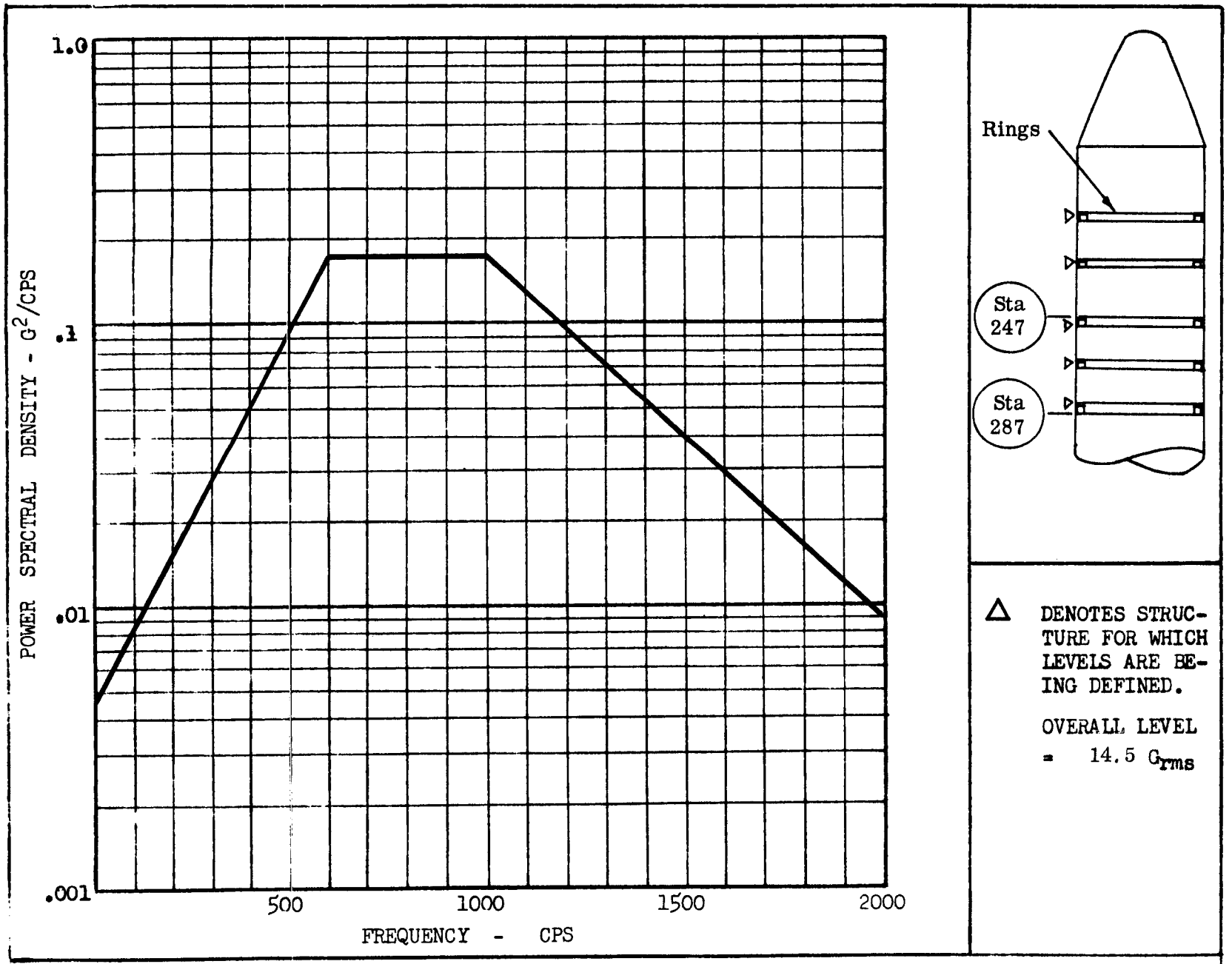

FIG. 32 BACKGROUND VIBRATION FOR PS AND FER OUTER STRUCTURE, THOR LAUNCH FROM "DRY" PAD

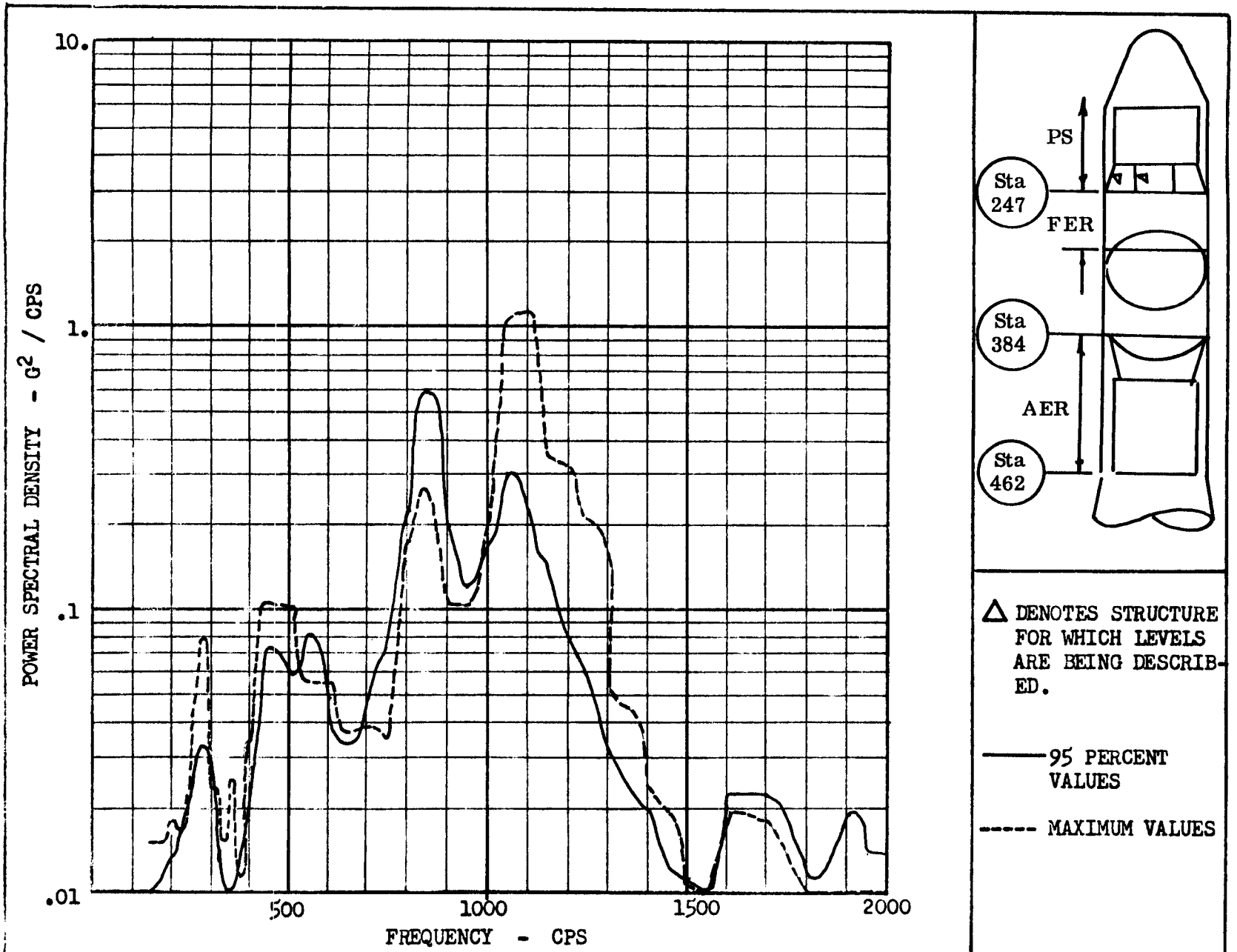

FIG. 33 95 PERCENT AND MAXIMUM VIBRATION FOR PS AND FER INNER STRUCTURE, THOR LAUNCH FROM "DRY" PAD

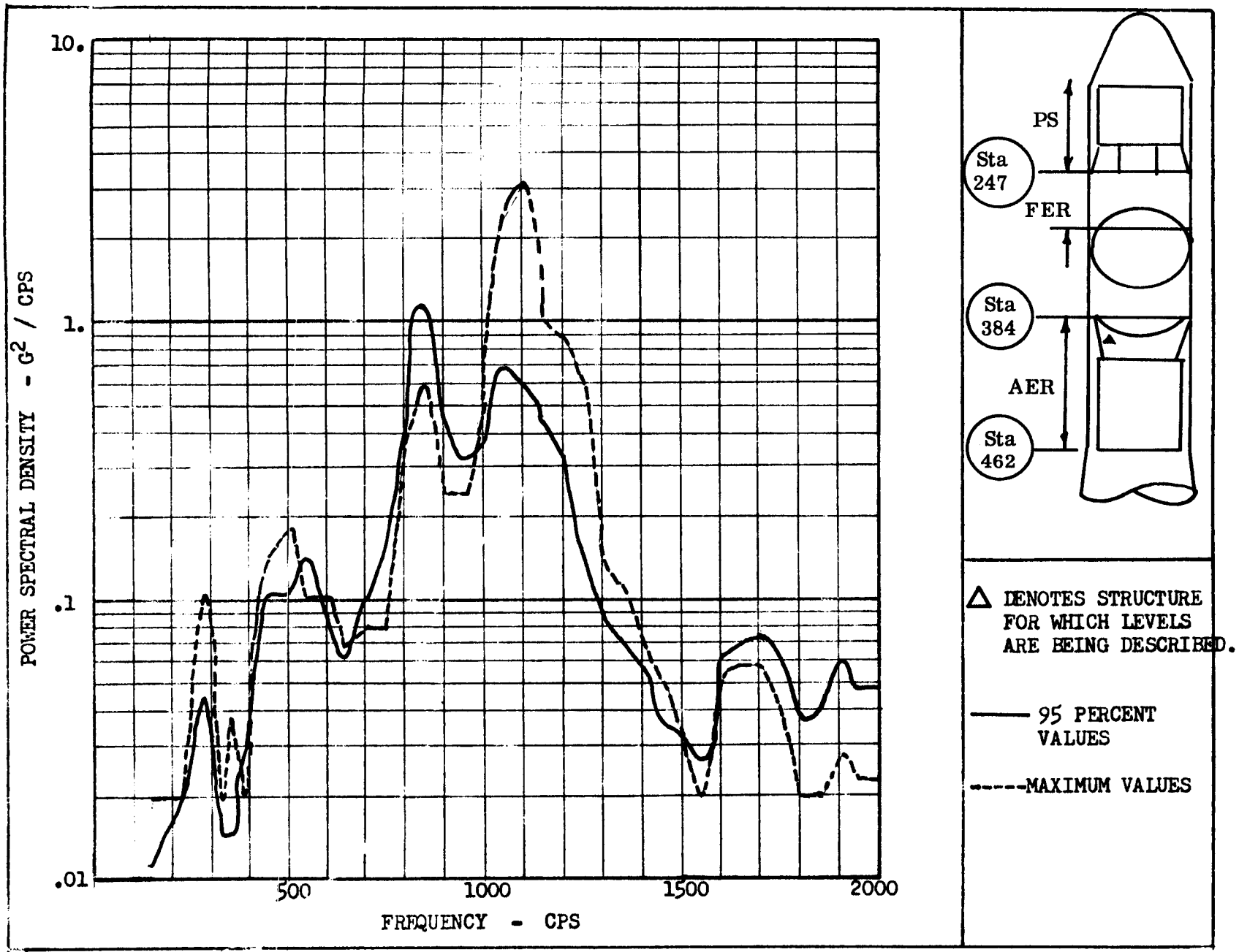

FIG. 34 95 PERCENT AND MAXIMUM VIBRATION FOR AER INNER STRUCTURE, THOR LAUNCH FROM "DRY" PAD

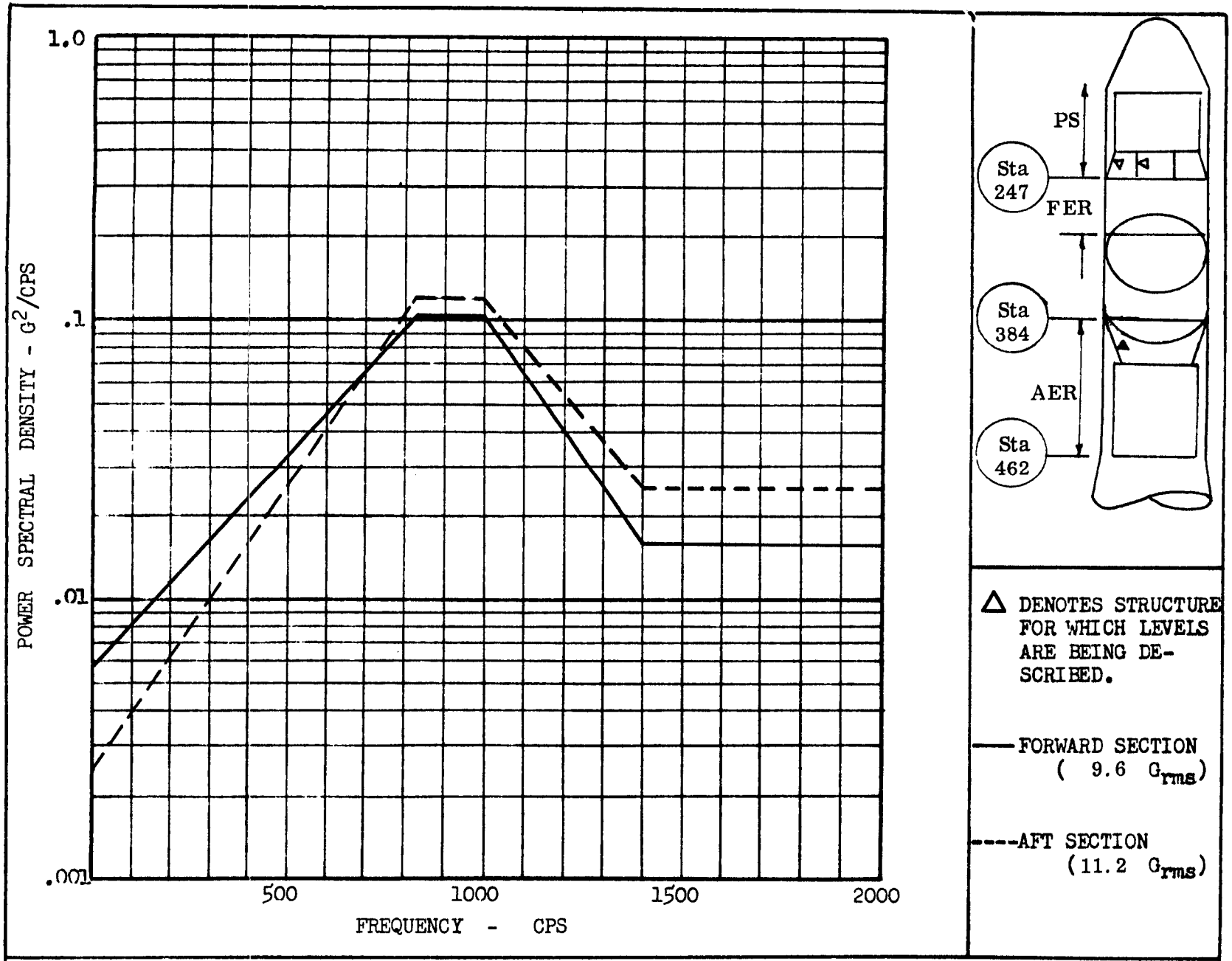

FIG. 35 BACKGROUND VIBRATION FOR PS, FER AND AER INNER STRUCTURE, THOR LAUNCH FROM "DRY" PAD

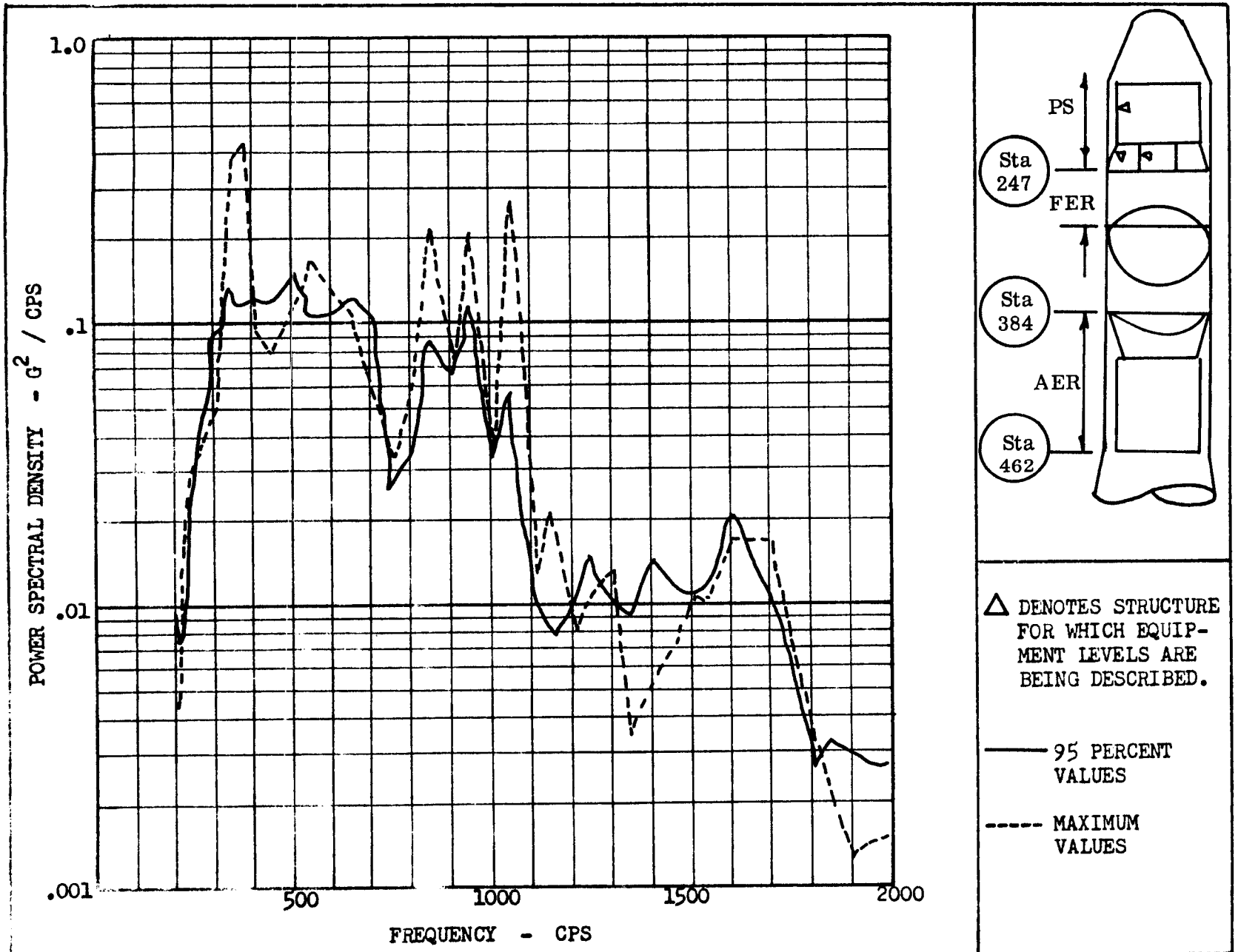

FIG. 36 95 PERCENT AND MAXIMUM VIBRATION FOR PS AND FER EQUIPMENT, THOR LAUNCH FROM "DRY" PAD

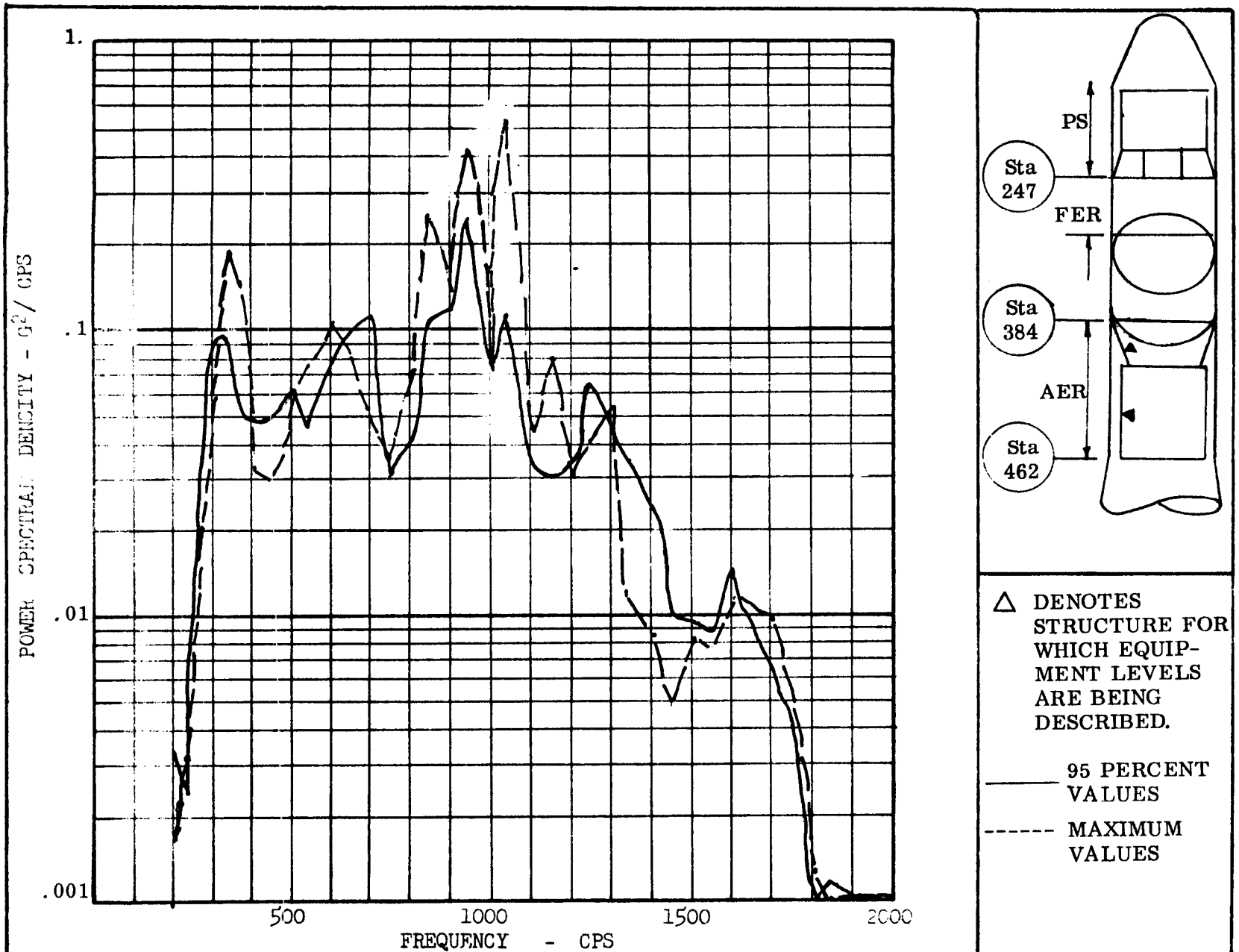

FIG. 37 95 PERCENT AND MAXIMUM VIBRATION FOR AER EQUIPMENT, THOR LAUNCH FROM "DRY," PAD

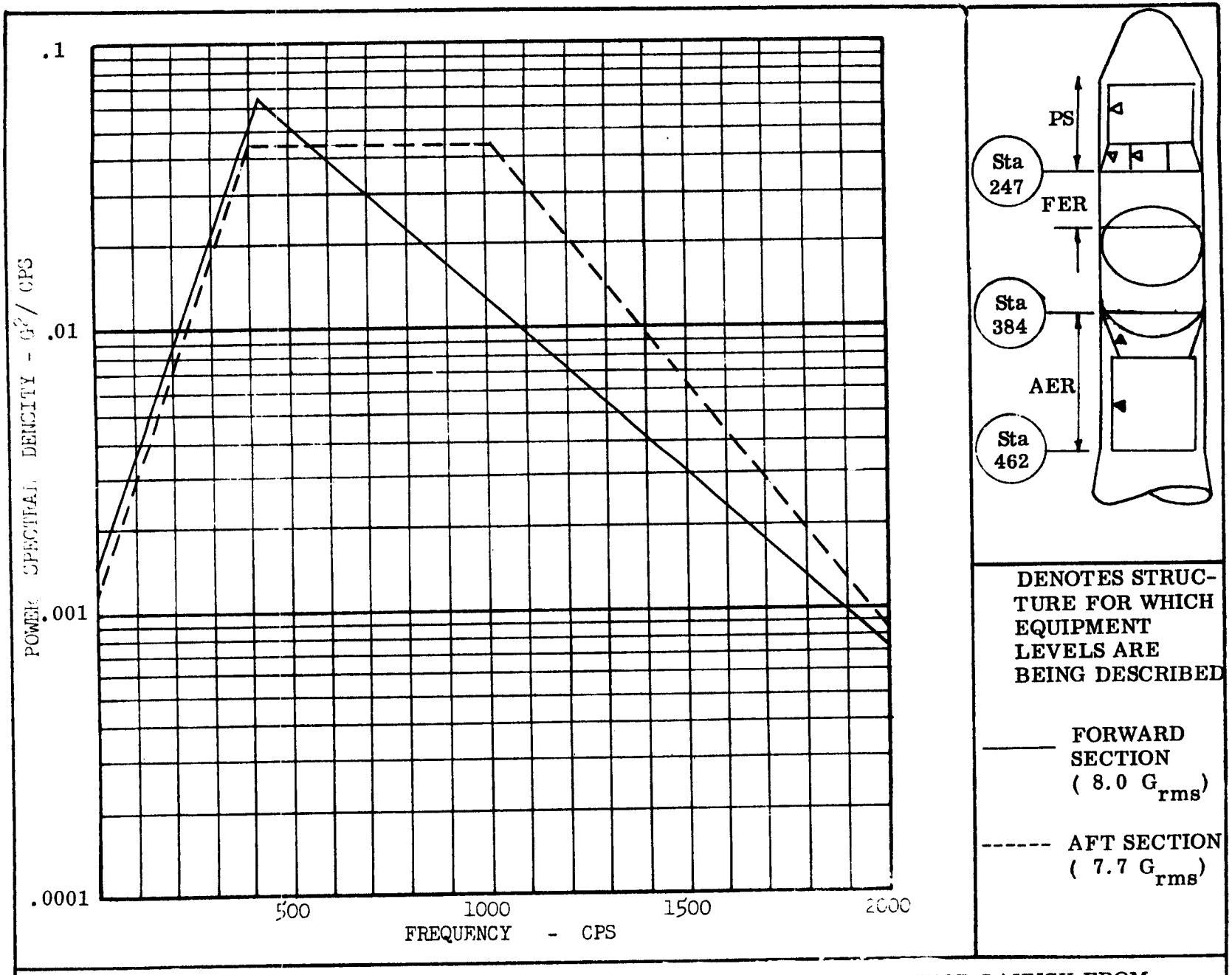

FIG. 38 BACKGROUND VIBRATION FOR PS, FER AND AER EQUIPMENT, THOR LAUNCH FROM "DRY" PAD

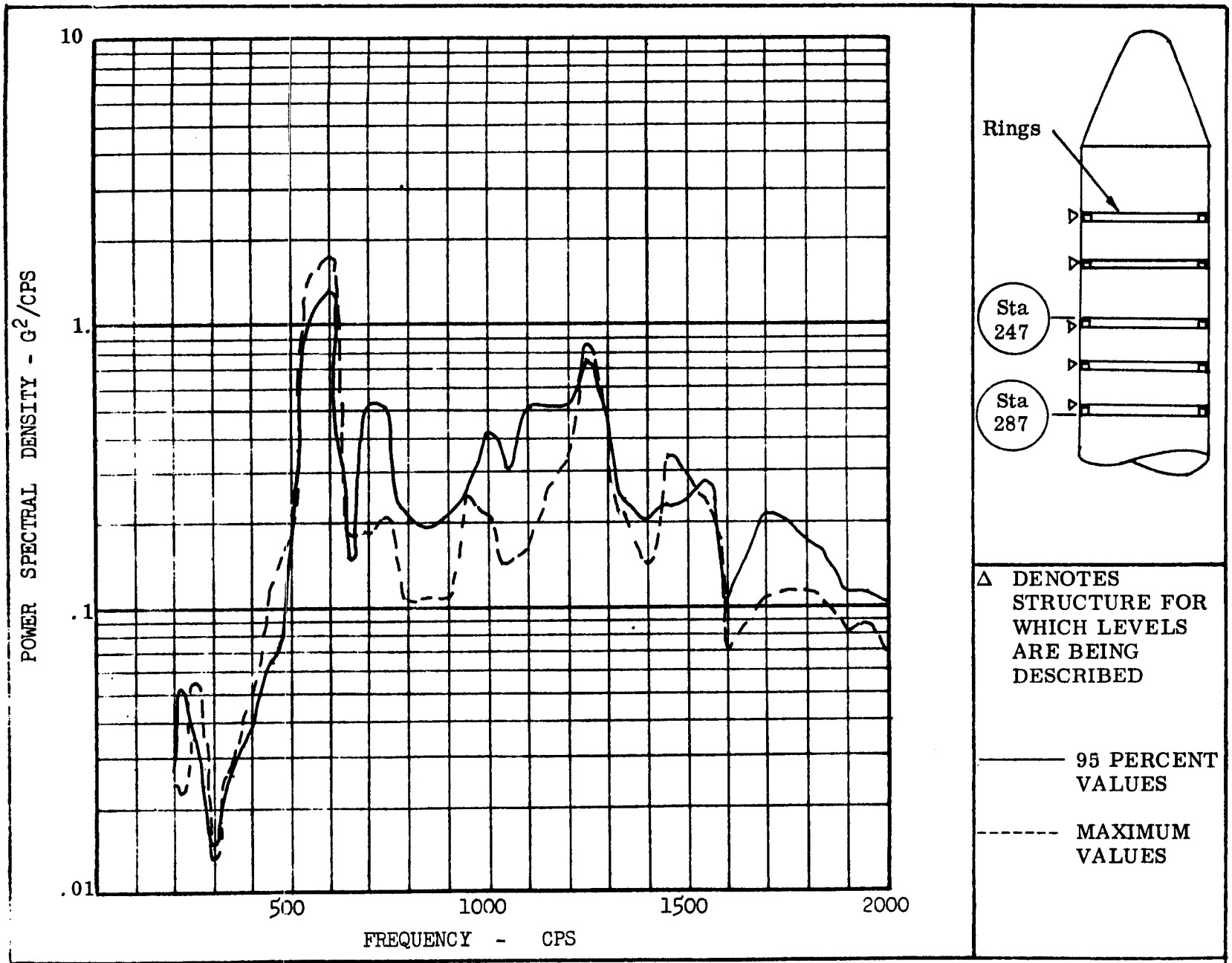

FIG. 39 95 PERCENT AND MAXIMUM VIBRATION FOR PS AND FER OUTER STRUCTURE, TAT LAUNCH FROM "WET" PAD

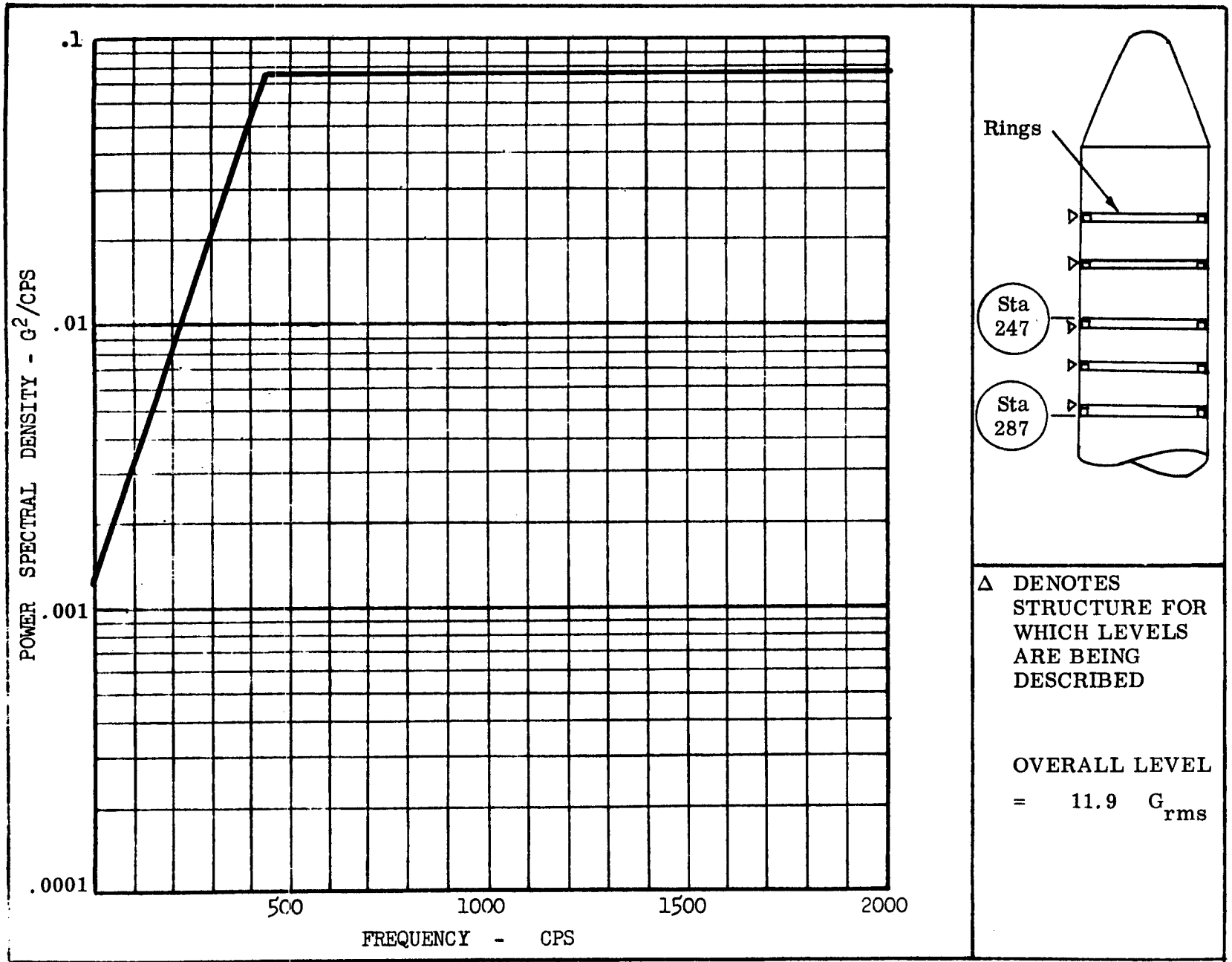

FIG. 40 BACKGROUND VIBRATION FOR PS AND FER OUTER STRUCTURE, TAT LAUNCH FROM "WET" PAD

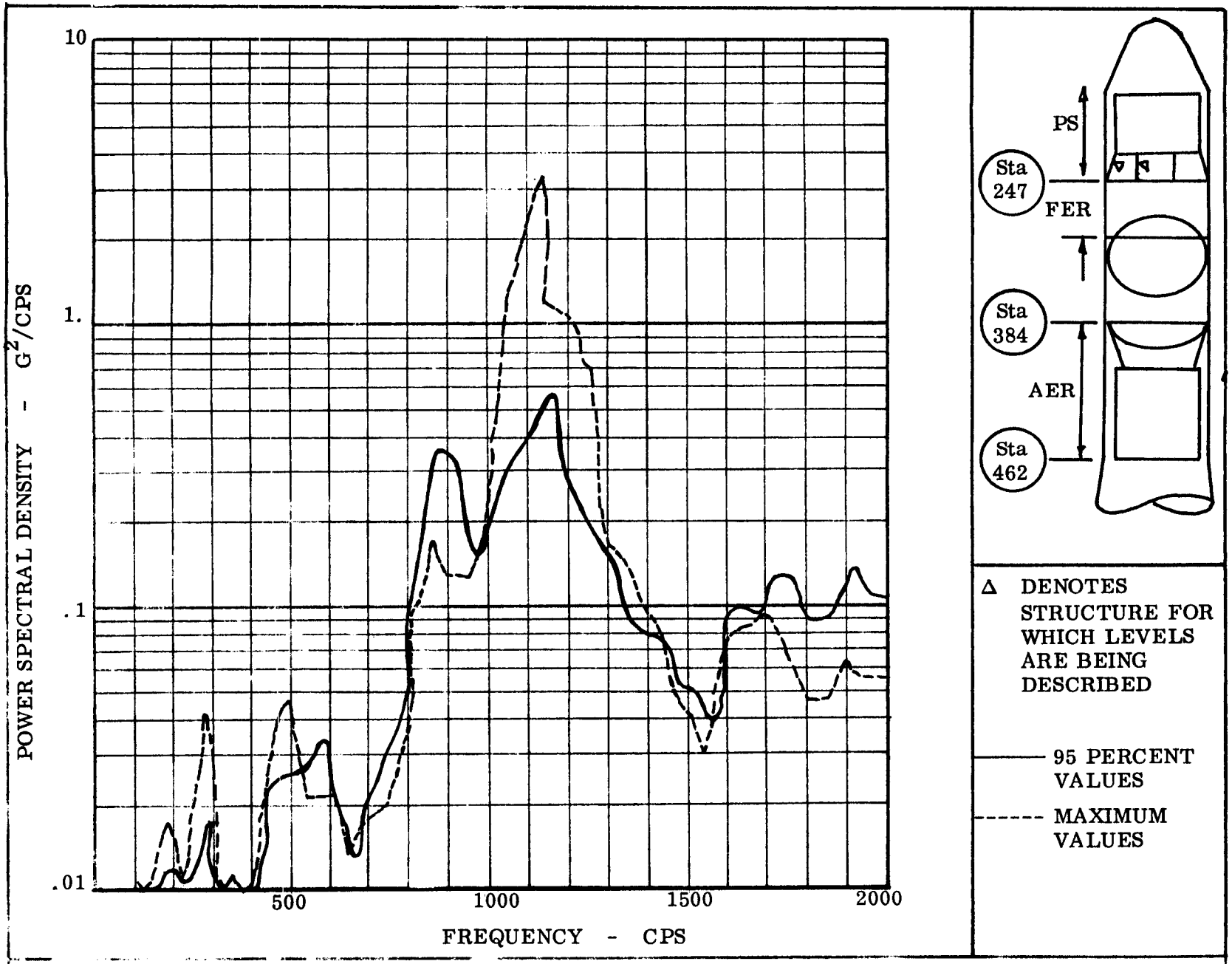

FIG. 41 95 PERCENT AND MAXIMUM VIBRATION FOR PS AND FER INNER STRUCTURE, TAT LAUNCH FROM "WET" PAD

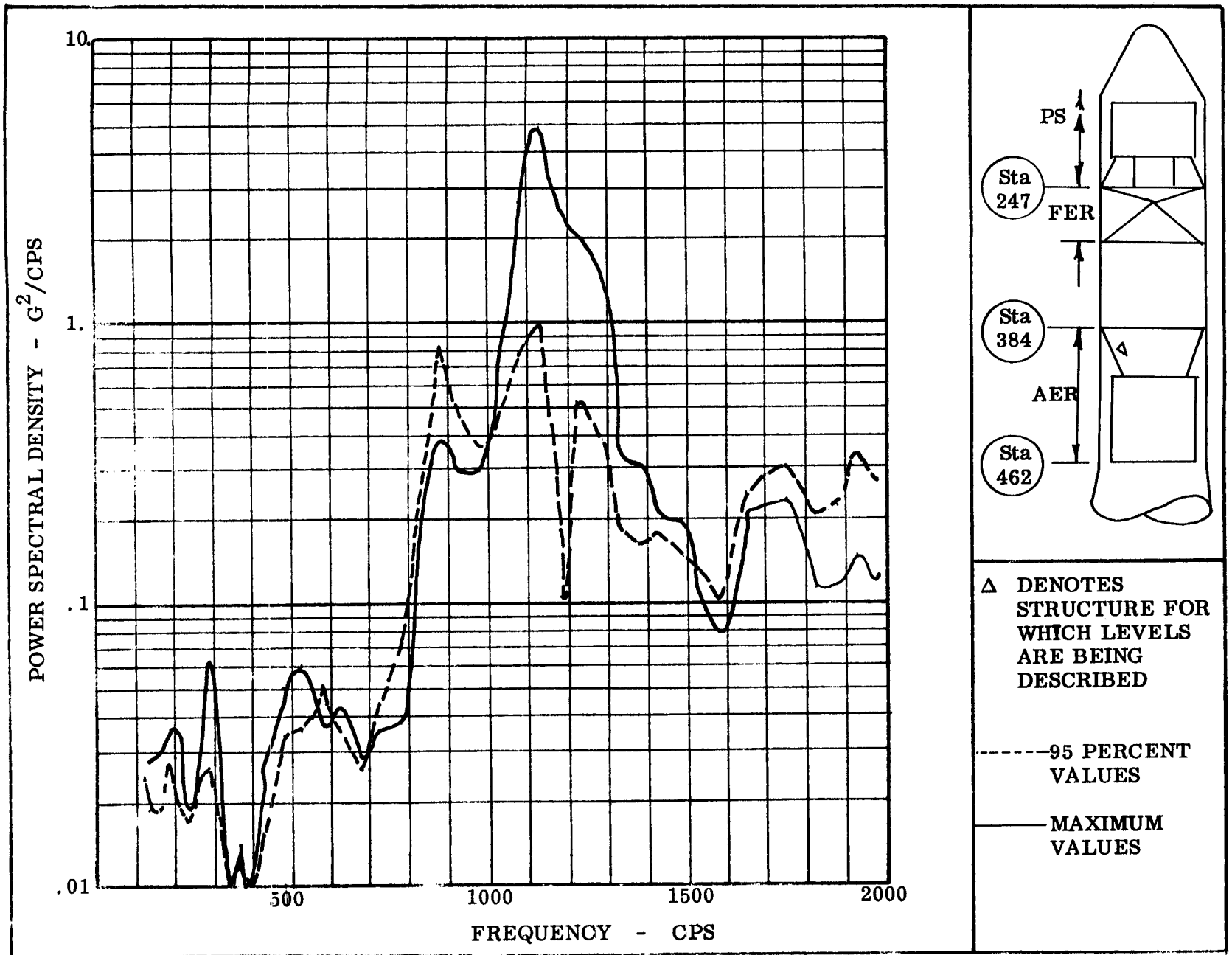

FIG. 42 95 PERCENT AND MAXIMUM VIBRATION FOR AER INNER STRUCTURE, TAT LAUNCH FROM "WET" PAD

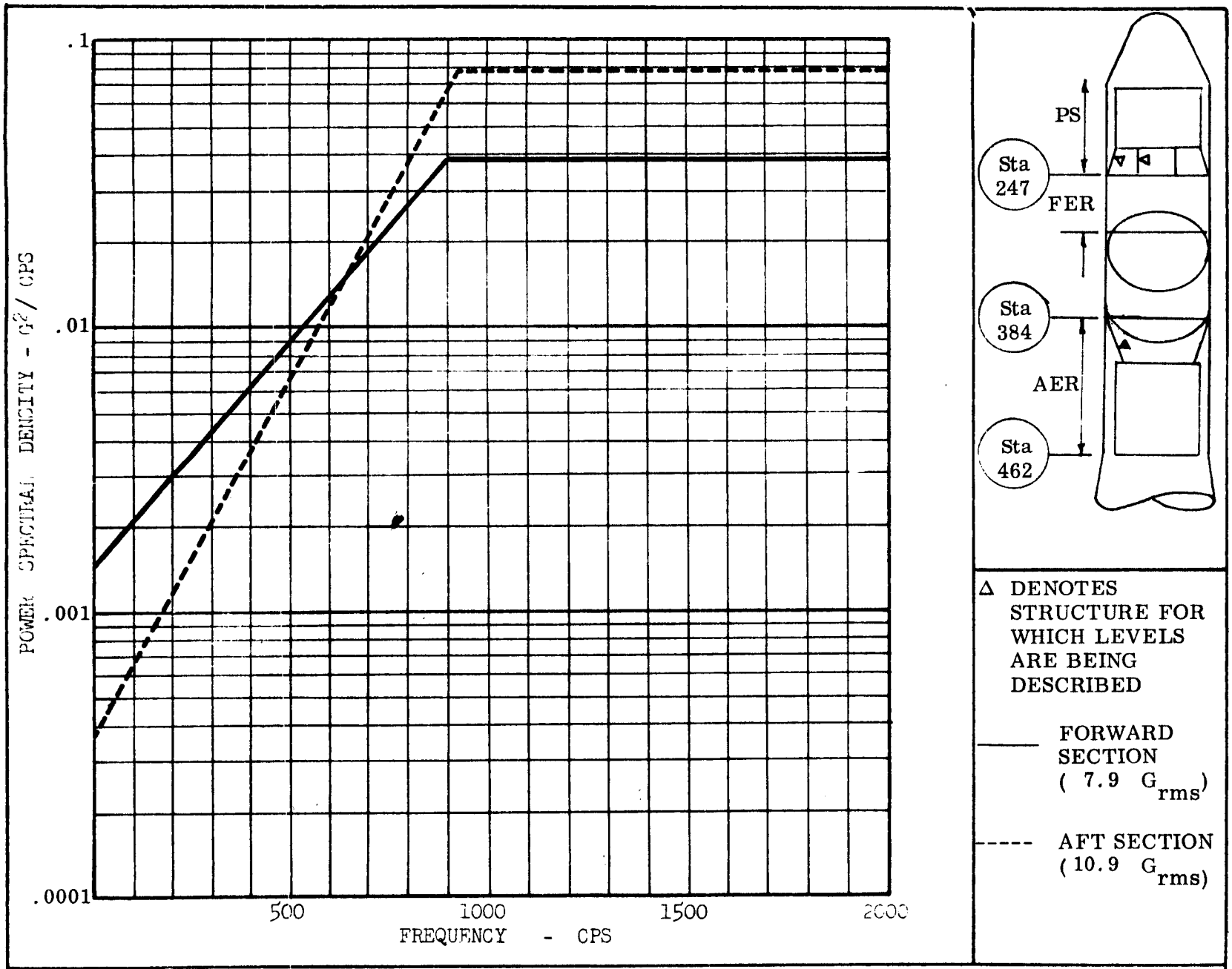

FIG. 43 BACKGROUND VIBRATION FOR PS, FER, AND AER INNER STRUCTURE, TAT LAUNCH FROM "WET" PAD

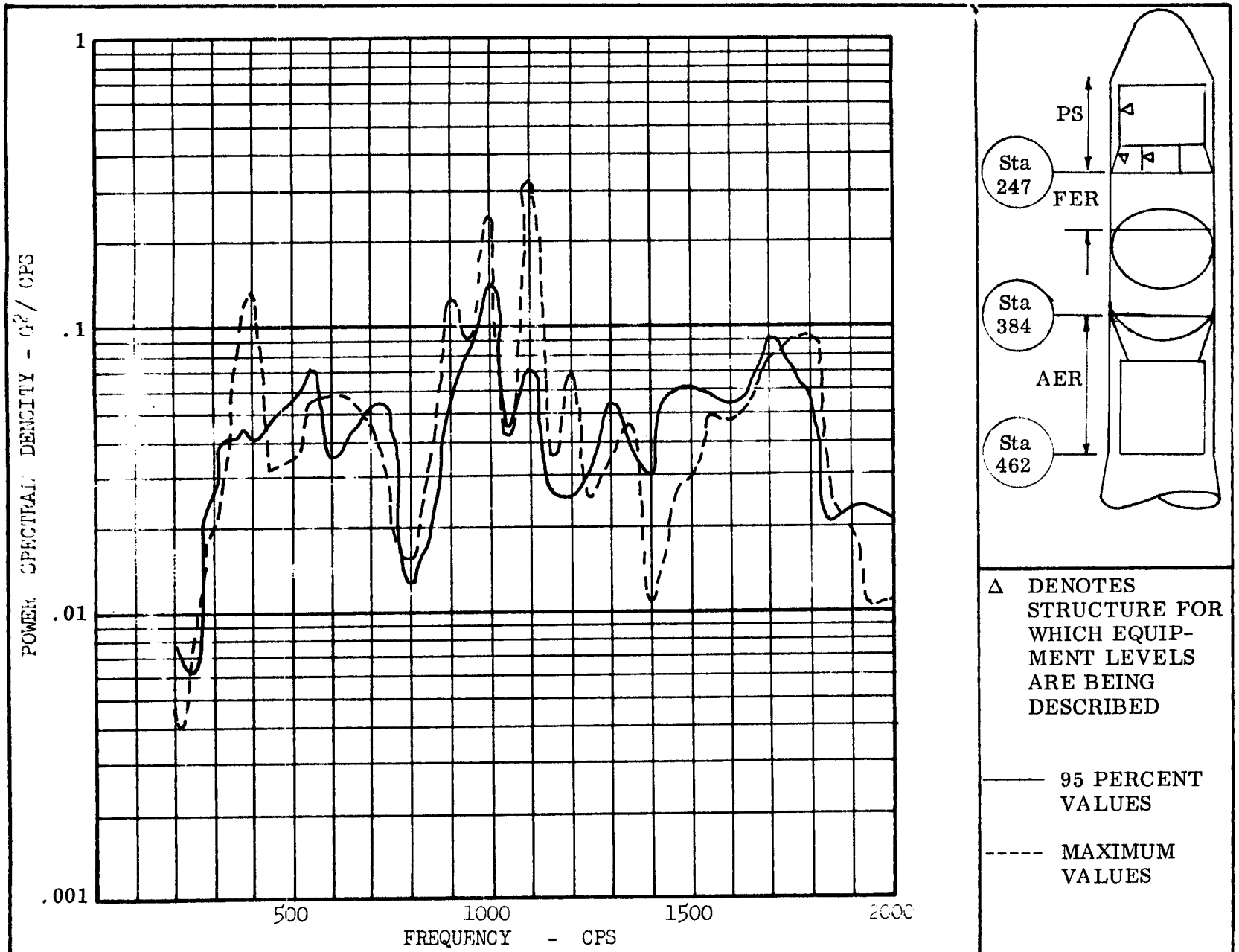

FIG. 44 95 PERCENT AND MAXIMUM VIBRATION FOR PS AND FER EQUIPMENT, TAT LAUNCH FROM "WET" PAD

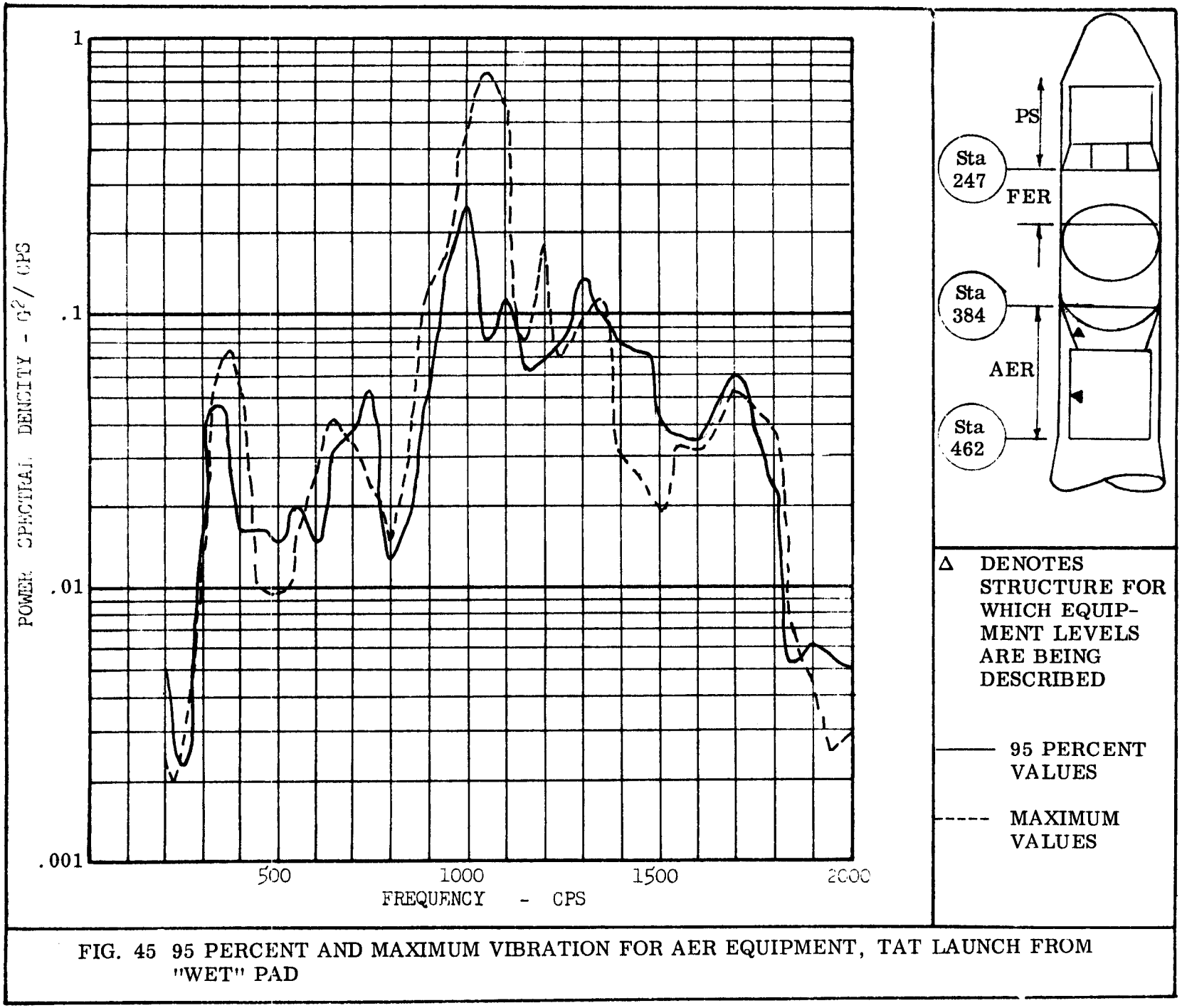

FIG. 45 95 PERCENT AND MAXIMUM VIBRATION FOR AER EQUIPMENT, TAT LAUNCH FROM "WET" PAD

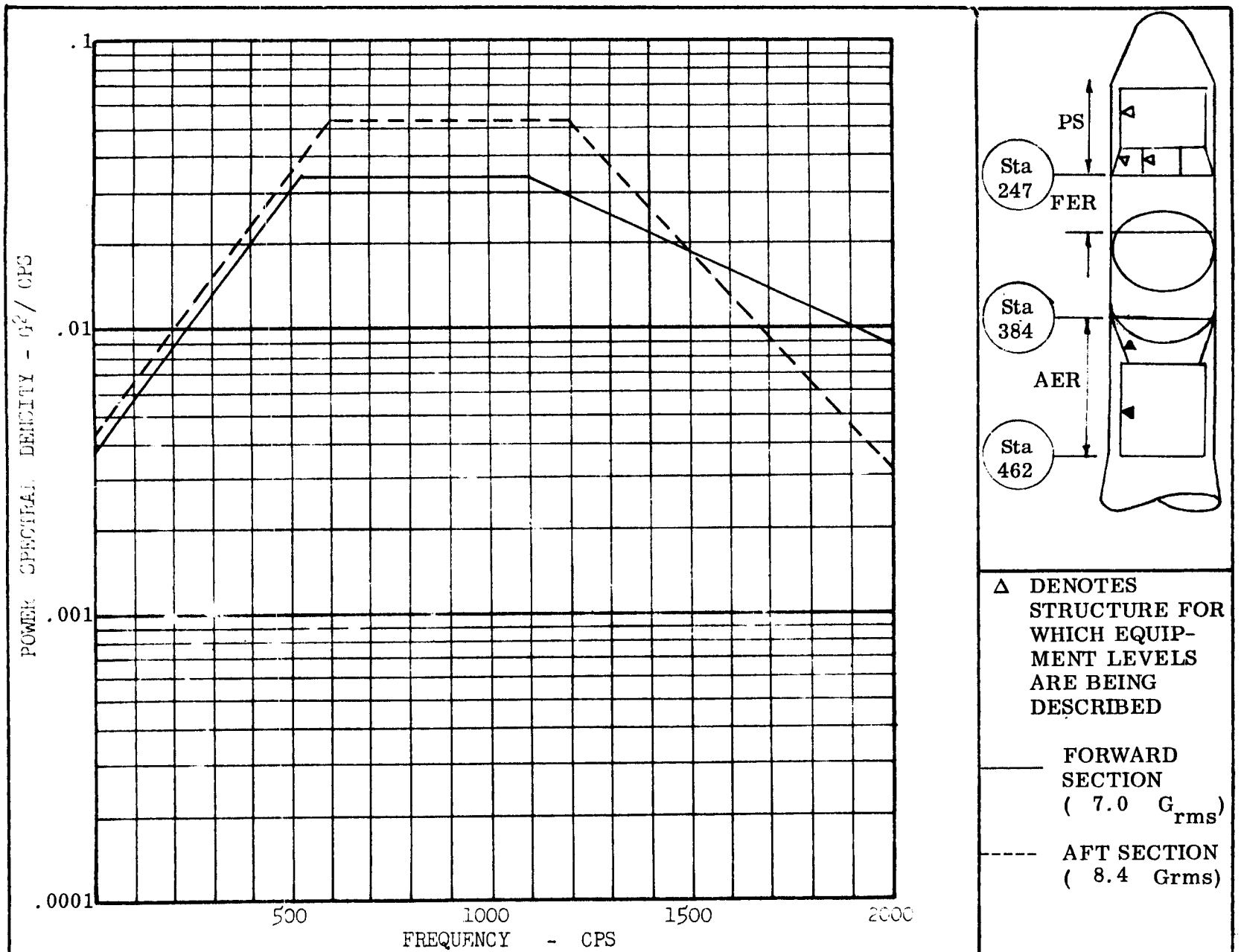

FIG. 46 BACKGROUND VIBRATION FOR PS, FER AND AER EQUIPMENT, TAT LAUNCH FROM "WET" PAD

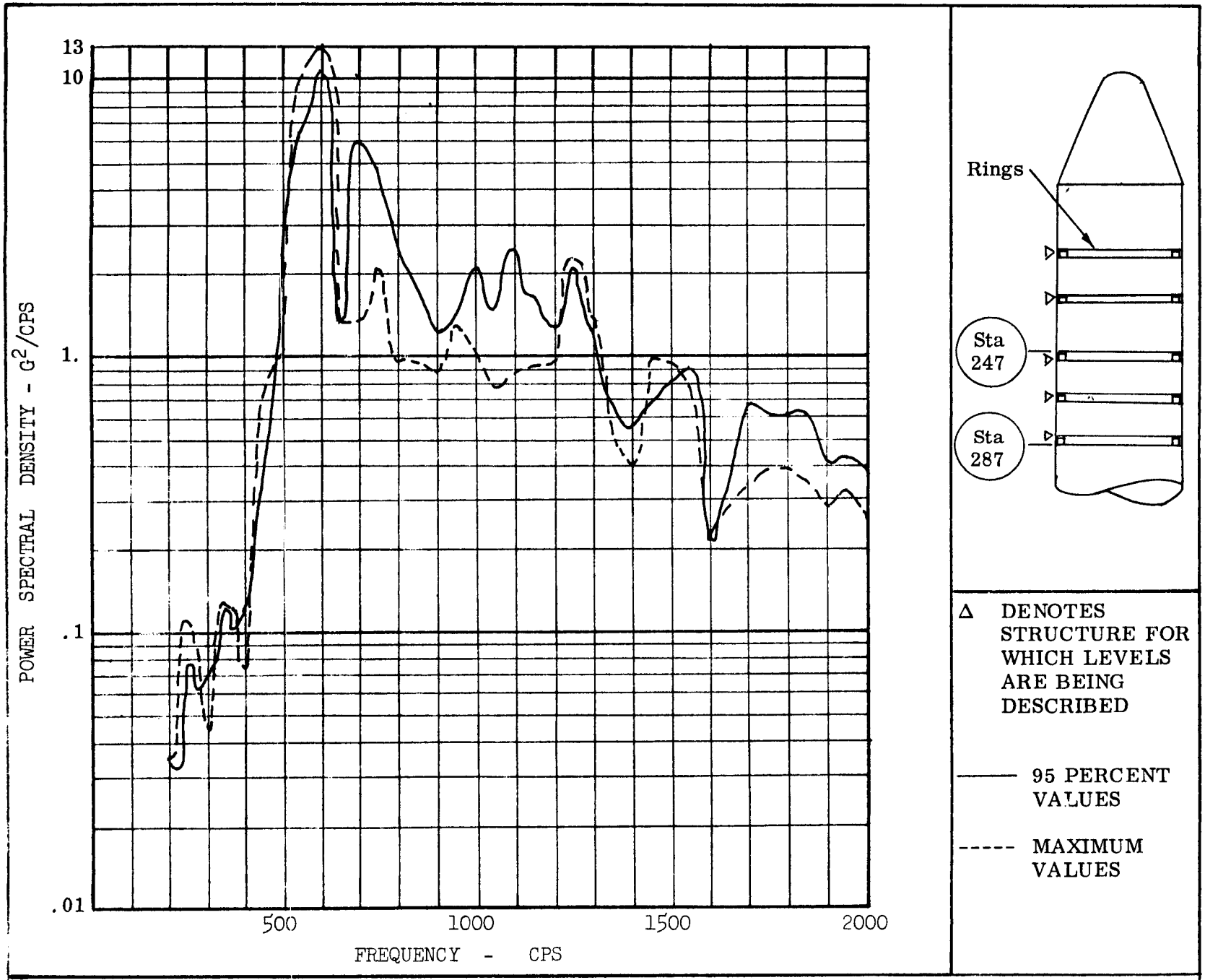

FIG. 47 95 PERCENT AND MAXIMUM VIBRATION FOR PS AND FER OUTER STRUCTURE, TAT LAUNCH FROM "DRY" PAD

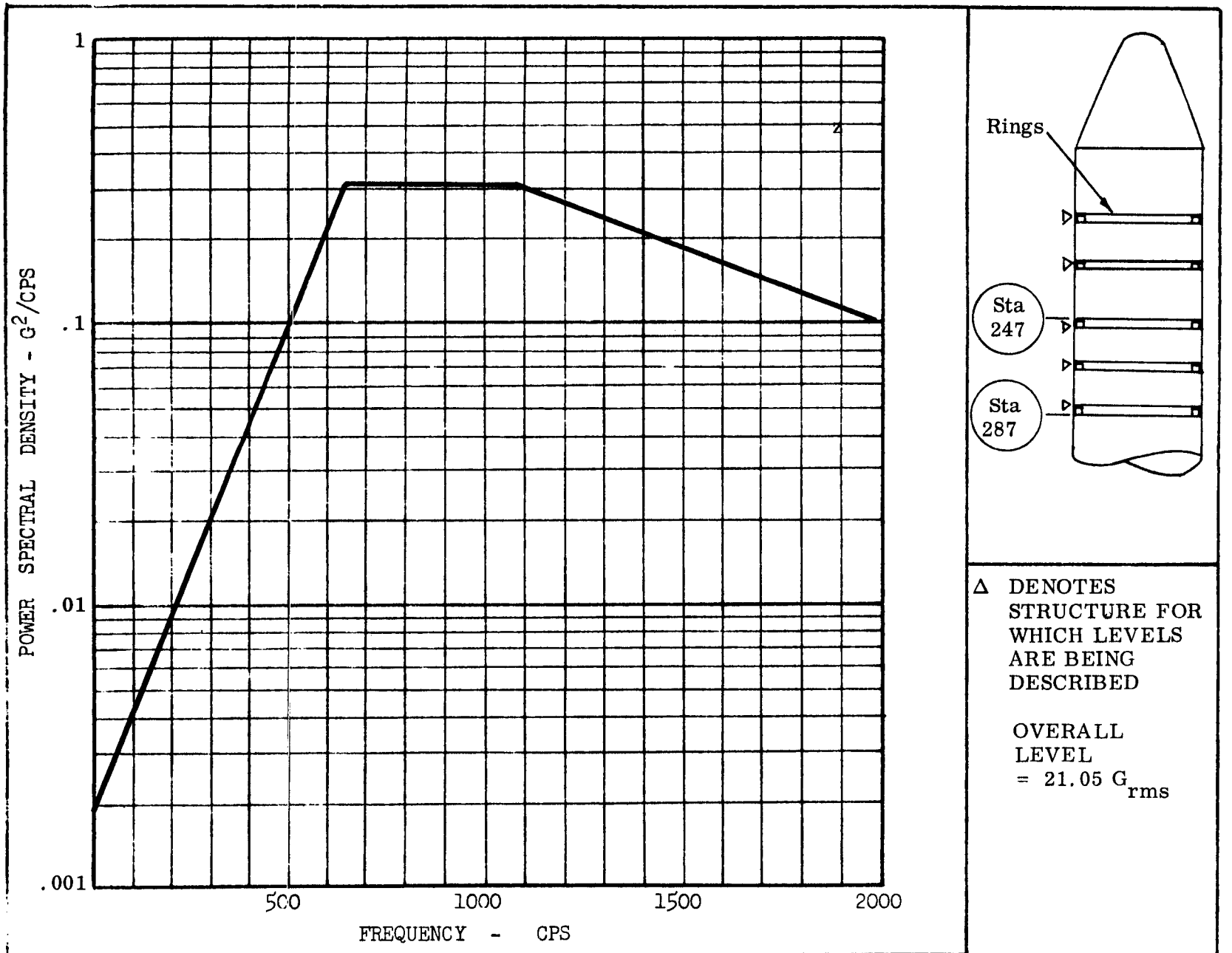

FIG. 48 BACKGROUND VIBRATION FOR PS AND FER OUTER STRUCTURE, TAT LAUNCH FROM "DRY" PAD

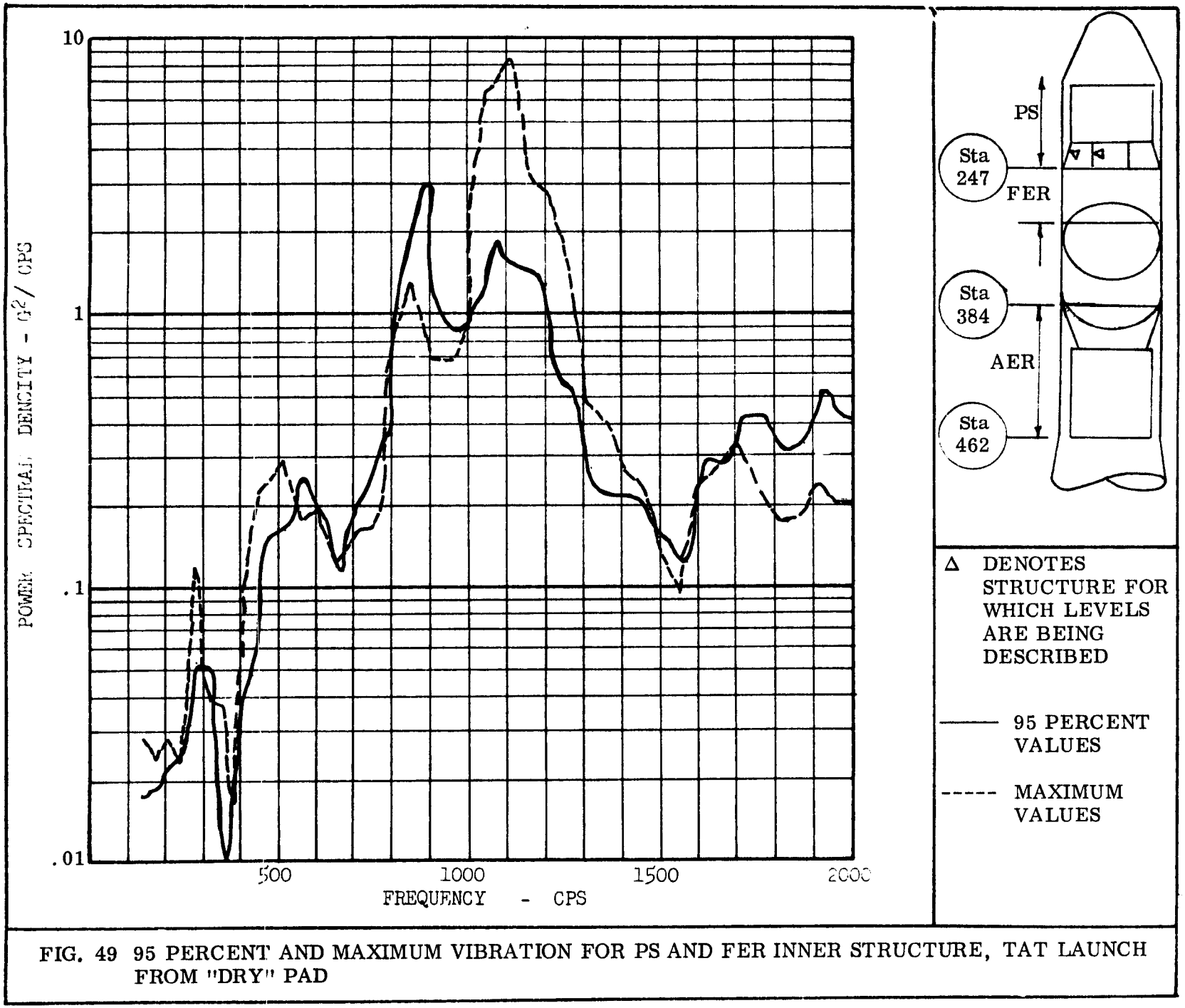

FIG. 49 95 PERCENT AND MAXIMUM VIBRATION FOR PS AND FER INNER STRUCTURE, TAT LAUNCH FROM "DRY" PAD

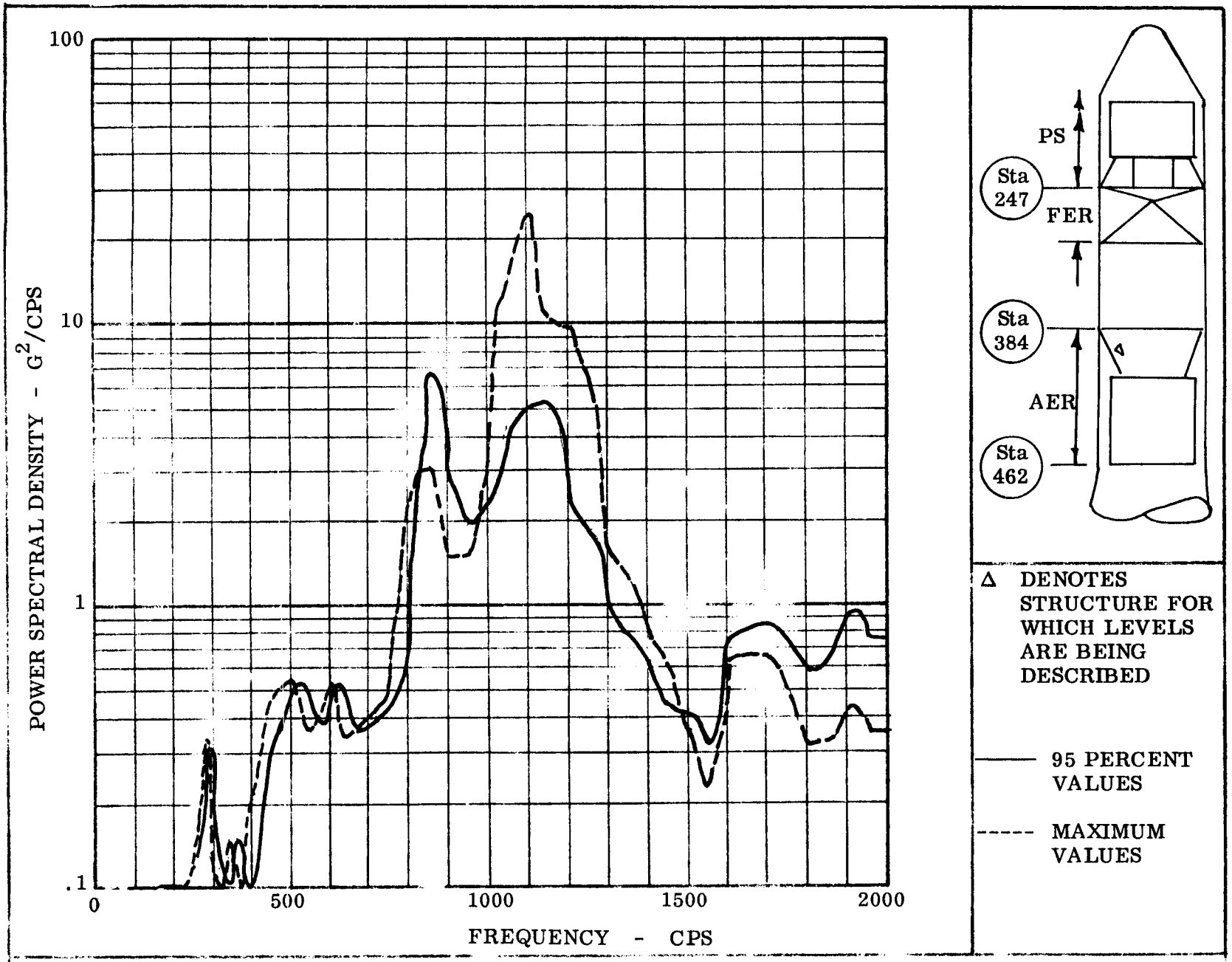

FIG. 50 95 PERCENT AND MAXIMUM VIBRATION FOR AER INNER STRUCTURE, TAT LAUNCH FROM "DRY" PAD

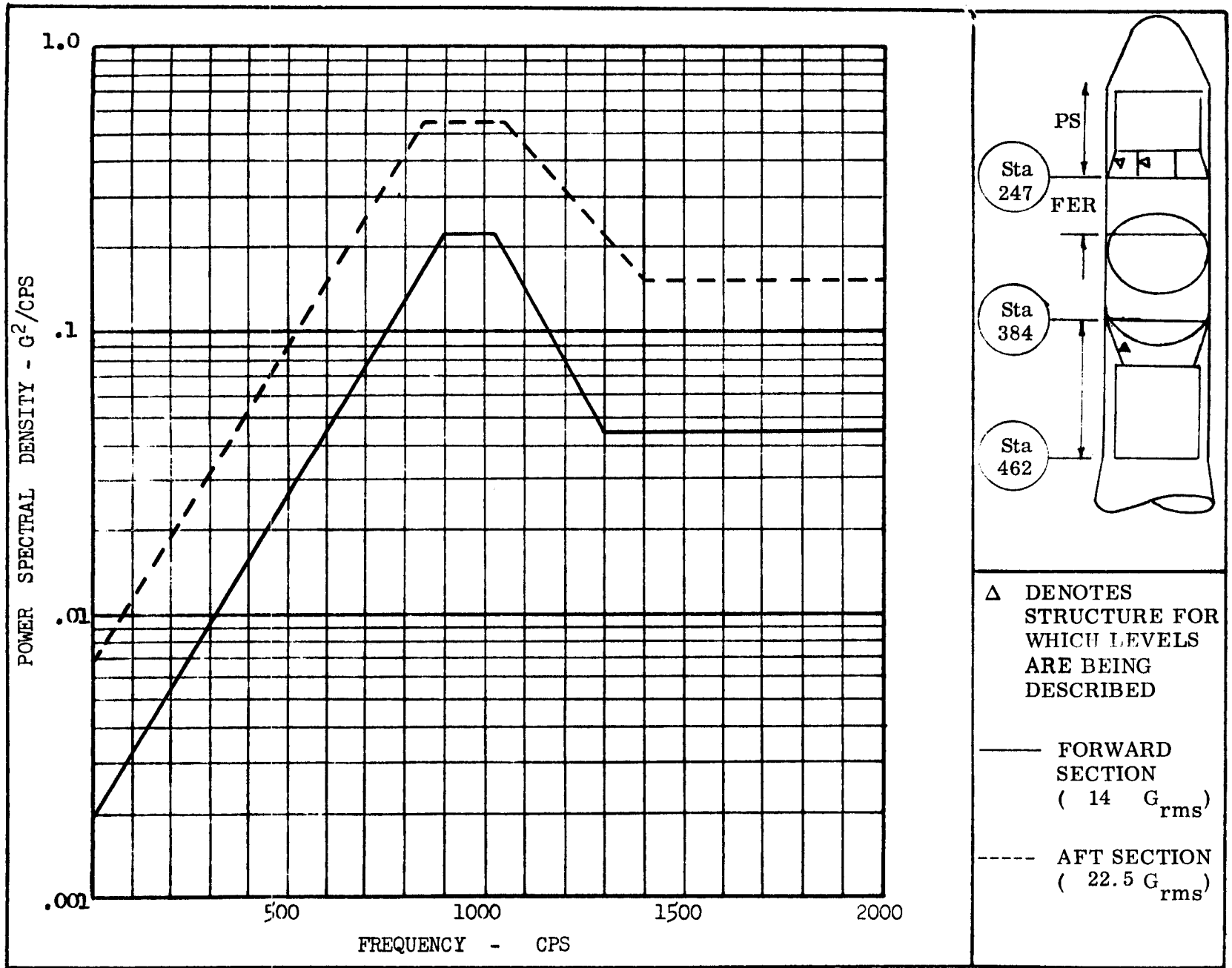

FIG. 51 BACKGROUND VIBRATION FOR PS, FER, AND AER INNER STRUCTURE, TAT LAUNCH FROM "DRY" PAD

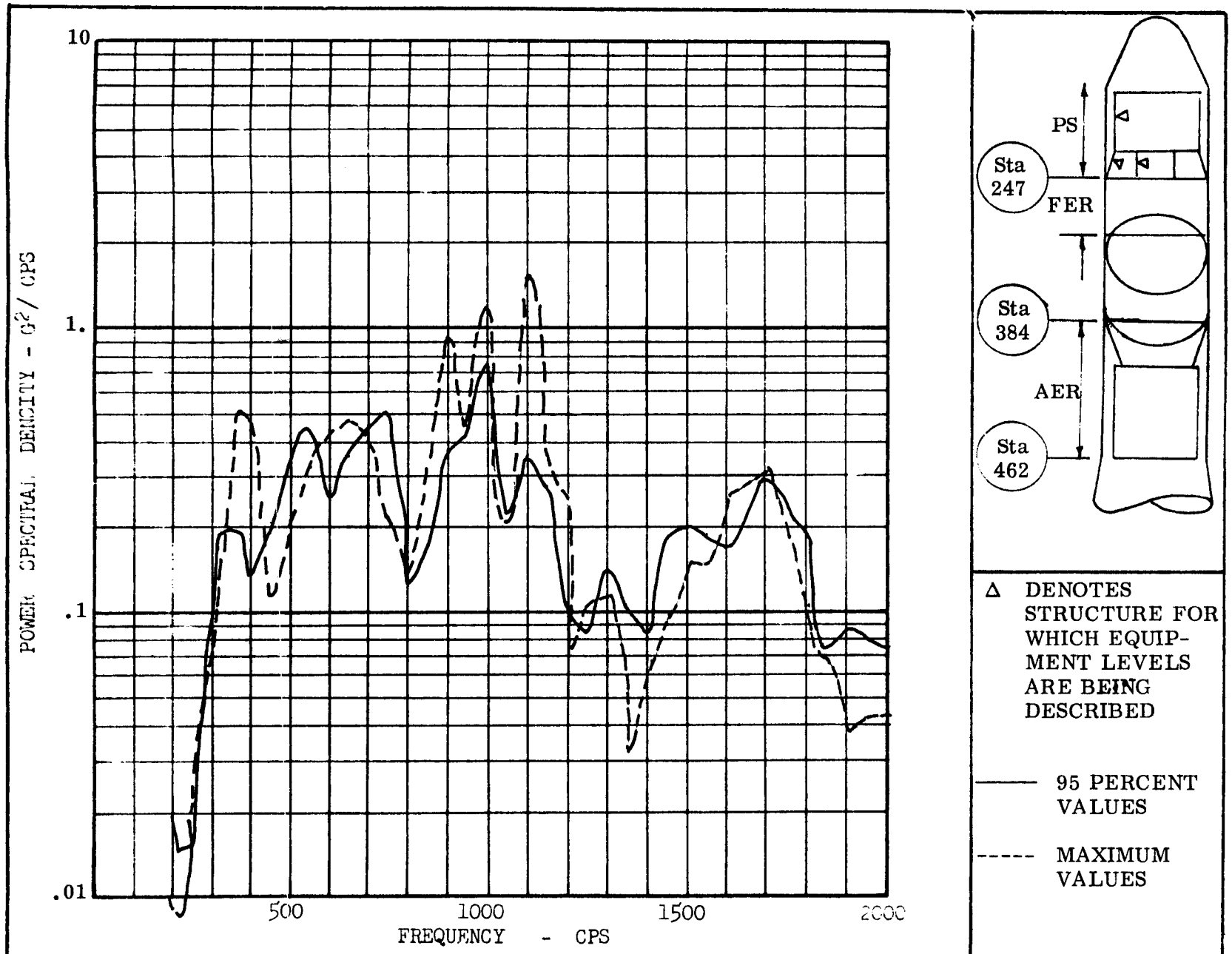

FIG. 52 95 PERCENT MAXIMUM VIBRATION FOR PS AND FER EQUIPMENT, TAT LAUNCH FROM "DRY" PAD

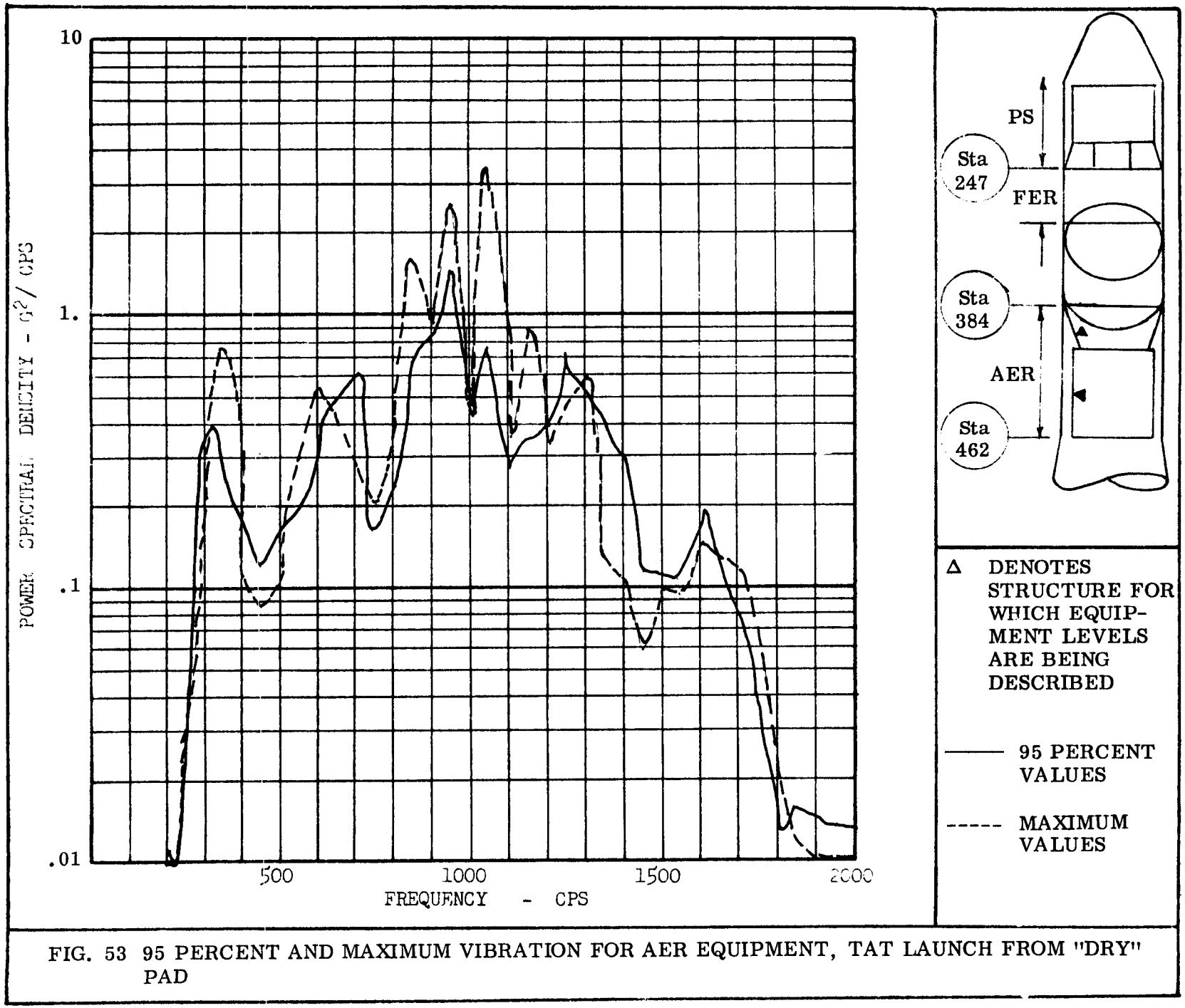

FIG. 53 95 PERCENT AND MAXIMUM VIBRATION FOR AER EQUIPMENT, TAT LAUNCH FROM "DRY" PAD

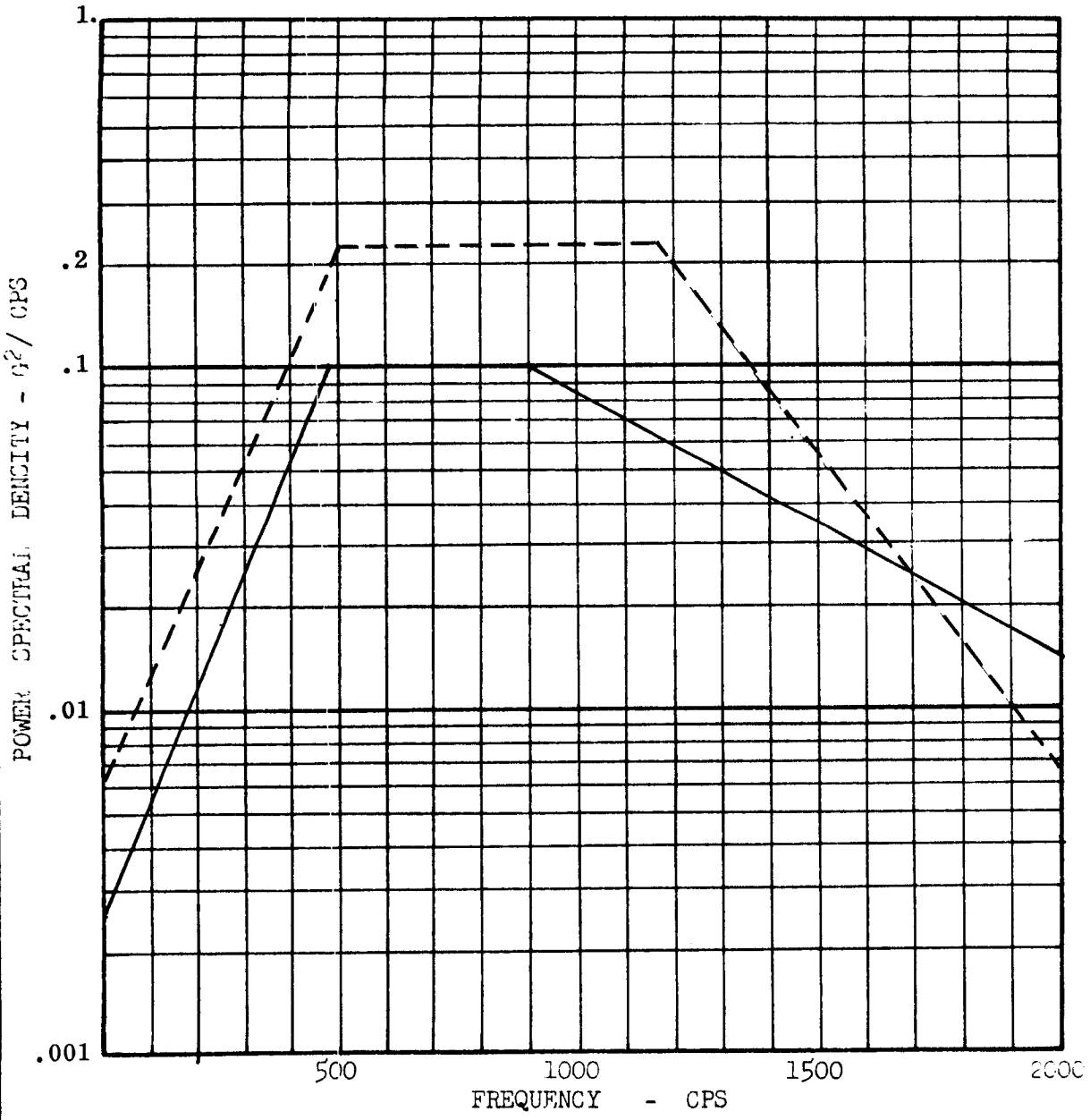

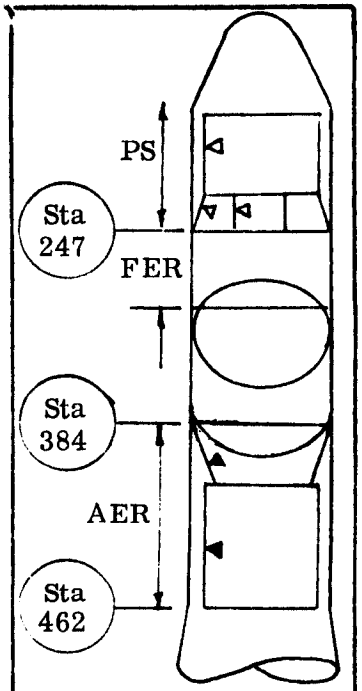

Δ DENOTES STRUCTURE FOR WHICH EQUIPMENT LEVELS ARE BEING DESCRIBED

——— FORWARD SECTION (11.85 G_{rms})

----- AFT SECTION (17.4 G_{rms})

FIG. 54 BACKGROUND VIBRATION FOR PS, FER AND AER EQUIPMENT TAT LAUNCH FROM "DRY" PAD

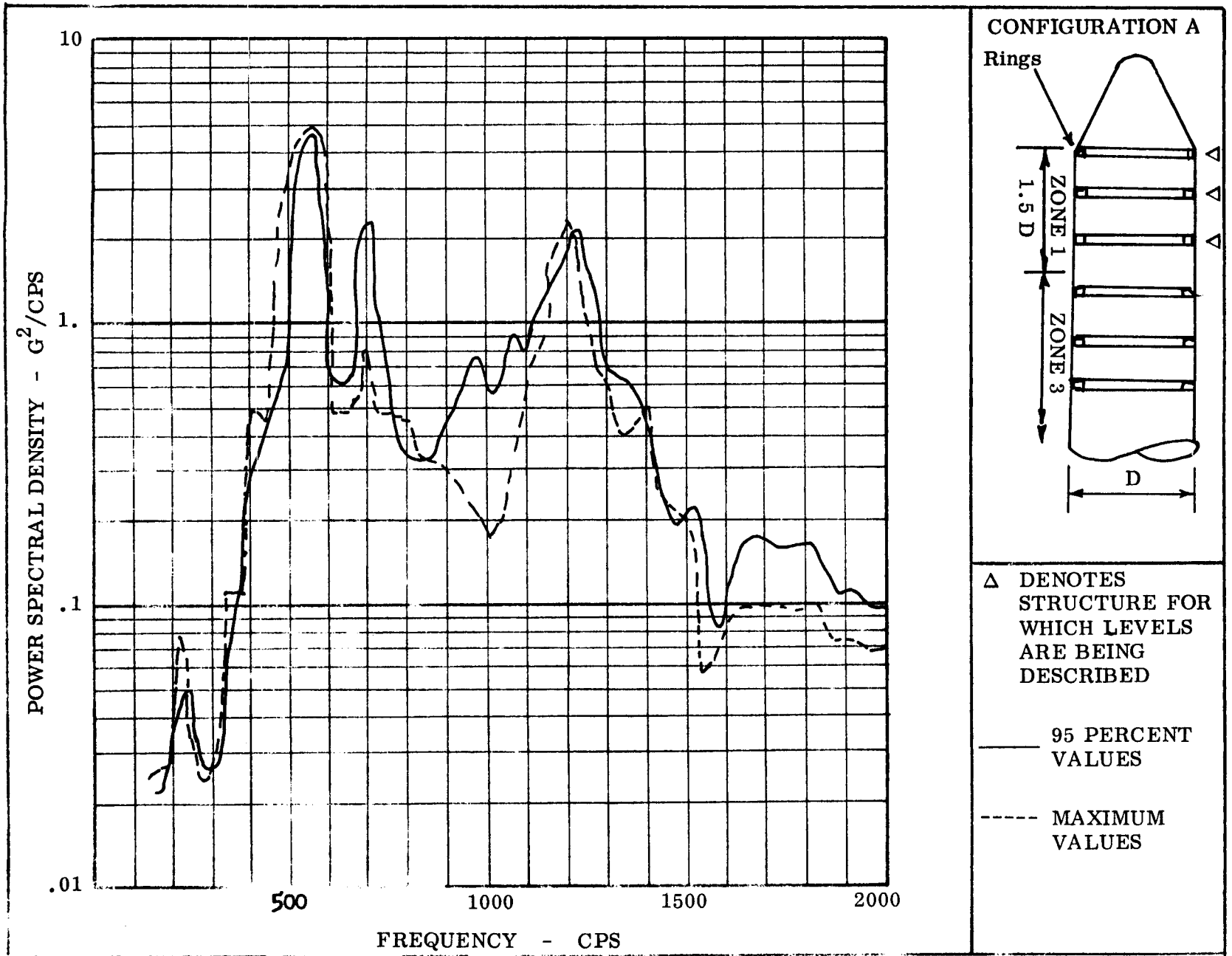

FIG. 55 95 PERCENT AND MAXIMUM PSD VALUES IN OUTER STRUCTURE - ATLAS AND THOR TRANSONIC FLIGHT, CONFIGURATION A, ZONE 1

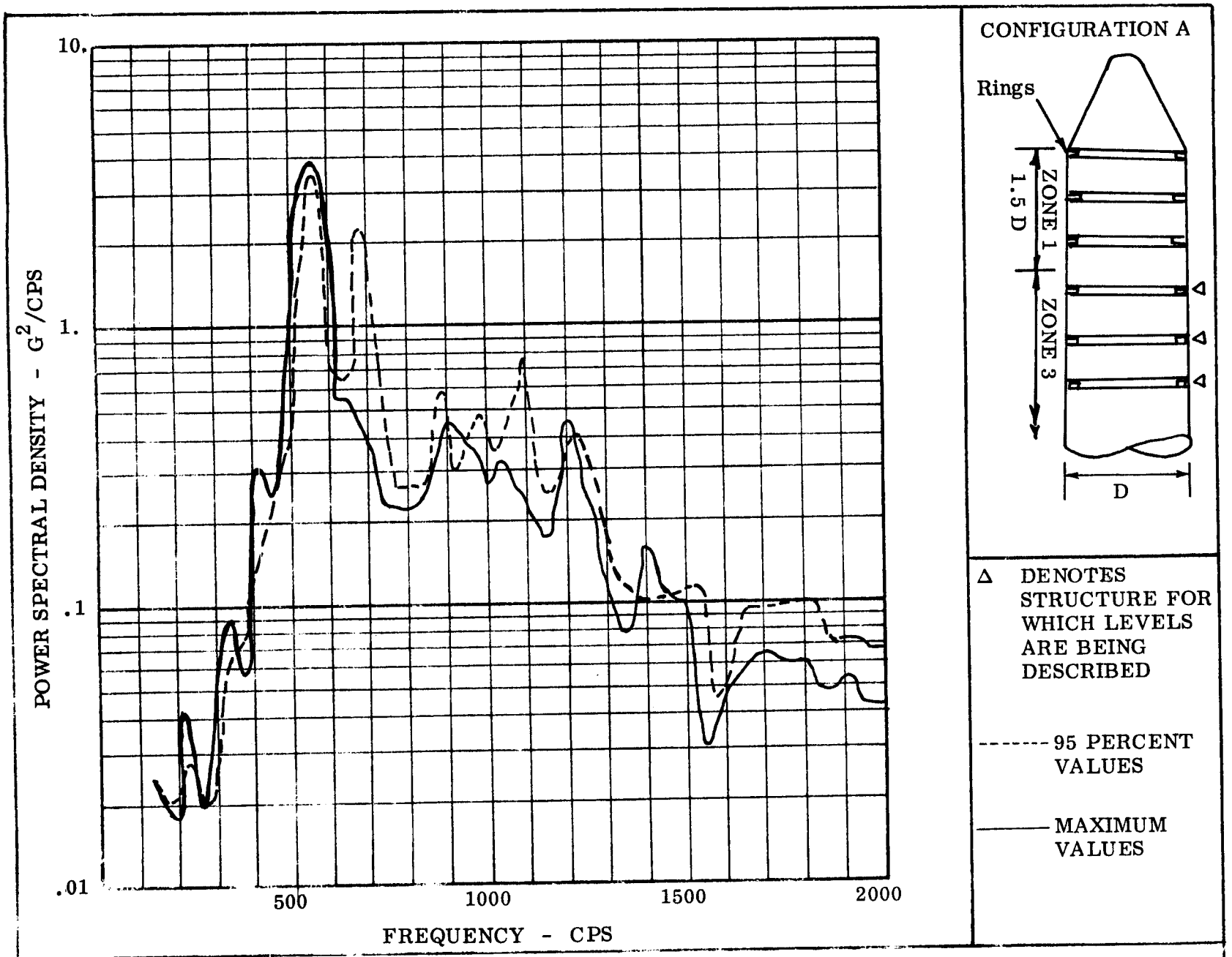

FIG. 56 95 PERCENT AND MAXIMUM PSD VALUES IN OUTER STRUCTURE - ATLAS AND THOR TRANSONIC FLIGHT, CONFIGURATION A, ZONE 3

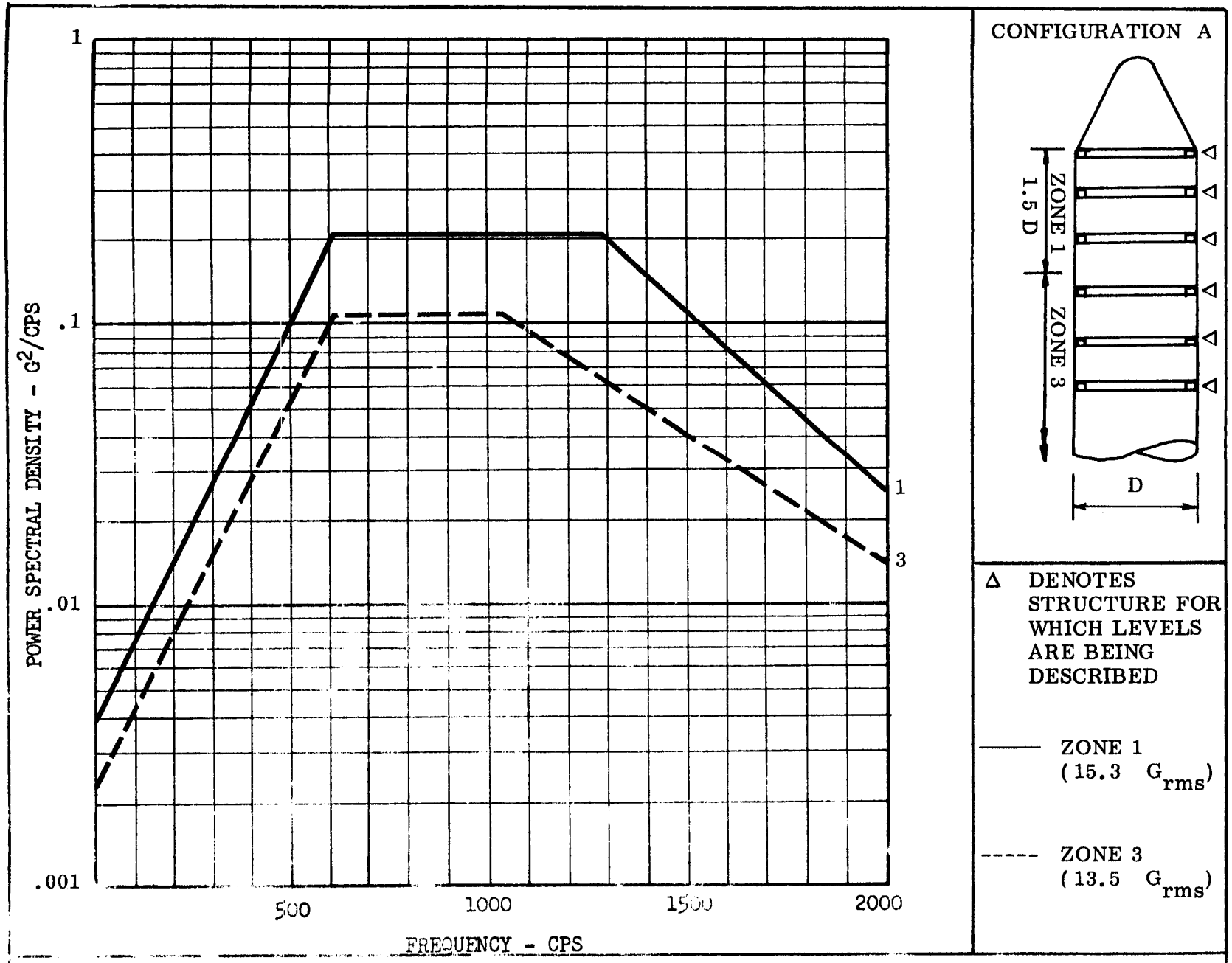

FIG. 57 BACKGROUND VIBRATION IN OUTER STRUCTURE - ATLAS AND THOR TRANSONIC FLIGHT, CONFIGURATION A, ZONES 1 AND 3

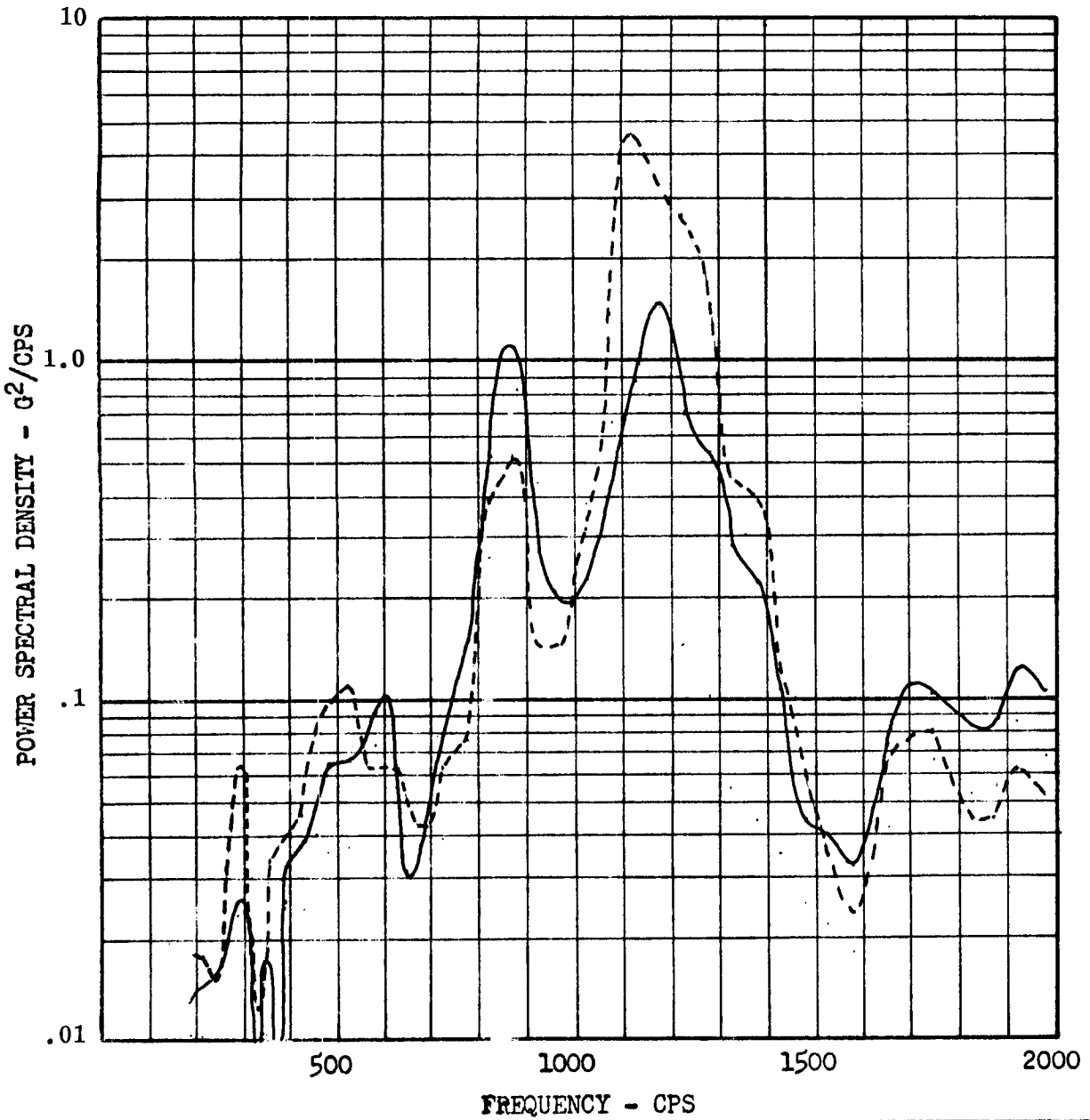

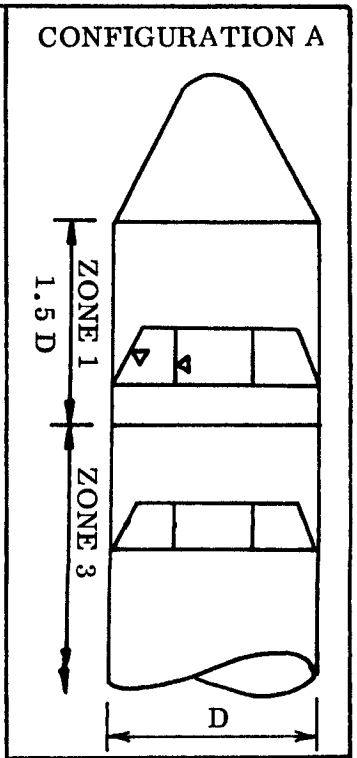

Δ DENOTES STRUCTURE FOR WHICH LEVELS ARE BEING DESCRIBED

——— 95 PERCENT VALUES

----- MAXIMUM VALUES

FIG. 58 95 PERCENT AND MAXIMUM PSD VALUES IN INNER STRUCTURE - ATLAS AND THOR TRANSONIC FLIGHT, CONFIGURATION A, ZONE 1

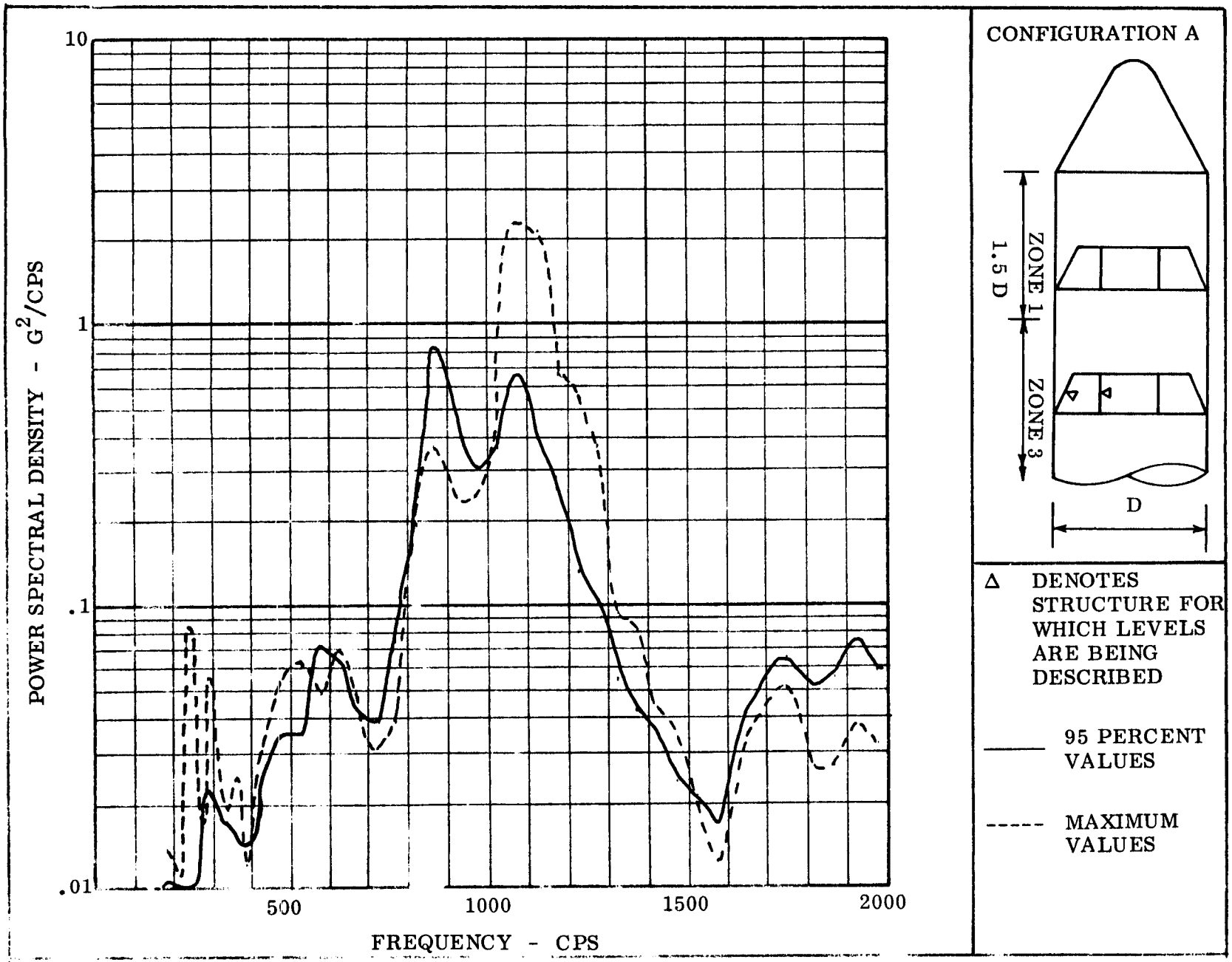

FIG. 59 95 PERCENT AND MAXIMUM PSD VALUES IN INNER STRUCTURE - ATLAS AND THOR TRANSONIC FLIGHT, CONFIGURATION A, ZONE 3

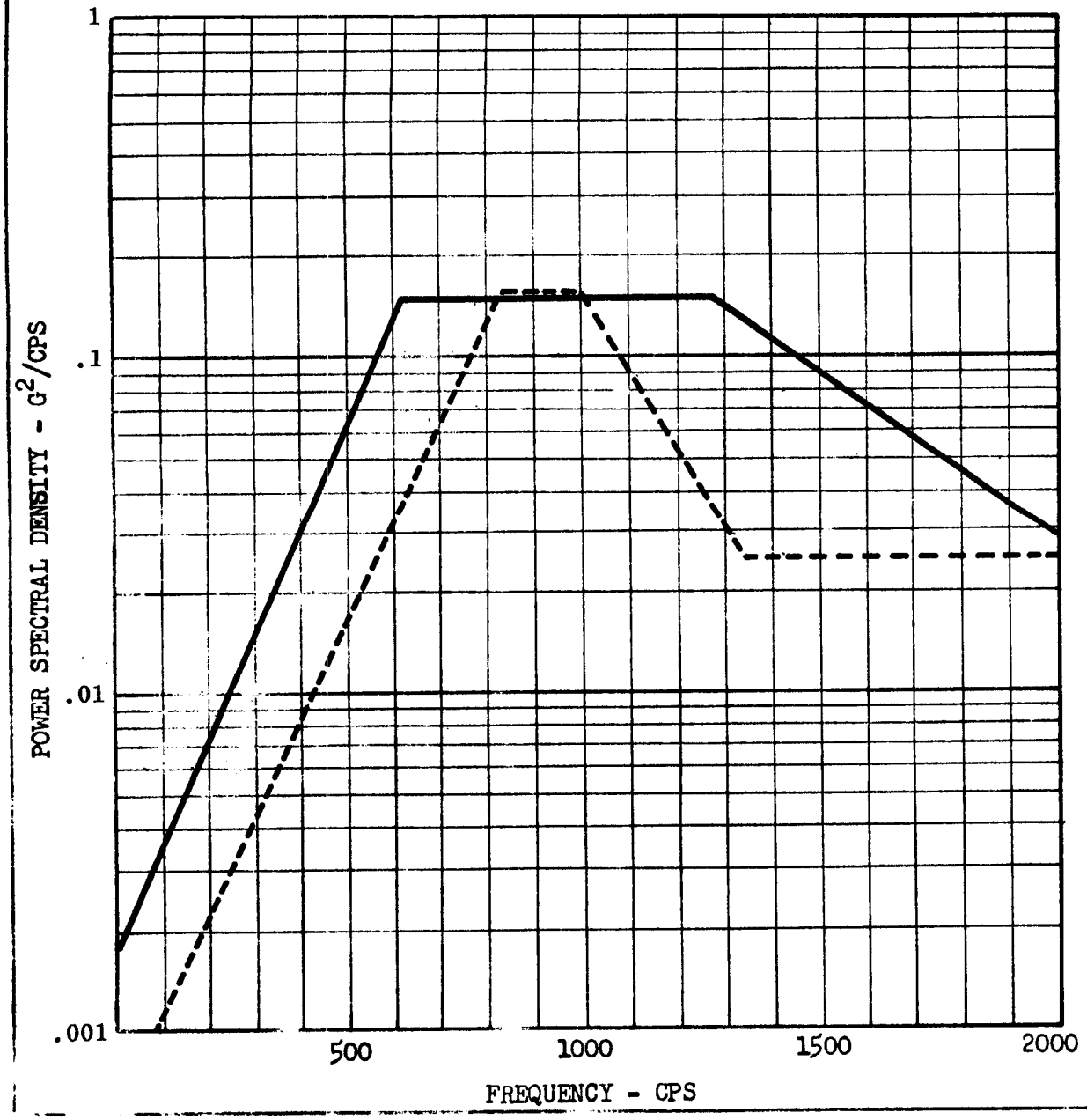

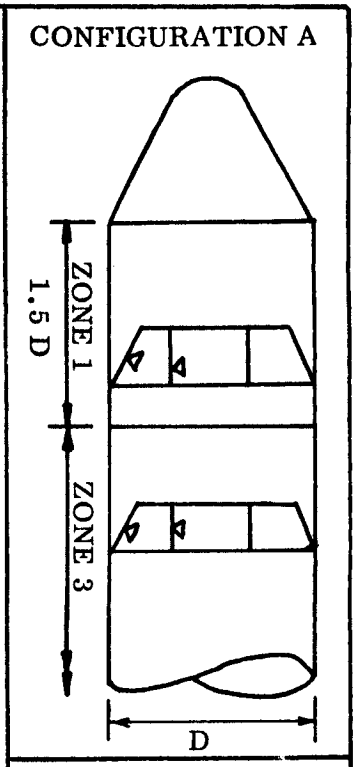

Δ DENOTES STRUCTURE FOR WHICH LEVELS ARE BEING DESCRIBED

——— ZONE 1 VALUES (13.6 G_{rms})

----- ZONE 3 VALUES (12 G_{rms})

FIG. 60 BACKGROUND VIBRATIONS IN INNER STRUCTURE - ATLAS AND THOR TRANSONIC FLIGHT, CONFIGURATION A, ZONES 1 AND 3

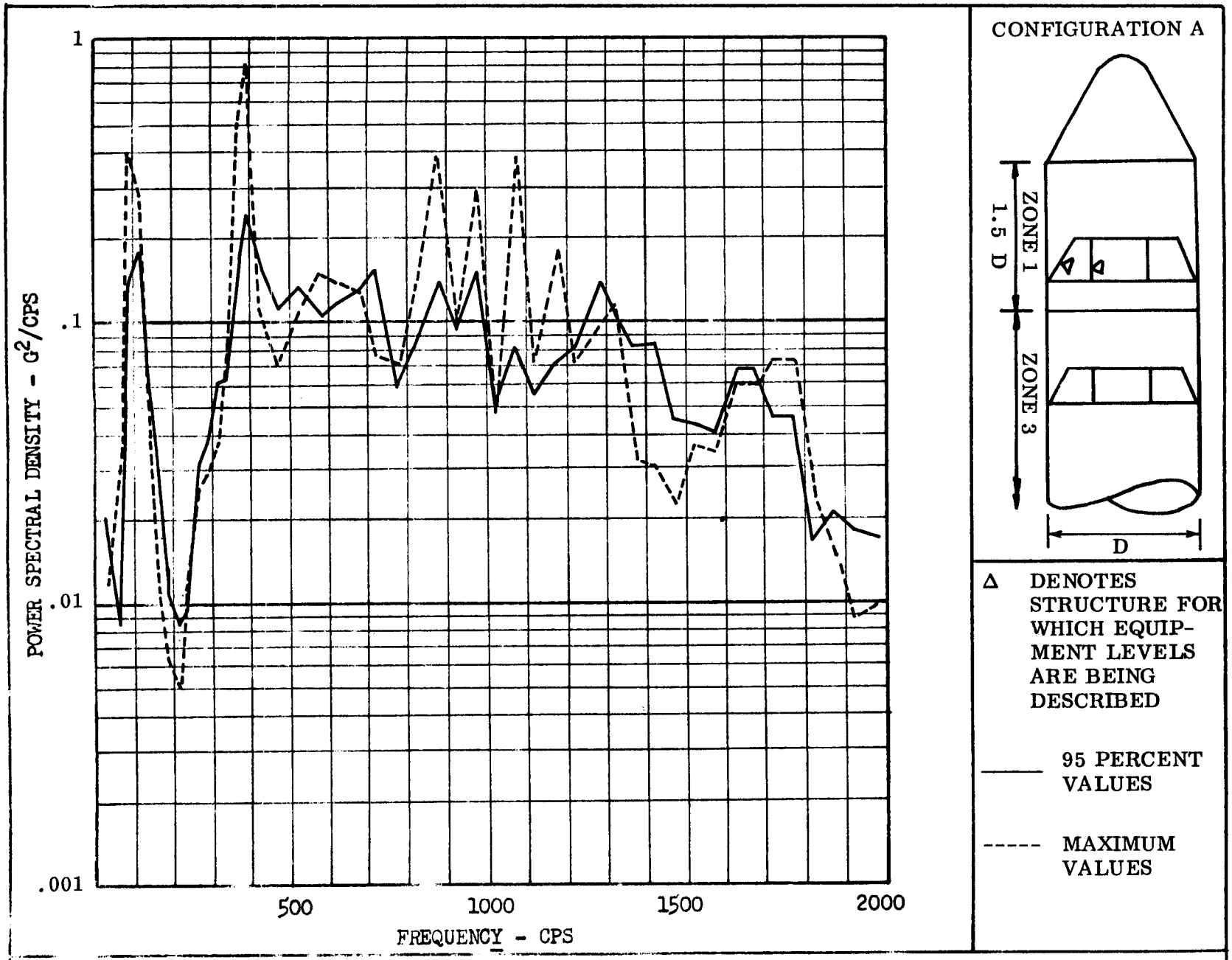

FIGURE 61 95 PERCENT AND MAXIMUM PSD VALUES FOR EQUIPMENT - ATLAS AND THOR TRANSONIC FLIGHT, CONFIGURATION A, ZONE 1

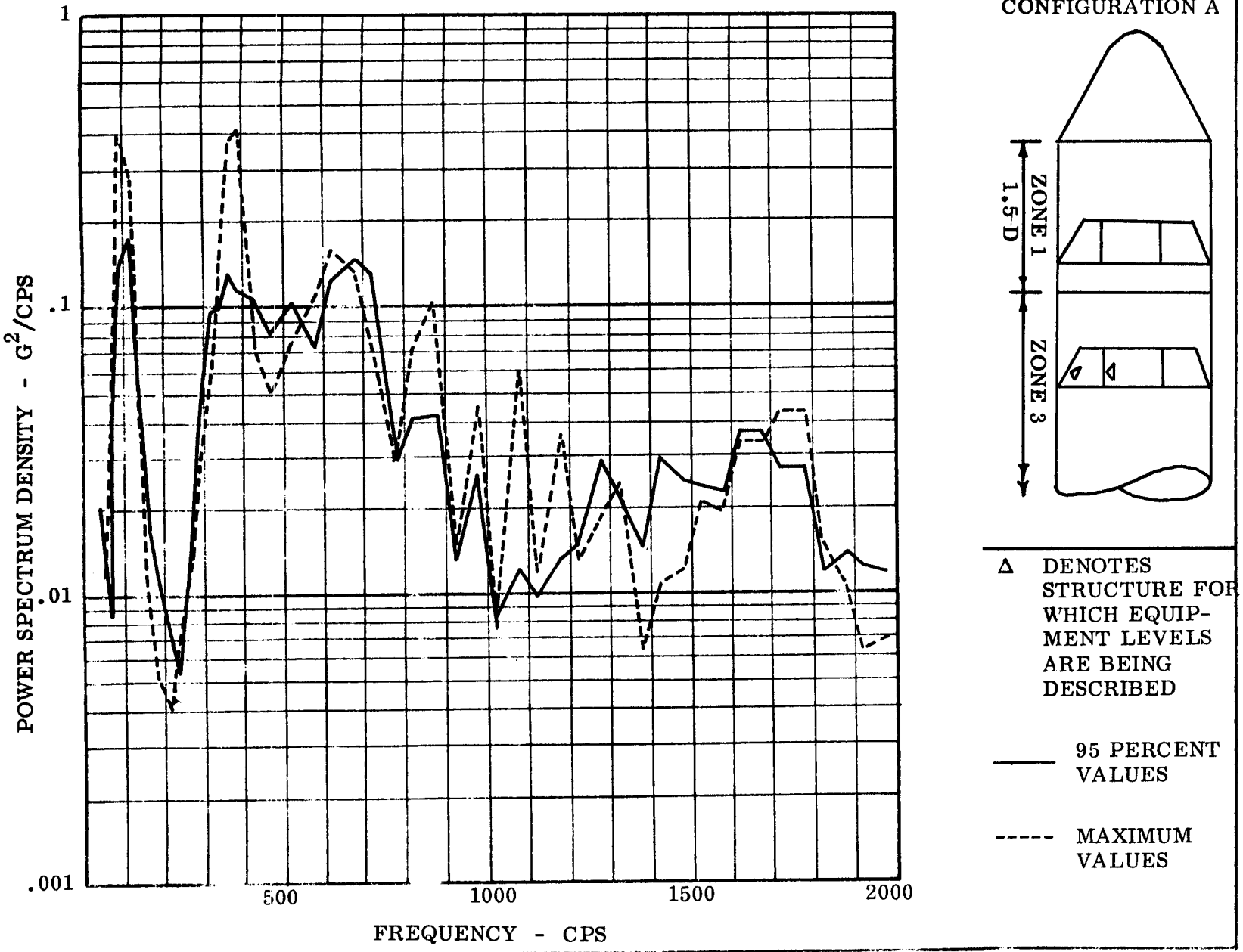

FIGURE 62 95 PERCENT AND MAXIMUM PSD VALUES FOR EQUIPMENT - ATLAS AND THOR TRANSONIC FLIGHT, CONFIGURATION A, ZONE 3

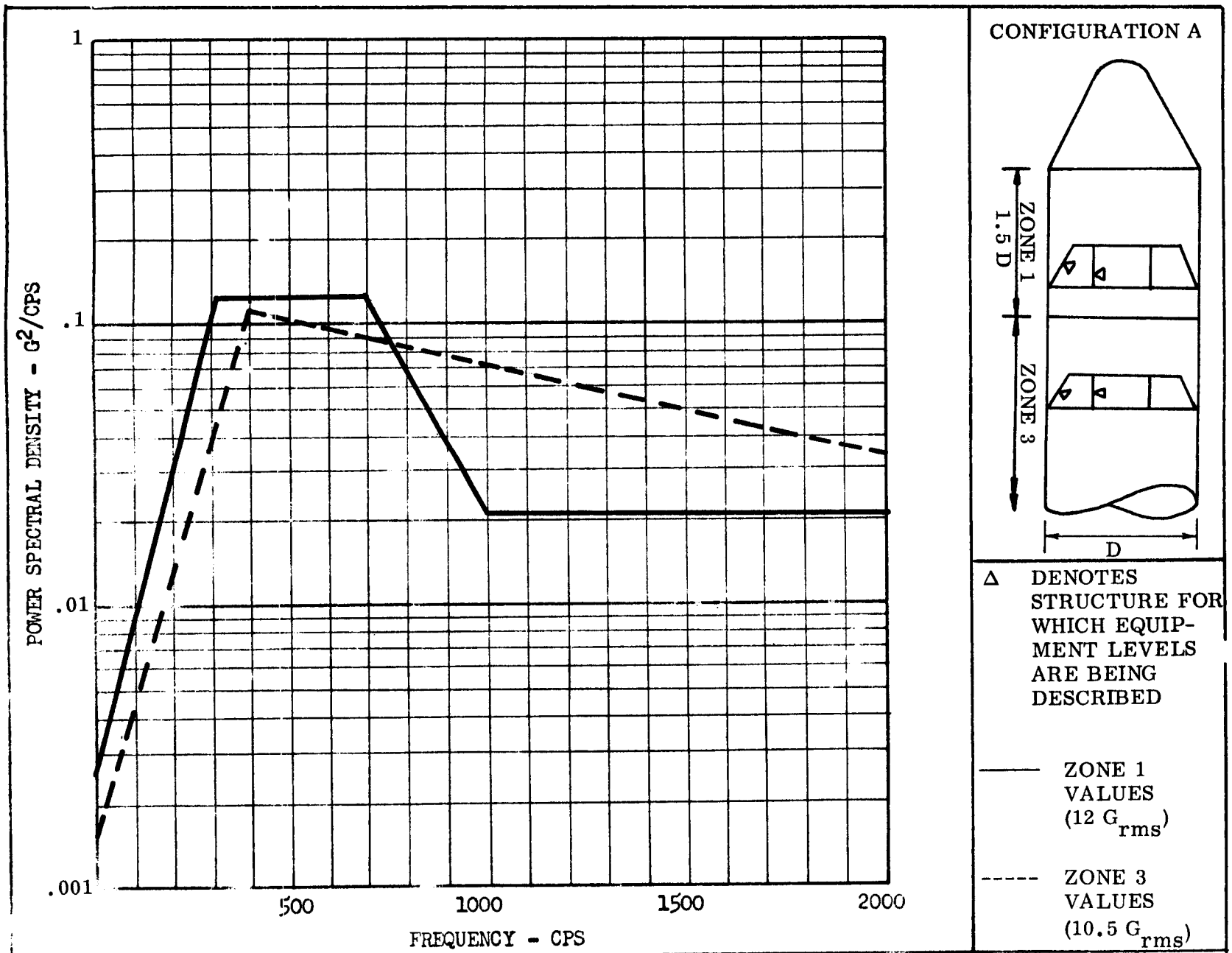

FIGURE 63 BACKGROUND VIBRATION FOR EQUIPMENT - ATLAS AND THOR TRANSONIC FLIGHT, CONFIGURATION A, ZONES 1 AND 3

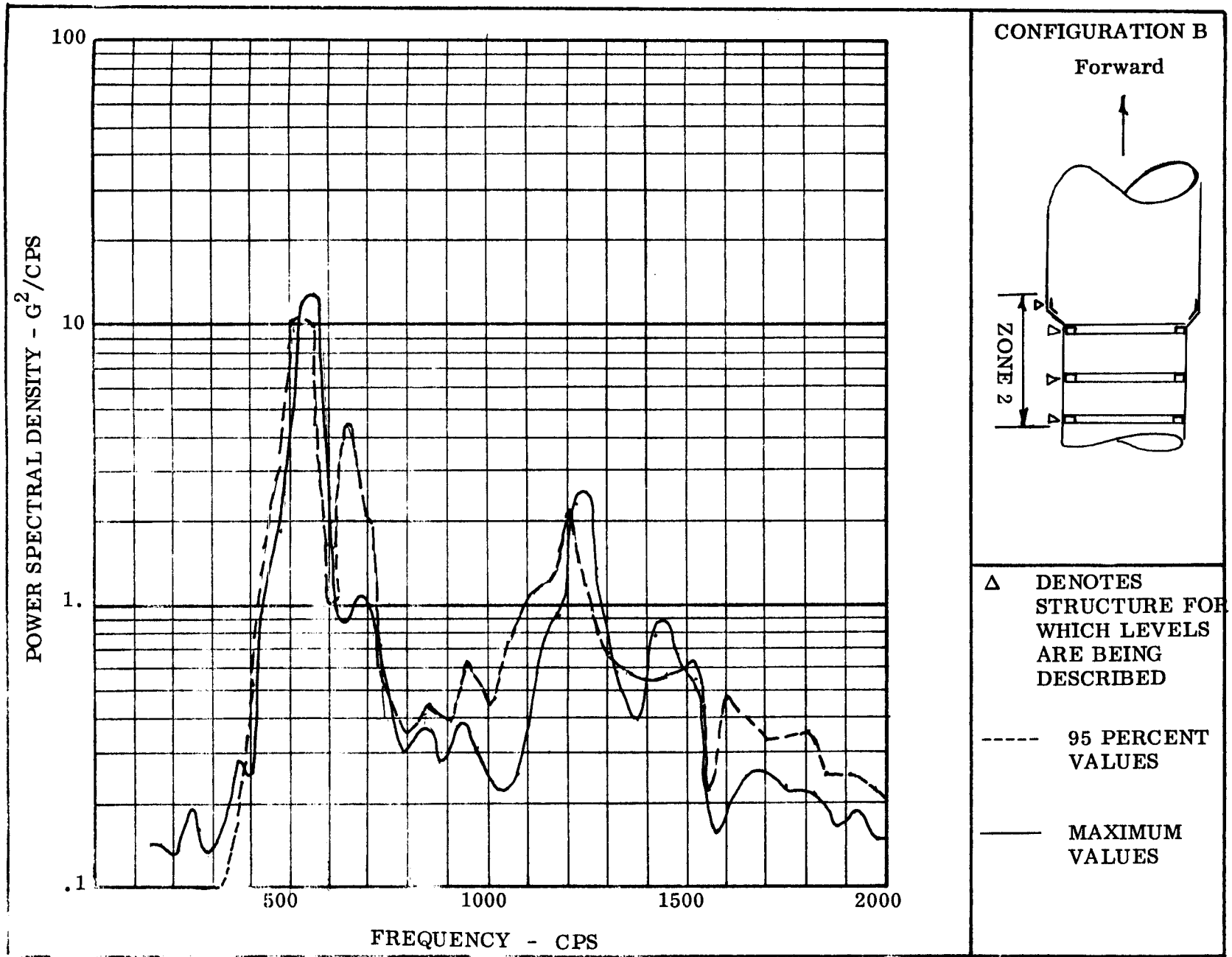

FIGURE 64 95 PERCENT AND MAXIMUM PSD VALUES FOR OUTER STRUCTURE - ATLAS AND THOR FLIGHT, CONFIGURATION B, ZONE 2

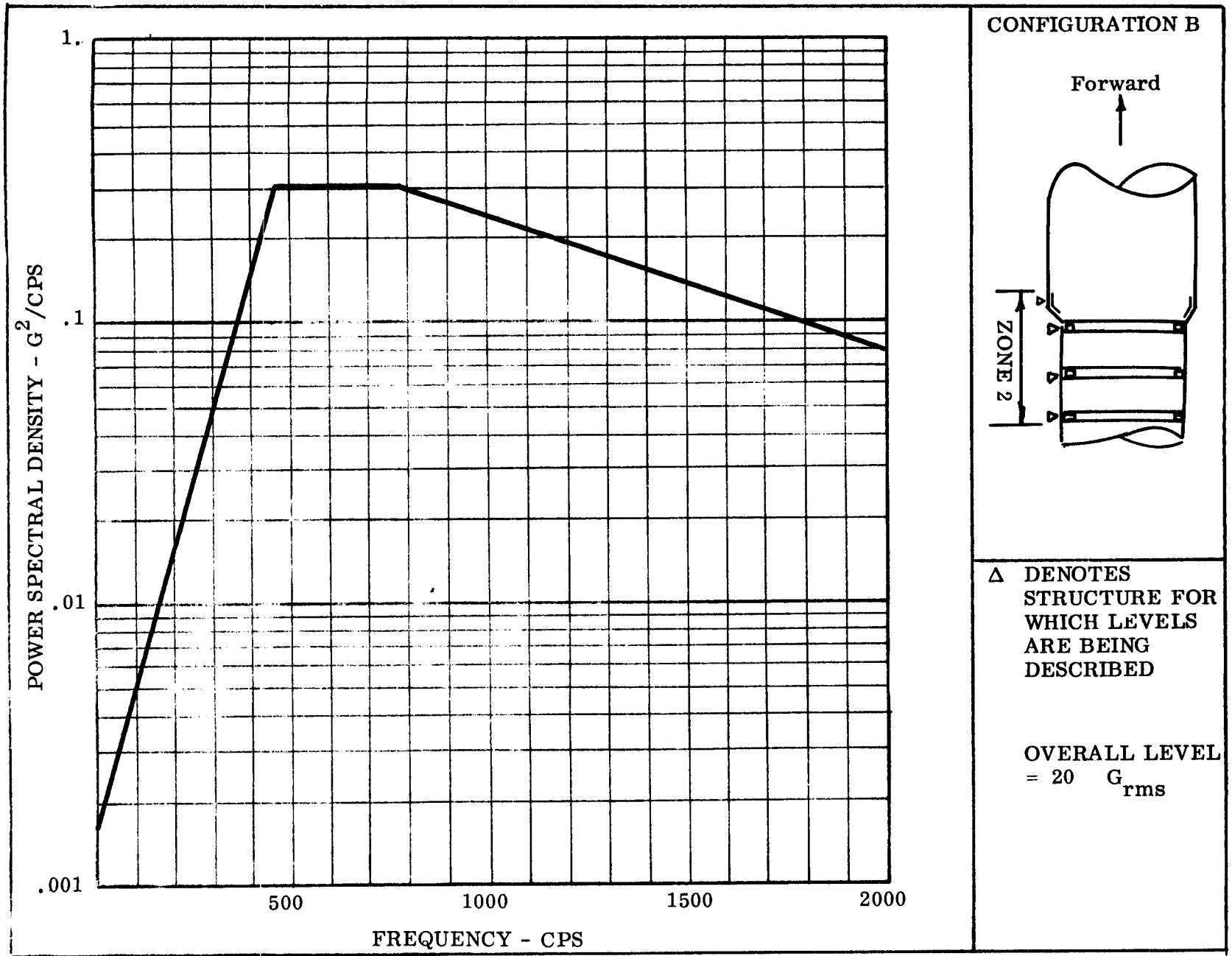

FIGURE 65 BACKGROUND VIBRATIONS FOR OUTER STRUCTURE - ATLAS AND THOR TRANSONIC FLIGHT, CONFIGURATION B, ZONE 2

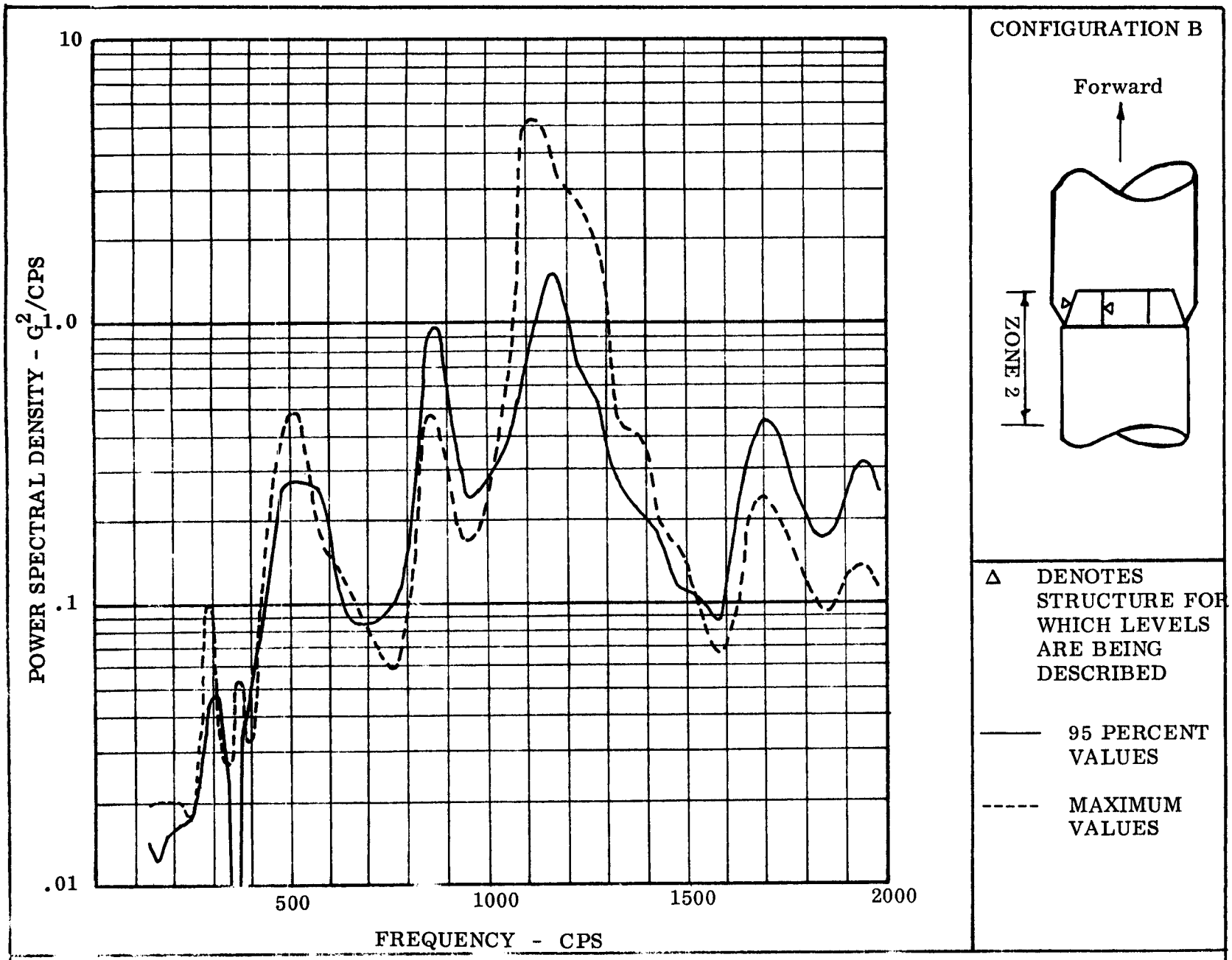

FIG. 66 95 PERCENT AND MAXIMUM PSD VALUES FOR INNER STRUCTURE, ATLAS AND THOR FLIGHT, CONFIGURATION B, ZONE 2

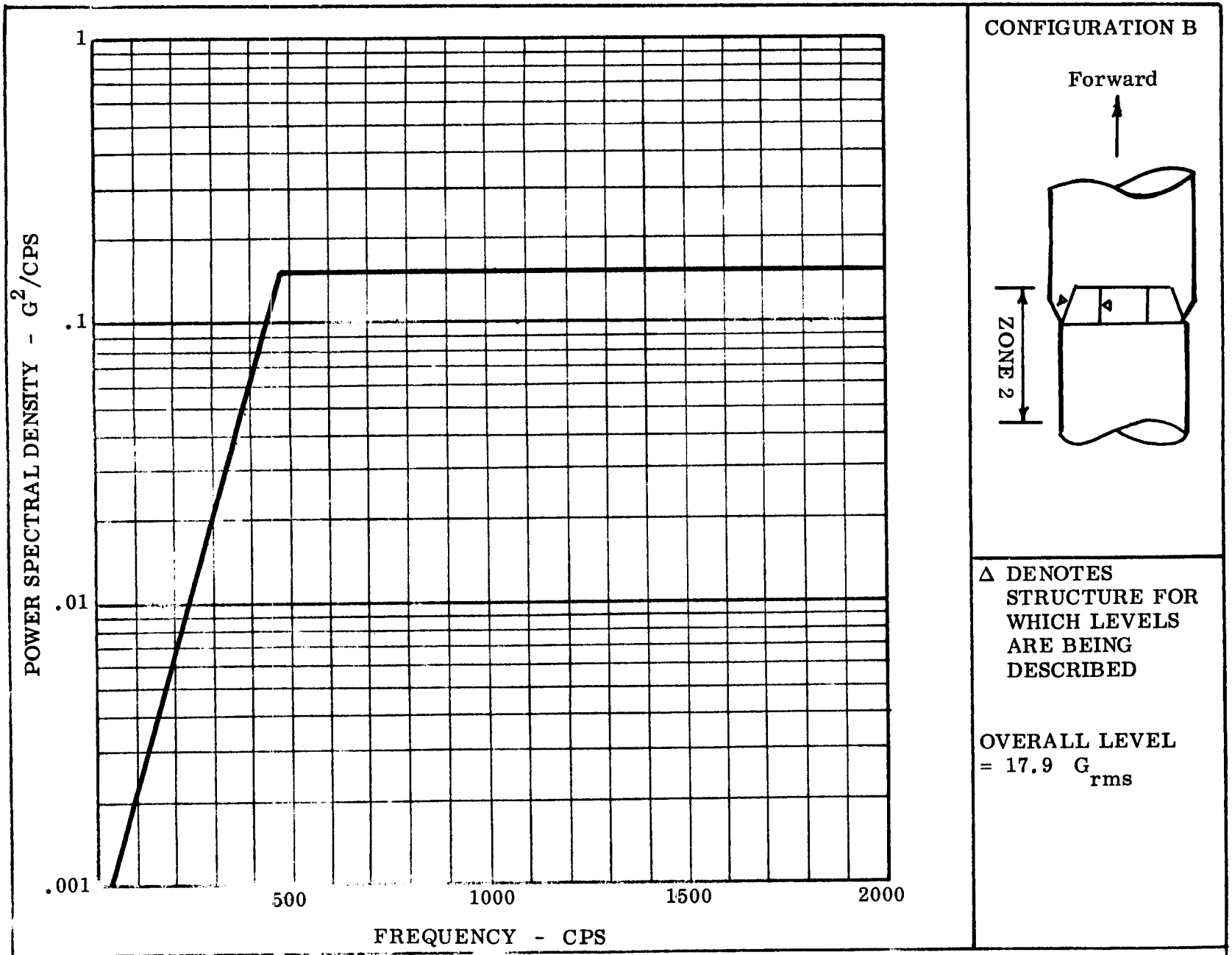

FIGURE 67 BACKGROUND VIBRATIONS FOR INNER STRUCTURE - ATLAS AND THOR FLIGHT CONFIGURATION B, ZONE 2

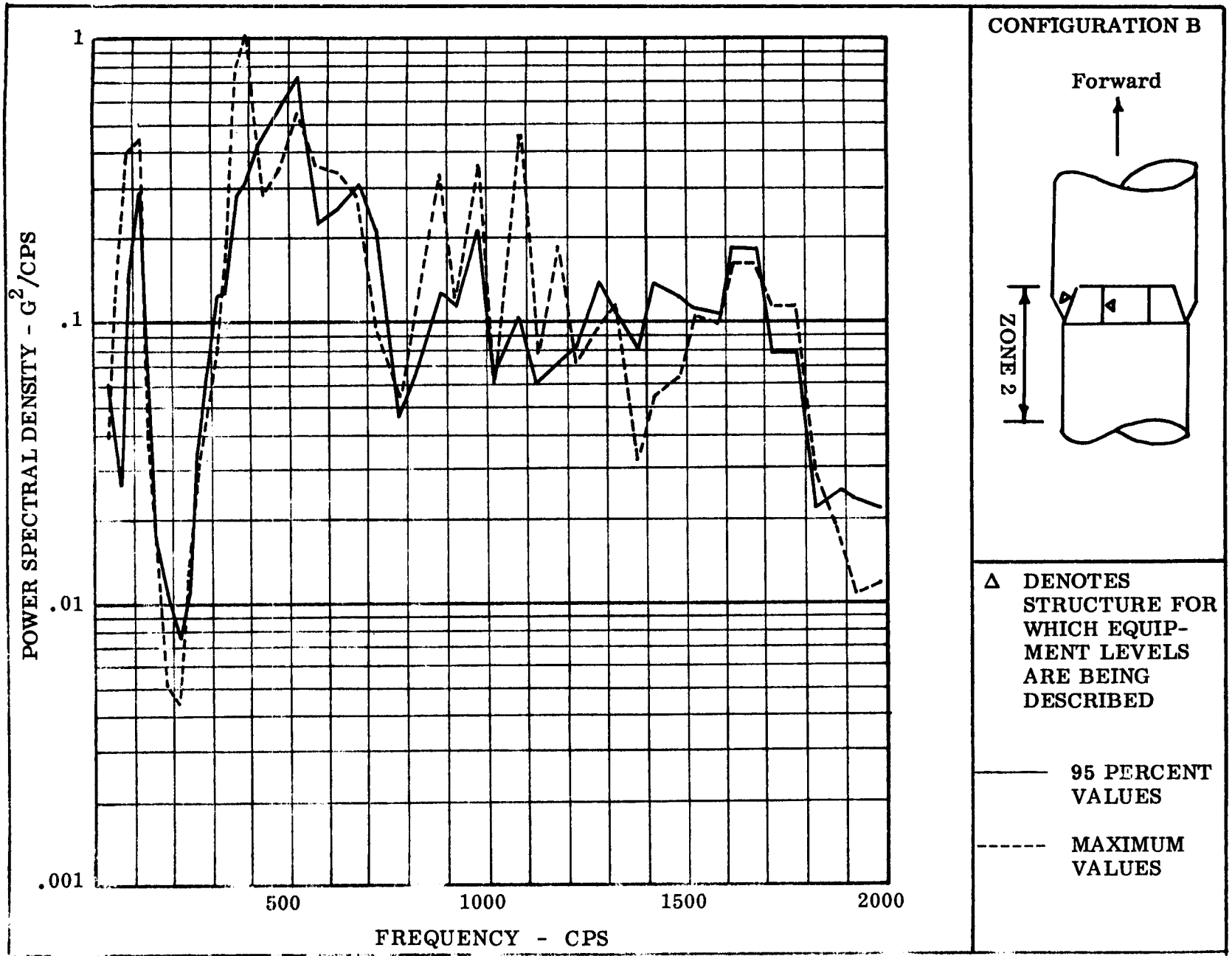

FIGURE 68 95 PERCENT AND MAXIMUM PSD VALUES FOR EQUIPMENT - ATLAS AND THOR FLIGHT, CONFIGURATION B, ZONE 2

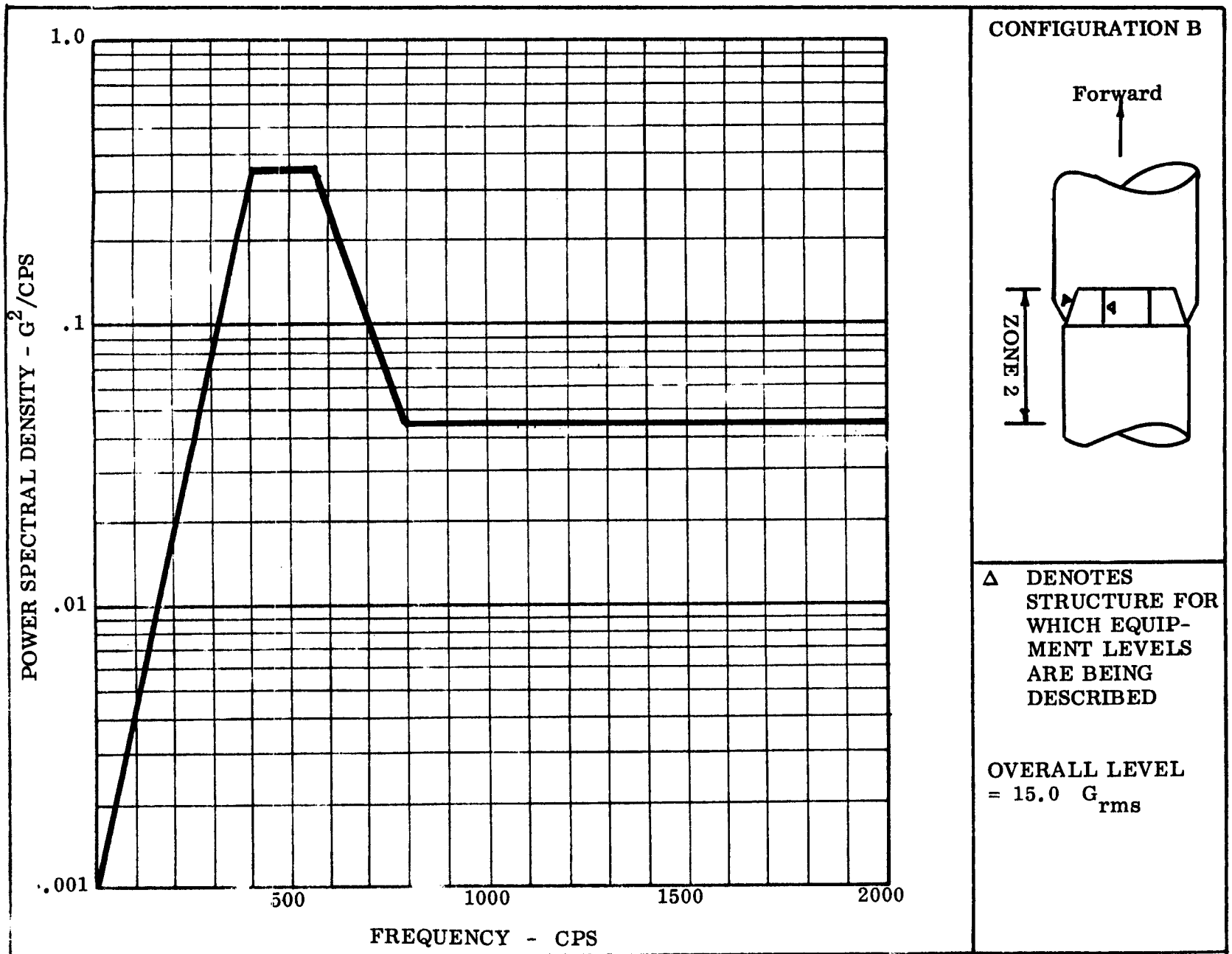

FIGURE 69 BACKGROUND VIBRATION FOR EQUIPMENT, ATLAS AND THOR FLIGHT CONFIGURATION B, ZONE 2

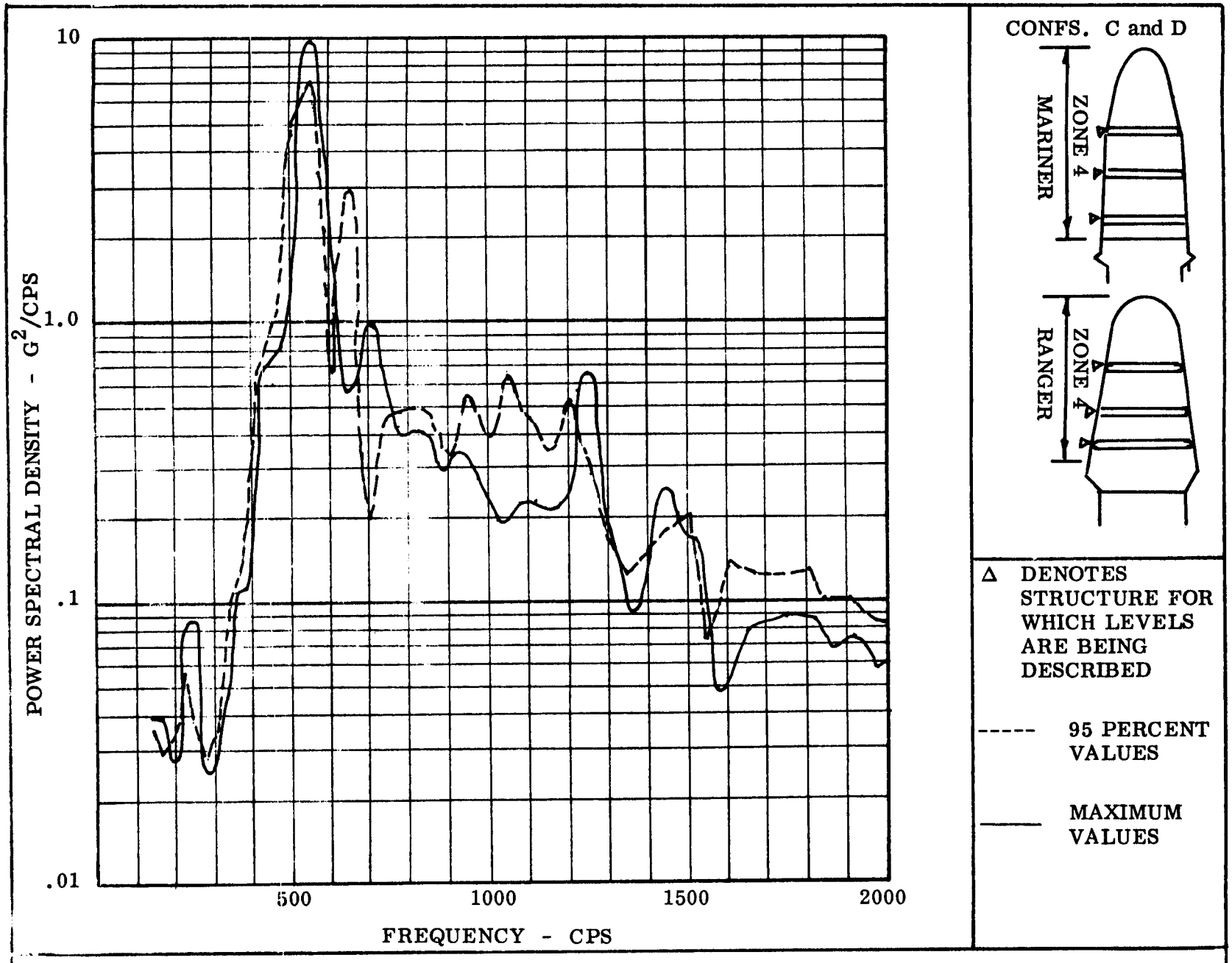

FIGURE 70 95 PERCENT AND MAXIMUM PSD VALUES FOR OUTER STRUCTURE - ATLAS AND THOR FLIGHT, CONFIGURATIONS C AND D, ZONE 4

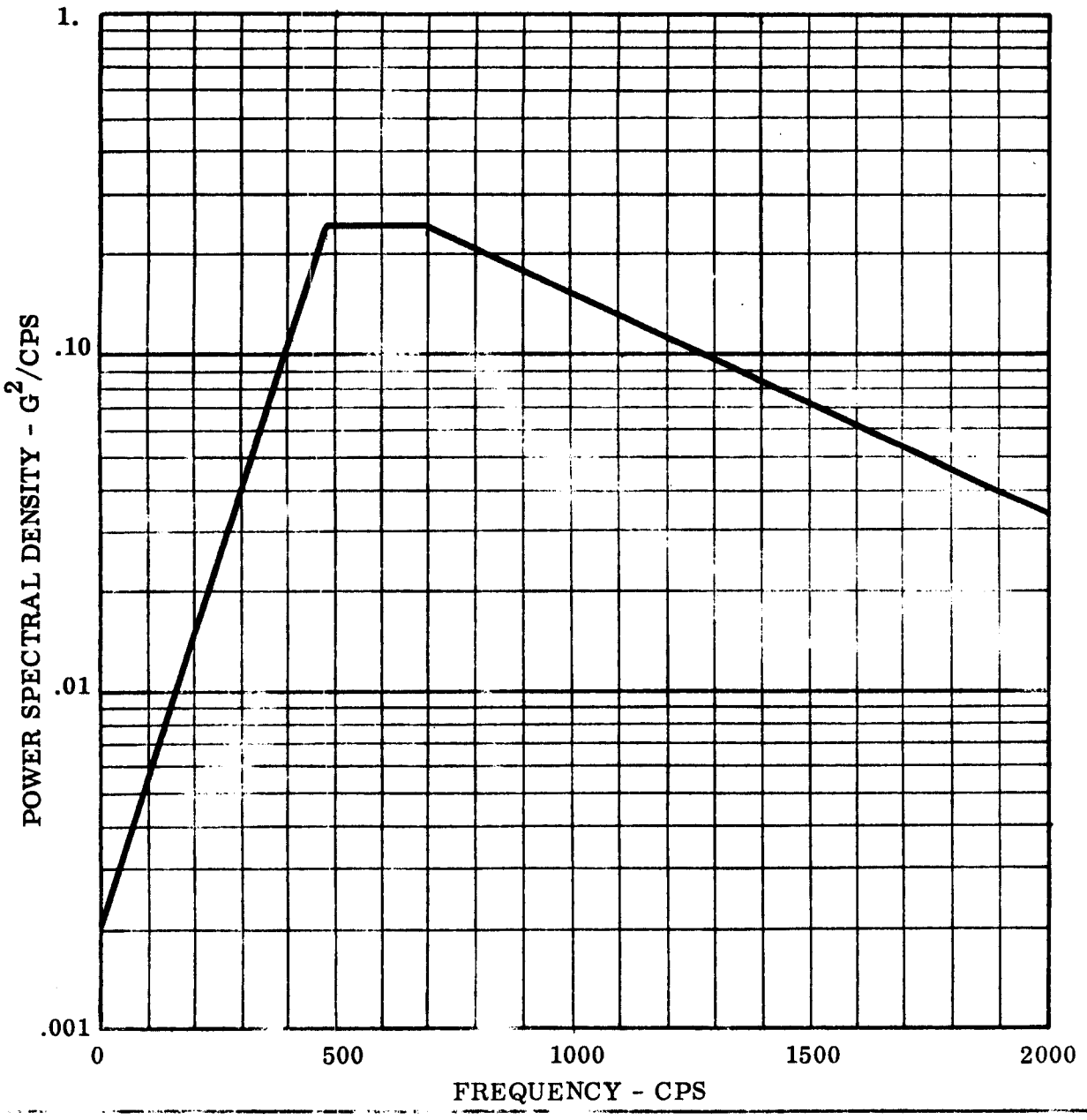

CONFS. C and D

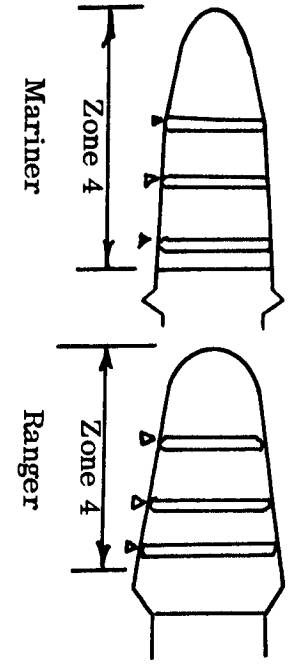

Δ – denotes structure for which levels are being described

Overall level = 17.0 G_{rms}

FIGURE 71 BACKGROUND VIBRATION FOR OUTER STRUCTURE – ATLAS AND THOR FLIGHT, CONFIGURATIONS C AND D, ZONE 4

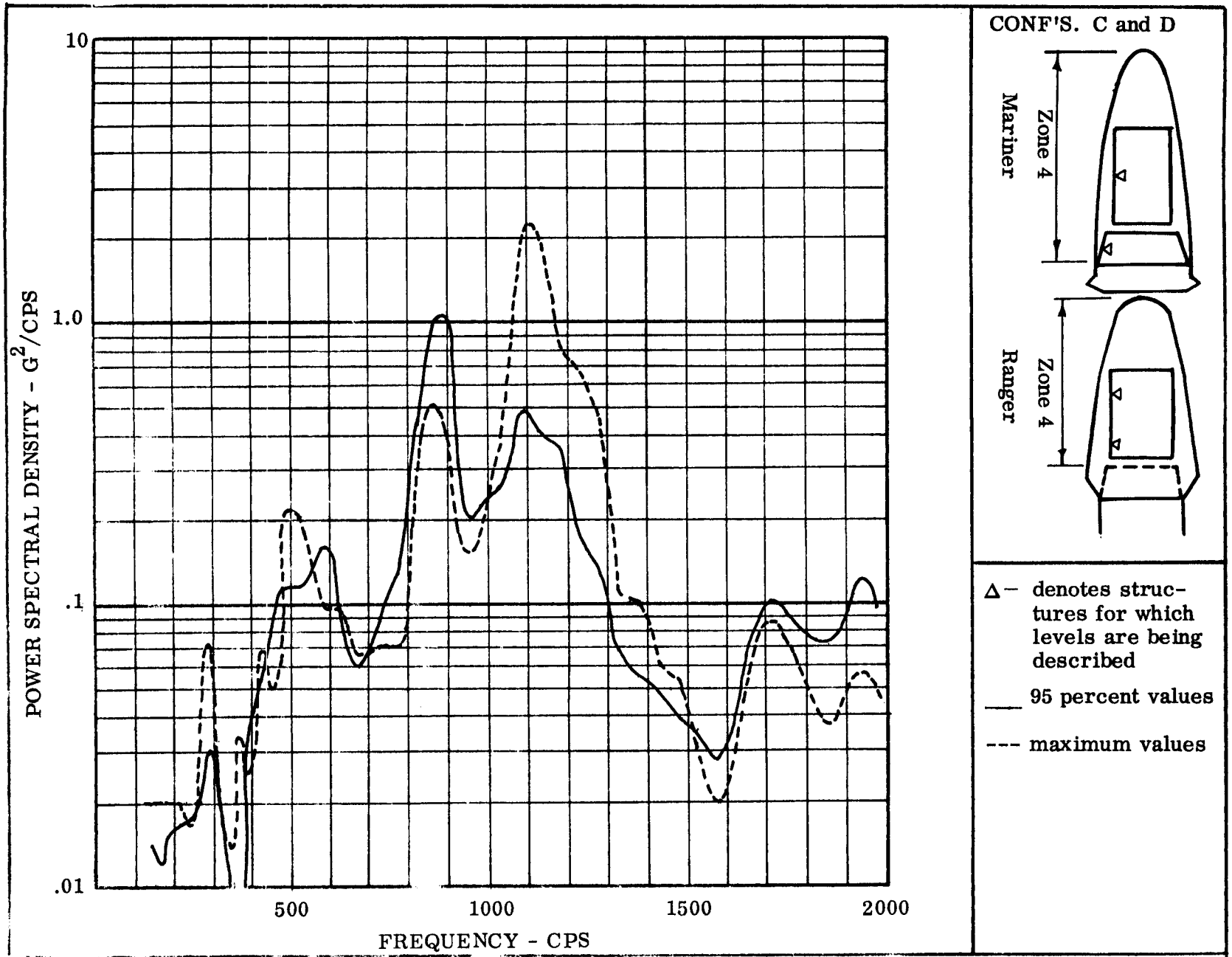

FIGURE 72 95 PERCENT AND MAXIMUM PSD VALUES FOR INNER STRUCTURE, ATLAS AND THOR FLIGHT CONFIGURATIONS C AND D, ZONE 4

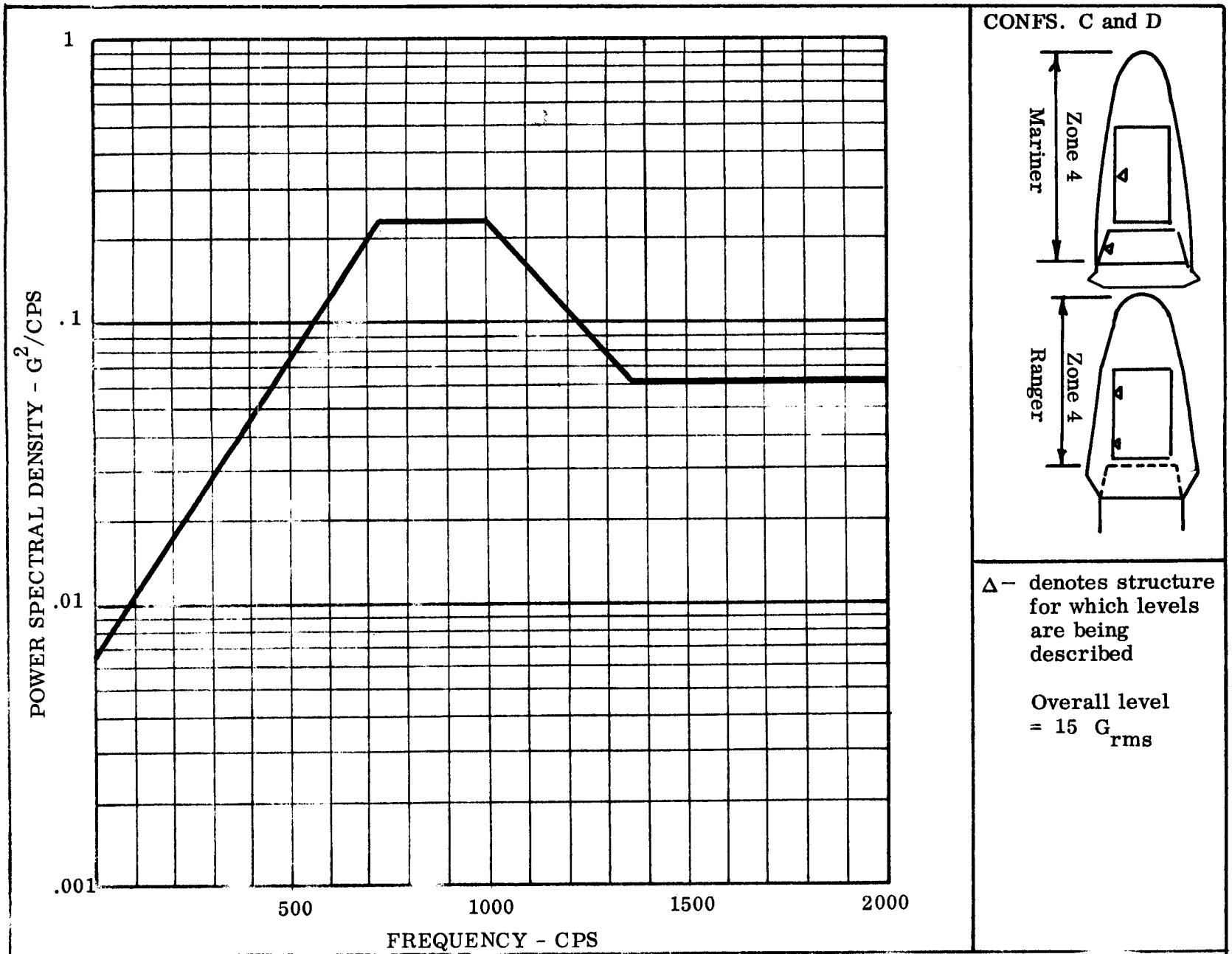

FIGURE 73 BACKGROUND VIBRATIONS FOR INNER STRUCTURE, ATLAS AND THOR FLIGHT, CONFIGURATIONS C AND D, ZONE 4

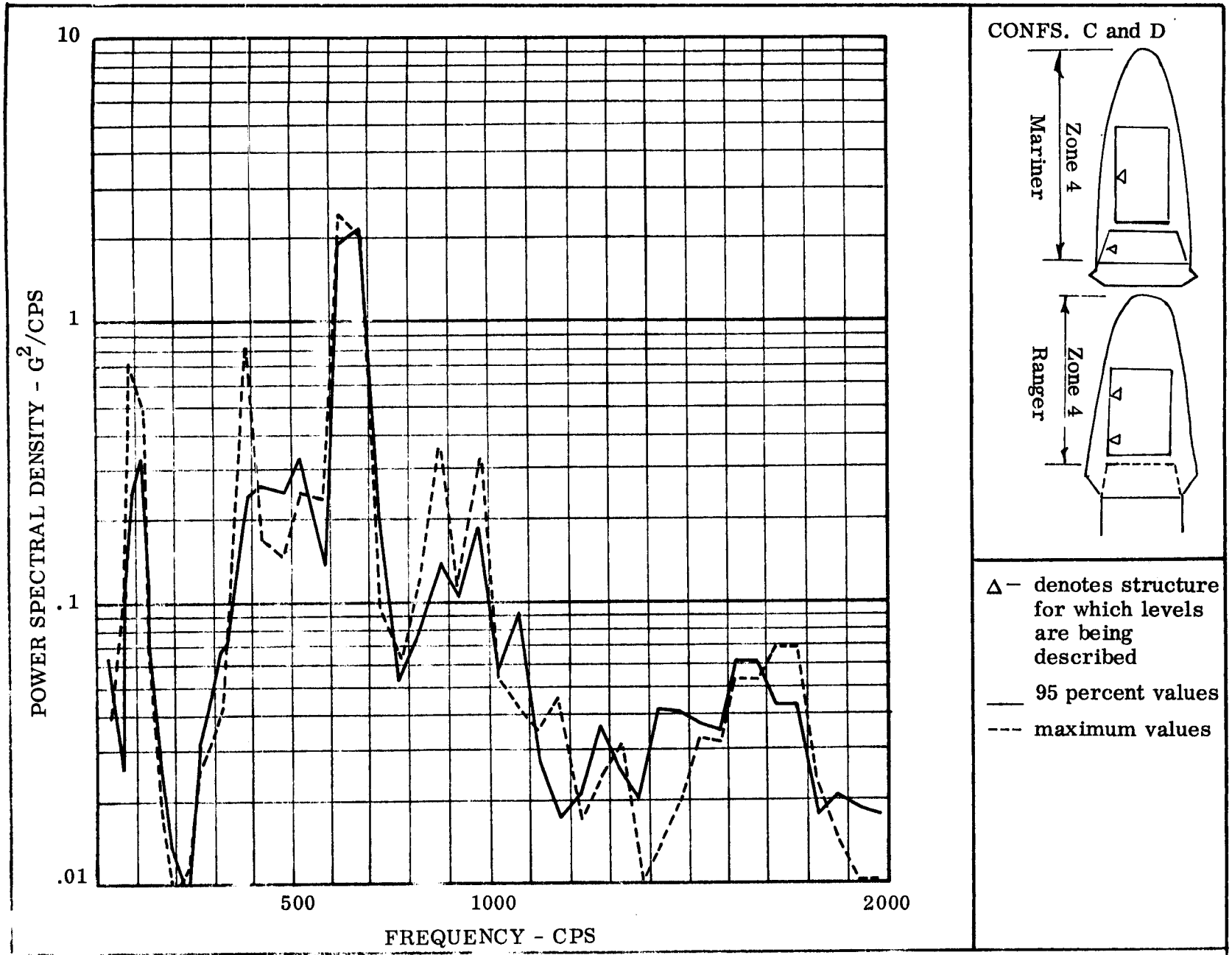

FIGURE 74 95 PERCENT AND MAXIMUM PSD VALUES FOR EQUIPMENT, ATLAS AND THOR FLIGHT, CONFIGURATIONS C AND D, ZONE 4

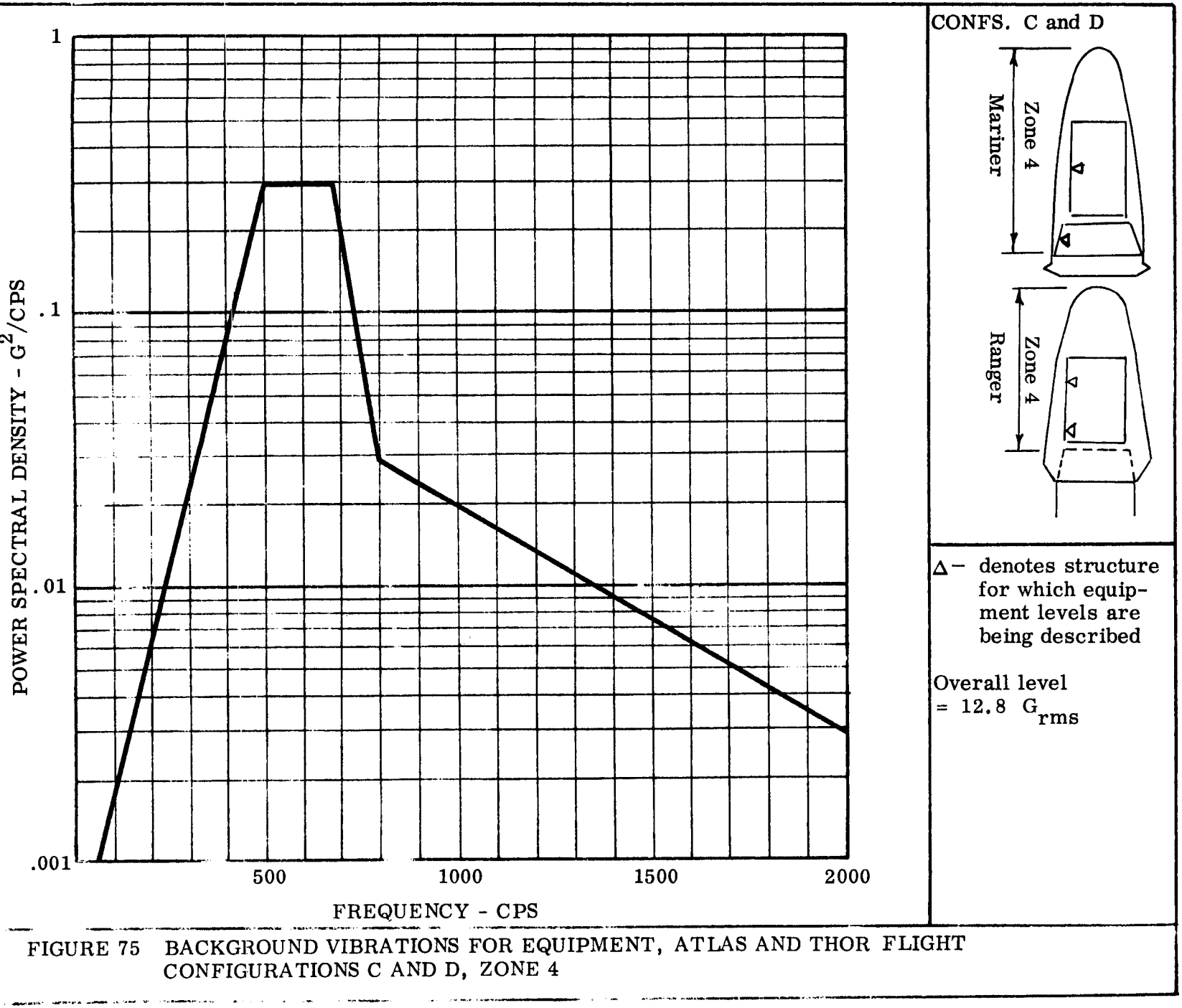

FIGURE 75 BACKGROUND VIBRATIONS FOR EQUIPMENT, ATLAS AND THOR FLIGHT CONFIGURATIONS C AND D, ZONE 4

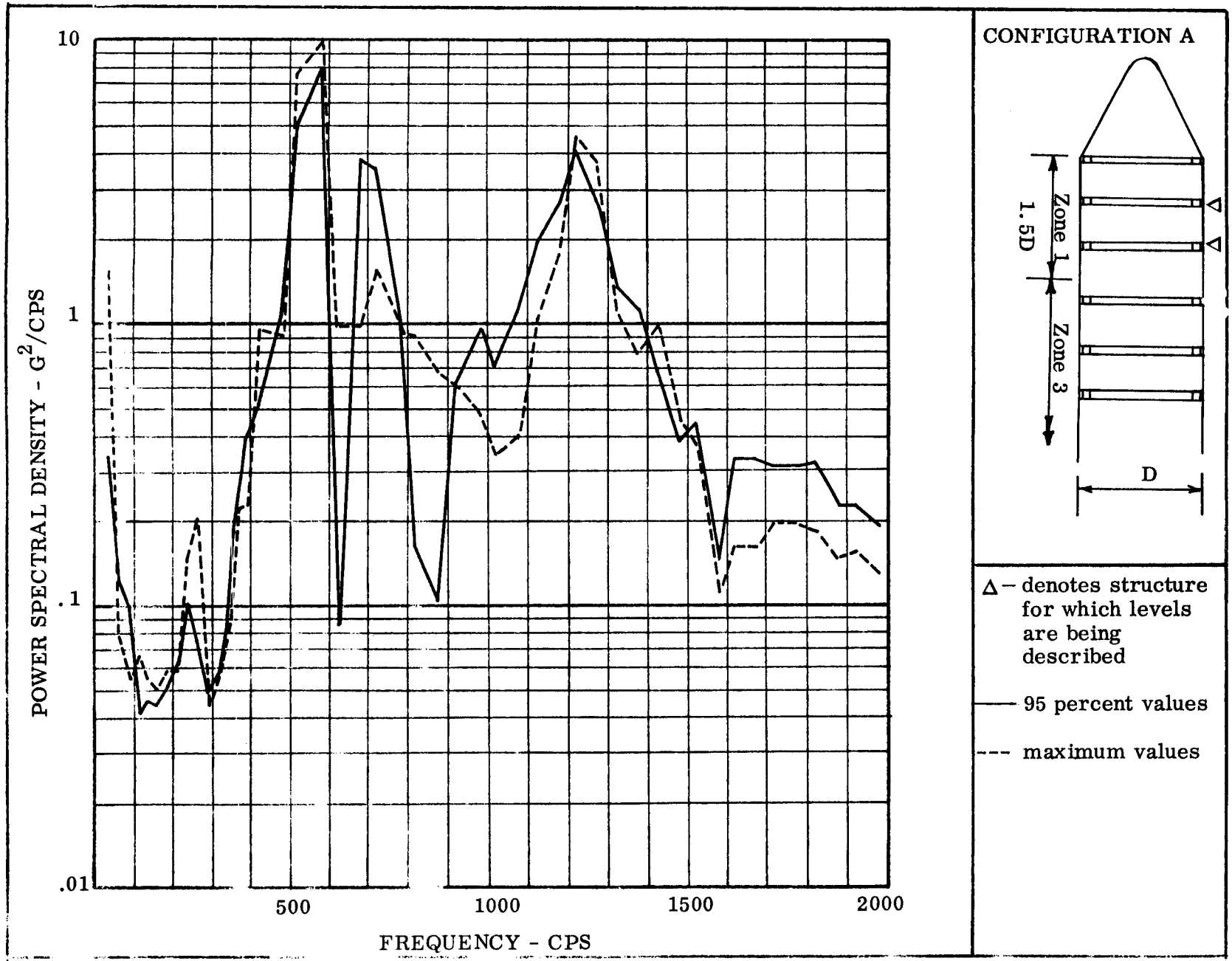

FIGURE 76 95 PERCENT AND MAXIMUM PSD VALUES IN OUTER STRUCTURE, TAT FLIGHT, CONFIGURATION A, ZONE 1

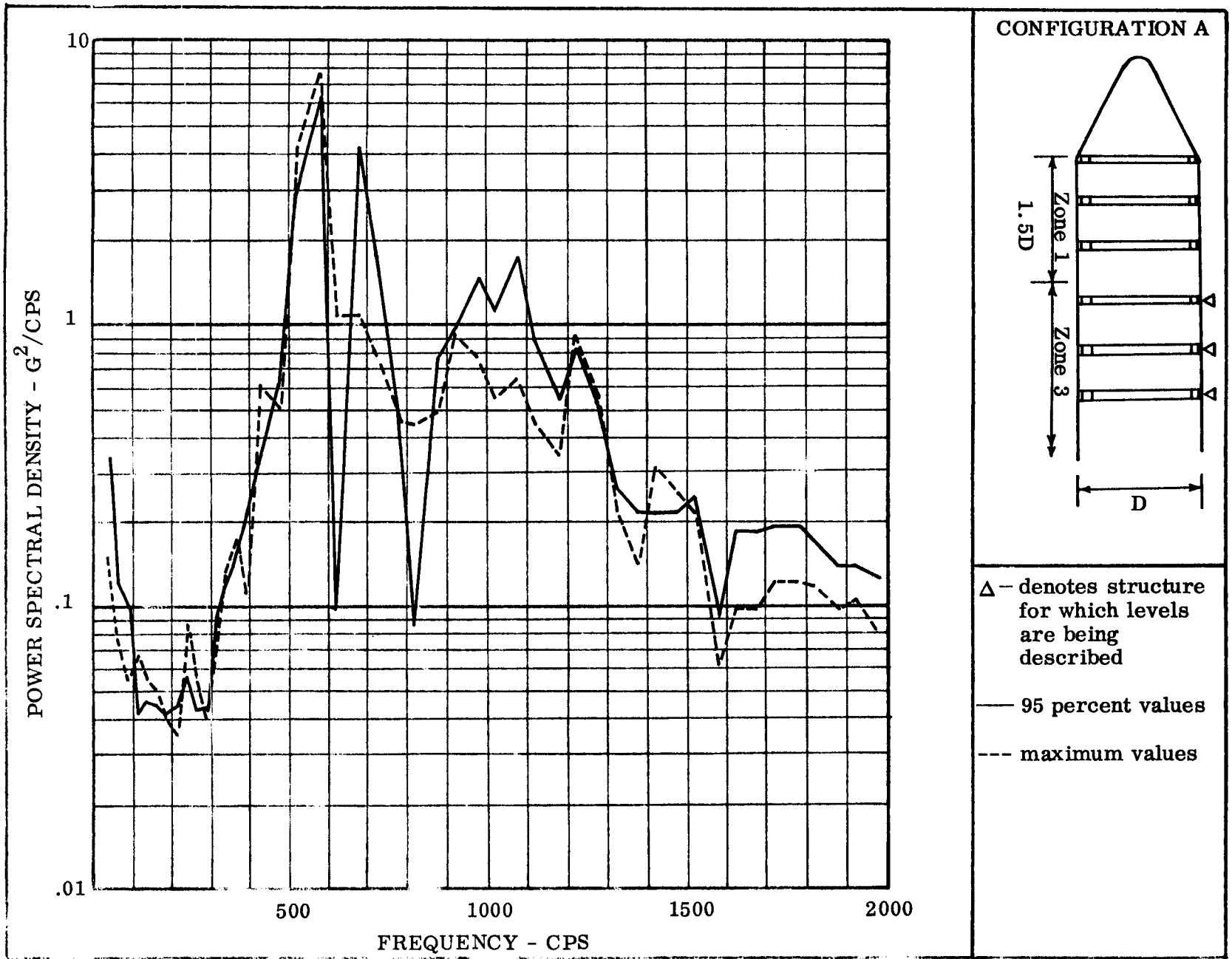

FIGURE 77 95 PERCENT AND MAXIMUM PSD VALUES IN OUTER STRUCTURE, TAT FLIGHT, CONFIGURATION A, ZONE 3

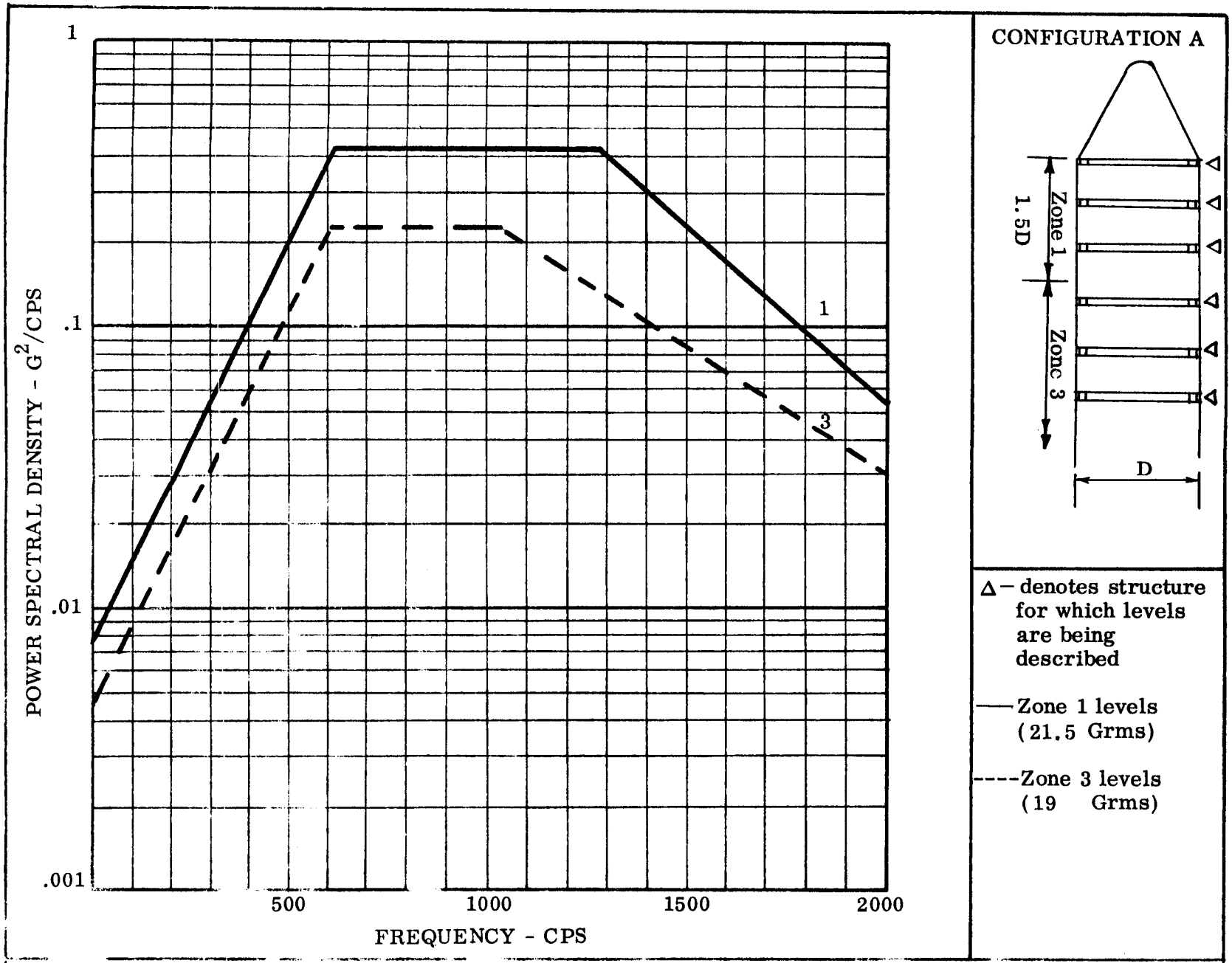

FIGURE 78 BACKGROUND VIBRATION IN OUTER STRUCTURE, TAT TRANSONIC FLIGHT, CONFIGURATION A, ZONES 1 AND 3

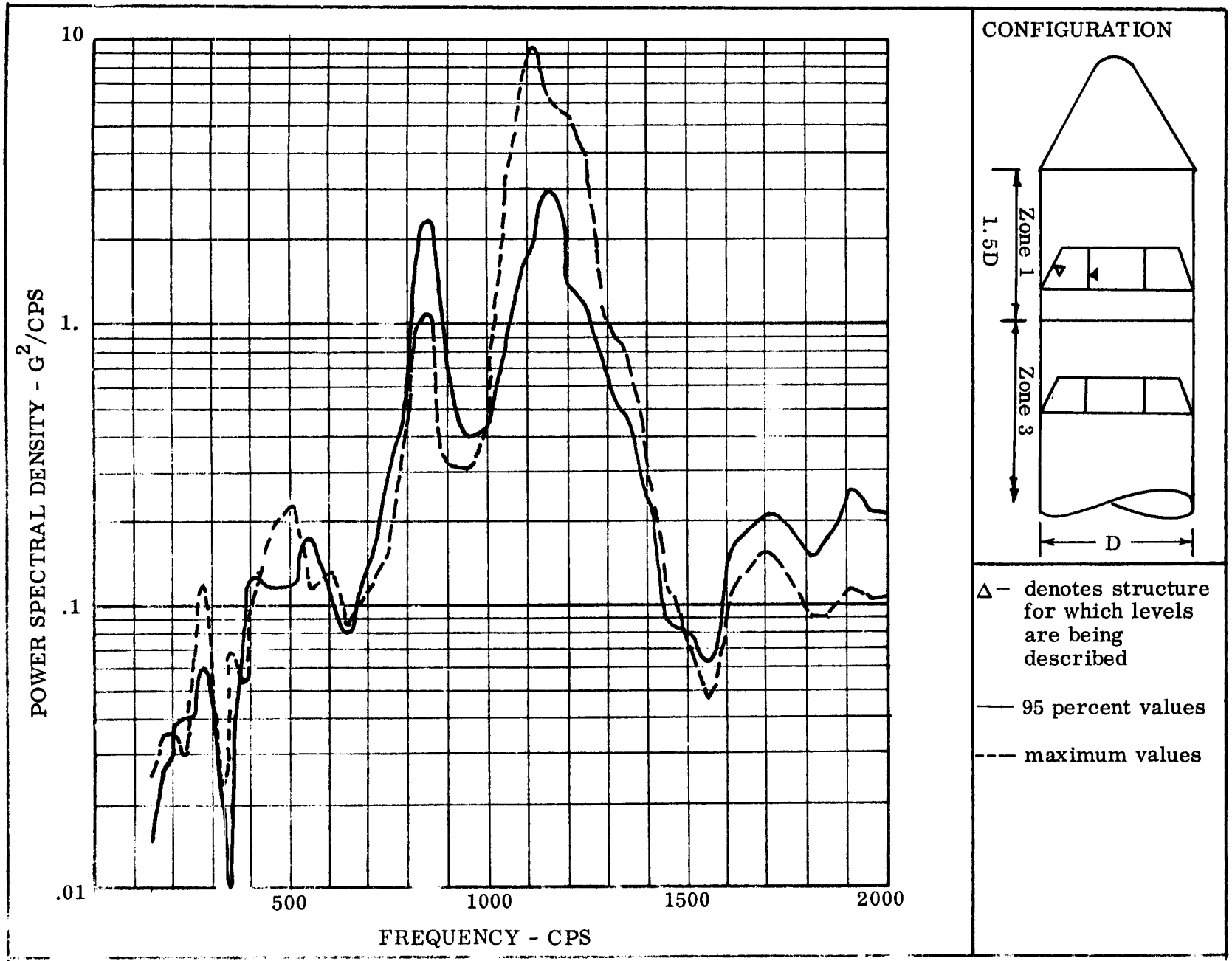

FIGURE 79 95 PERCENT AND MAXIMUM PSD VALUES IN INNER STRUCTURE, TAT FLIGHT, CONFIGURATION A, ZONE 1

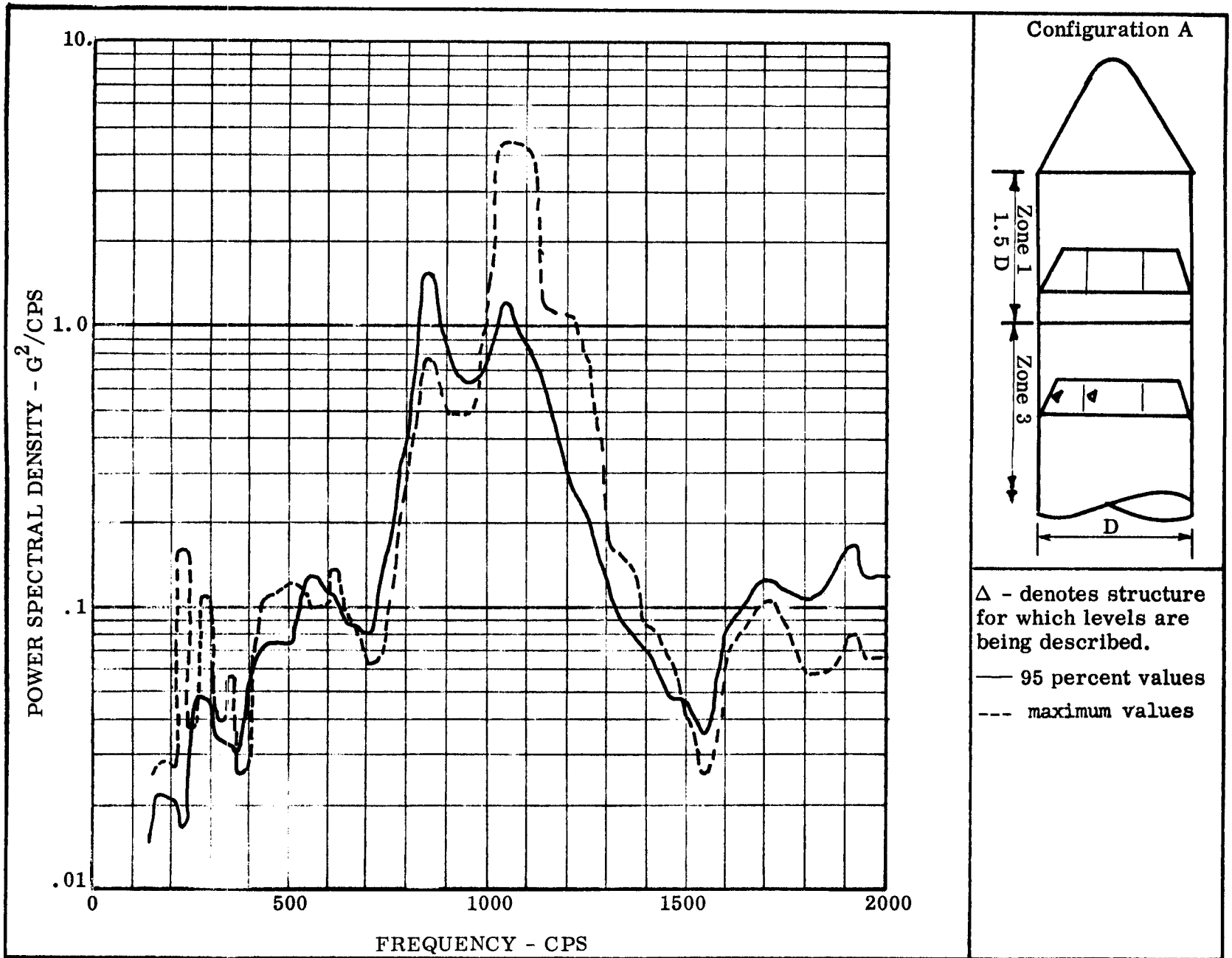

Figure 80 95 Percent and Maximum PSD Values for Inner Structure, TAT Transonic Flight, Configuration A, Zone 3

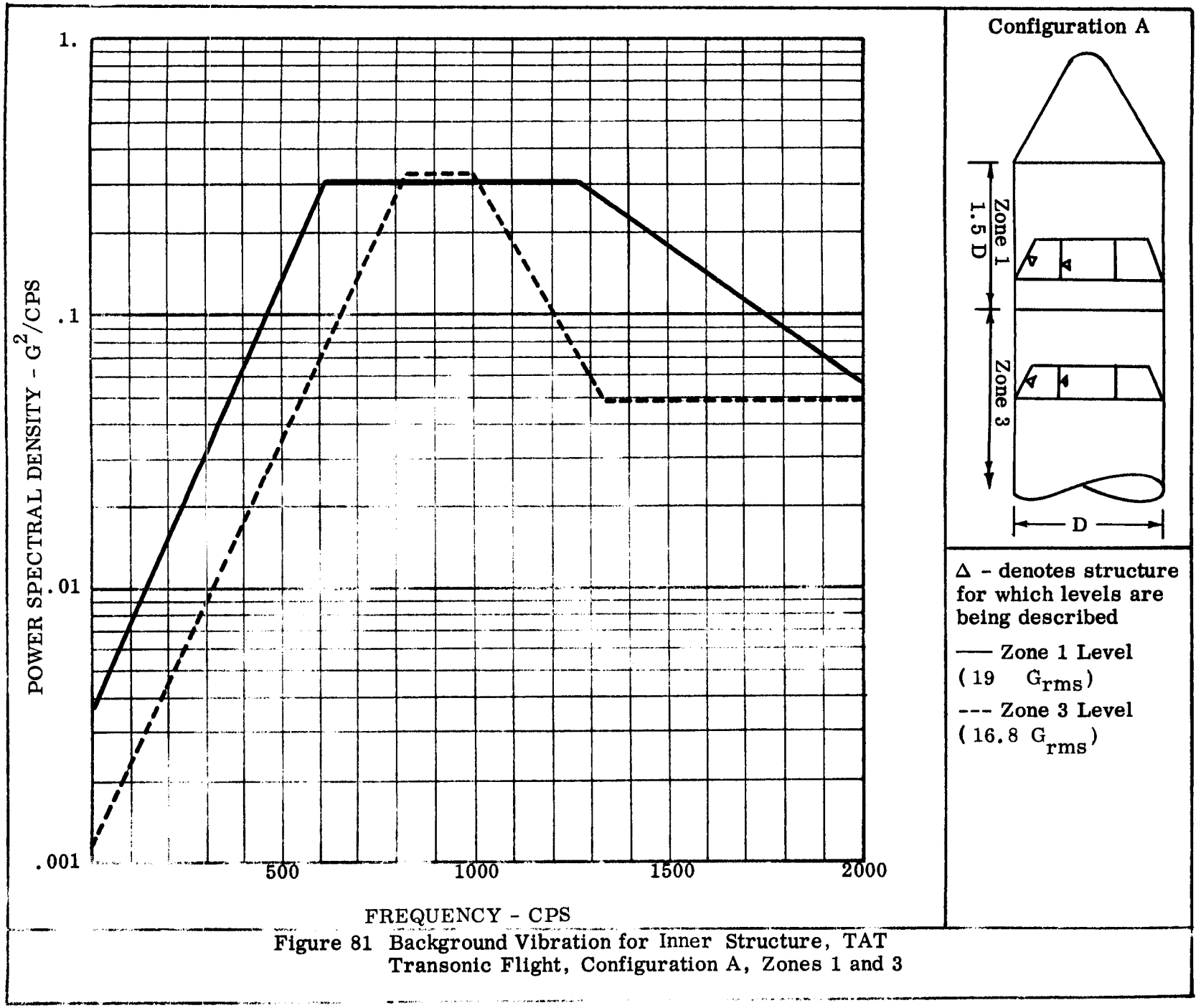

Figure 81 Background Vibration for Inner Structure, TAT Transonic Flight, Configuration A, Zones 1 and 3

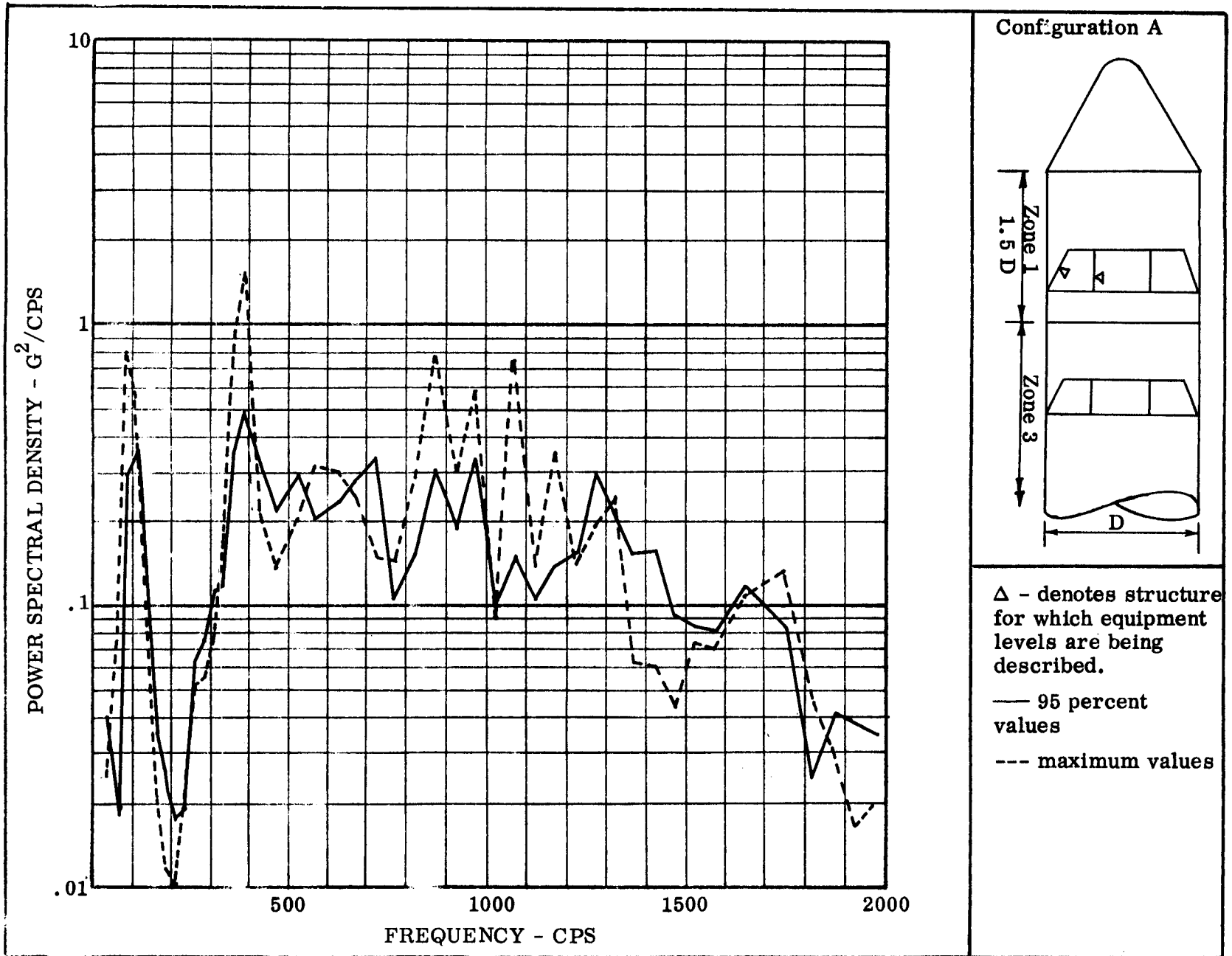

FIGURE 82 95 PERCENT AND MAXIMUM PSD VALUES FOR EQUIPMENT, TAT FLIGHT CONFIGURATION A, ZONE 1

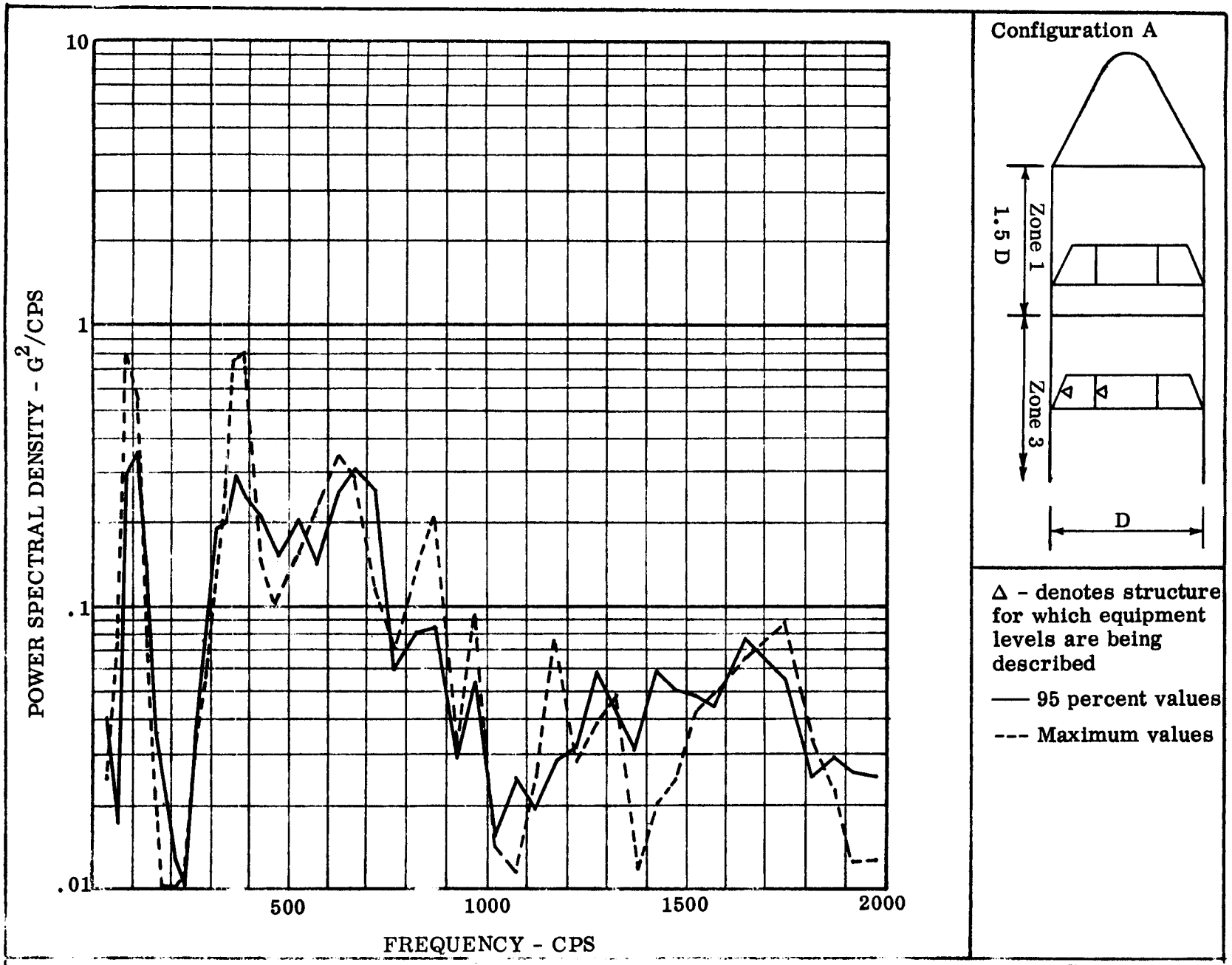

FIGURE 83 95 PERCENT AND MAXIMUM PSD VALUES FOR EQUIPMENT, TAT FLIGHT, CONFIGURATION A, ZONE 3

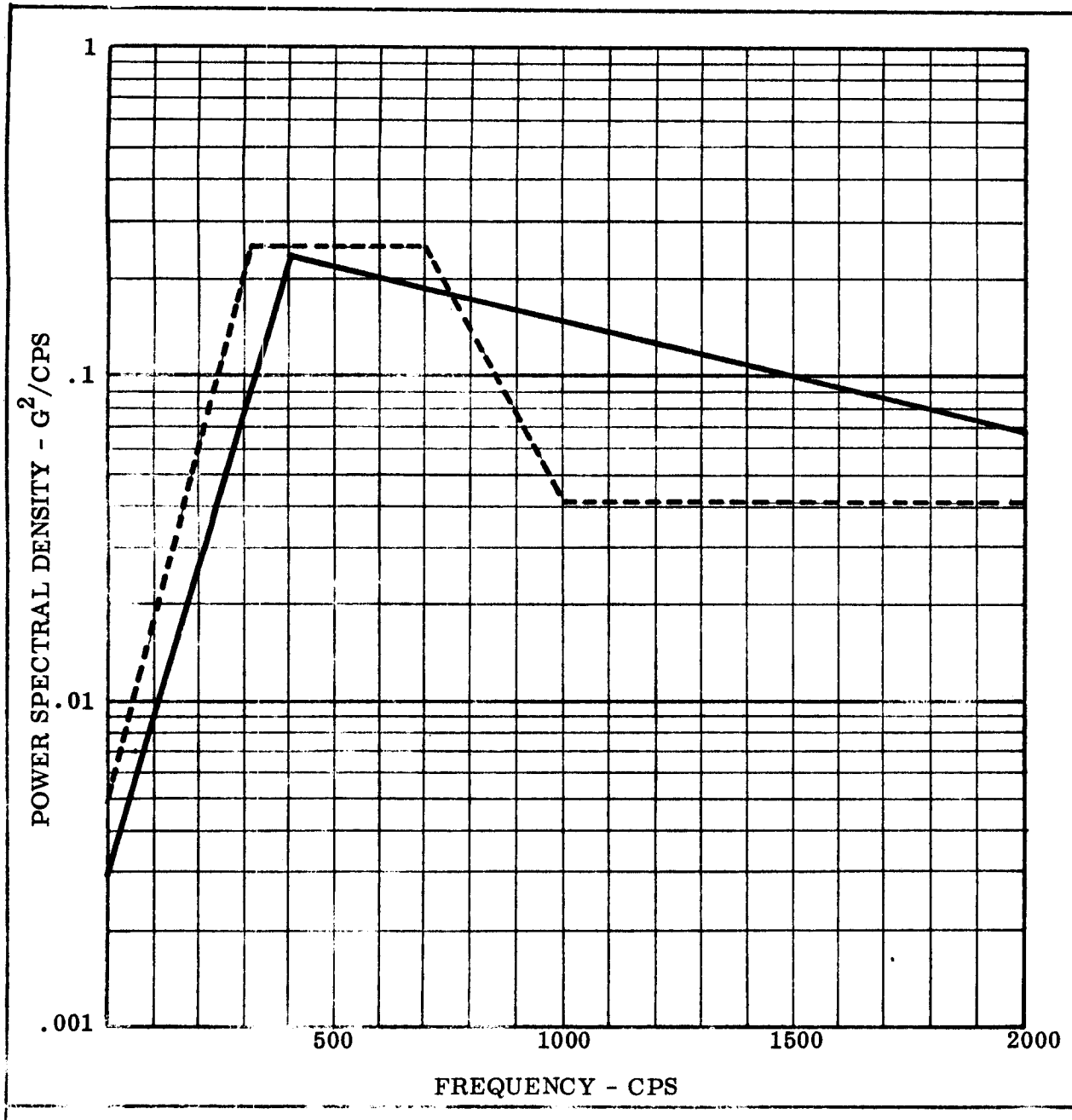

Configuration A

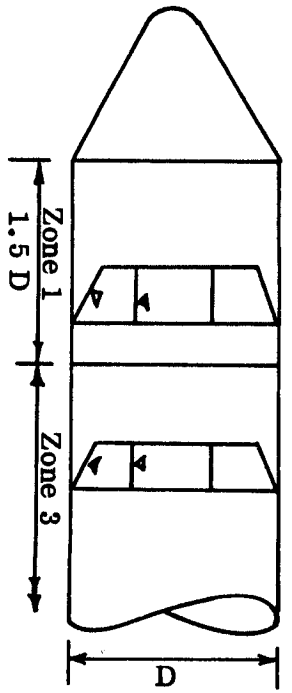

Δ - denotes structure for which equipment levels are being described

--- Zone 1 Level (16.8 G_{rms})

—— Zone 3 Level (14.7 G_{rms})

Figure 84 Background Vibration for Equipment, TAT Transonic Flight, Configuration A, Zones 1 and 3

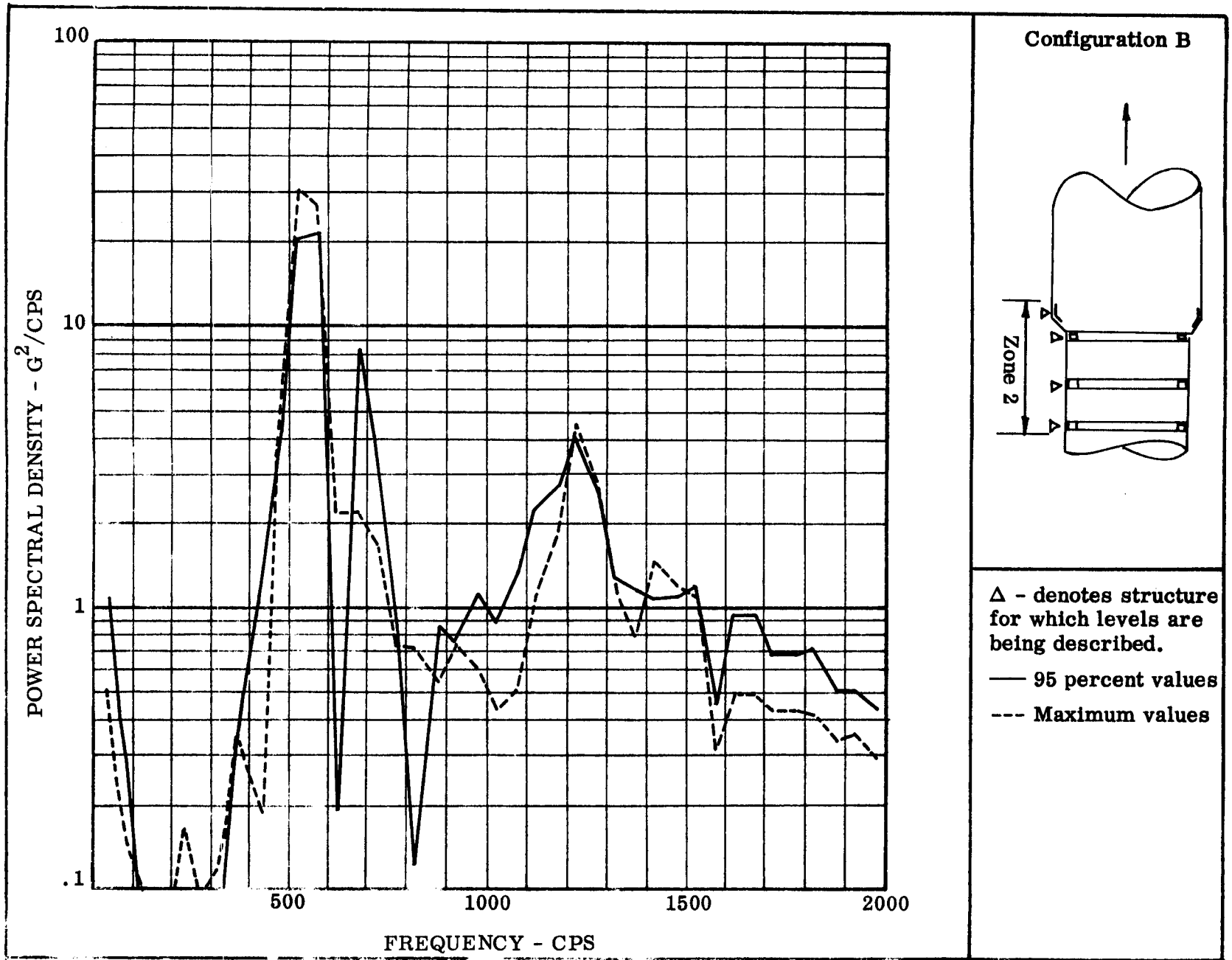

Figure 85 95 Percent and Maximum PSD Values for Outer Structure, TAT Transonic Flight, Configuration B, Zone 2

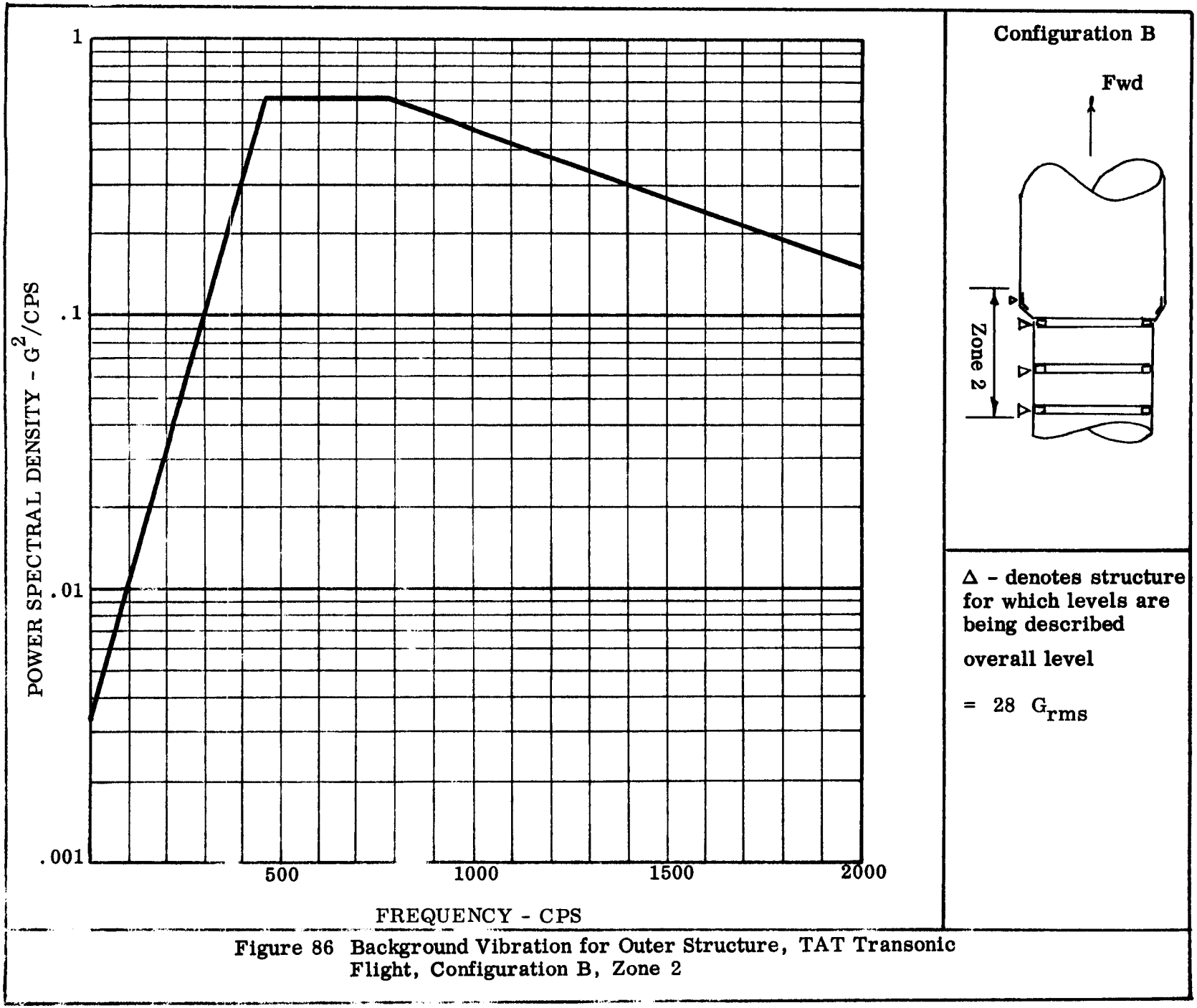

Figure 86 Background Vibration for Outer Structure, TAT Transonic Flight, Configuration B, Zone 2

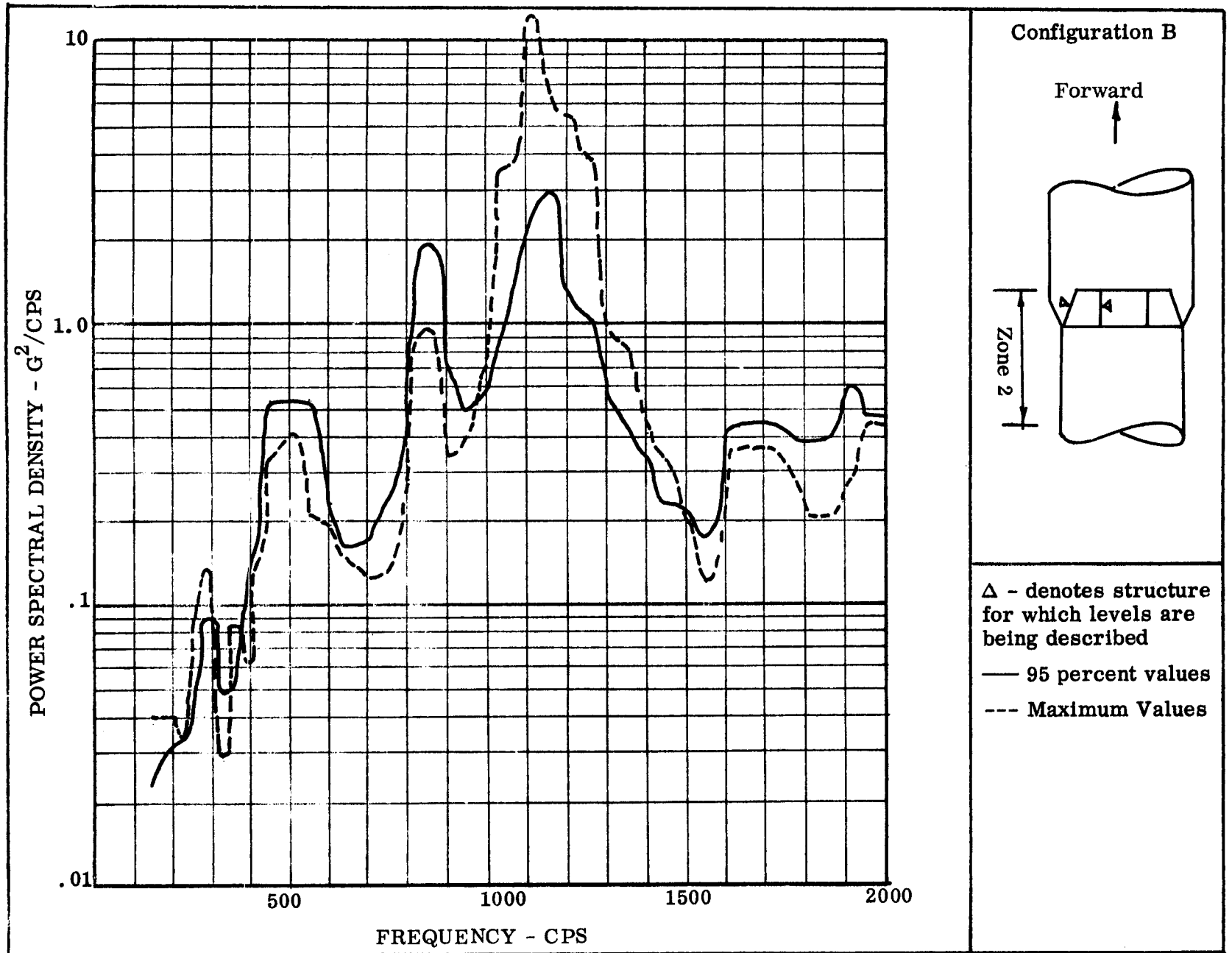

Figure 87 95 Percent and Maximum PSD Values for Inner Structure, TAT Transonic Flight, Configuration B, Zone 2

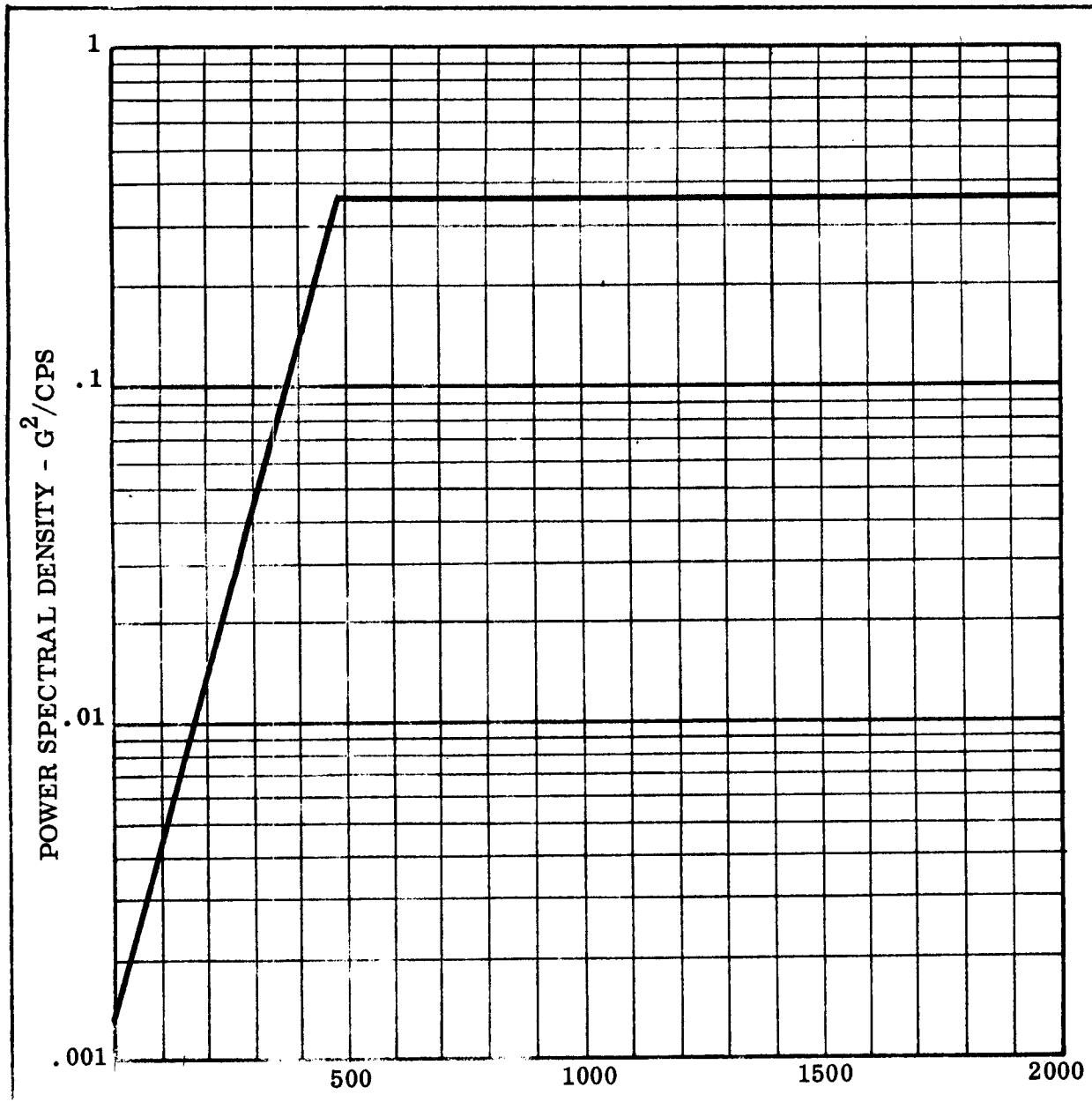

Configuration B

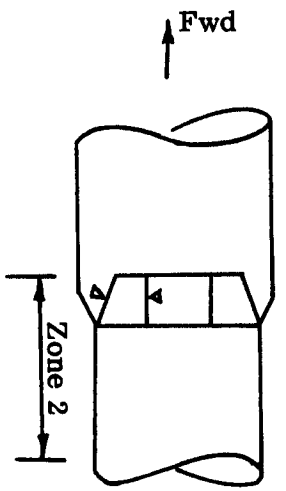

Δ - denotes structure for which levels are being described

Overall Level

= 25 G_{rms}

Figure 88 Background Vibration for Inner Structure, TAT Transonic Flight, Configuration B, Zone 2

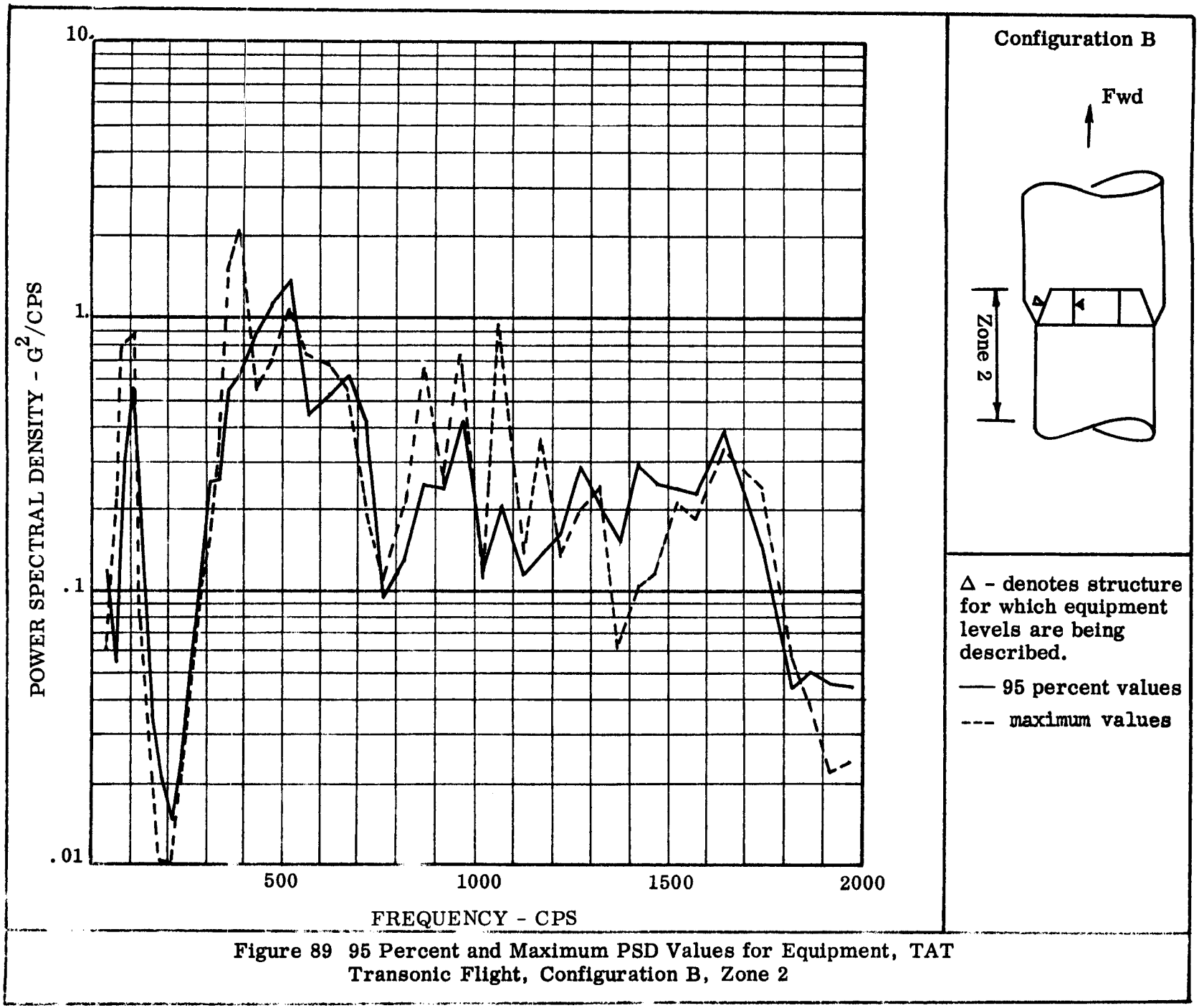

Figure 89 95 Percent and Maximum PSD Values for Equipment, TAT Transonic Flight, Configuration B, Zone 2

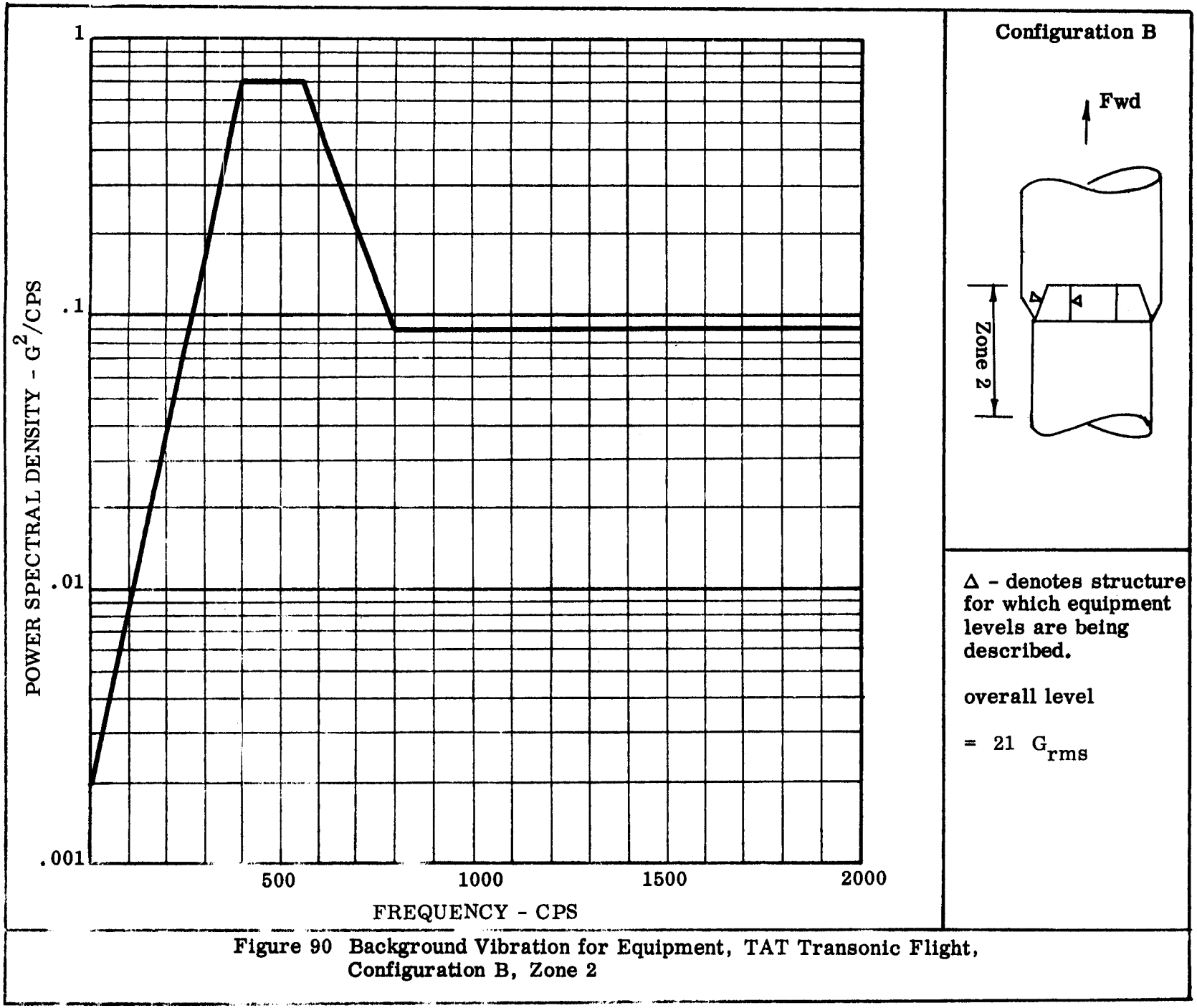

Figure 90 Background Vibration for Equipment, TAT Transonic Flight, Configuration B, Zone 2

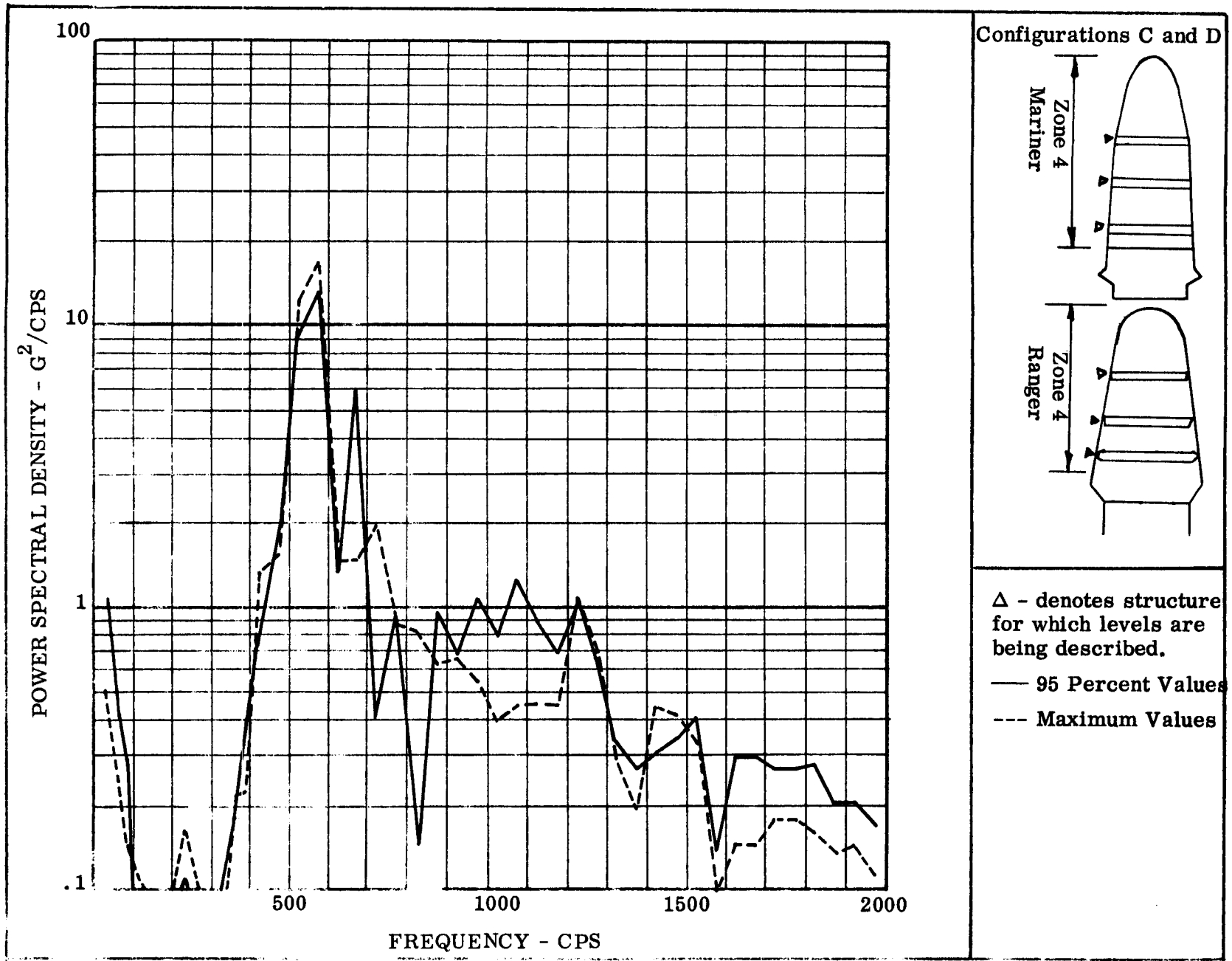

Figure 91 95 Percent and Maximum PSD Values for Outer Structure, TAT Transonic Flight, Configurations C and D, Zone 4

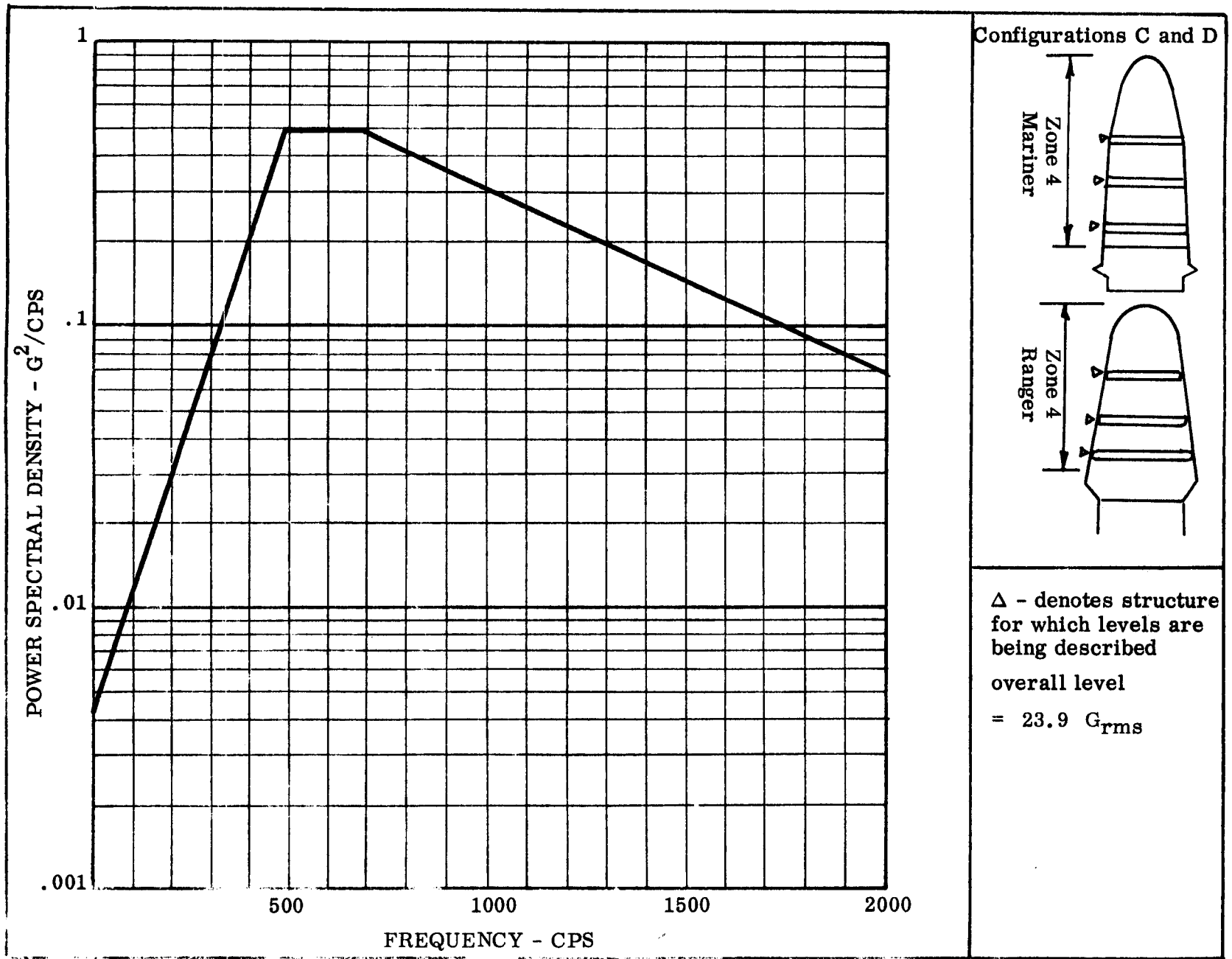

Figure 92 Background Vibration for Outer Structure, TAT Transonic Flight, Configurations C and D, Zone 4

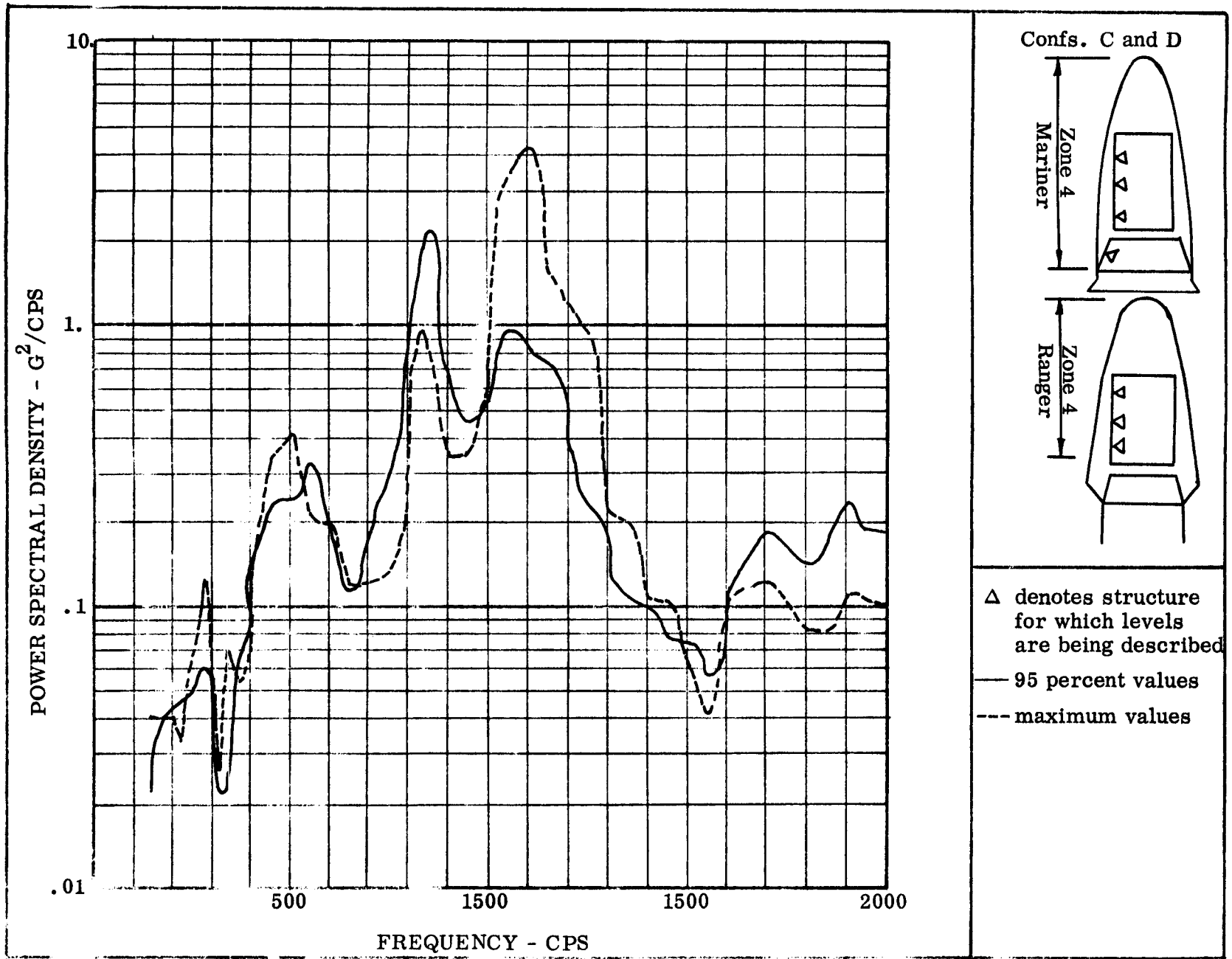

Figure 93 95 Percent and Maximum PSD Values for Inner Structure, TAT Transonic Flight, Configuration C and D, Zone 4.

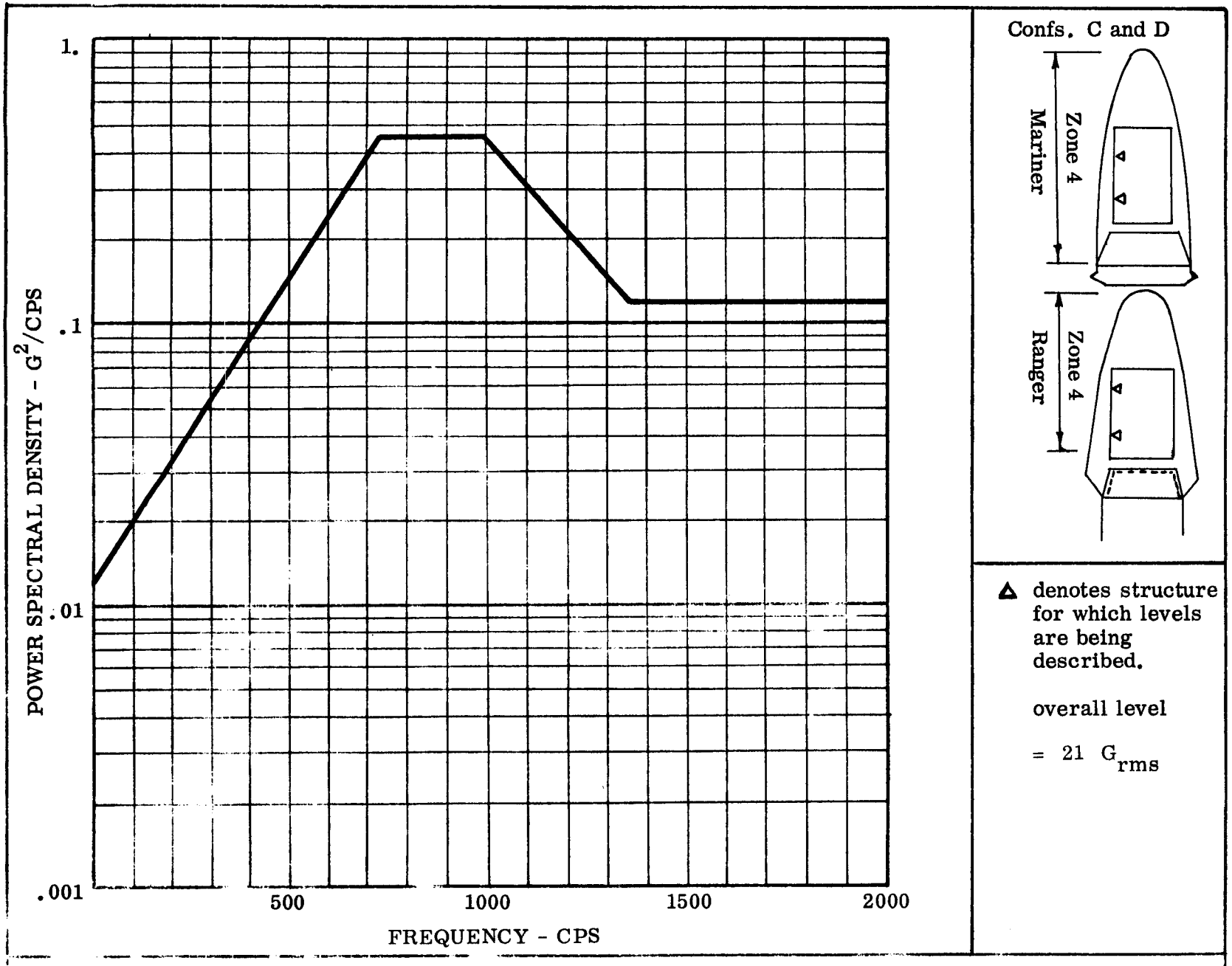

Figure 94 Background Vibration of Inner Structure, TAT Transonic Flight, Configurations C and D, Zone 4

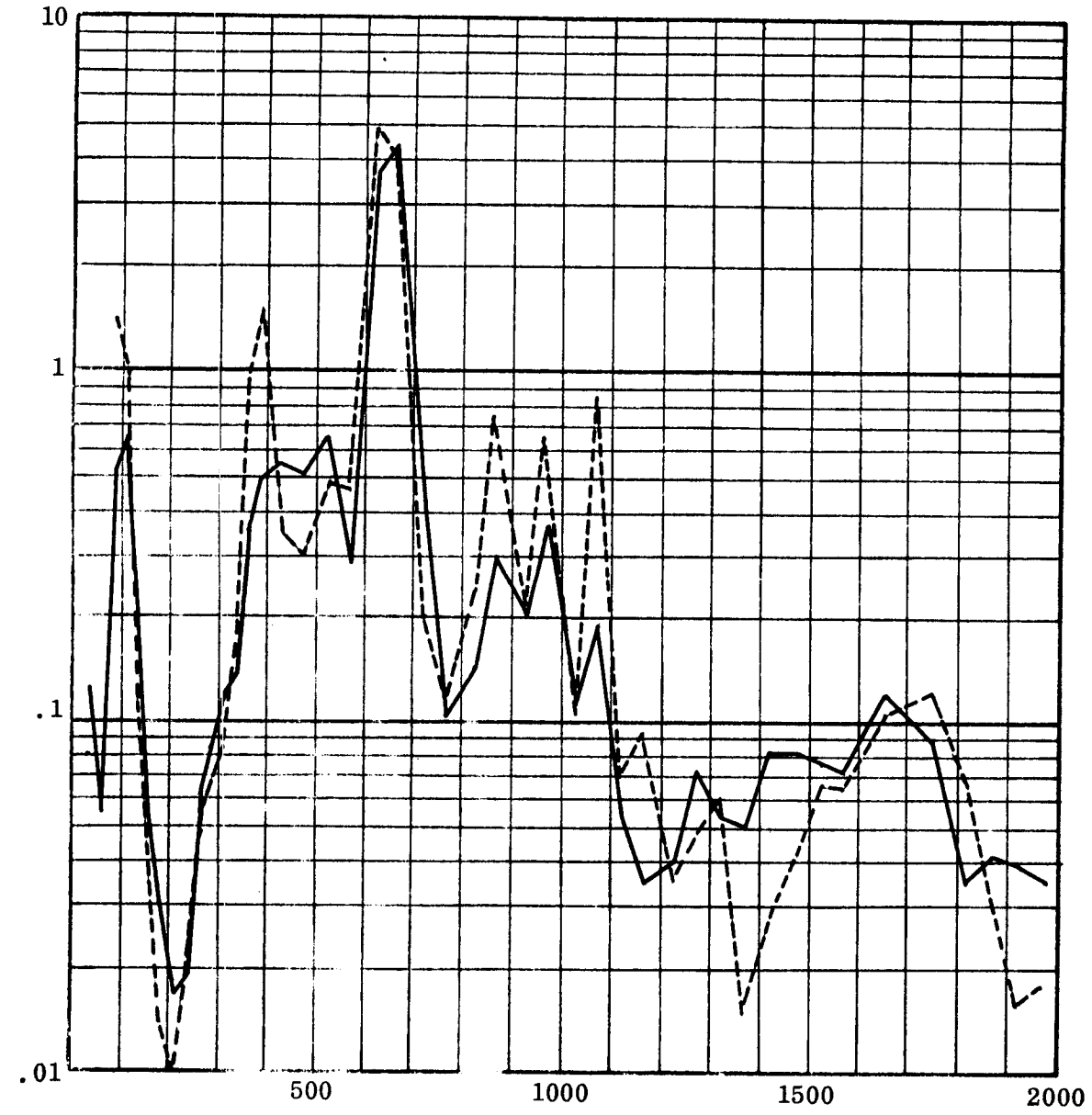

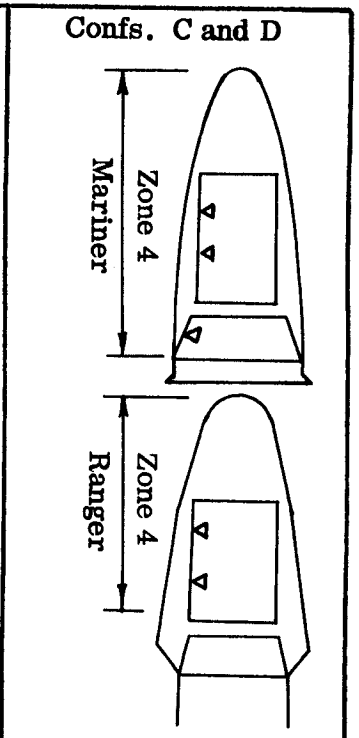

△ denotes structure for which equipment levels are being described.

——— 95 percent values

– – – maximum values

Figure 95 95 Percent and Maximum PSD Values for Equipment, TAT Transonic Flight, Configurations C and D, Zone 4.

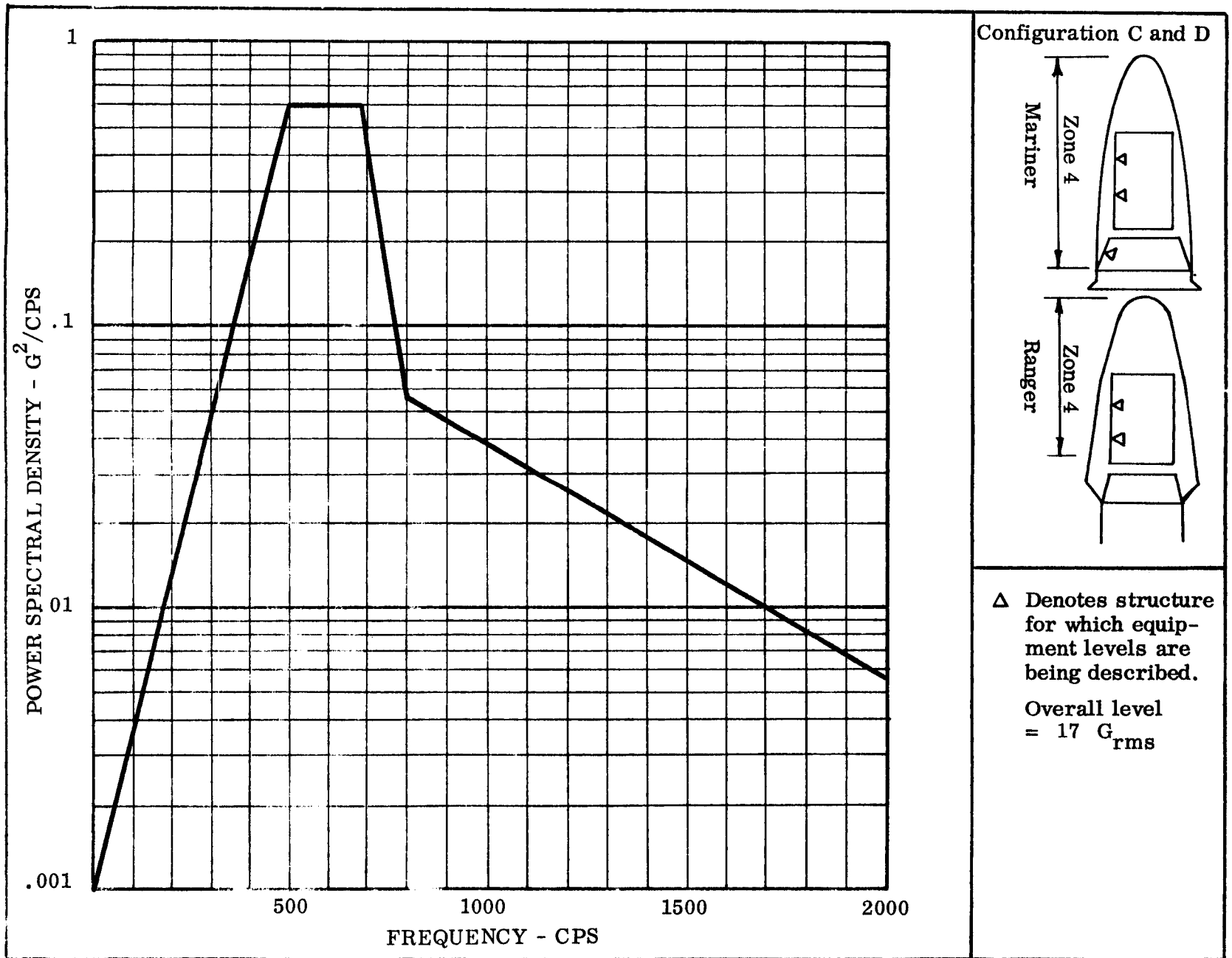

Fig. 96 Background Vibration for Equipment, TAT Transonic Flight, Configuration C and D, Zone 4

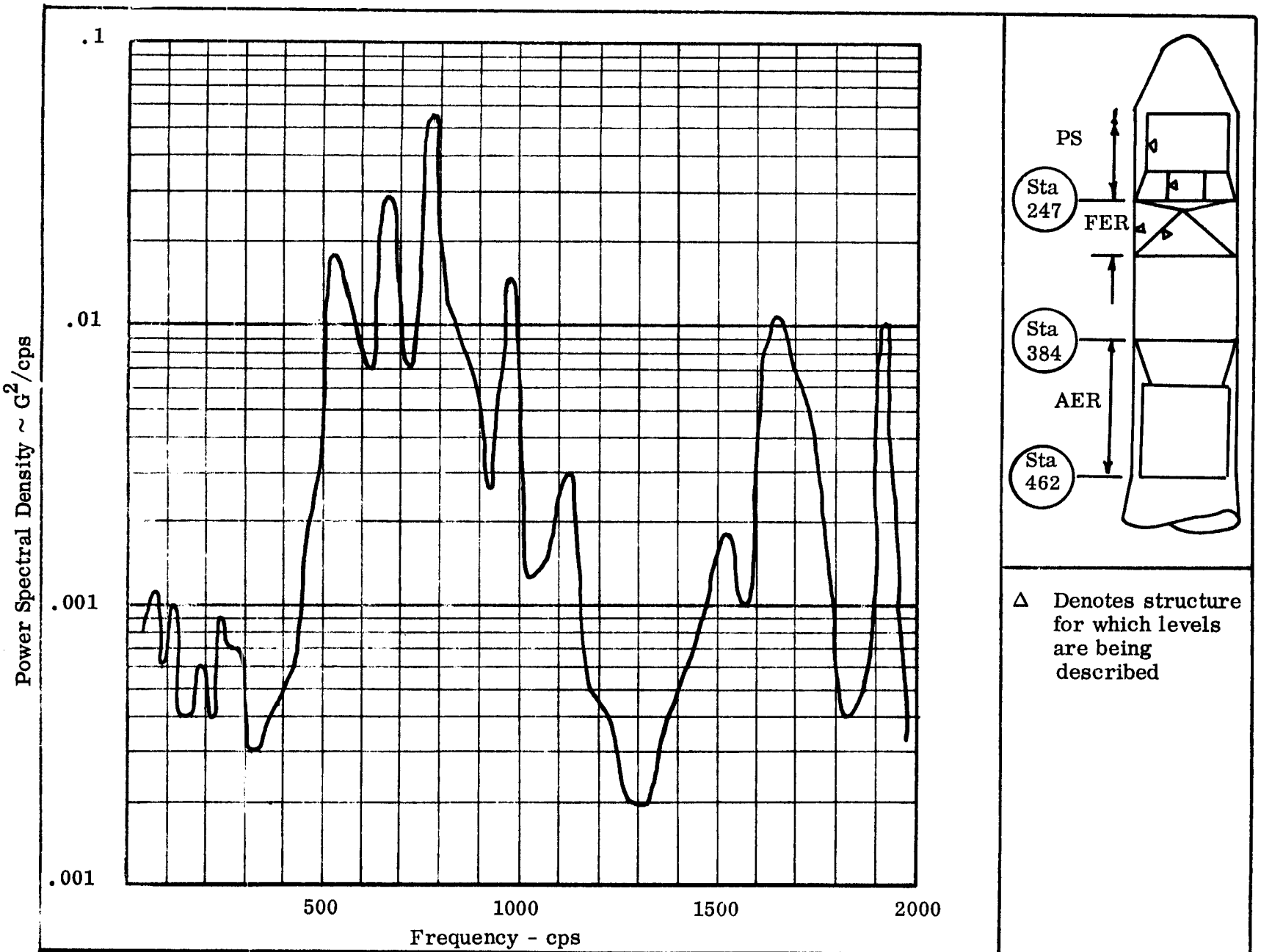

Fig. 97 Agena Main Engine Steady Burn Vibration Environment – PS and FER

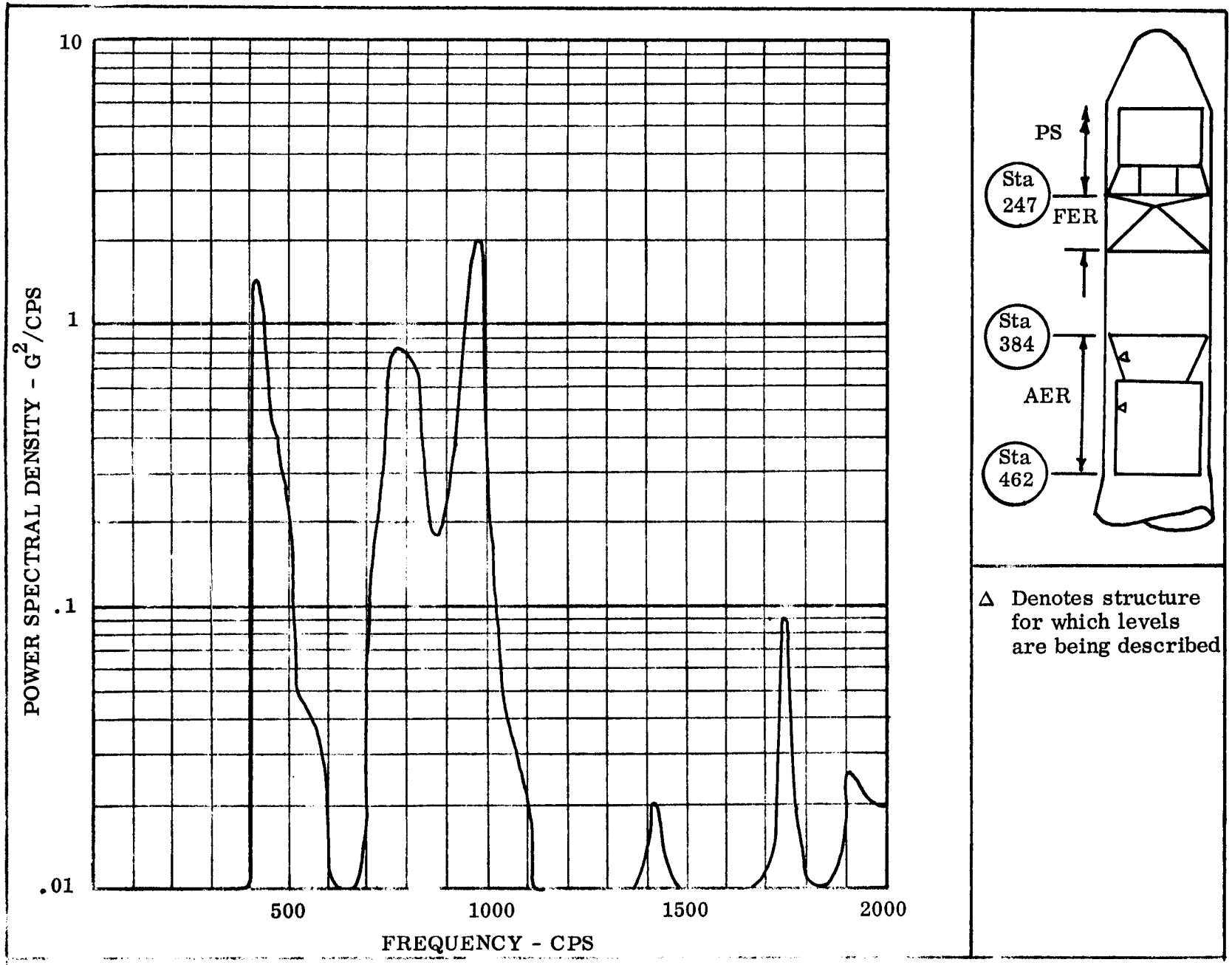

Fig. 98 Agena Main Engine Steady Burn Vibration Environment – AER

Section 3
QUASI-PERIODIC ENVIRONMENTS

The transient quasi-periodic environment of the Agena and payload structure is caused by the ignition and shutdown of the propulsion systems, POGO instabilities and resonances generated by the propulsion system, wind gusts and aerodynamic buffeting. Design load criteria for primary and secondary structure are generally established by these environments rather than by mechanically or acoustically induced random vibrations. The information presented in this section is, therefore, of particular significance with respect to the formulation of qualification test criteria for primary and secondary structure.

The flight data used to define the above environments were obtained from transducers attached to the structure of payloads, the Agena forward equipment rack and the Agena aft equipment rack. Therefore, this data is representative of the coupled response of primary structure loaded by equipment and/or payloads. No rational procedure is presently available to derive from this data the environment for the completely different configuration. However, this data is useful for defining test requirements for similar configurations.

Appendix A summarizes the vehicle measurements which were considered in the analyses of the above environments. The specific vehicles from which data was collected for defining the environment generated by POGO instabilities have not been separately identified since these data were obtained from all successful Agena B and D flights made to date.

Engine Ignition and Shutdown Transients

Transient oscillations of the vehicle structure are induced by rapid changes in steady state thrust levels occurring at the ignition and shutdown sequences of the various

booster engines. The transients observed at these events are in the form of a mixture of decaying oscillations, the frequency contents of which are primarily associated with the gross vehicle fundamental longitudinal vibration mode. However, local structure motions, not identifiable with gross vehicle natural vibration modes, are also present in the form of decaying oscillations.

Form of Transients. A review of oscillogram records of transients obtained from several vehicles (see Appendix A) has revealed that decay characteristics fall into the three categories shown in Figure 99.

The first category has the traditional decay characteristic of a simple viscously damped system while the second displays two distinct damping rates which appear to be amplitude-dependent. The third category has the characteristic of a decaying amplitude modulated sine wave and possesses a distinct periodic "beat." Table 7 summarizes the maximum, minimum and average values of equivalent viscous damping observed at the various flight events during which transients occur. Also included are representative values of rigid body acceleration resulting from changes in engine thrust level.

Peak accelerations and associated frequencies for observed flight transients occurring during Agena main engine ignition and shutdown operations, are shown in Figure 100. During these events the peak values observed were significantly different for the three zones of the vehicle examined (PS, FER and AER), and were therefore specified separately. The values shown represent motions of the vehicle primary structure.

Figure 101 presents peak acceleration values, again for primary structure, observed during ignition and shutdown operations of the Thor, TAT and Atlas engines. Since no significant variation between the peak values observed in the three vehicle zones examined, no attempt was made to distinguish them separately.

Based upon the available flight data, the estimated peak transient accelerations experienced by equipment during the Agena ignition and shutdown events are as shown

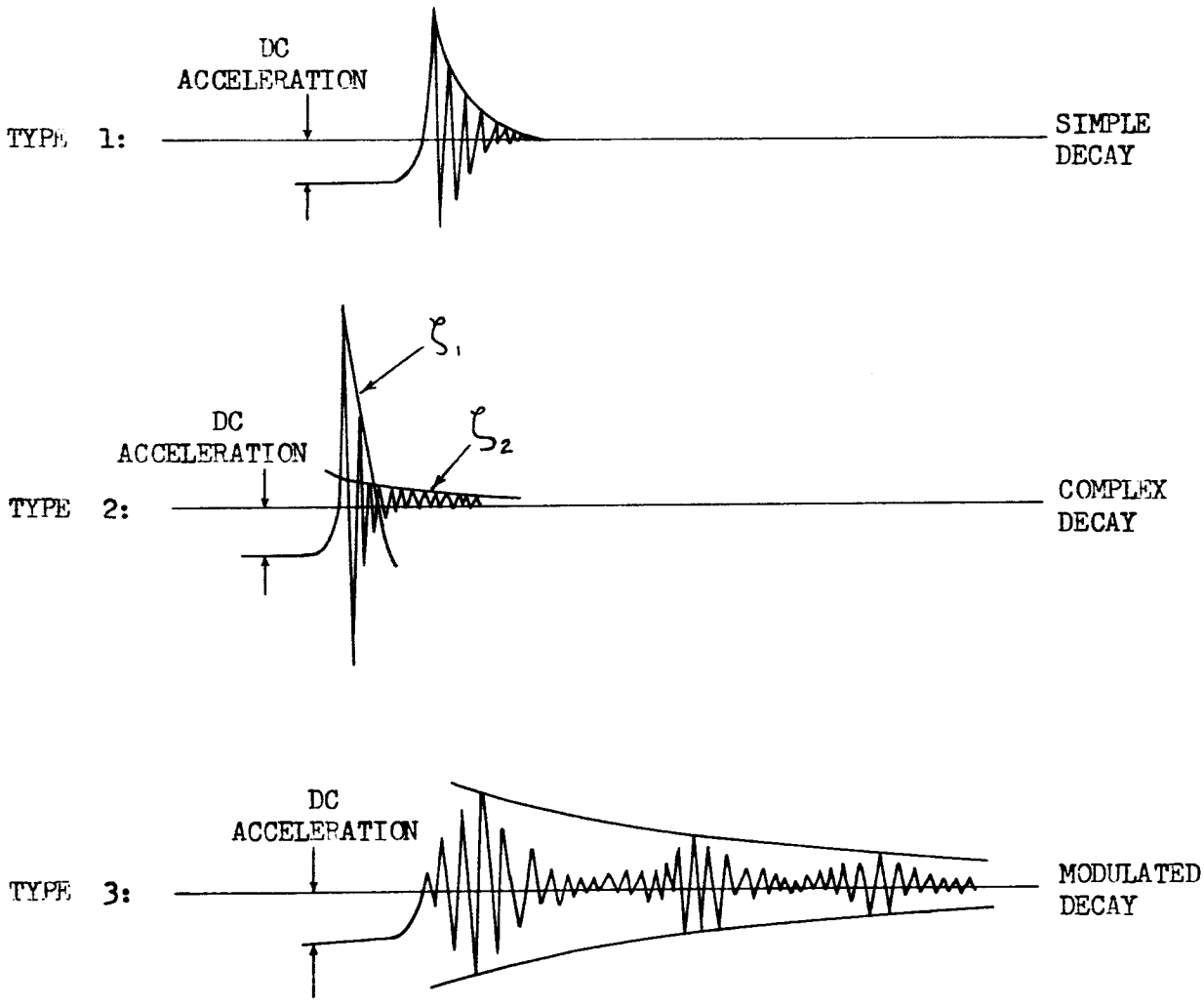

ζ = Percentage of Critical Damping

Figure 99 Characteristic Types of Transient Decay

Table 7

SUMMARY OF MAXIMUM, MINIMUM AND AVERAGE VALUES OF TRANSIENT DAMPING RATES

EVENT	D. C. ACCEL.	NUMBER OF TRANSIENTS ANALYZED	APPROXIMATE FREQUENCIES (cps)	TYPE* OF DECAY	ζ (PERCENT OF CRITICAL DAMPING)		
					Min.	Average	Max.
Atlas Liftoff	1.6	4 1 6	5,12 12 12,18,30,50	1 2 3(2 cps beat)	0.6 6(1.5)** 0.3	1.0 6(1.5) 1.2	1.5 6(1.5) 1.9
Atlas MECO	6	9 1 4	10,22,45 24,50 20,75	1 2 3(7&5 cps beat)	.9 1.7(.8)** .3	1.7 1.7(.8) .7	2.8 1.7(.8) 1.1
Atlas SECO		4 4	5,40 35	1 3(7 cps beat)	1.1 2	2.0 2	3.6 2
TAT & Thor Liftoff	2 4 2.2	4 2 11	15,70 15 15,27	1 2 3(2 cps beat)	.5 1.2(.4)** .4	1.1 2.0(.45) .9	1.9 2.8(.52) 1.9
Thor & TAT MECO	8	3	20	1	2	2.3	2.8
Agena 1st Ignition	1.5	4	30,50,75	1	1.4	1.6	2.0
Agena 1st Shutdown	6.5	10 1	35,60,75 80	1 2	0.5 1.7(.2)**	1.1 1.7(.2)	2.1 1.7(.2)
Agena 2nd Ignition	6.5	1 1	80 55	1 2	1.0 1.6(.1)**	1.0 1.6(.1)	1.0 1.6(.1)
Agena 2nd Shutdown	7.7		50,80	2	.9(.5)**	1.3(.4)	1.6(.3)

*Types of transient decay:
(1) Simple
(2) Complex
(3) Modulated
} See Figure 99

** Value in parenthesis refers to ζ_2 in type 2 decay (See Figure 1)

in Table 8. Due to the lack of sufficient vibration measurements made on actual equipment during flight, extensive use of recent transient simulation tests conducted on an Agena aft section has been made in order to estimate equipment maximum transient environments, which, in the majority of cases occurs at the Agena ignition and shutdown sequences. This transient test, described in Reference (5), was conducted on the Agena Program P-50 aft section configuration which contained 17 equipments having a wide variety of mounting arrangements and masses (5 to 200 pounds). The applied test transient was a close simulation of an Agena shutdown transient, evidenced by comparing the shock spectra analysis of the transient produced on the specimen with that predicted for flight (Figure 102). Measured equipment responses during the test indicated that the maximum amplification of peak transient accelerations induced by equipment support structure was 3.0. It is felt that the use of this amplification value of 3.0 will provide a good indication of the peak transient accelerations which are experienced by equipment during flight, in the frequency range where equipment mounting resonances generally occur. This transmissibility data was also applied to establish representative equipment peak responses in the payload and Agena forward section since, it is assumed, similar kinds of mounting structures and equipment masses are used in these areas as are used in the aft section.

Table 8

ESTIMATED PEAK TRANSIENT ACCELERATIONS FOR EQUIPMENT DURING AGENA IGNITION AND SHUTDOWN EVENTS (GS)

Location	Primary Structural Peak Acceleration	Assumed Amplification of Transient	Approximate Peak Transient Acceleration for Equipment
PS	4.5	3	14
FER	2.3	3	7
AER	3.5	3	11

Shock Spectra Data. Shock spectra analysis data is presented since it provides an indication of energy distribution (with respect to frequency) of the various transient oscillations. This data has been used in the past in qualification testing for transients to establish an equivalent steady state sinusoidal test level which produces the same peak response in a viscously damped single-degree-of-freedom system as would the transient being tested for. Recently, a transient excitation technique has been developed which uses shock spectra as the control media, rather than waveform which is examined to ensure that peak transient acceleration values exceeded predicted flight levels and that frequency content is consistent with flight values. Reference (5) describes a typical LMSC transient test program.

The shock spectra presented represent the maximum response of a simple, viscously-damped, base-driven single-degree-of-freedom system to the given transient excitation being studied. This response, obtained by digital computer techniques, is plotted against the frequency of resonance of the single-degree-of-freedom system. The response plotted represents the absolute value of response of the "mass element" of the hypothetical single-degree-of-freedom system rather than the differential response between the "mass element" and the driven base. It should be noted that, for the contract extension vehicles, shock spectra analyses of the ignition and shutdown events were run using base excitations which included oscillatory motions and also the rigid body motions associated with the changes in "rigid-body" accelerations resulting from changes in vehicle thrust levels. In order to completely define the effects of the transient environment in shock spectra form, it is considered necessary to include the effects of changes of "rigid-body" acceleration level since these motions also affect the responses of equipment and secondary structure. The LMSC computer program did not have capability for including these effects until recently. For this reason only the contract extension vehicles were analyzed in this fashion.

The computer program can be run for various values of viscous damping for the hypothetical single-degree-of-freedom system, defined by the amplification at resonance (Q value).

Envelopes of shock spectrums of transients observed on primary airframe during various significant events are presented in Figures 103 through 149 for Q values of, in most cases, 5, 10, and 30.

In some cases, the "flat" frequency responses of the measurements were limited by the vehicle telemetry system to values as low as 100 cps, however substantial data was provided which was based upon measurements having minimum frequency response in excess of 400 cps. Table 9 summarizes the "flat" frequency responses of measurements used in establishing envelopes of the shock spectrums, and establishes the number of measurements for which the "flat" frequency responses exceed the values of 100 cps, 200 cps, 300 cps, and 400 cps.

The series of shock spectrums corresponding to the Thor and TAT liftoff events (Figures 103 through 107, and 113 through 117) reveal that substantial excitation of the vehicle primary longitudinal natural frequency, approximately 15 cps, occurs. Other response frequencies are thought to be associated by dynamic characteristics of the structure adjacent to the measurements.

The series of shock spectra plots for Thor and TAT main engine shutdown event (Figures 108 through 112) again reveals excitation of the vehicle fundamental longitudinal vibration mode. Also, significant energy is present at approximately 60 cps which corresponds to a theoretical fourth longitudinal vibration modal frequency of the vehicle.

Figures 118 through 127 present shock spectra data for Atlas liftoff, main engine shutdown and sustainer shutdown. A unique disturbance, in the form of a torsional response of the vehicle, has persistently appeared during the Atlas main engine and sustainer engine shutdown sequences, especially in the Ranger vehicle configuration. This phenomena, thought to be due to a coupling between the axial, bending, and torsional vehicle vibration modes when excited by perturbations in the combustion processes occurring at the engine shutdown, is displayed in the form of a transient oscillation having a principal frequency of approximately 70 cps. Large shock spectra responses for this event appear at this frequency in Figure 123.

Table 9

NUMBER OF MEASUREMENTS USED TO ESTABLISH SHOCK SPECTRA ENVELOPES VERSUS MEASUREMENT TELEMETRY FREQUENCY RESPONSE

Event	Location in Vehicle	Number of Measurements			
		Frequency Response			
		100 cps	200 cps	300 cps	400 cps
Atlas Liftoff	PS	6	5	2	2
	FER	8	5	5	5
	AER	–	–	–	–
Atlas MECO	PS	18	15	9	–
	FER	4	1	–	–
	AER	1	1	1	1
Atlas SECO	PS	8	5	2	2
	FER	–	–	–	–
	AER	–	–	–	–
Thor Liftoff	PS	5	2	1	1
	FER	4	1	–	–
	AER	1	1	1	1
Thor and TAT MECO	PS	4	2	1	1
	FER	7	–	–	–
	AER	1	1	1	1
TAT Liftoff	PS	3	2	1	1
	FER	3	–	–	–
	AER	1	–	–	–
Agena First Ignition	PS	17	13	11	11
	FER	14	5	3	3
	AER	12	7	1	1
Agena First Shutdown	PS	17	11	7	7
	FER	16	8	7	7
	AER	9	6	–	–
Agena Second Ignition	PS	8	8	8	8
	FER	1	–	–	–
	AER	1	–	–	–
Agena Second Shutdown	PS	7	5	3	3
	FER	7	5	2	2
	AER	1	–	–	–

As in the case of the Atlas, Thor, and TAT booster systems, the significant responses of the payload and Agena forward section during the Agena ignition and shutdown events occur primarily at frequencies corresponding to the fundamental longitudinal natural frequency of the vehicle which can vary from 50 to 60 cps. Payload responses often occur in the frequencies associated with the primary payload branch vibration mode (e.g., see responses at 36−40 cps in Figure 134).

Responses in the Agena aft section are principally associated with the primary aft section branch vibration mode which falls in the frequency range 70−90 cps. Shock spectra data for primary airframe corresponding to Agena events are shown in Figures 128 through 149.

Because of the scarcity of data, maximum shock spectra for equipment in the payload, Agena forward section and Agena aft section, were established by making extensive use of data obtained from the Reference (5) transient simulation test. The Agena ignition and shutdown events are assumed to produce the most severe transient environments on equipment since experience during tests of Agena structures has revealed that equipment substructure primary resonances generally occur in the frequency ranges excited during these events. During the transient tests, transient responses of equipment and of adjacent primary airframe were recorded on magnetic tape from which shock spectrum analyses were prepared. Using these shock spectrums, equipment support structure transmissibility curves, plotted as a function of frequency, were established by dividing the shock spectra response for each equipment at discrete frequencies by the corresponding shock spectrum responses for the adjacent primary structure. An envelope of the most severe transmissibility characteristics of all equipment support structures is shown in Figure 150. This was applied to envelopes of shock spectrums established for the Agena ignition and shutdown events for the payload, Agena forward section and Agena aft sections, to arrive at maximum shock spectrums for equipment in these areas of the vehicle. These are shown in Figures 151, 152, and 153.

Gust and Aerodynamic Buffet Responses

Oscillogram data from 19 Atlas-boosted, 13 Thor-boosted, and 8 TAT-boosted vehicles was examined for indications of structural dynamic responses due to forces produced by wind gust and aerodynamic buffeting during the periods of atmospheric flight. The vehicles selected represent a wide variety of payload weight and payload shroud configurations. Among the vehicles analyzed were two Thor-boosted vehicles having "hammerhead" shrouds with maximum diameters of 72 inches (Agena diameter 60 inches) and three Atlas-boosted vehicles each having a maximum shroud diameter of 65 inches. These large diameter shroud configurations were chosen since it was felt that they would exhibit the most severe buffet characteristics.

In providing data regarding wind gust and buffet responses, extensive use was made of measurements obtained from accelerometers located on the guidance module in the Agena forward section. The natural frequencies of these Y axis and Z axis accelerometer installations are 35 cps and 50 cps, respectively. Since the response data observed was confined to the frequency range 2 to 19 cps, the data is considered to be valid.

Appendix B (Tables A, B, and C) summarize the responses observed at the Agena forward section, including frequencies excited, flight time of occurrence, and Mach number at time of occurrence.

In general, the largest responses have been observed at transonic Mach numbers and on the vehicles having "hammerhead" shroud configurations (i.e., vehicles having maximum shroud diameters larger than that of the Agena). It is therefore felt that the most severe vehicle responses observed are due to aerodynamic buffeting rather than wind gust, since these configurations and flight conditions more readily promote vehicle buffeting.

Table 10 summarizes the maximum gust and buffet responses observed in the Agena forward section at Station 255.

Table 10

MAXIMUM WIND GUST AND BUFFET RESPONSES OBSERVED AT AGENA FORWARD SECTION (STATION 255)

Booster	Mode	Approximate Frequency (cps)	Response at Station 255 G's (0-Peak)	Configuration Observed; Maximum Shroud Diameter (inches)	Theoretical Maximum Gust Response (G's)	Theoretical Maximum Buffet Response (G's)
Atlas	1	2.5	0.16	65	.16	.18
	2	7.0	0.17	65	.012	.16
	3	10.0	0.15	62	.16	.41
	P/L Mode	20.0	0.22	60	–	.13
Thor	1	4.5	0.10	72	.07	–
	2	10.0	0.08	60	.06	–
	3	13.0	0.34	60	.03	–
	P/L Mode	None Observed	–	–	–	–
TAT	1	3.5	0.08	60	.15	–
	2	8.0	0.06	60	.02	–
	3	12.0	0.07	60	0	–
	P/L Mode	None Observed	–	–	–	–

Appendix B (Table D) shows payload responses for two vehicle configurations. These responses, which represent approximately the motions of the payload centroid, are substantially larger than those measured in the Agena forward section. This is expected because of the modal ratio between the Agena forward section and the payload centroid. The magnitude of these responses are such that they may represent potential design conditions of payload/Agena interface structure.

Table 10 also contains vehicle responses at Station 255 which were established from theoretical buffet and wind gust analyses of representative vehicle configurations.

Theoretical 3σ buffet responses were established using the dynamic model and fluctuating pressure field data corresponding to the Ranger configuration. The method of analysis, which is described in Reference (6), was conducted using a one percent critical damping factor.

The theoretical gust responses presented were obtained by the method of analysis described in Reference (7). One TAT, one Thor and two Atlas configurations were examined. The TAT configuration (vehicle 1172) was analyzed for a (1-cosine) gust having a maximum velocity of 40 feet per second and the Thor configuration (Vehicle 6101) for a trapezoidal gust profile having a maximum velocity of 30 feet per second. The Atlas configurations analyzed were Vehicle 1351 (Program 461) and the OAO program vehicle, for which trapezoidal gust profiles having peak velocities of 30 feet per second and 25 feet per second, respectively, were assumed. The gust responses shown in Table 10 for Atlas vehicles represents the larger of the responses in each mode of the two configurations examined. In all cases the period of the gust was "tuned" to the primary bending mode of the total vehicle.

In general, the responses obtained in the theoretical buffet analysis were consistent with the responses observed in the first and second vehicle modes which contribute the majority of the total vehicle loads. In the higher modes, there is variance between the theoretical and observed response values. In these cases, a review of the assumptions made in the analysis is recommended.

The theoretical gust responses in the primary vehicle bending mode, which contributes the majority of total vehicle load, are also consistent with the observed responses, within the accuracy of the flight data analysis.

In the opinion of LMSC, theoretical analysis of projected new Agena vehicle configurations should be used to establish gust and buffet loads rather than establishing loads

from the historical response data contained in this document. This procedure is recommended since the response of the individual vehicle is very sensitive to parameters such as aerodynamic pressure distribution, and vehicle natural vibration mode shapes. Also, qualification of structures should be based upon statically, rather than dynamically, applied load.

Propulsion-Structure System Instability Oscillation

During the latter portion of Thor (and TAT) booster operations, a sinusoidal oscillation persistently appears on all vehicles which has a frequency corresponding very closely to the primary longitudinal natural frequency of the vehicle (20 cps). The oscillation, gradually builds up to a maximum amplitude at the time approximately 8 seconds prior to main engine shutdown, gradually decays again and disappears completely before main engine shutdown. This phenomena, known as propulsion-structure system instability (or "POGO"), is a result of coupling between the propulsion system and the primary longitudinal natural frequency of the vehicle.

Data has been obtained from 39 Agena B flights and 50 from Agena D flights, and due to this large data sampling it was decided to employ statistical techniques to define the environment associated with this phenomena.

All of the Agena D measurements were located in the forward section at Station 255 while the remaining Agena B data described aft section Station 409 responses. It was decided to combine both sets of data into a single population by modifying the Station 255 data by a factor of 1.4 corresponding to the primary longitudinal mode ratio between Station 255 and Station 409.

A least-square fit of all the data revealed it to be distributed more in log-normal fashion rather than in a "normal" one. Figure 154 shows the "least square fit" line for the aft section data which represents amplitude of oscillation versus percentage probability of occurrence. The corresponding plot for the forward section Station 255 was established by multiplying the aft section values by the 1.4 modal ratio.

LMSC is presently using 99% probability values as a basis for design and environmental data. These levels are: 6.5 g's and 4.64 g's (peak-to-peak) for the forward and aft sections of the Agena, respectively.

Relatively mild lateral excitation is induced by this phenomena and LMSC is presently using a 99% value of 0.74 g (peak-to-peak) for Station 255 as a basis for design.

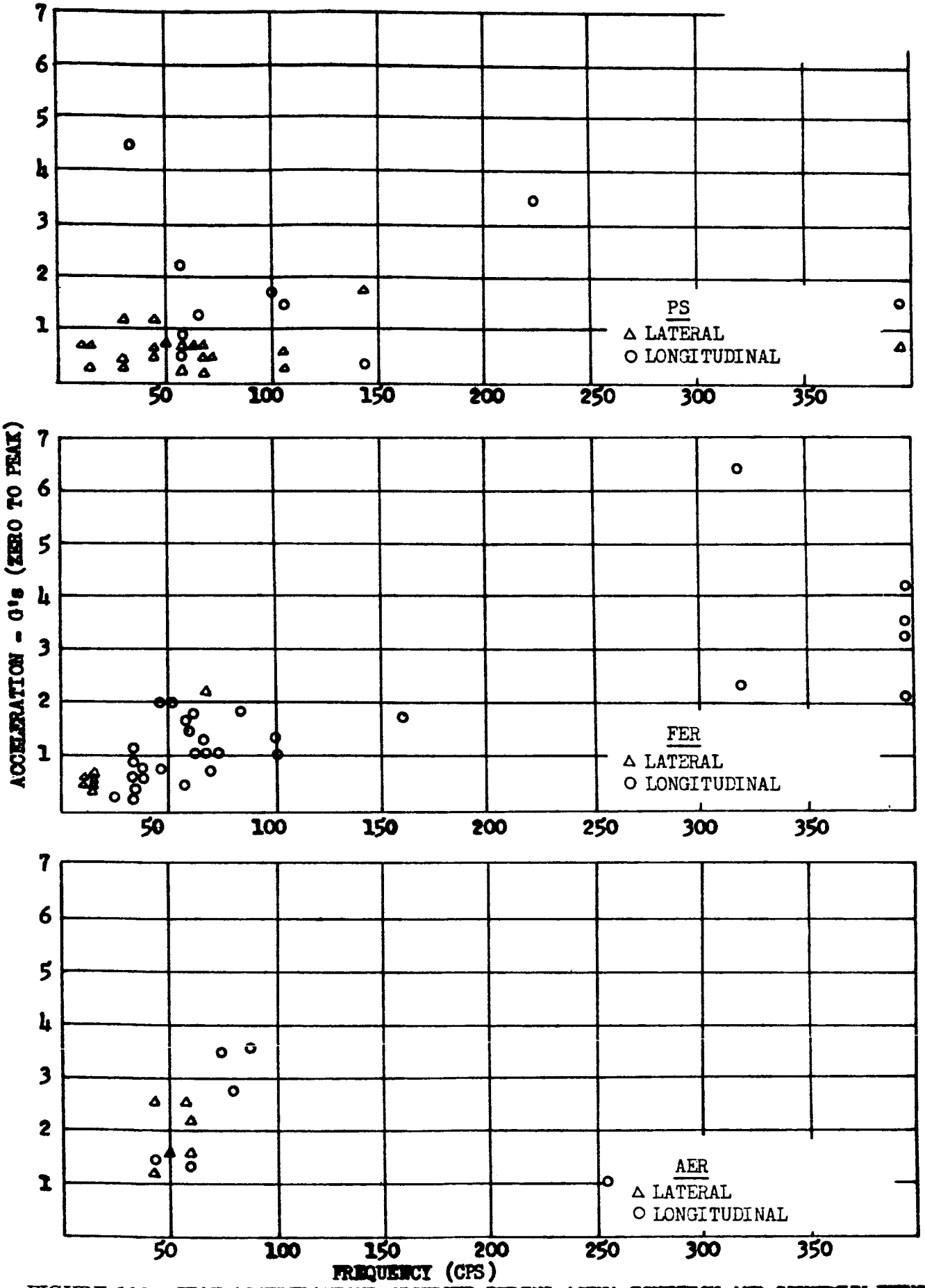

FIGURE 100 - PEAK ACCELERATIONS OBSERVED DURING AGENA IGNITION AND SHUTDOWN EVENTS

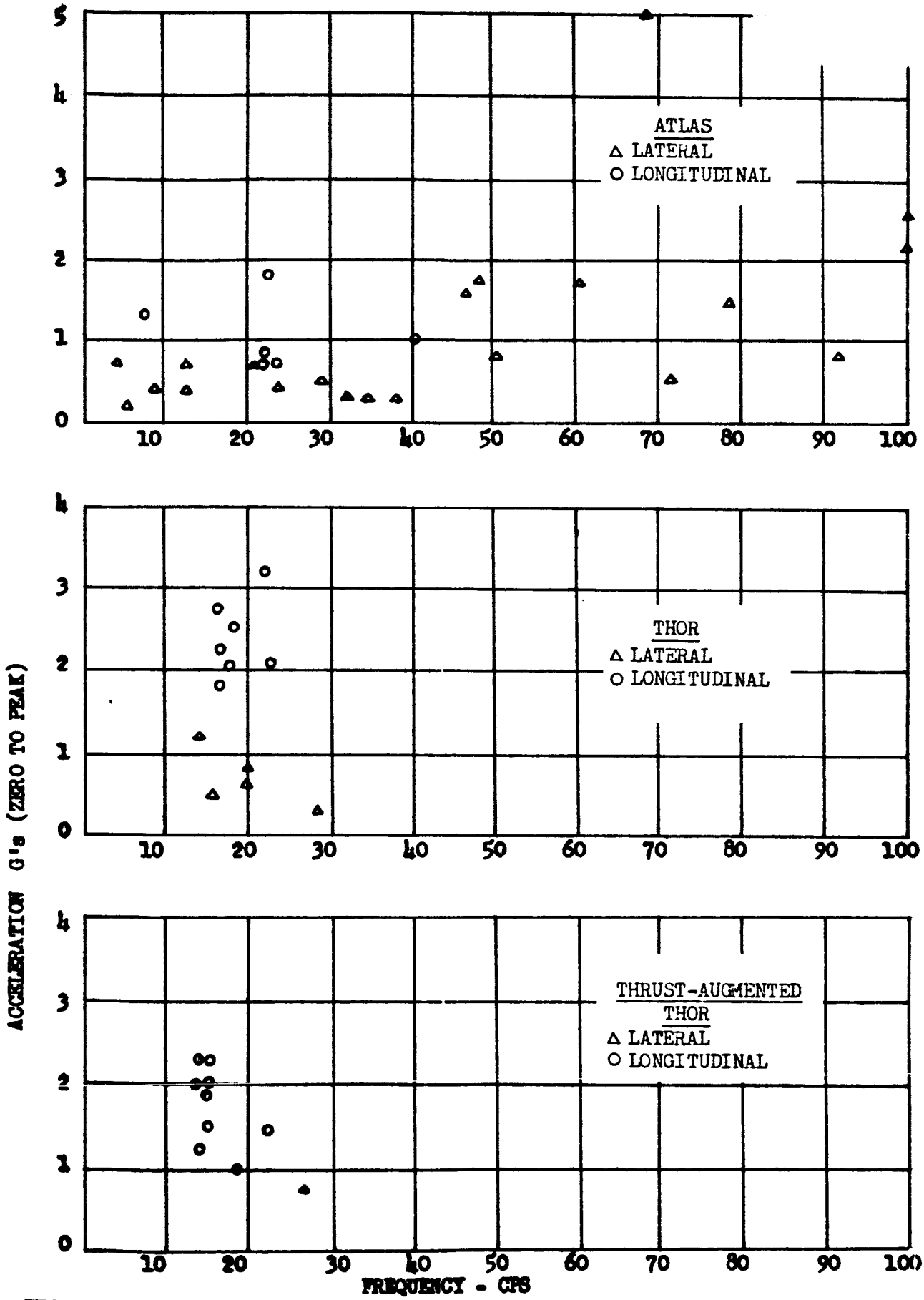

FIGURE 101 - **PEAK ACCELERATIONS OBSERVED DURING IGNITION AND SHUTDOWN EVENTS OF ATLAS, THOR AND THRUST-AUGMENTED THOR OPERATION** (ALL SECTIONS)

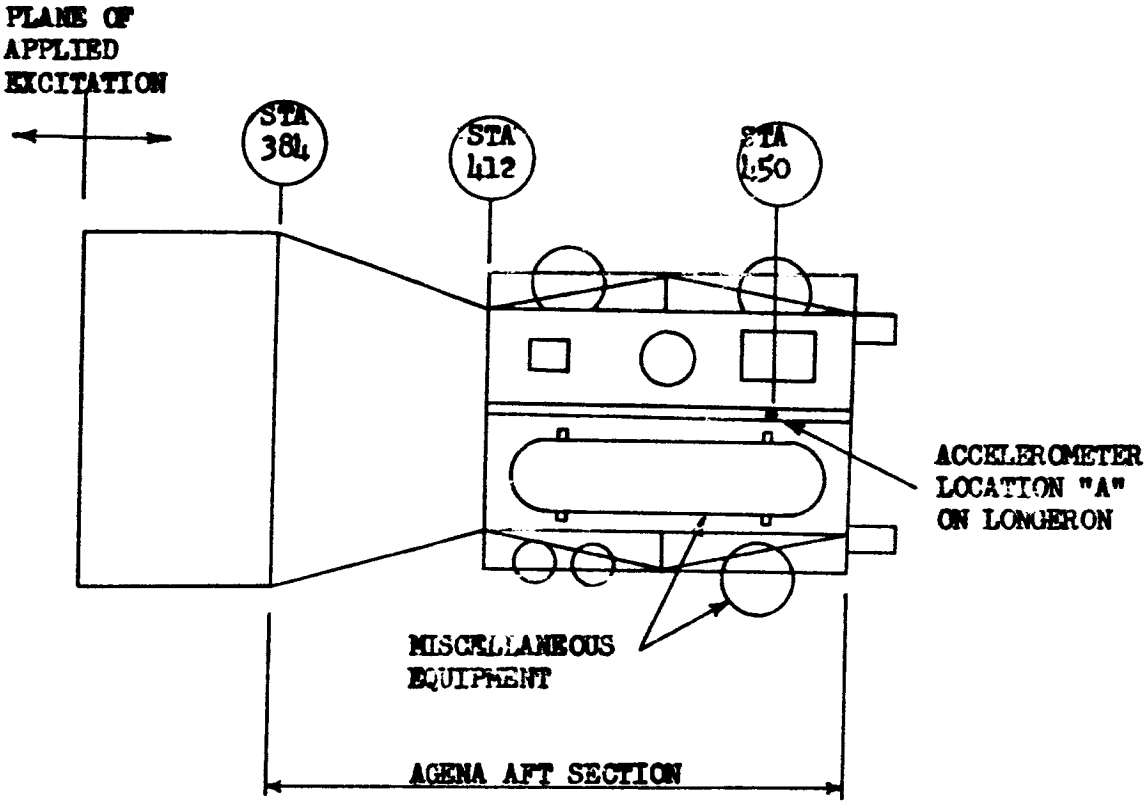

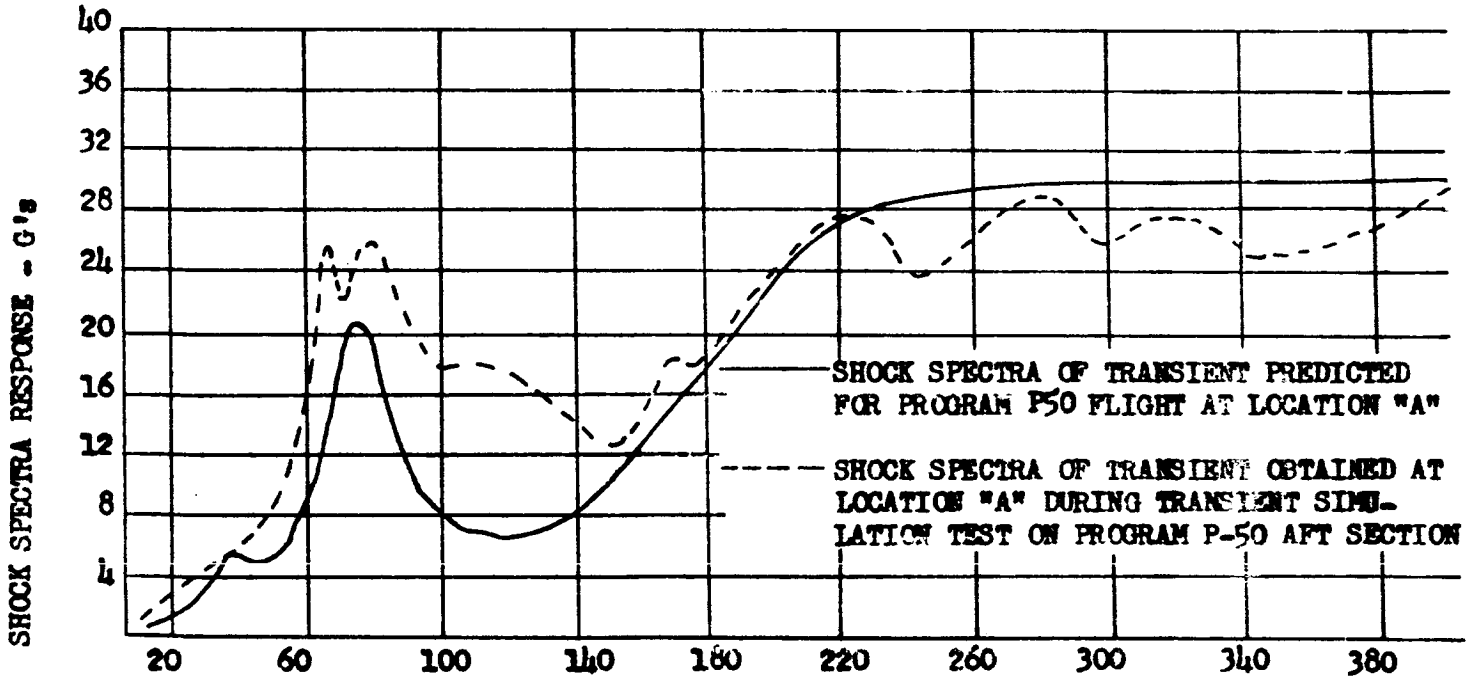

FIGURE 102 - SHOCK SPECTRA ANALYSIS OF TRANSIENT APPLIED DURING PROGRAM P-50 AER SECTION TEST VS. SHOCK SPECTRA OF TRANSIENT PREDICTED FOR PROGRAM P-50 FLIGHT

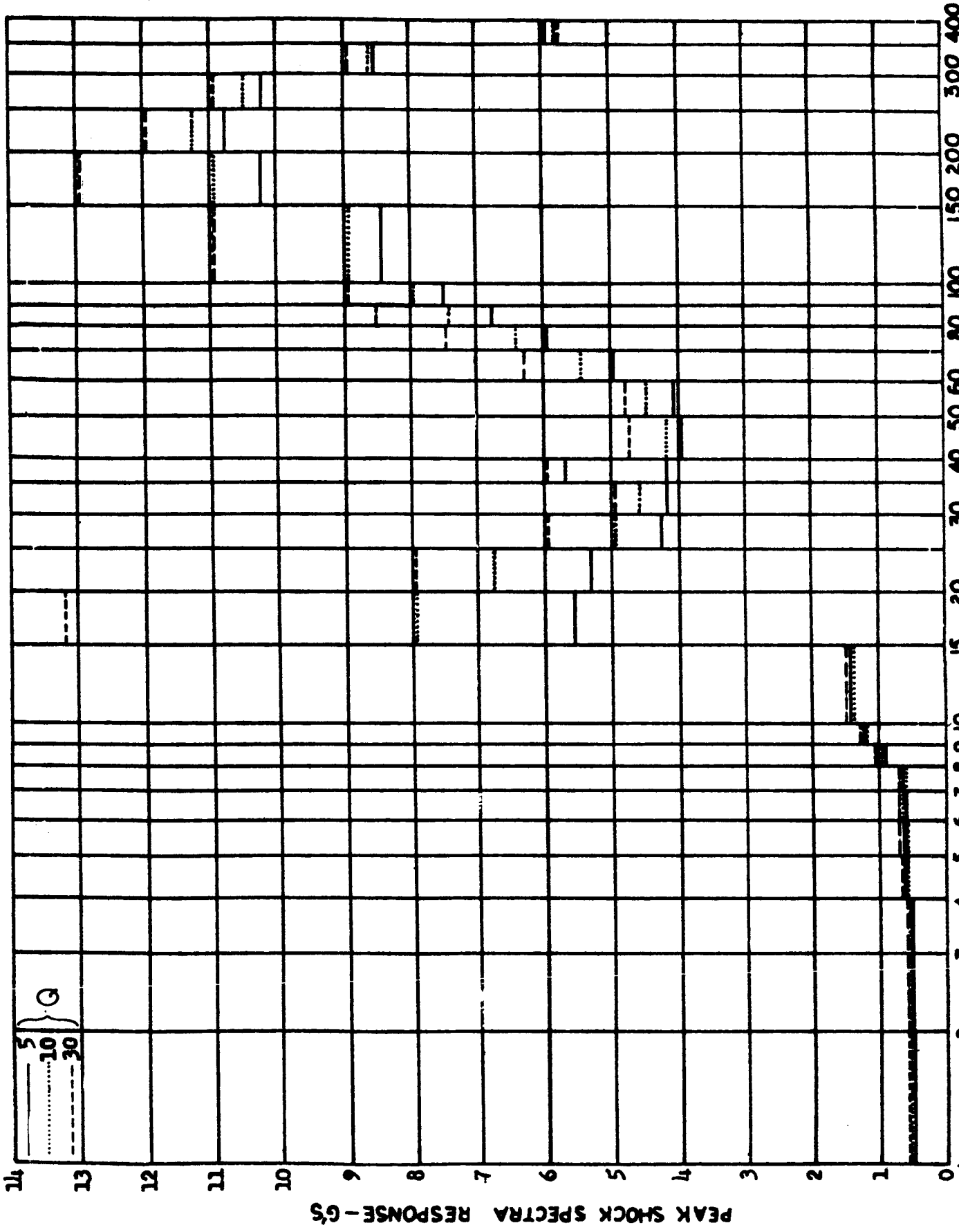

FIGURE 103 - SHOCK SPECTRUM ENVELOPE FOR THOR LIFT-OFF AT PAYLOAD (AXIAL)

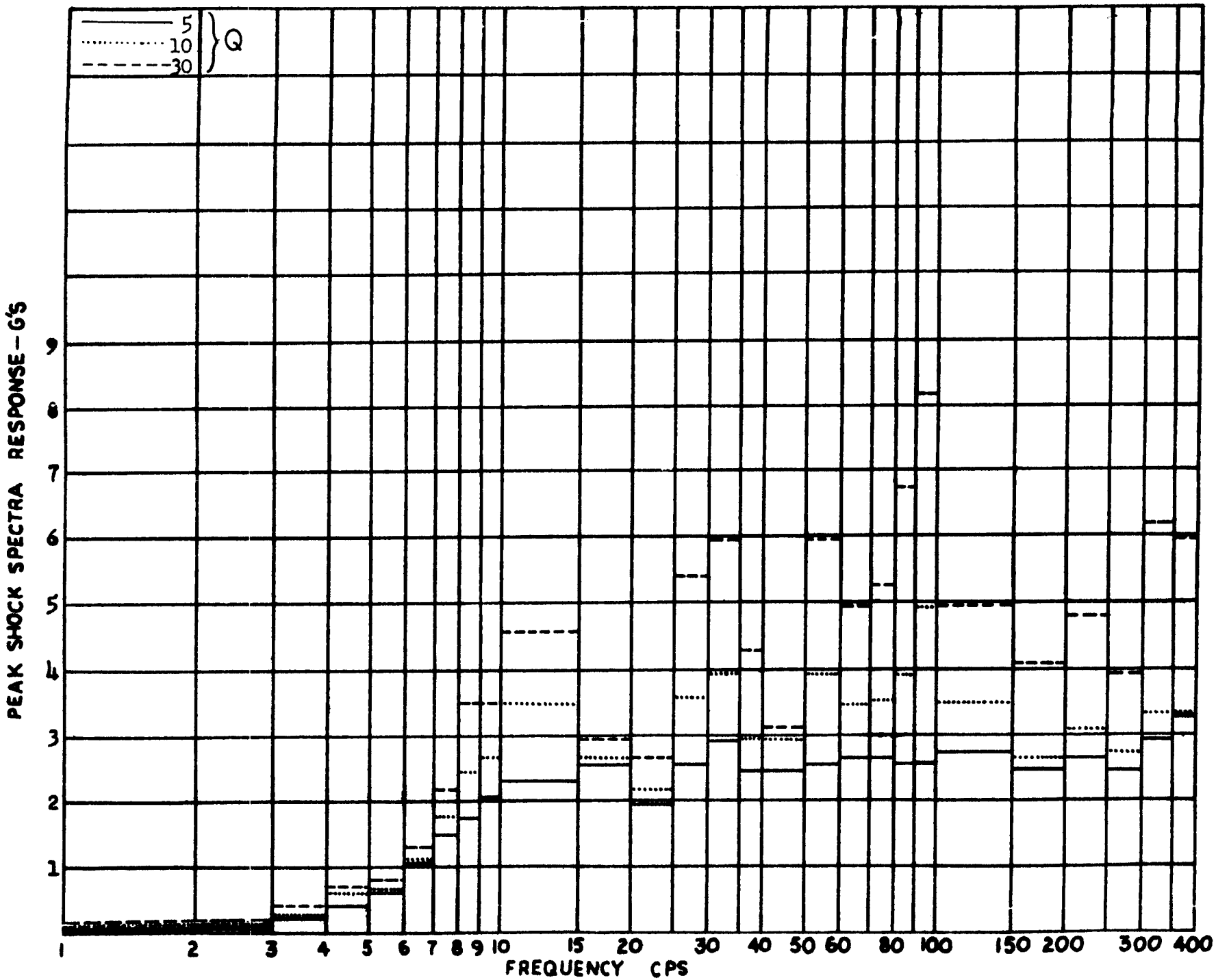

FIGURE 104 -SHOCK SPECTRUM ENVELOPE FOR THOR LIFT-OFF AT PAYLOAD (TRANSVERSE)

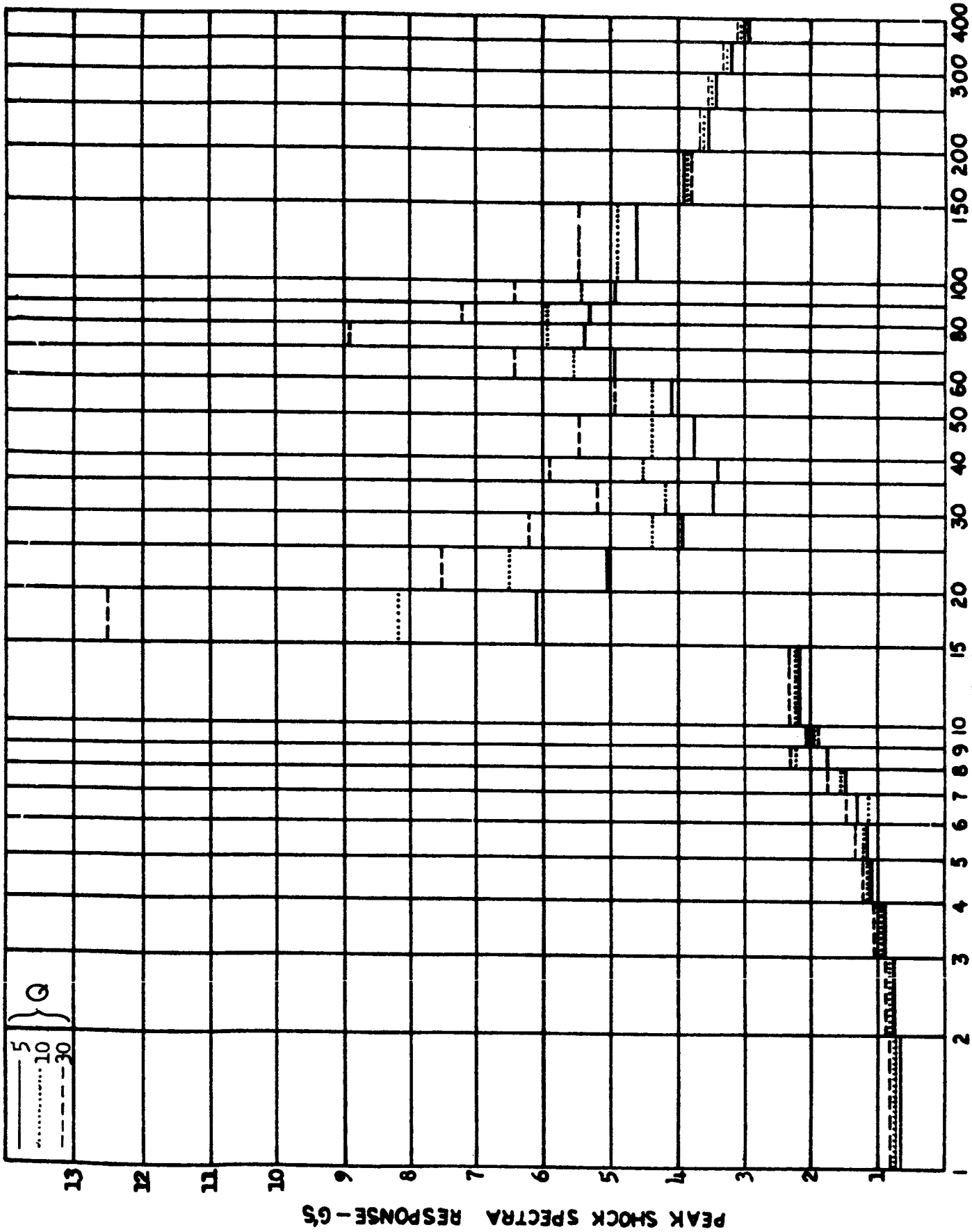

FIGURE 105 -SHOCK SPECTRUM ENVELOPE FOR THOR LIFT-OFF AT FER (AXIAL)

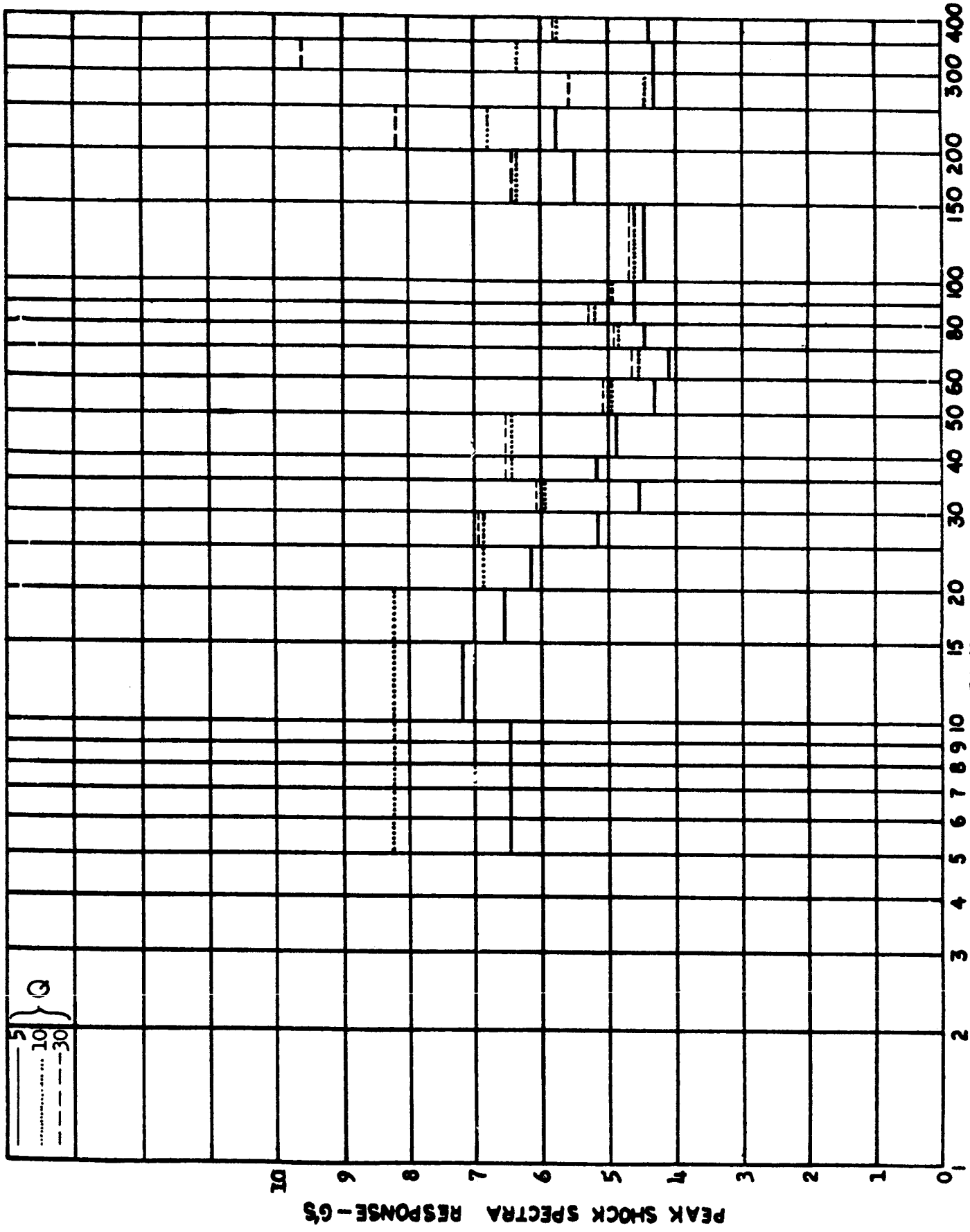

FIGURE 106 -SHOCK SPECTRUM ENVELOPE FOR THOR LIFT-OFF AT FER (TRANSVERSE)

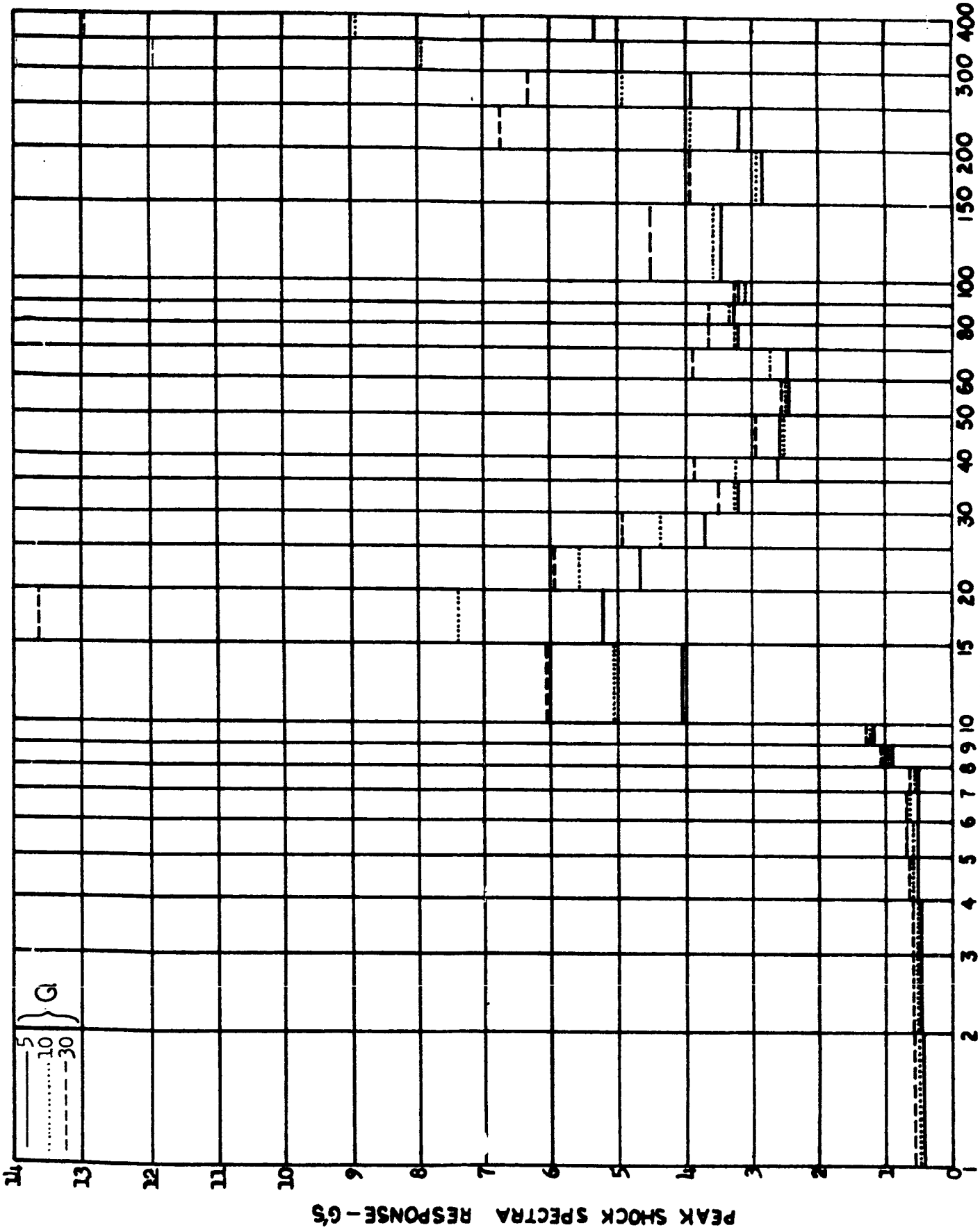

FIGURE 107 - SHOCK SPECTRUM ENVELOPE FOR THOR LIFT-OFF AT AER (AXIAL)

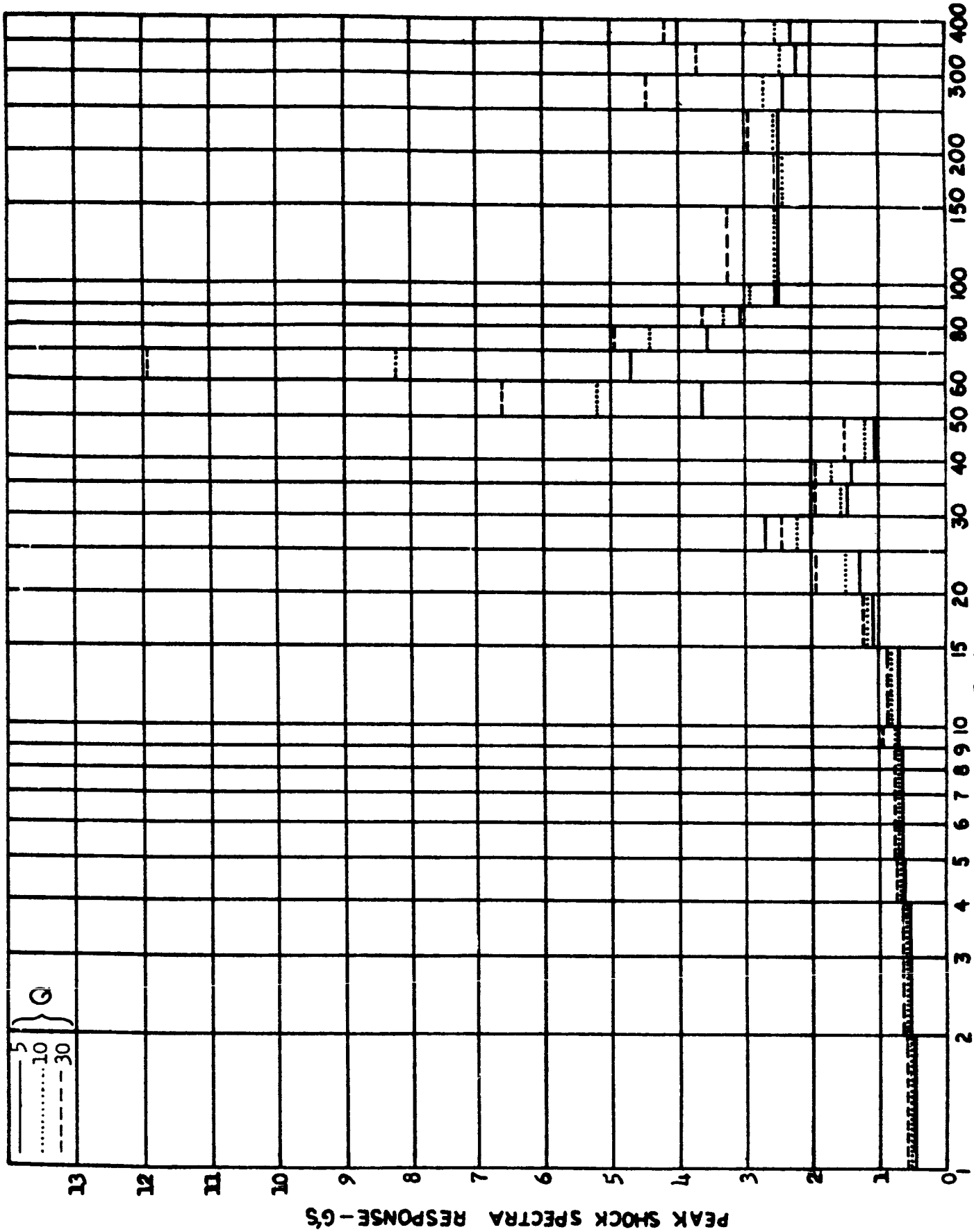

FIGURE 108 - SHOCK SPECTRUM ENVELOPE FOR THOR AND TAT MECO AT P S (Axial)

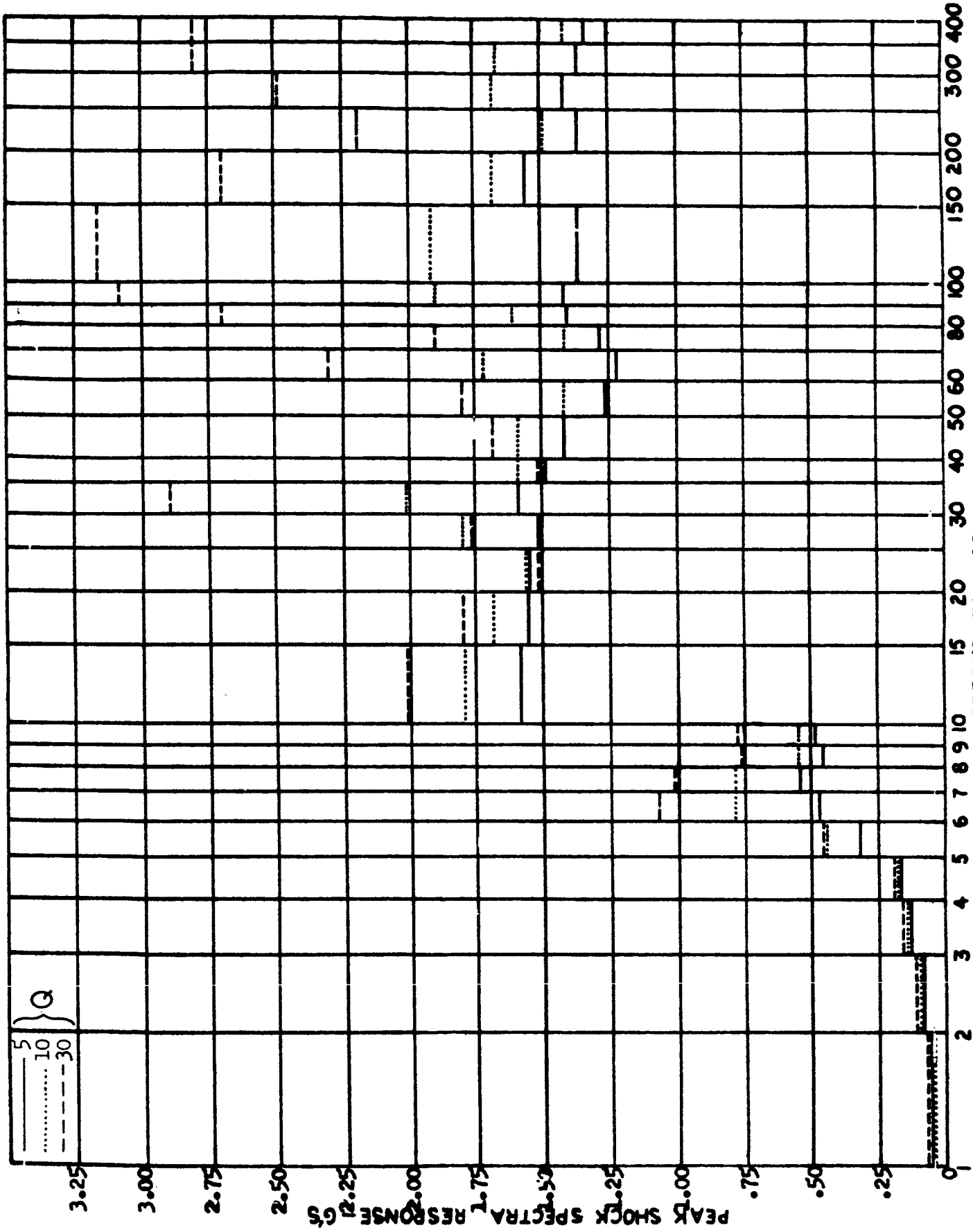

FIGURE 109 - SHOCK SPECTRUM ENVELOPE FOR THOR AND TAT MECO AT PS (TRANSVERSE)

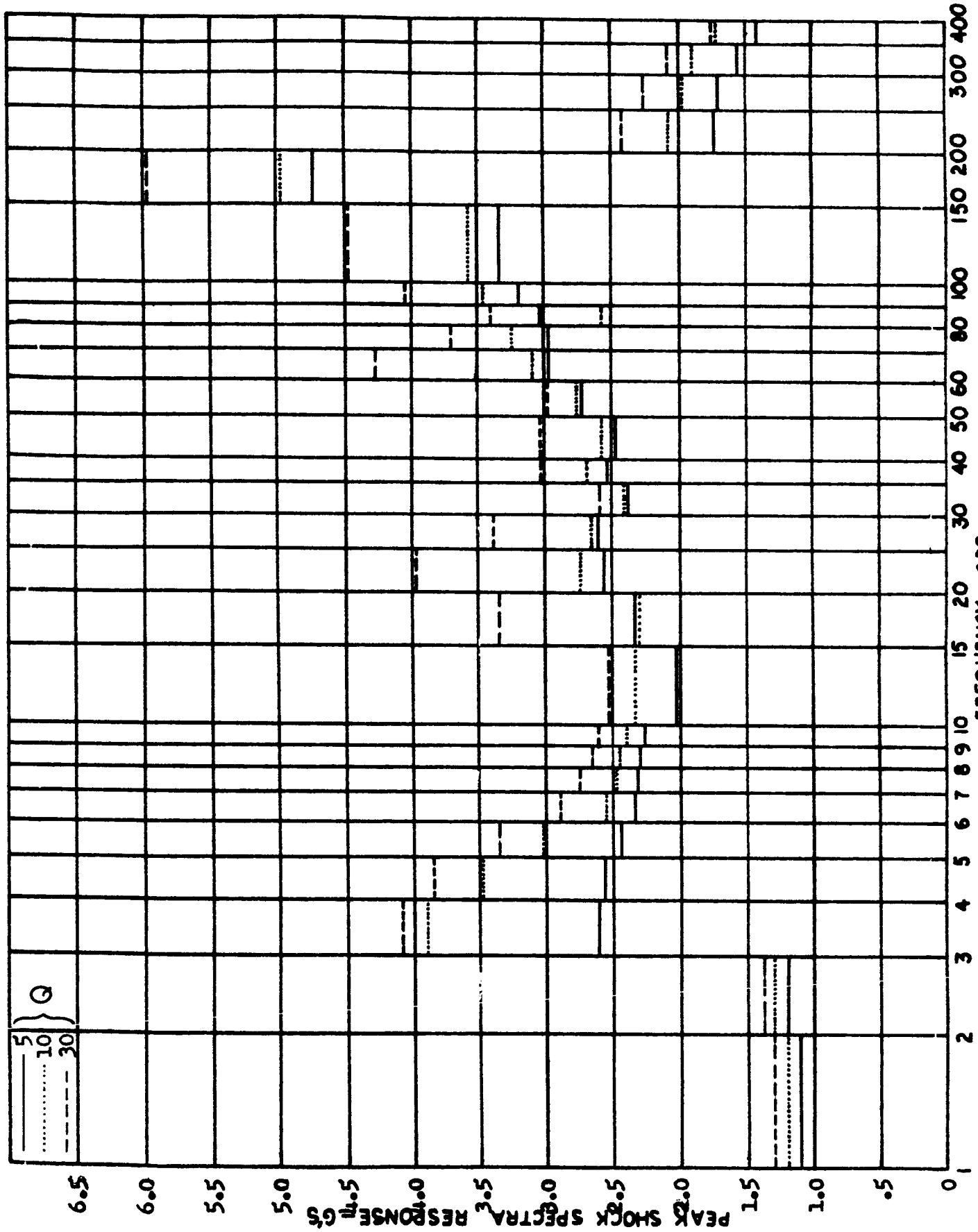

FIGURE 110 - SHOCK SPECTRUM ENVELOPE FOR THOR AND TAT MECO AT FER (AXIAL)

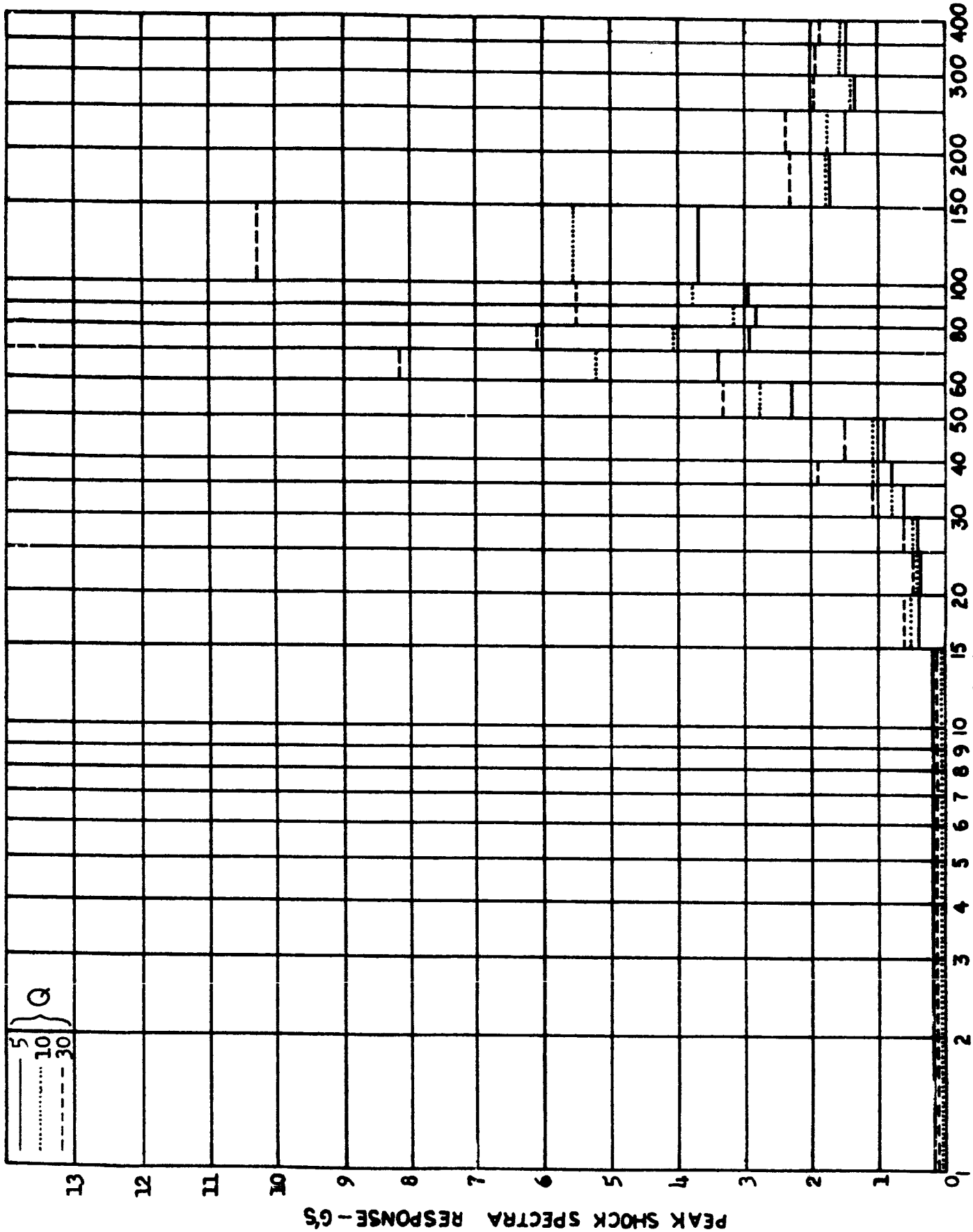

FIGURE 111 - SHOCK SPECTRUM ENVELOPE FOR THOR AND TAT MECO AT FER (TRANSVERSE)

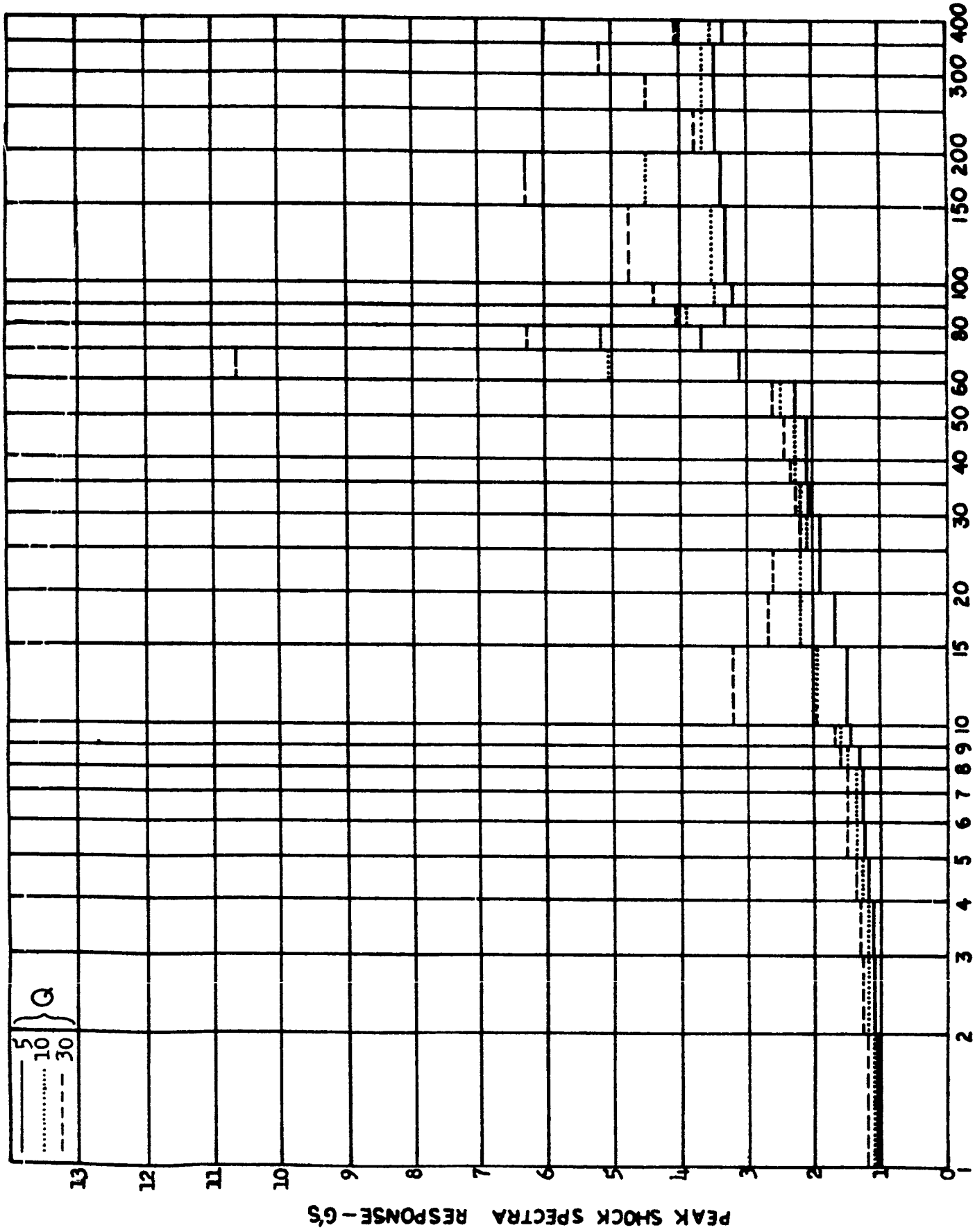

FIGURE 112 - SHOCK SPECTRUM ENVELOPE FOR THOR AND TAT MECO AT AER (AXIAL)

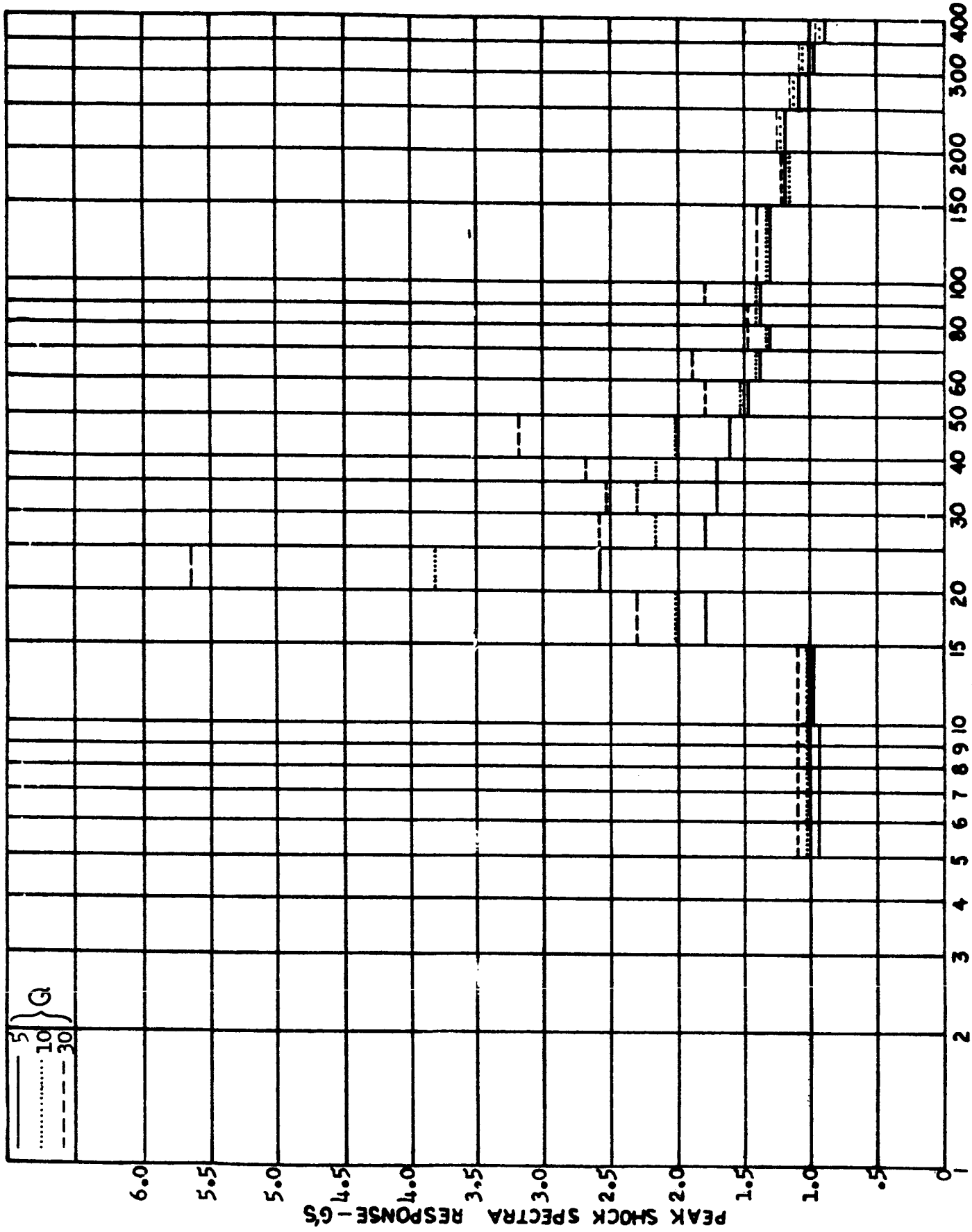

FIGURE 113 - SHOCK SPECTRUM ENVELOPE FOR TAT LIFT-OFF AT PAYLOAD (AXIAL)

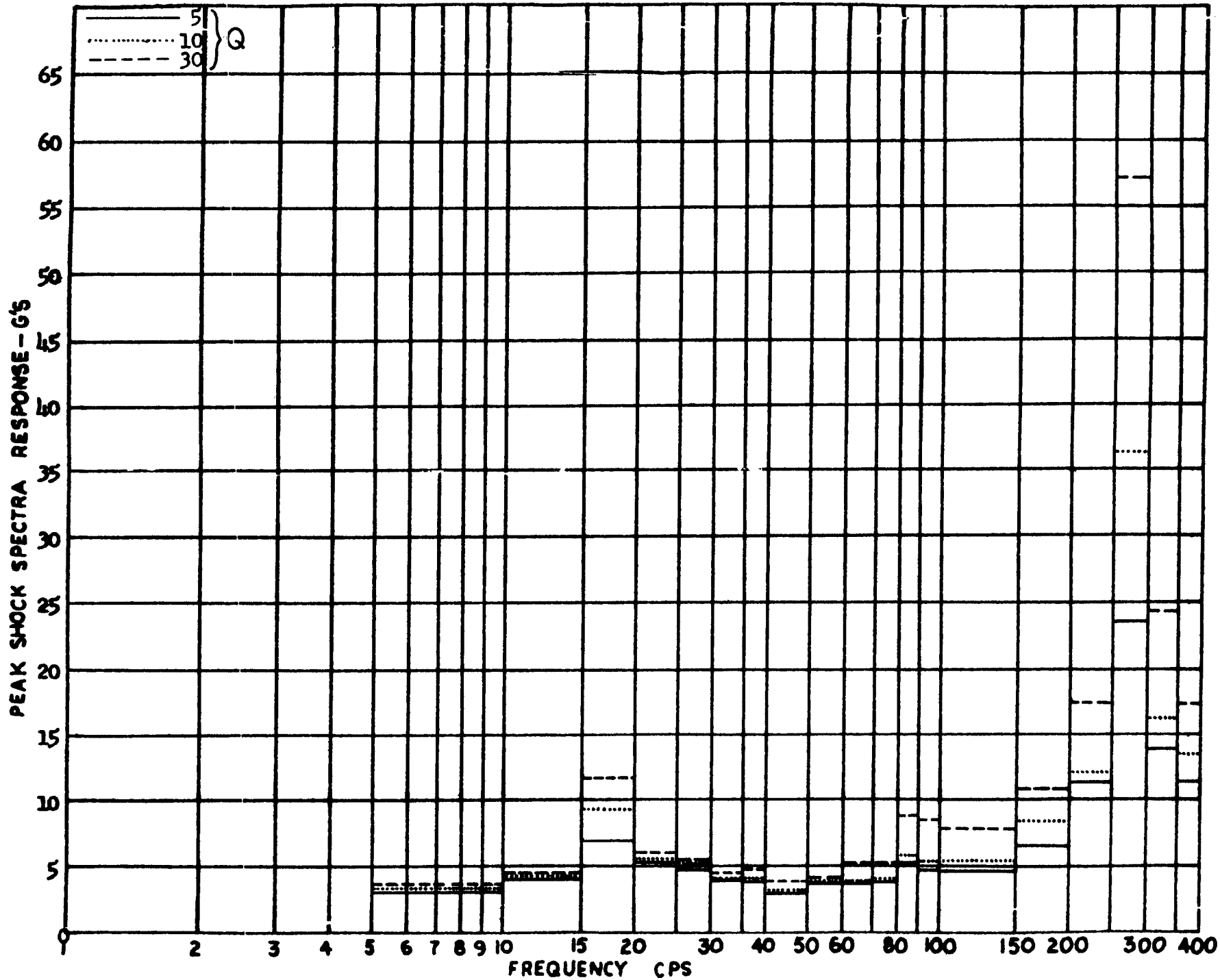

FIGURE 114 -SHOCK SPECTRUM ENVELOPE FOR TAT LIFT-OFF AT PAYLOAD (TRANSVERSE)

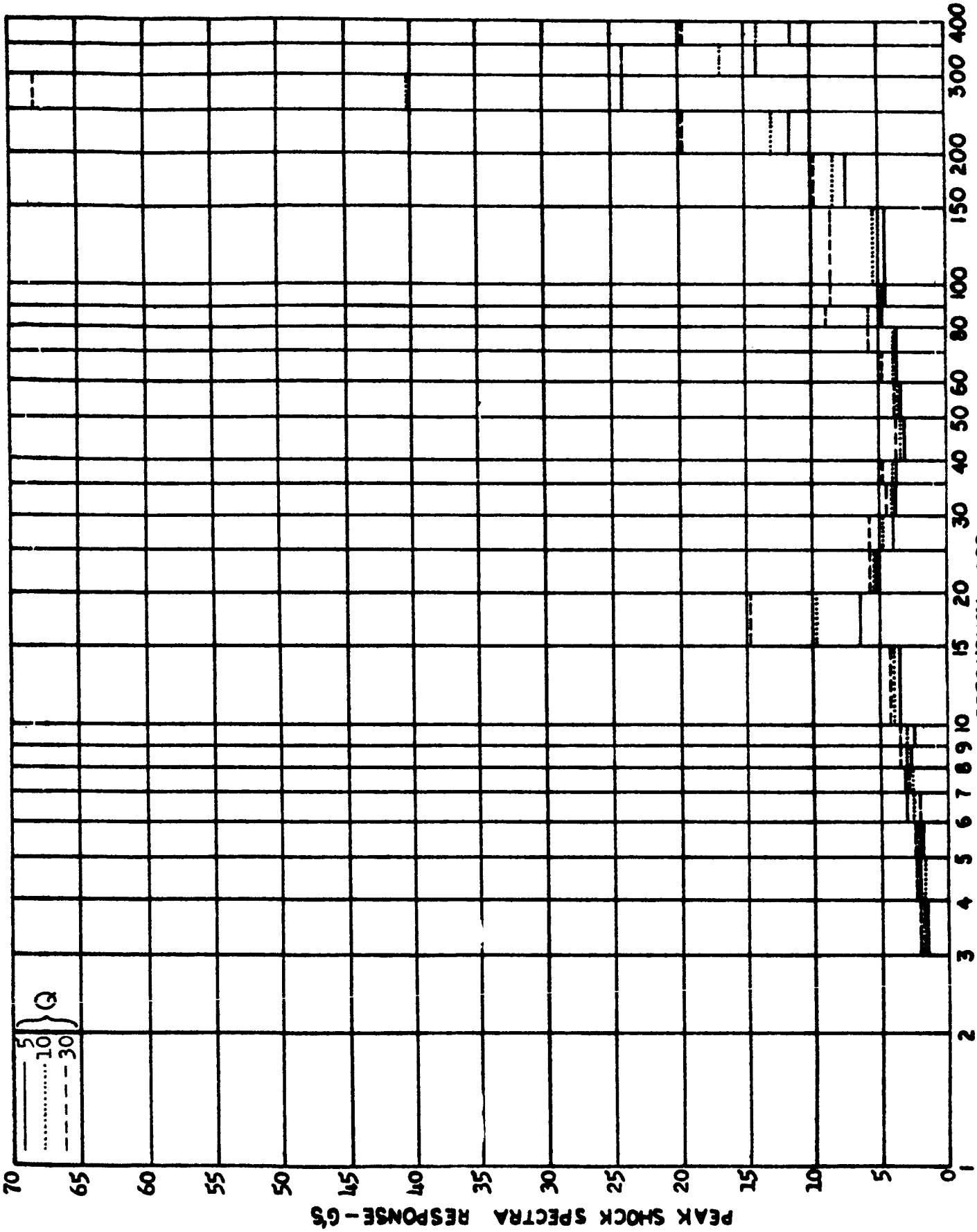

FIGURE 115 - SHOCK SPECTRUM ENVELOPE FOR TAT LIFT-OFF AT FER (AXIAL)

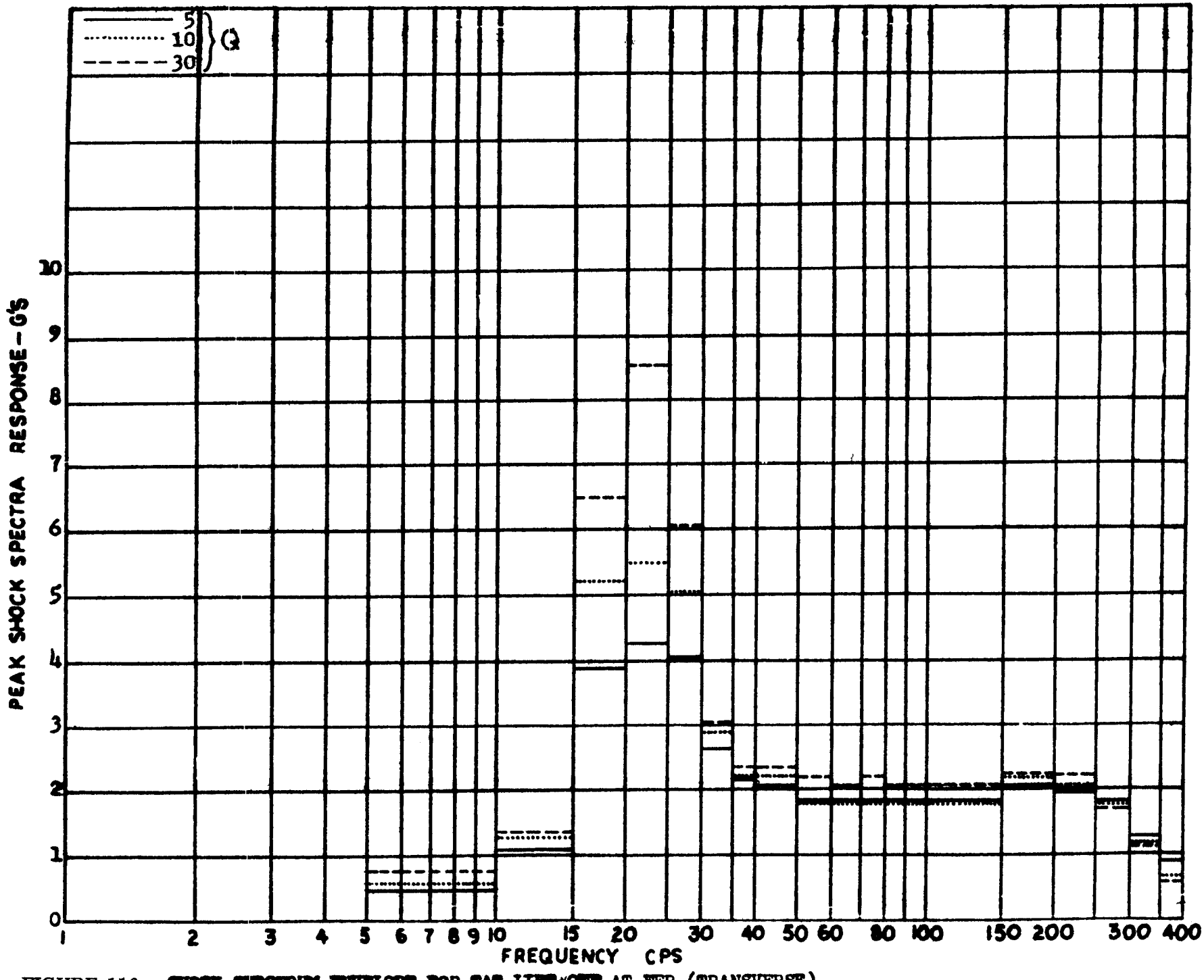

FIGURE 116 - SHOCK SPECTRUM ENVELOPE FOR TAT LIFT-OFF AT FER (TRANSVERSE)

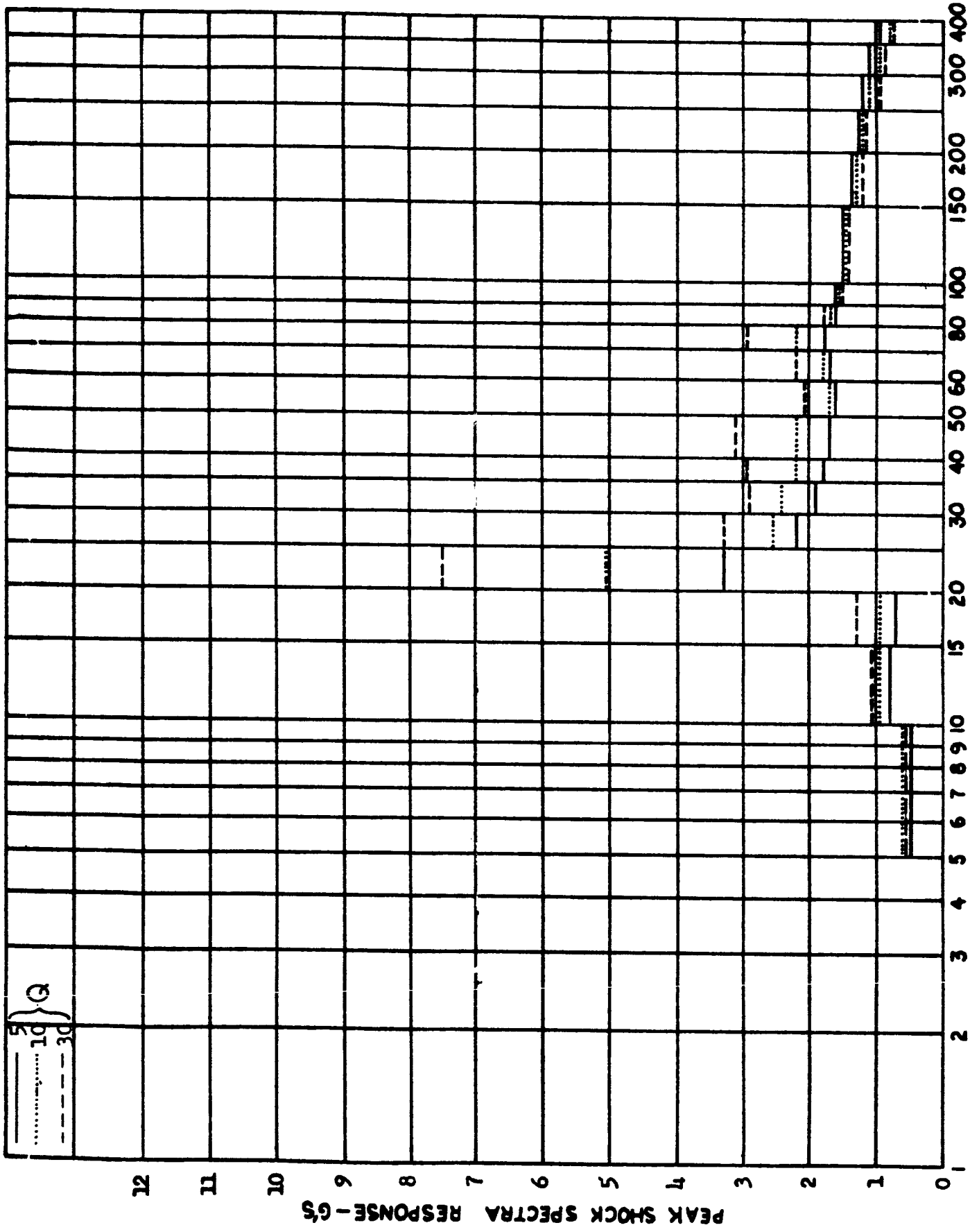

FIGURE 117 - SHOCK SPECTRUM ENVELOPE FOR TAT LIFT-OFF AT AMR (TRANSVERSE)

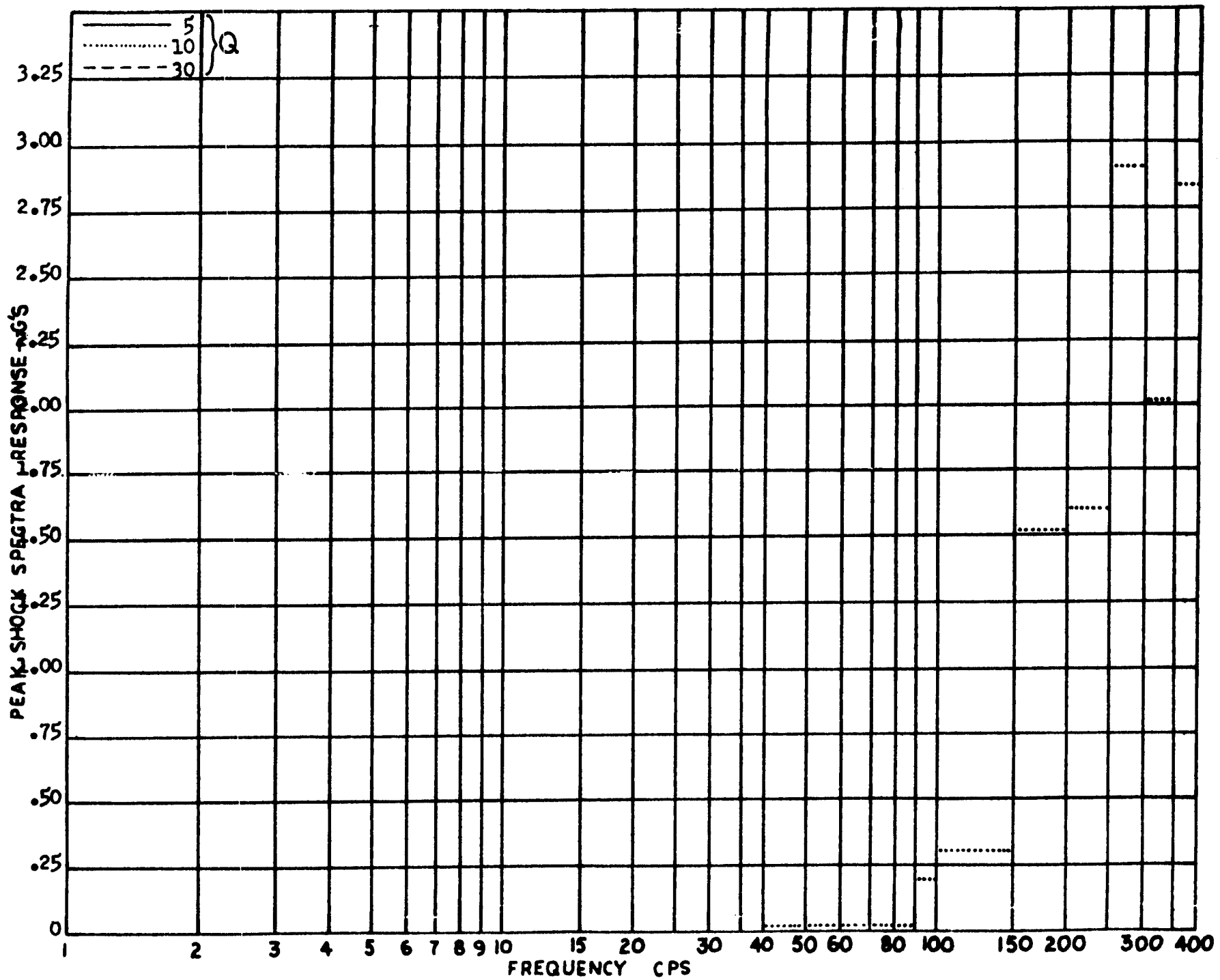

FIGURE 118 - SHOCK SPECTRUM ENVELOPE FOR ATLAS LIFT-OFF AT PS (AXIAL)

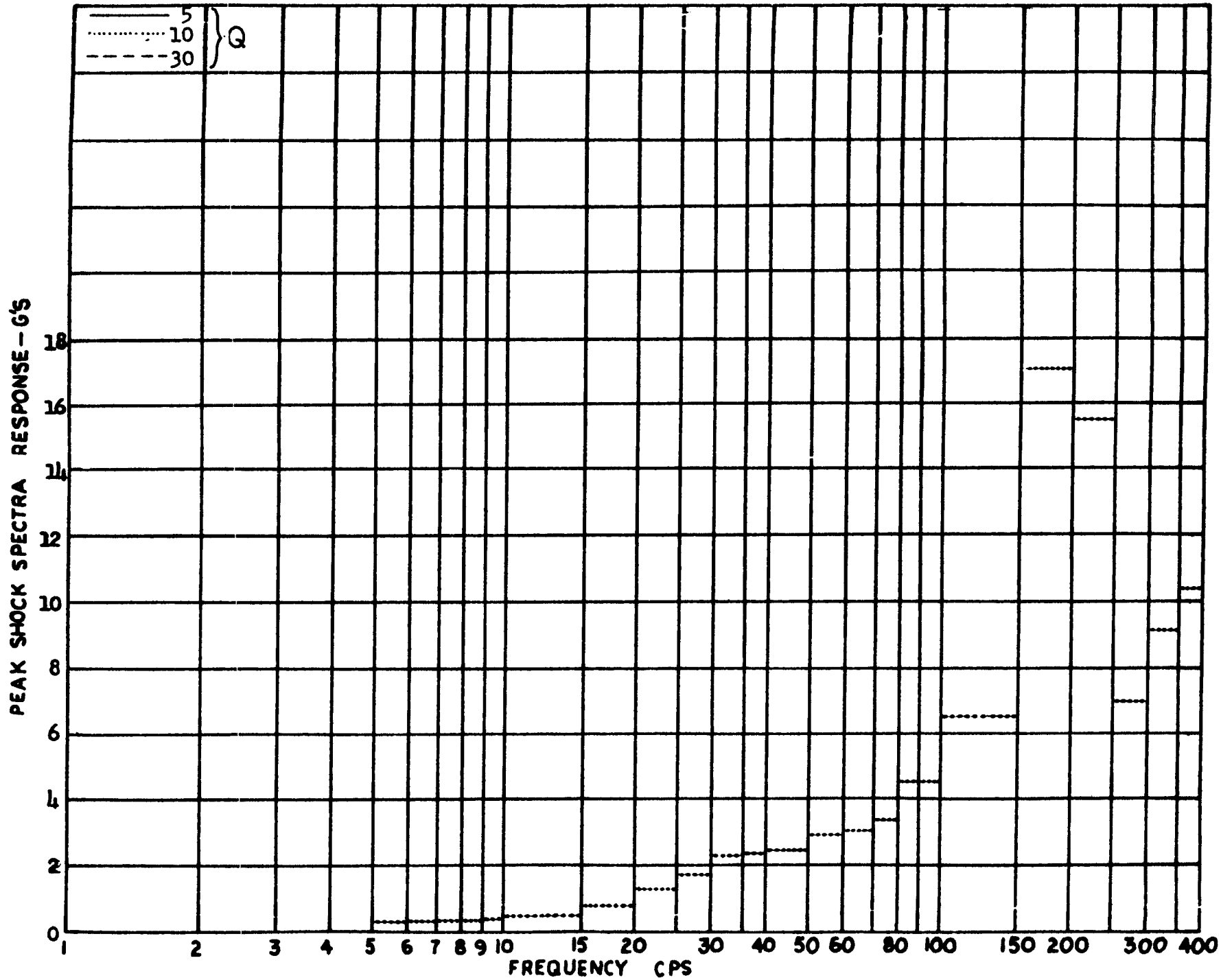

FIGURE 119 - SHOCK SPECTRUM ENVELOPE FOR ATLAS LIFT-OFF AT PS (TRANSVERSE)

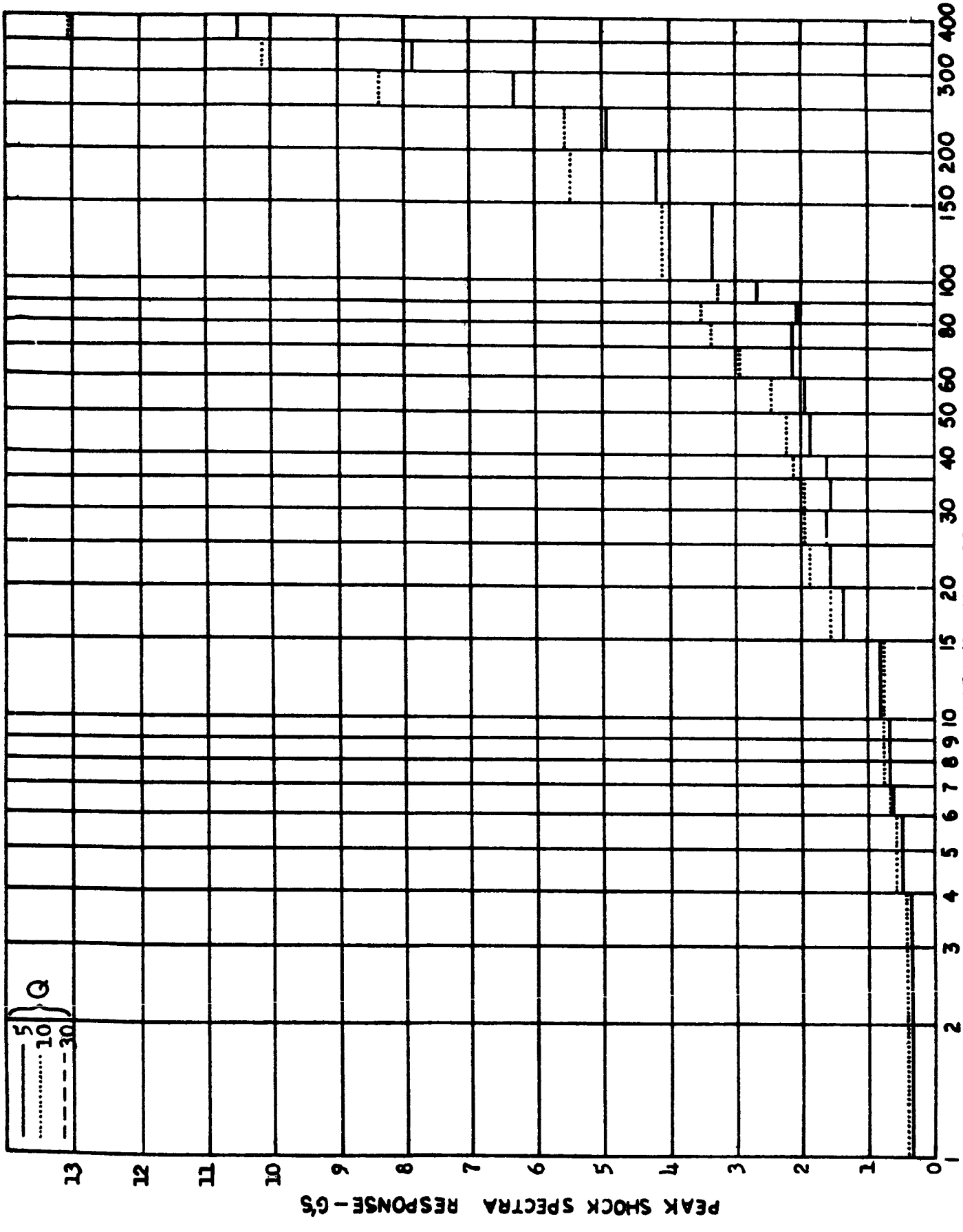

FIGURE 120 - SHOCK SPECTRUM ENVELOPE FOR ATLAS LIFT-OFF AT FER (AXIAL)

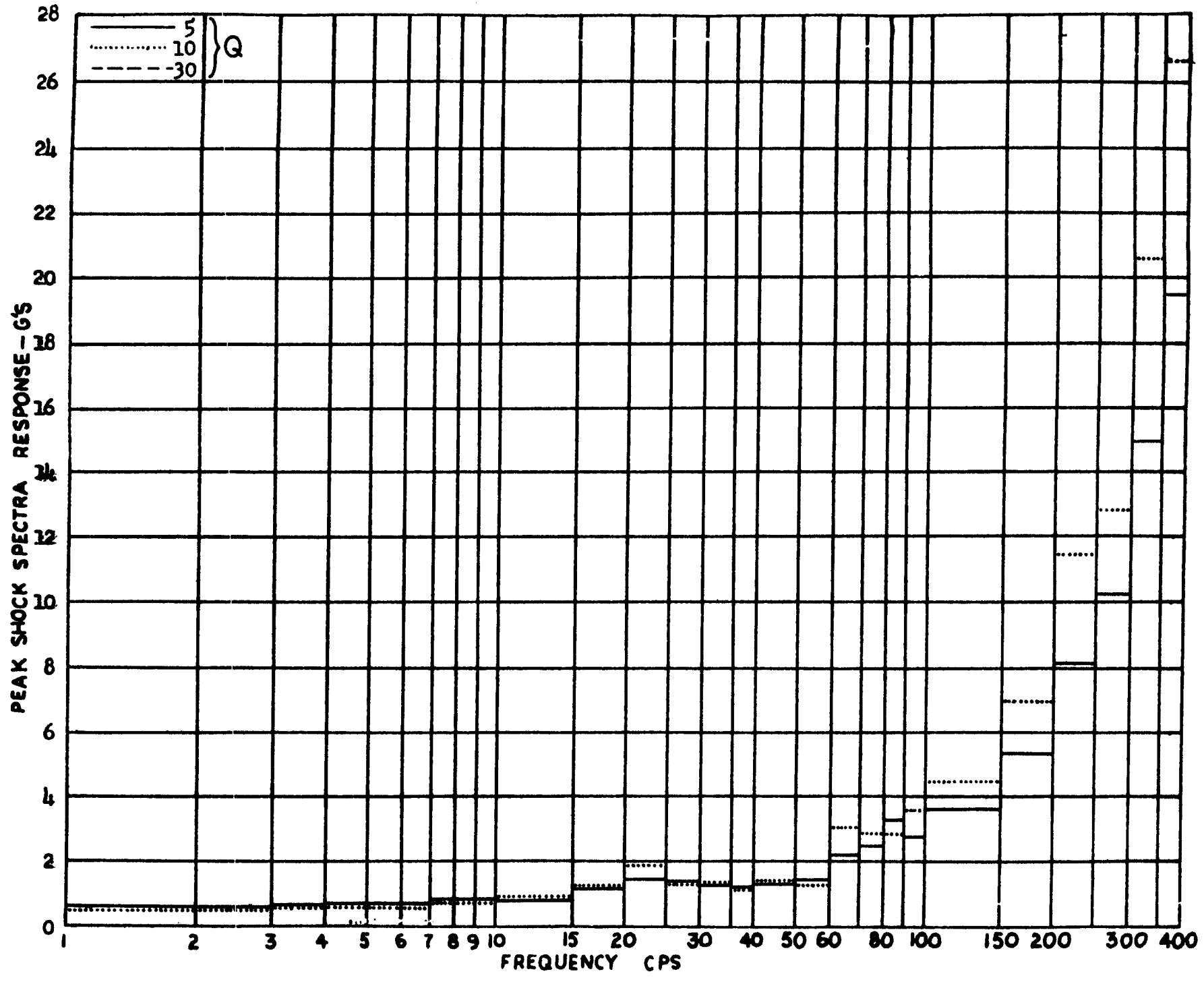

FIGURE 121 - SHOCK SPECTRUM ENVELOPE FOR ATLAS LIFT-OFF AT FER (TRANSVERSE)

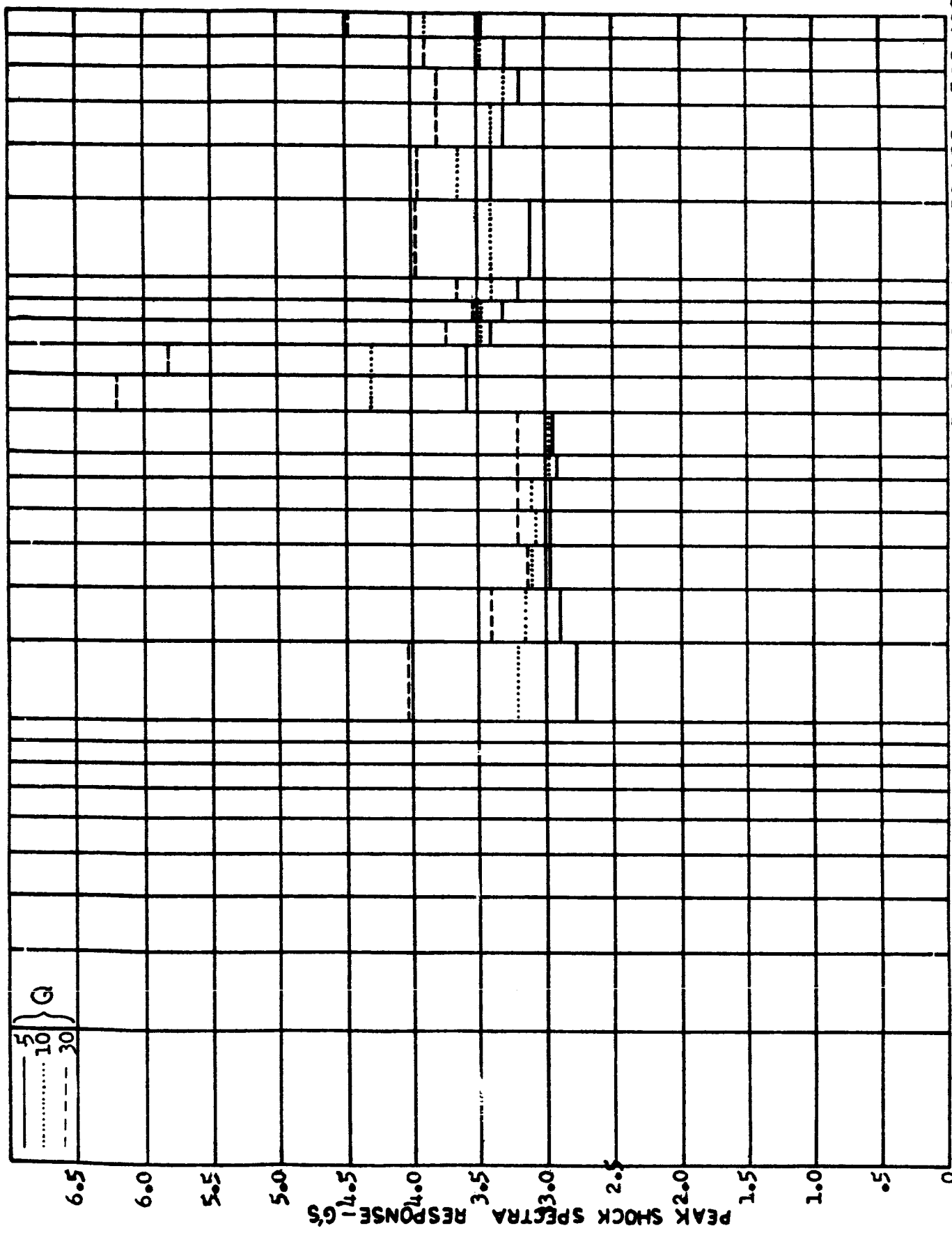

FIGURE 122 - SHOCK SPECTRUM ENVELOPE FOR ATLAS MECO AT PS (AXIAL)

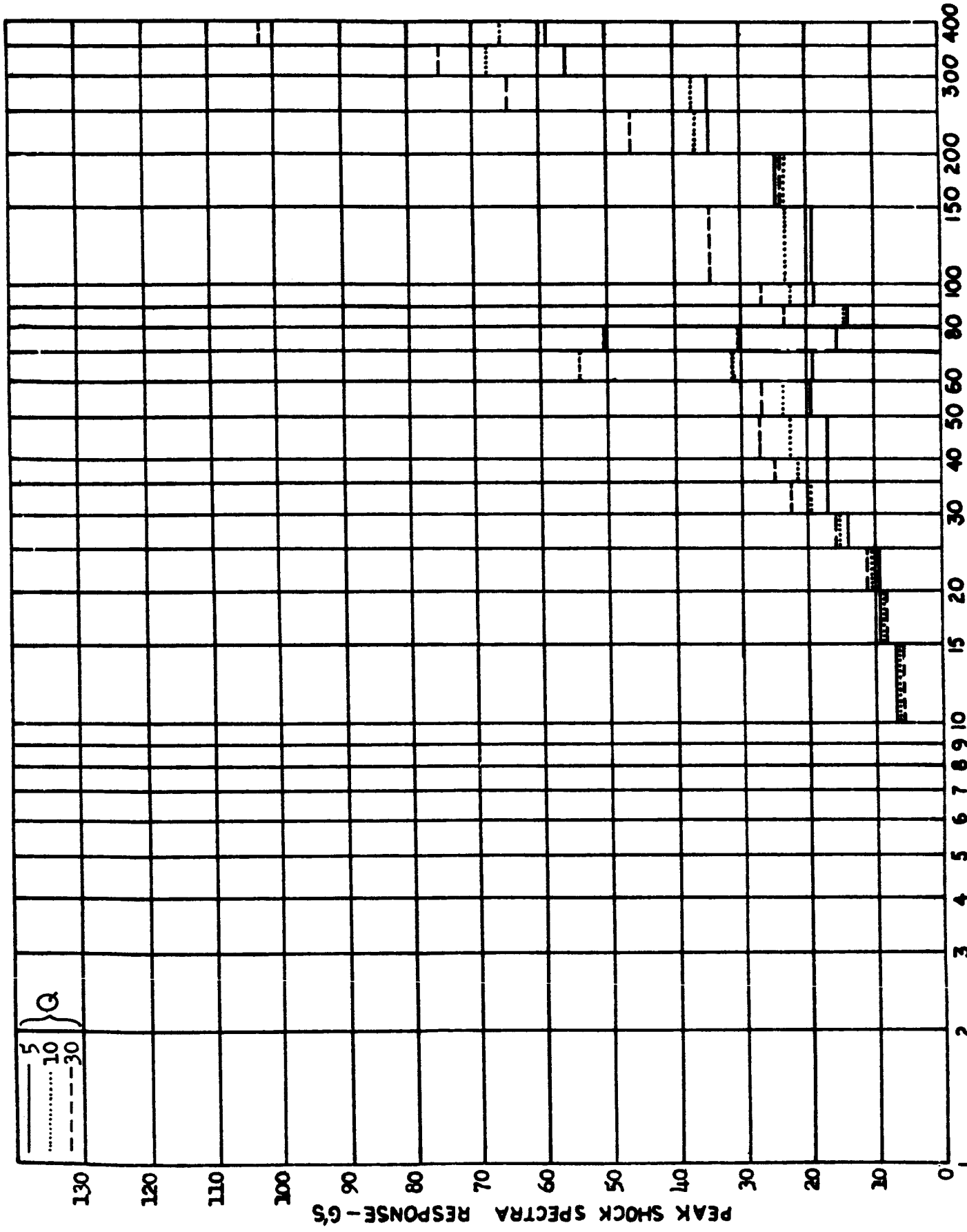

FIGURE 123 - SHOCK SPECTRUM ENVELOPE FOR ATLAS MECO AT PS (TRANSVERSE)

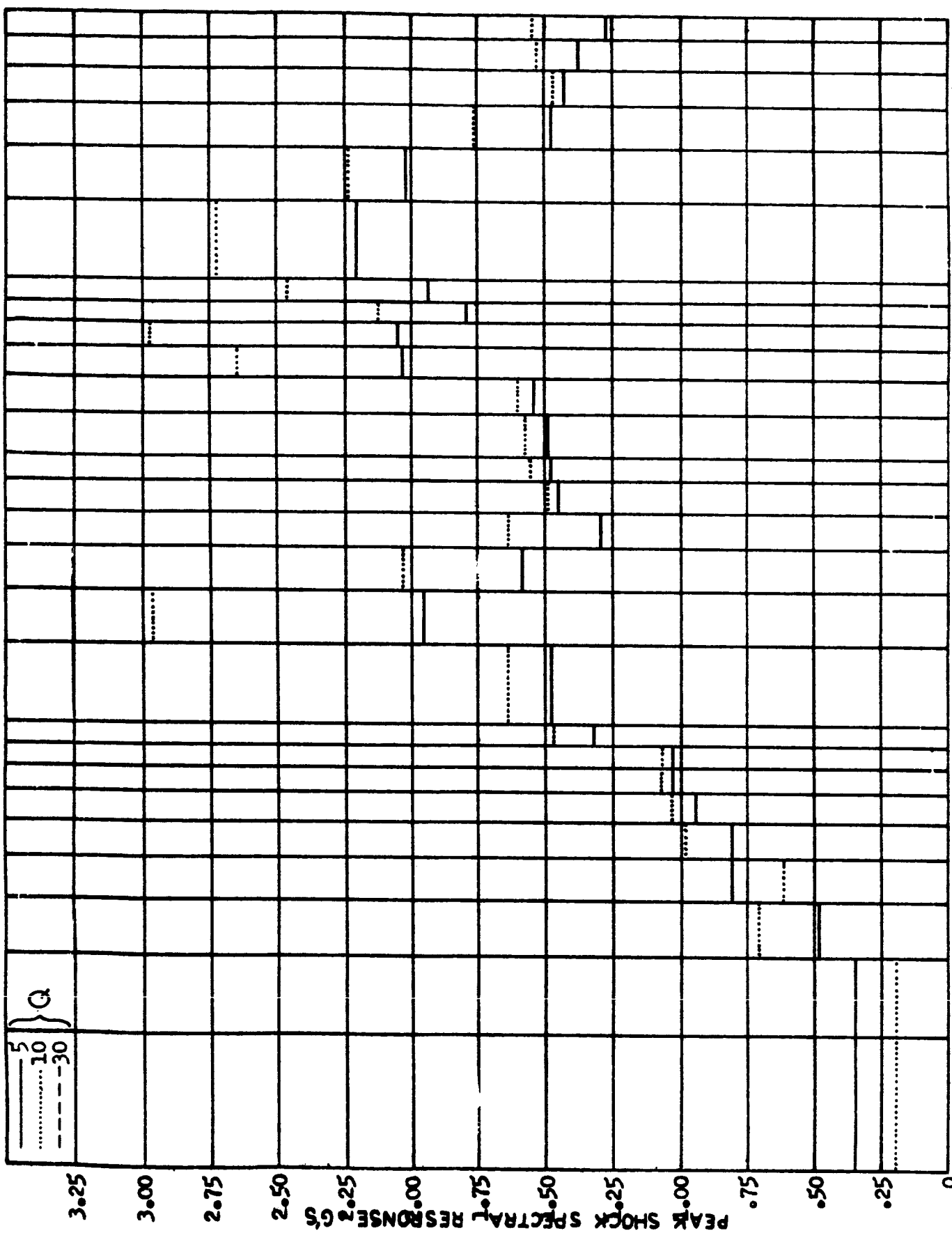

FIGURE 124 - SHOCK SPECTRUM ENVELOPE FOR ATLAS MECO AT FER (AXIAL)

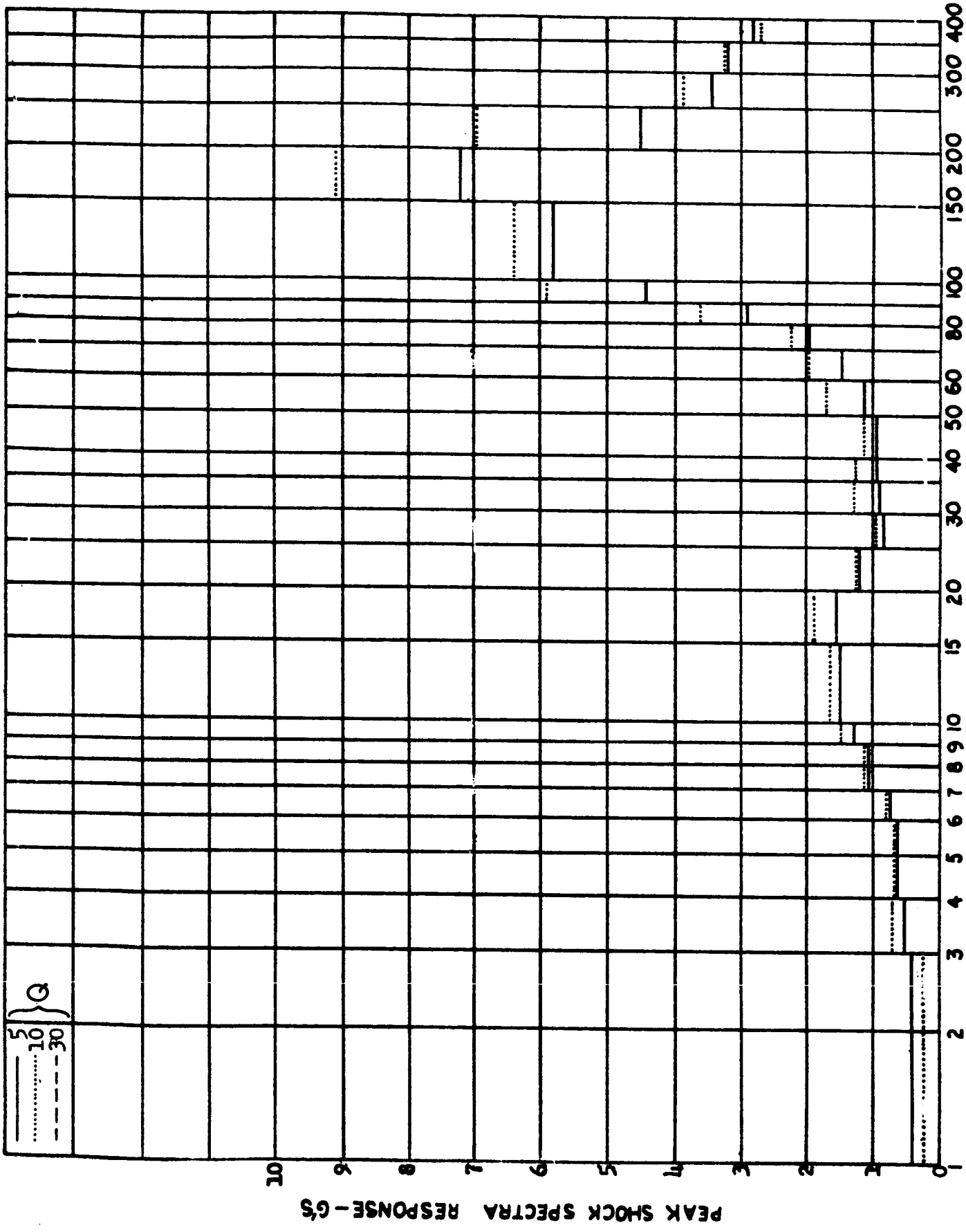

FIGURE 125 - SHOCK SPECTRUM ENVELOPE FOR ATLAS MECO AT FER (TRANSVERSE)

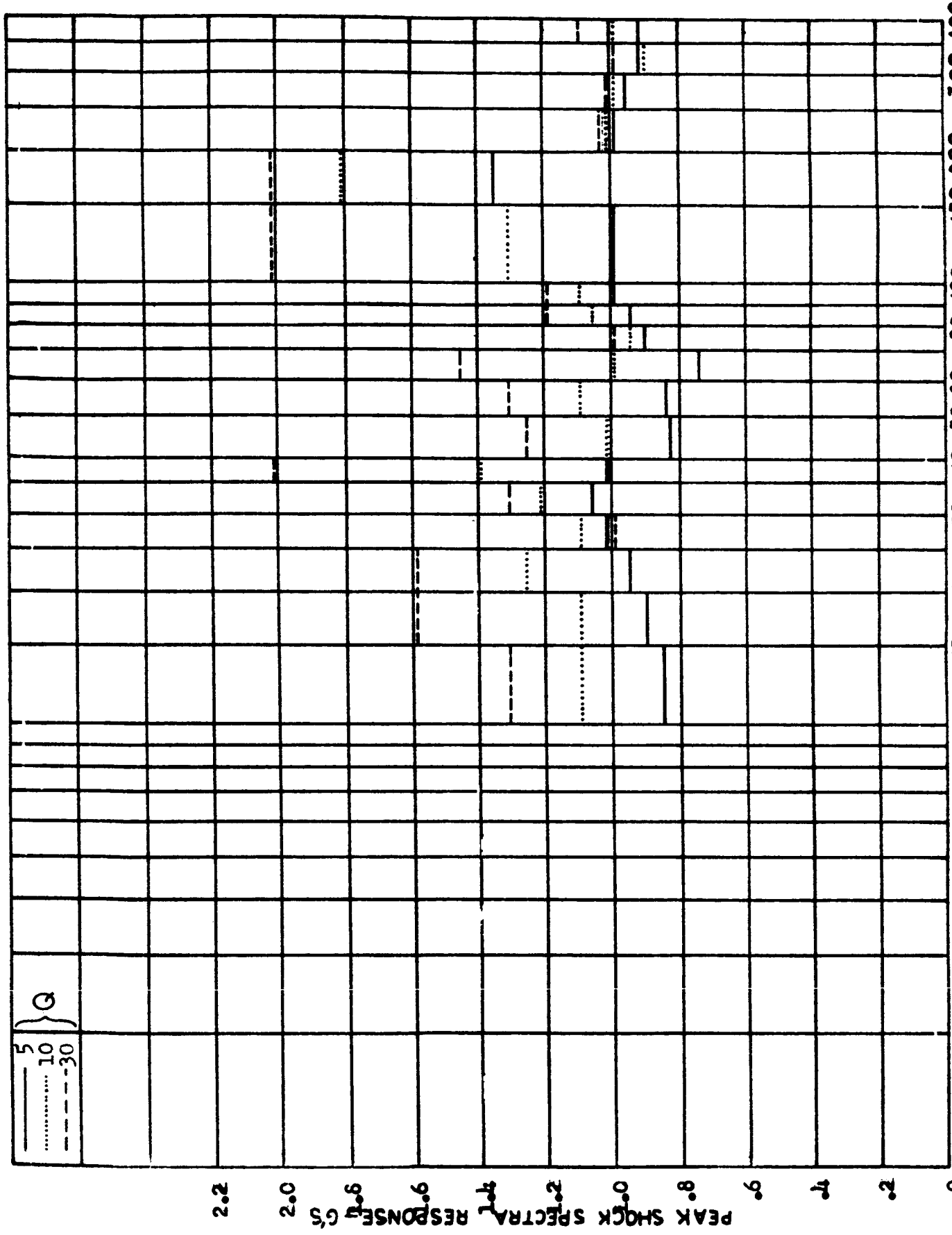

FIGURE 126 - SHOCK SPECTRUM ENVELOPE FOR ATLAS SECO AT PS (AXIAL)

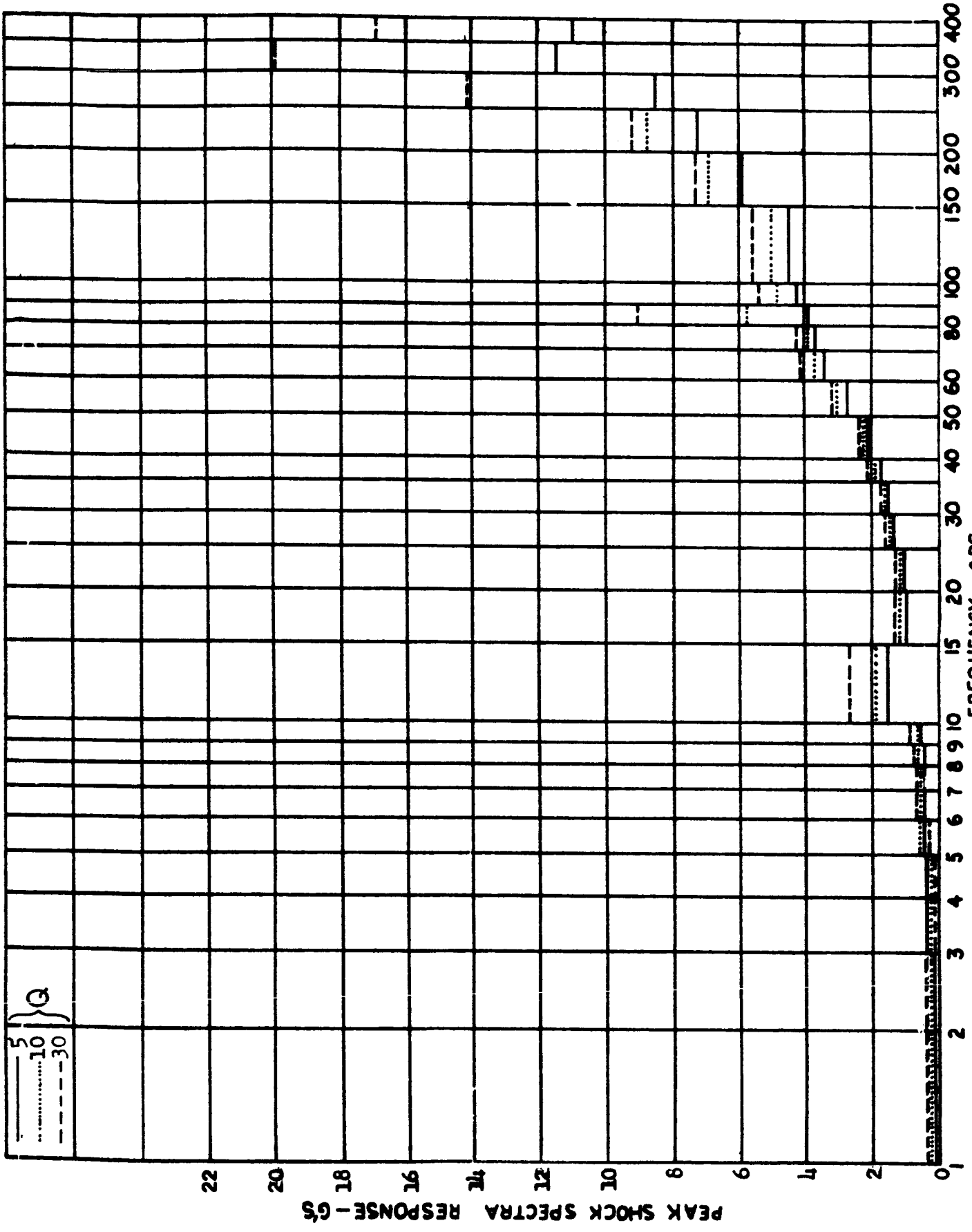

FIGURE 127 - SHOCK SPECTRUM ENVELOPE FOR ATLAS SECO AT PS (TRANSVERSE)

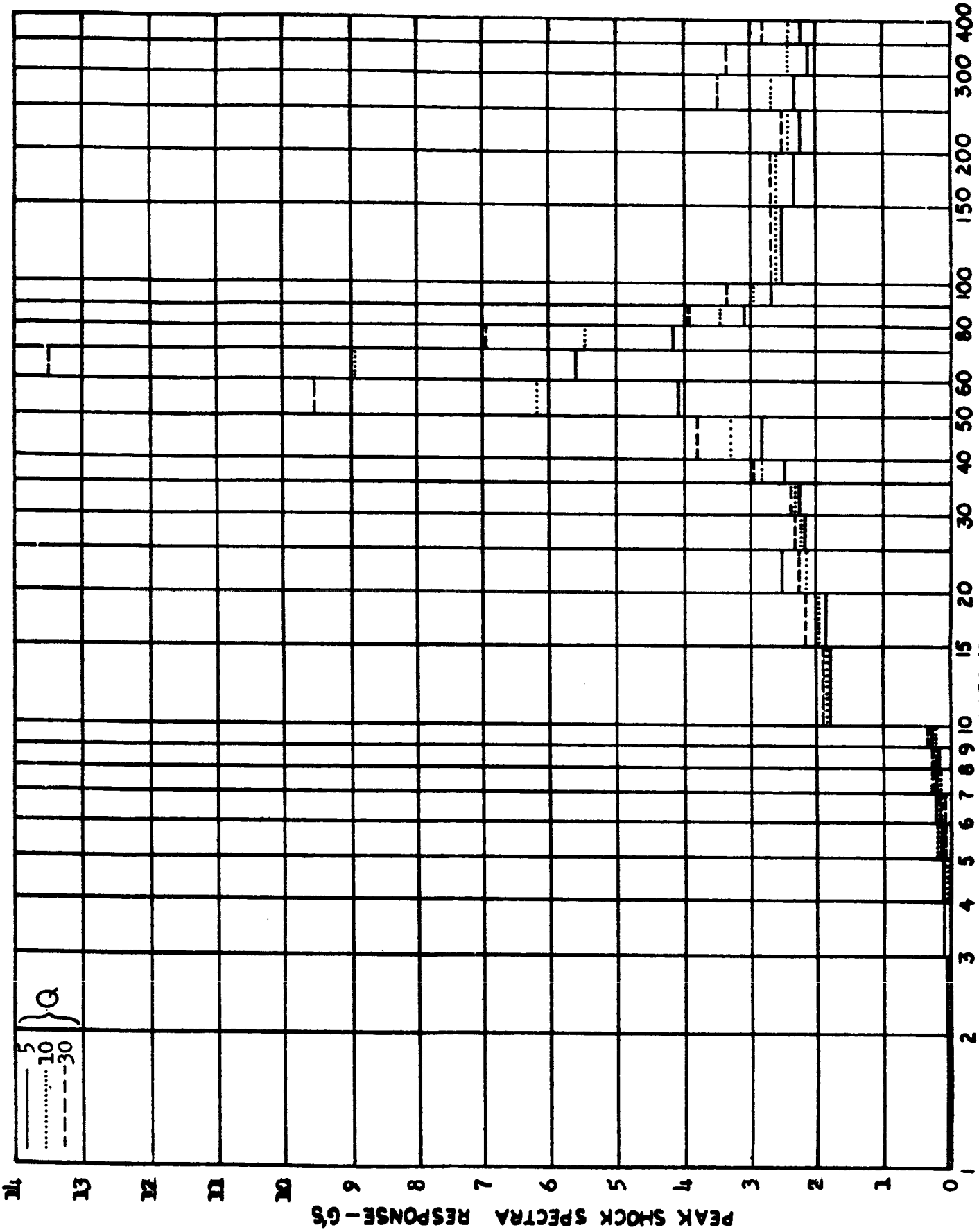

FIGURE 128 - SHOCK SPECTRUM ENVELOPE FOR AGENA FIRST IGNITION AT PS (AXIAL)

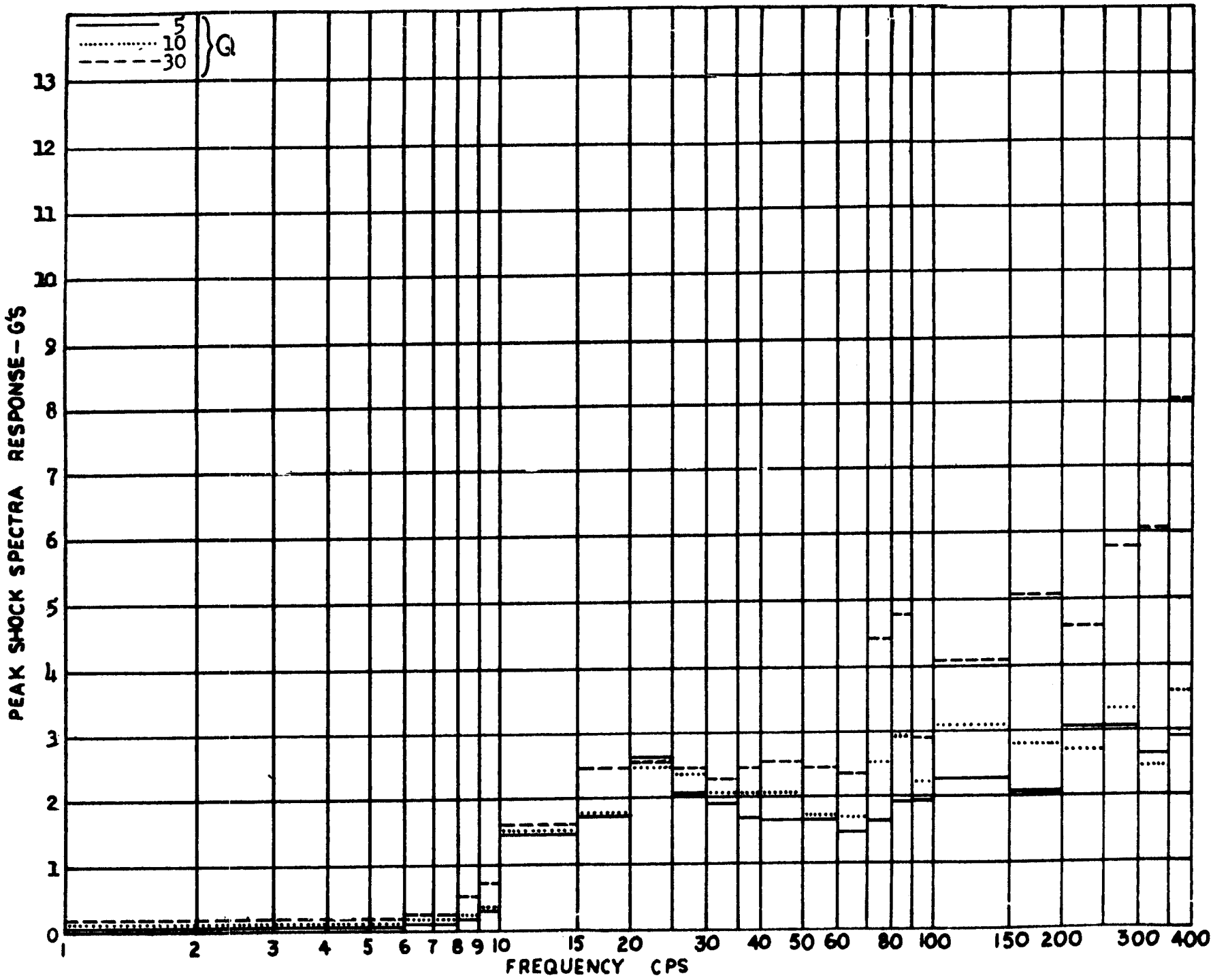

FIGURE 129 - SHOCK SPECTRUM ENVELOPE FOR AGENA FIRST IGNITION AT PS (TRANSVERSE)

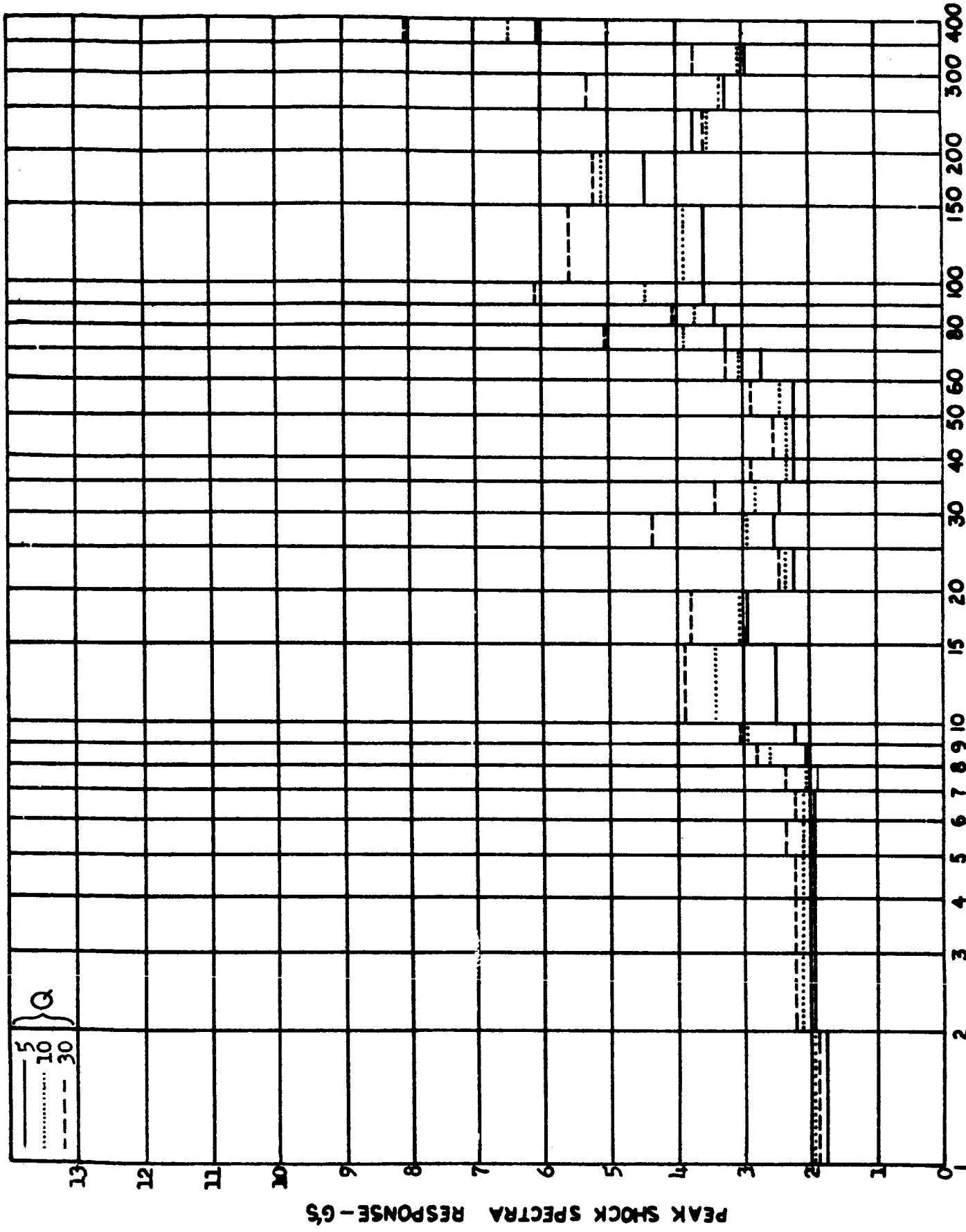

FIGURE 130 - SHOCK SPECTRUM ENVELOPE FOR ACENA FIRST IGNITION AT FER (AXIAL)

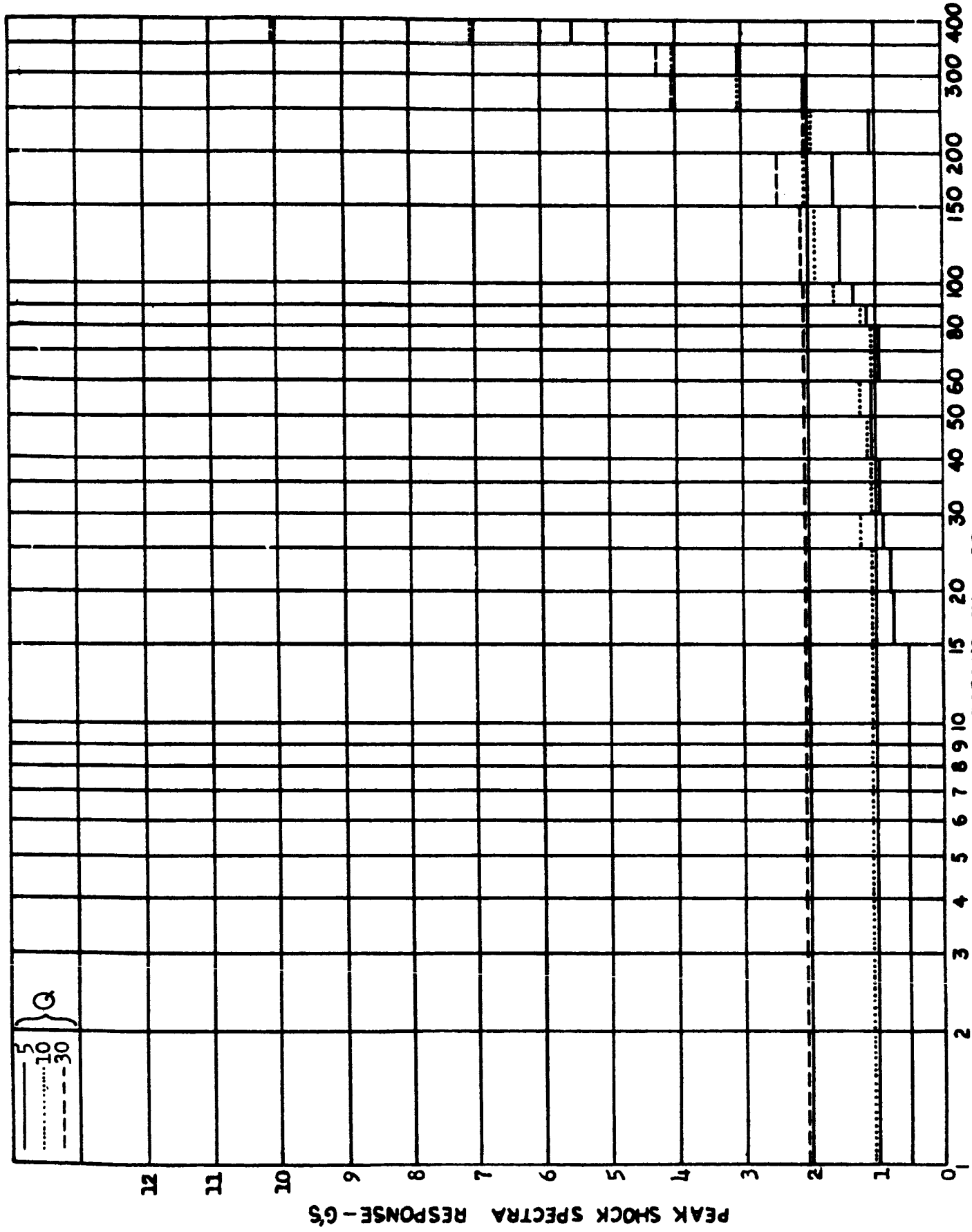

FIGURE 131 - SHOCK SPECTRUM ENVELOPE FOR AGENA FIRST IGNITION AT FER (TRANSVERSE)

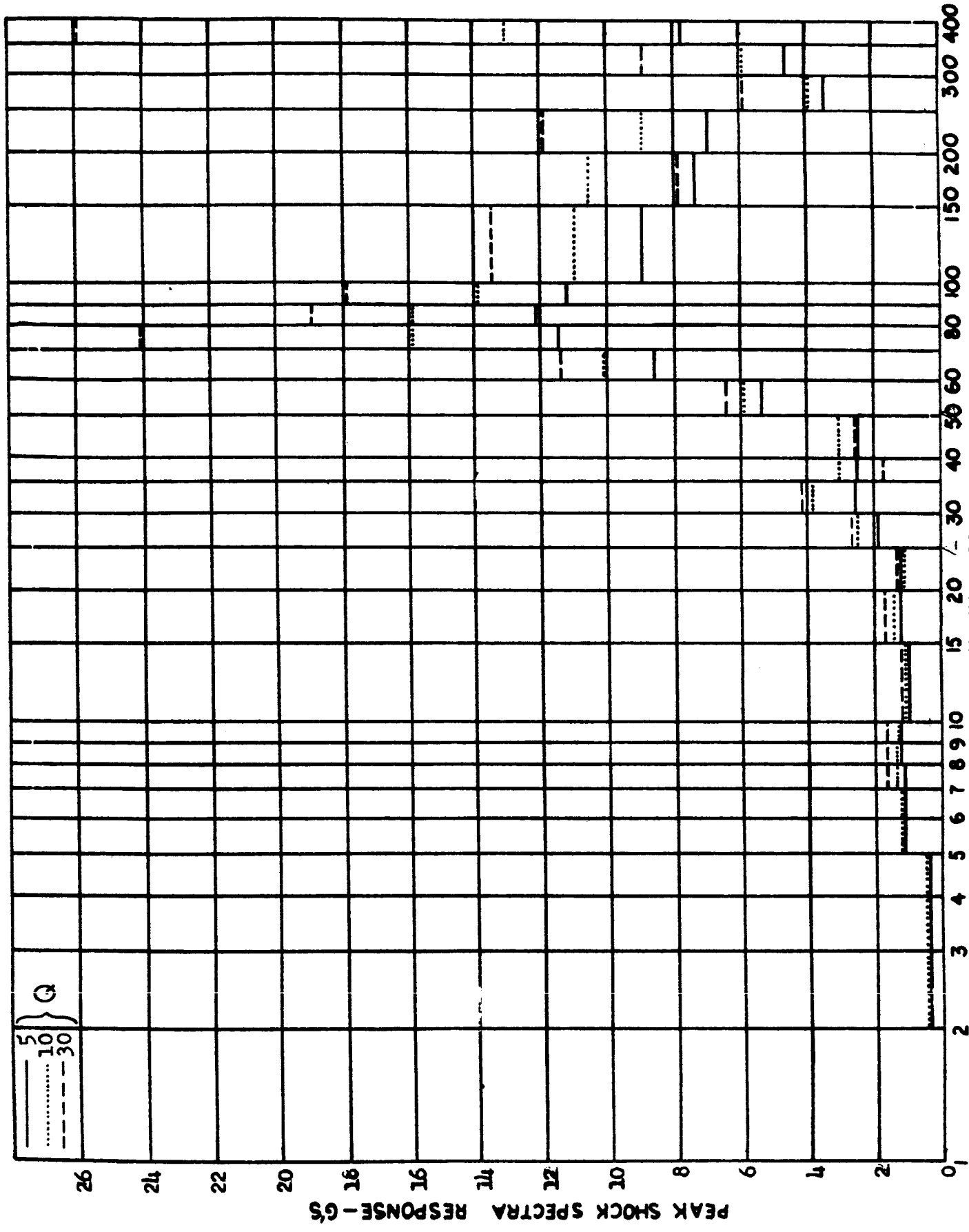

FIGURE 132 - SHOCK SPECTRUM ENVELOPE FOR AGENA FIRST IGNITION AT AER (AXIAL)

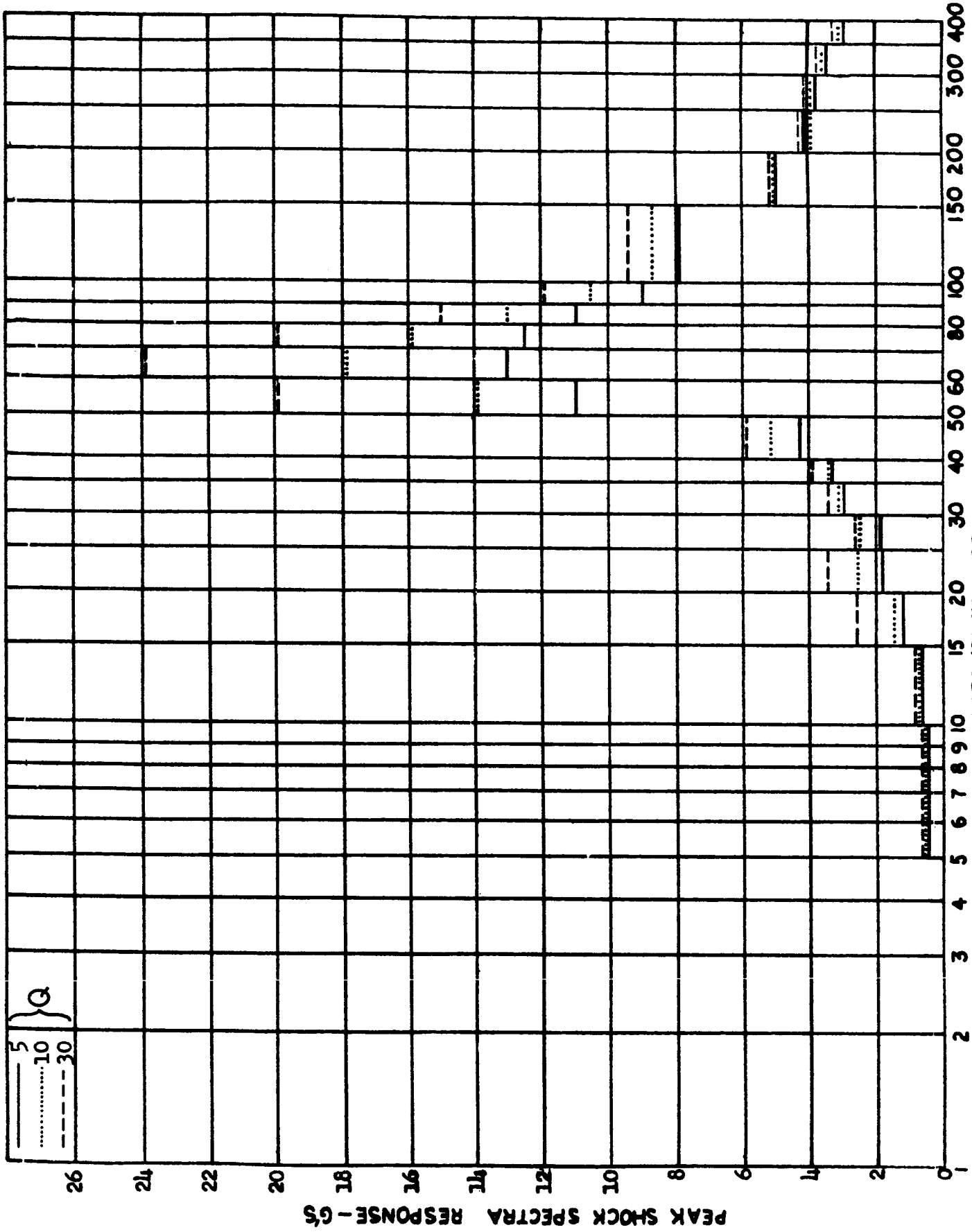

FIGURE 133 - SHOCK SPECTRUM ENVELOPE FOR AGENA FIRST IGNITION AT AER (TRANSVERSE)

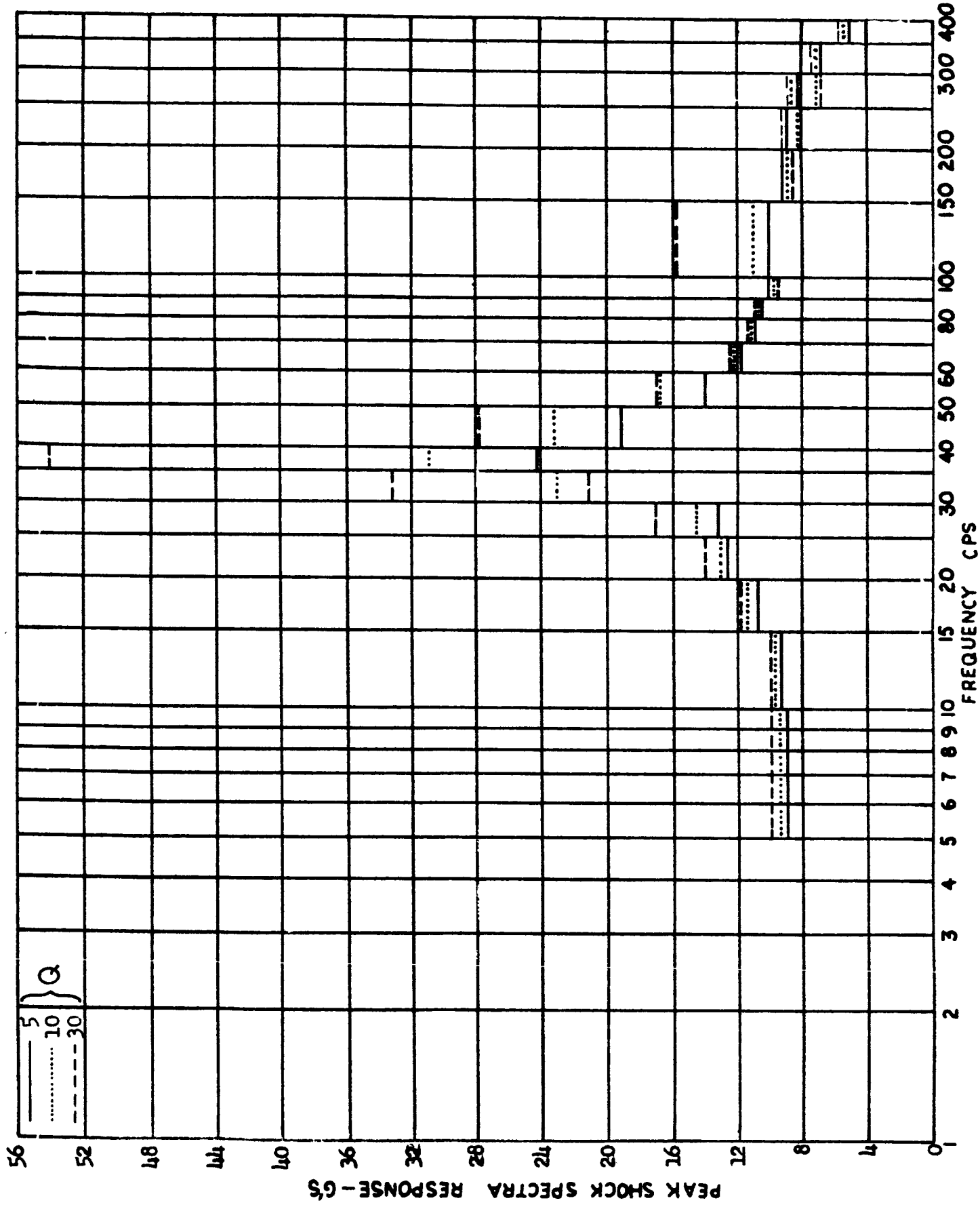

FIGURE 134 - SHOCK SPECTRUM ENVELOPE FOR AGENA FIRST SHUTDOWN AT PS (AXIAL)

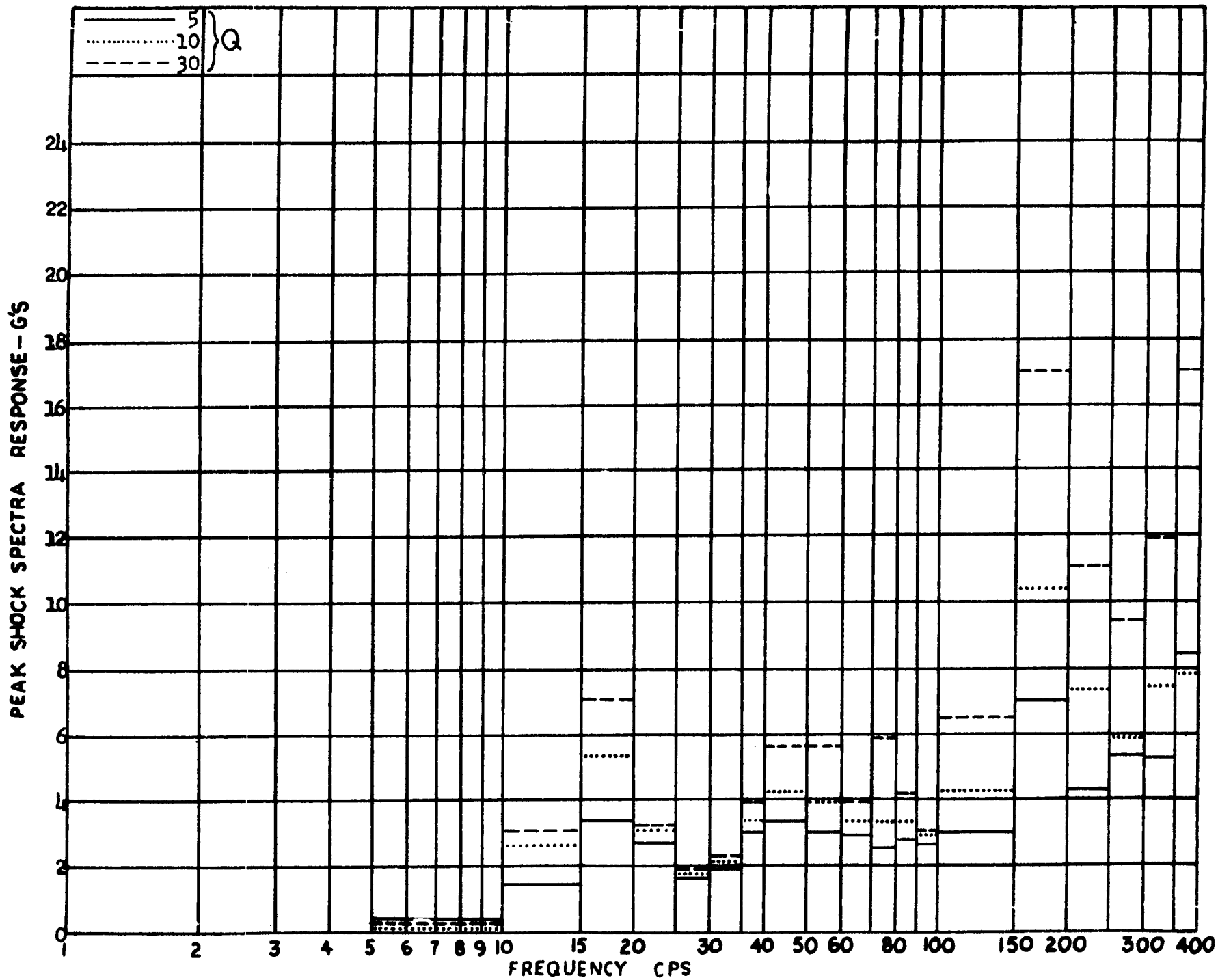

FIGURE 135 - SHOCK SPECTRUM ENVELOPE FOR AGENA FIRST SHUTDOWN AT PS (TRANSVERSE)

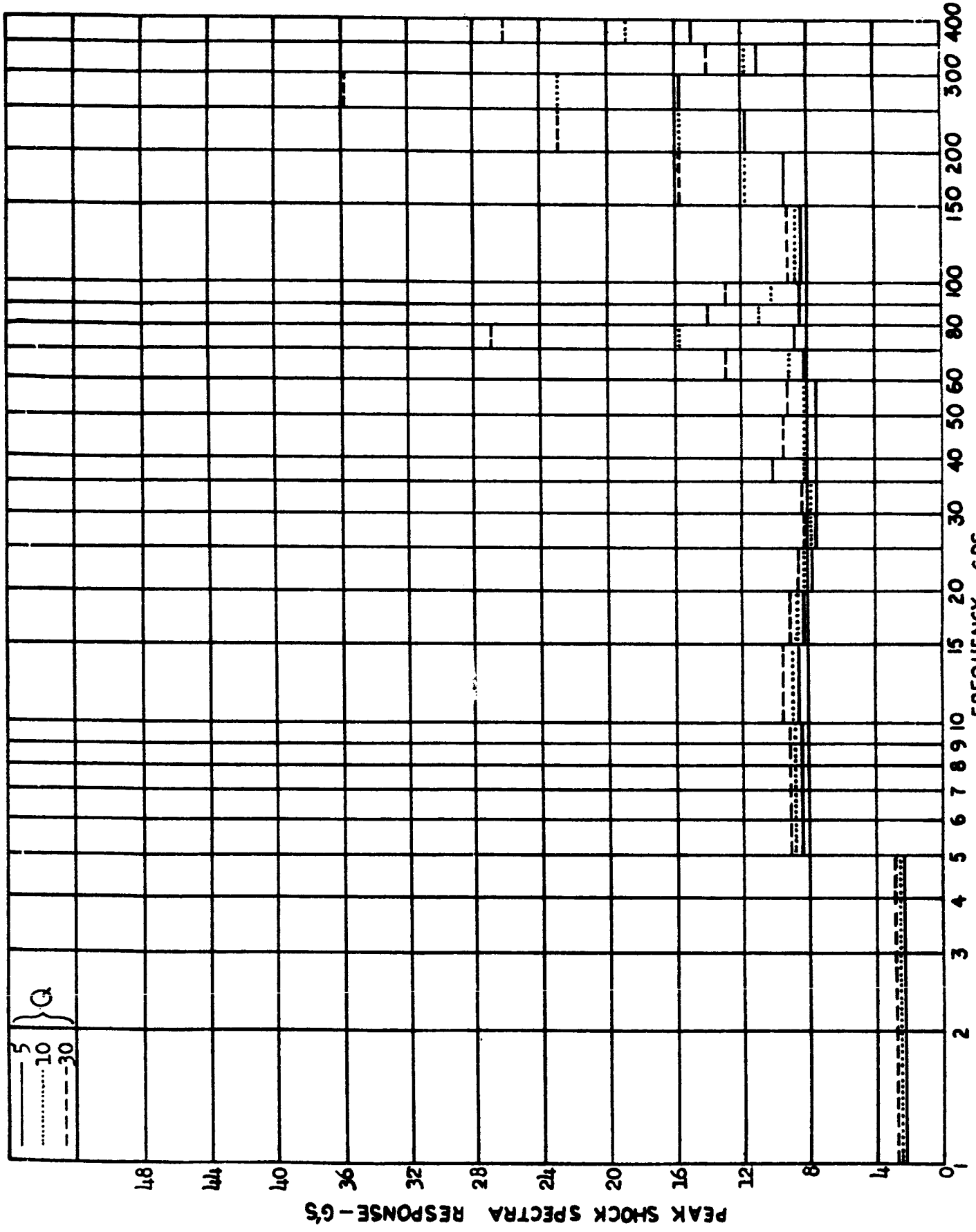

FIGURE 136 - SHOCK SPECTRUM ENVELOPE FOR AGENA FIRST SHUTDOWN AT FER (AXIAL)

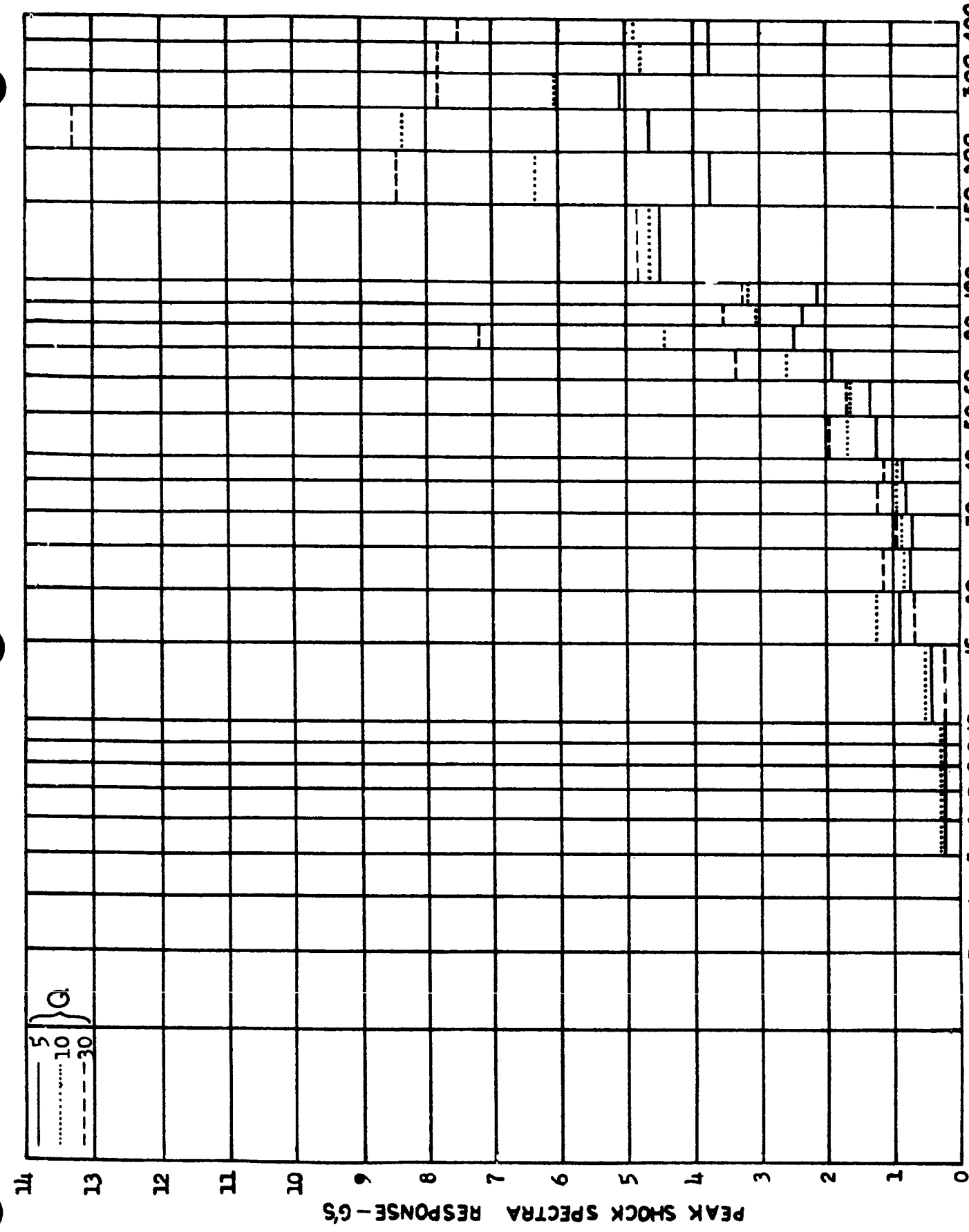

FIGURE 137 - SHOCK SPECTRUM ENVELOPE FOR AGENA FIRST SHUTDOWN AT FER (TRANSVERSE)

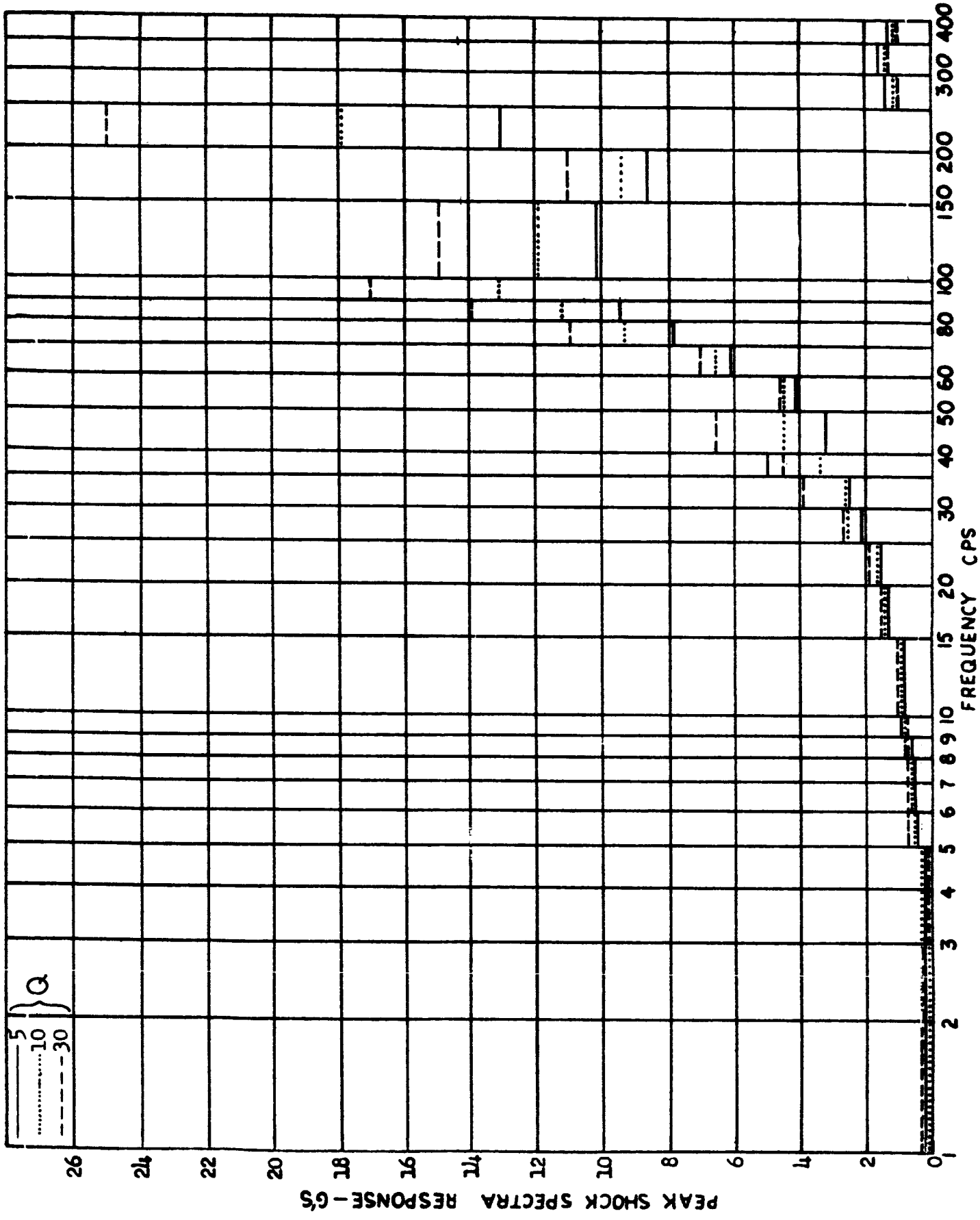

FIGURE 138 - SHOCK SPECTRUM ENVELOPE FOR AGENA FIRST SHUTDOWN AT AER (AXIAL)

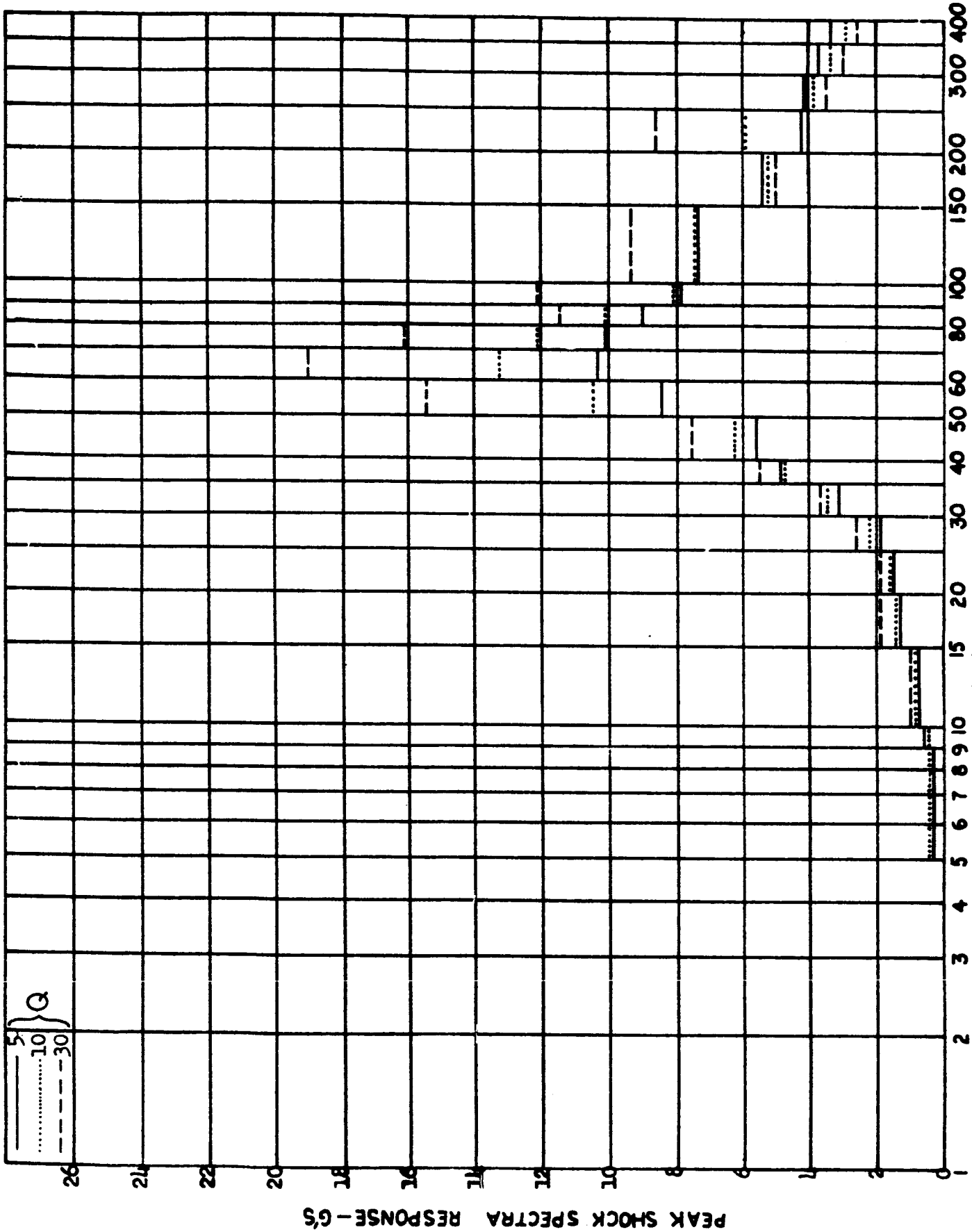

FIGURE 139 - SHOCK SPECTRUM ENVELOPE FOR AGENA FIRST SHUTDOWN AT AER (TRANSVERSE)

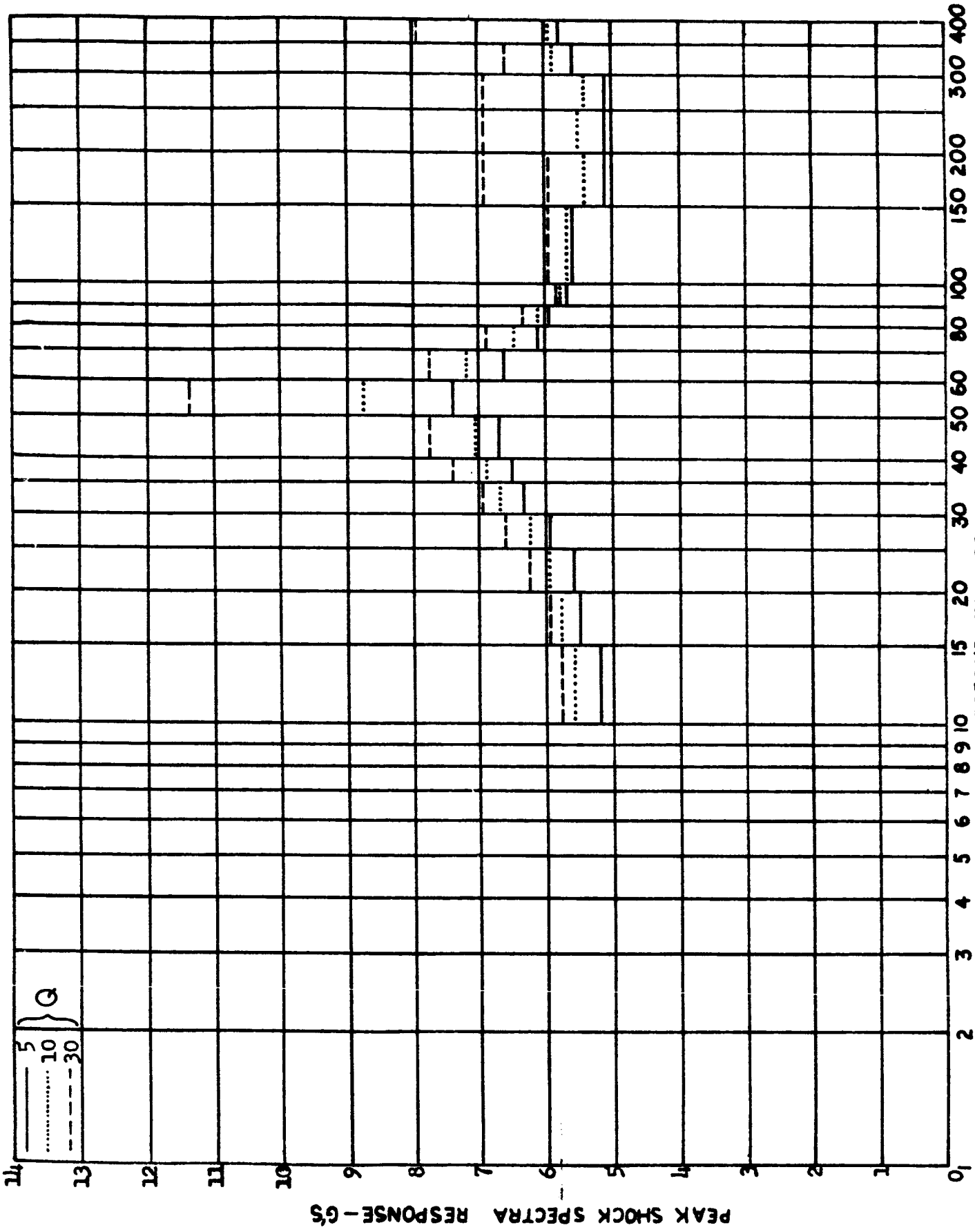

FIGURE 140 - SHOCK SPECTRUM ENVELOPE FOR AGENA SECOND IGNITION AT PS (AXIAL)

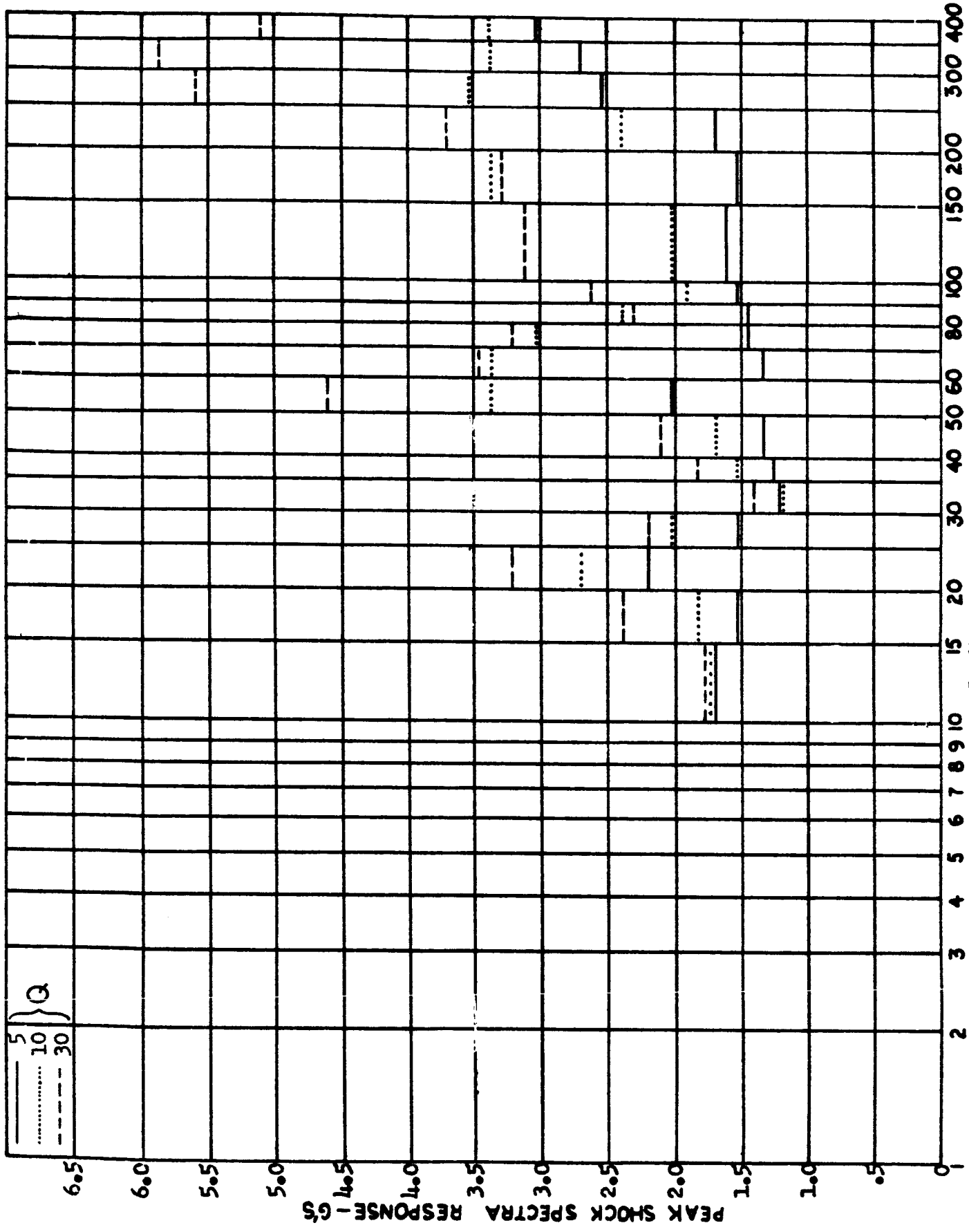

FIGURE 141 - SHOCK SPECTRUM ENVELOPE FOR AGENA SECOND IGNITION AT PS (TRANSVERSE)

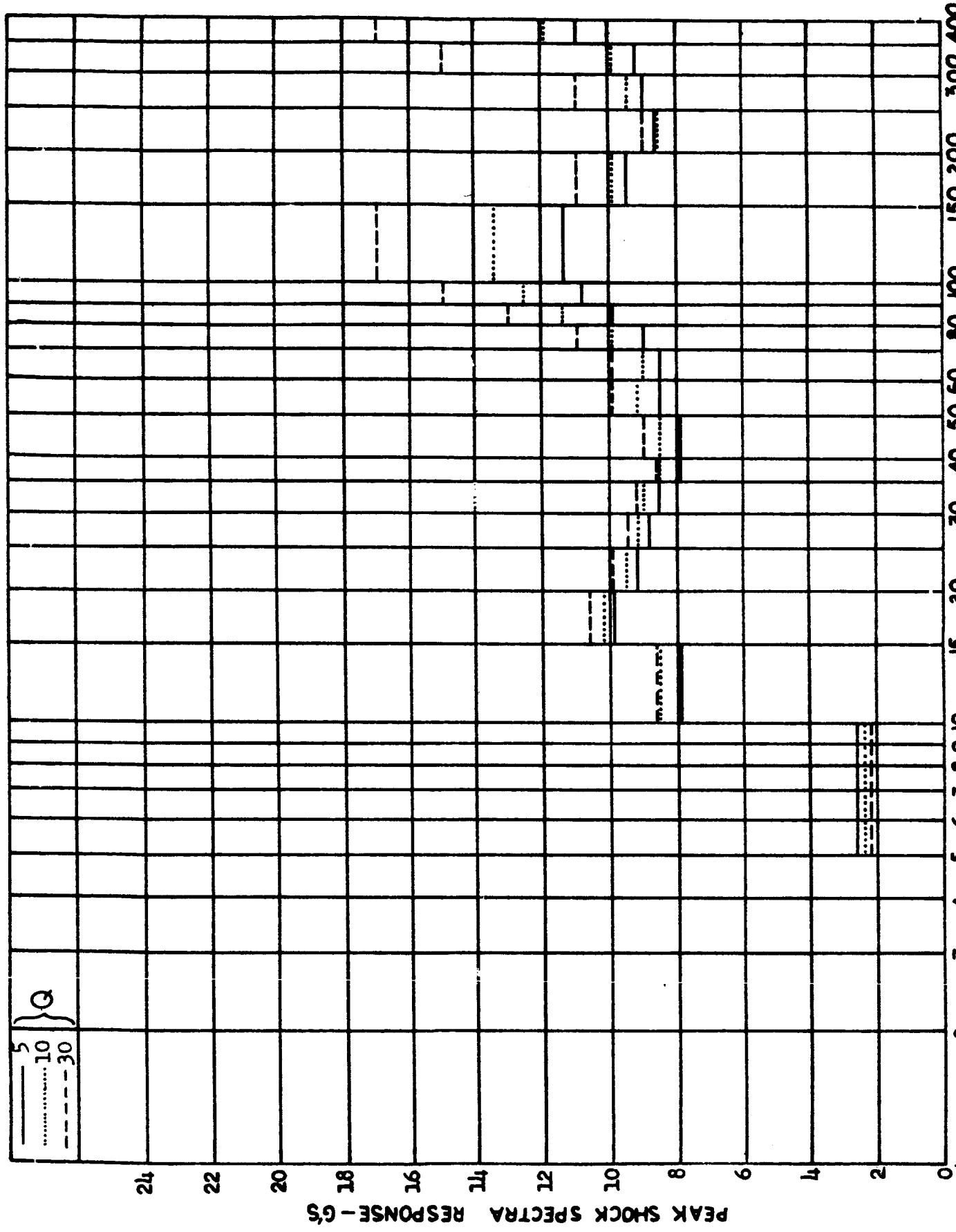

FIGURE 142 - SHOCK SPECTRUM ENVELOPE FOR AGENA SECOND IGNITION AT FER (AXIAL)

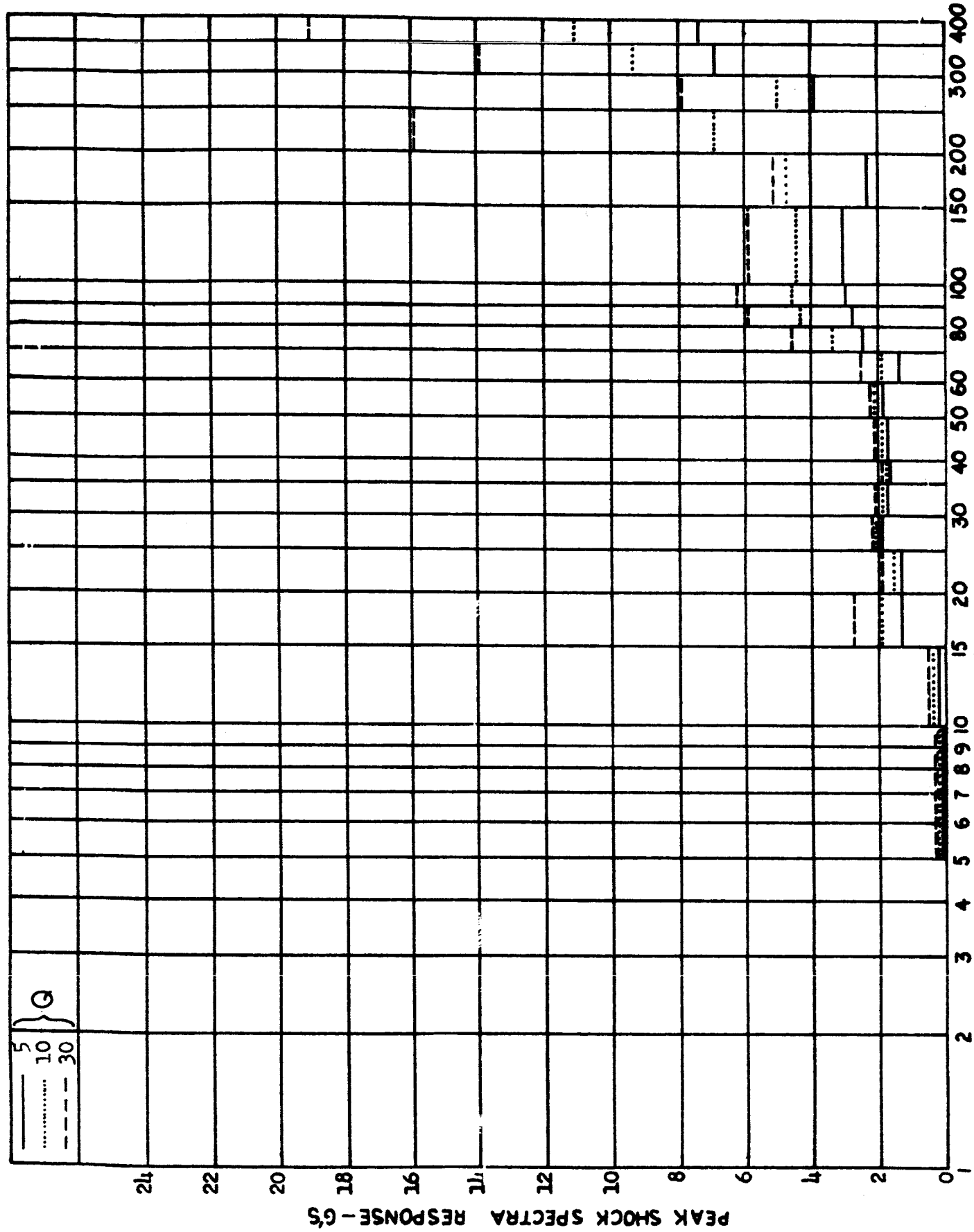

FIGURE 143 - SHOCK SPECTRUM ENVELOPE FOR AGENA SECOND IGNITION AT FER (TRANSVERSE)

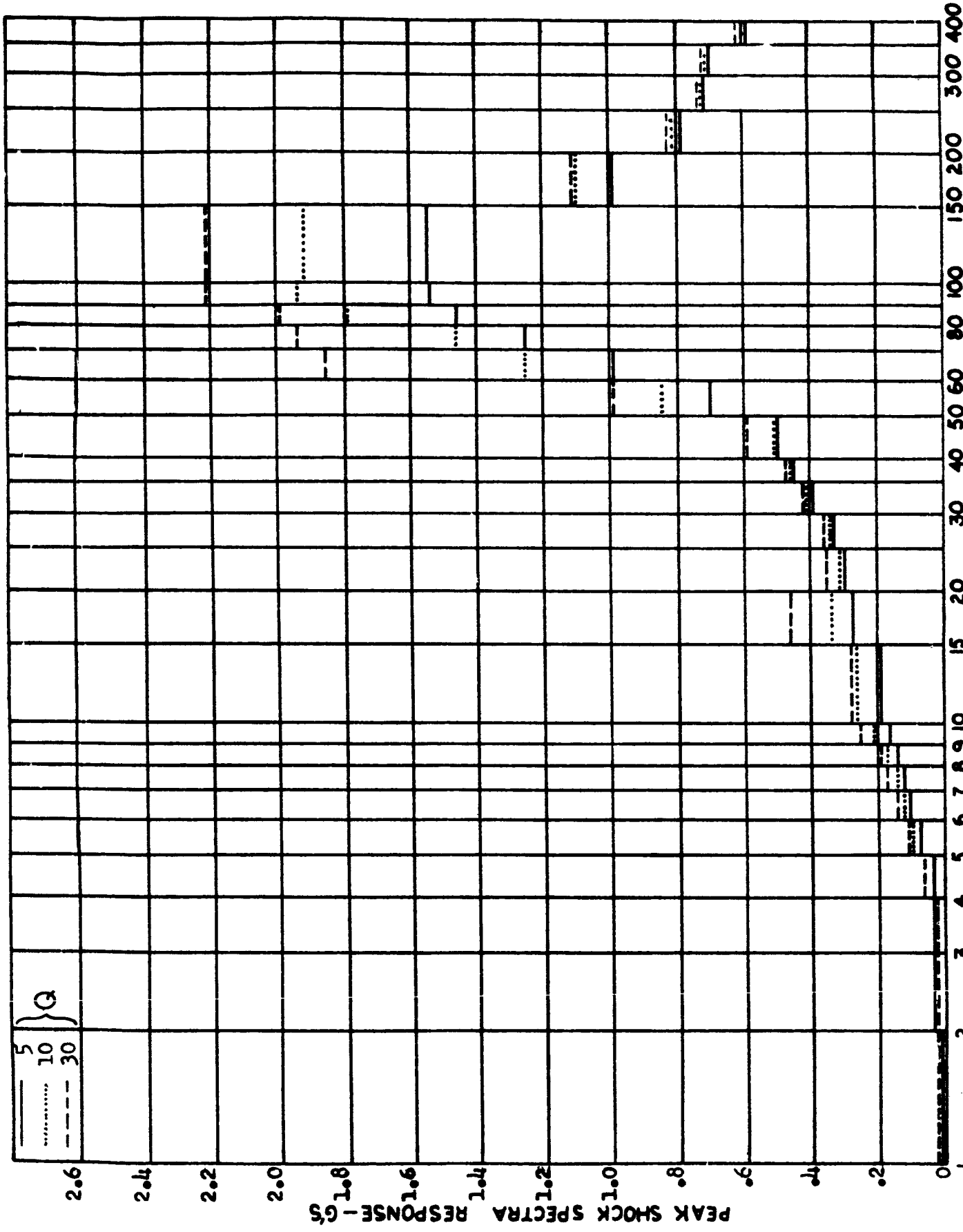

FIGURE 144 - SHOCK SPECTRUM ENVELOPE FOR AGENA SECOND IGNITION AT AER (AXIAL)

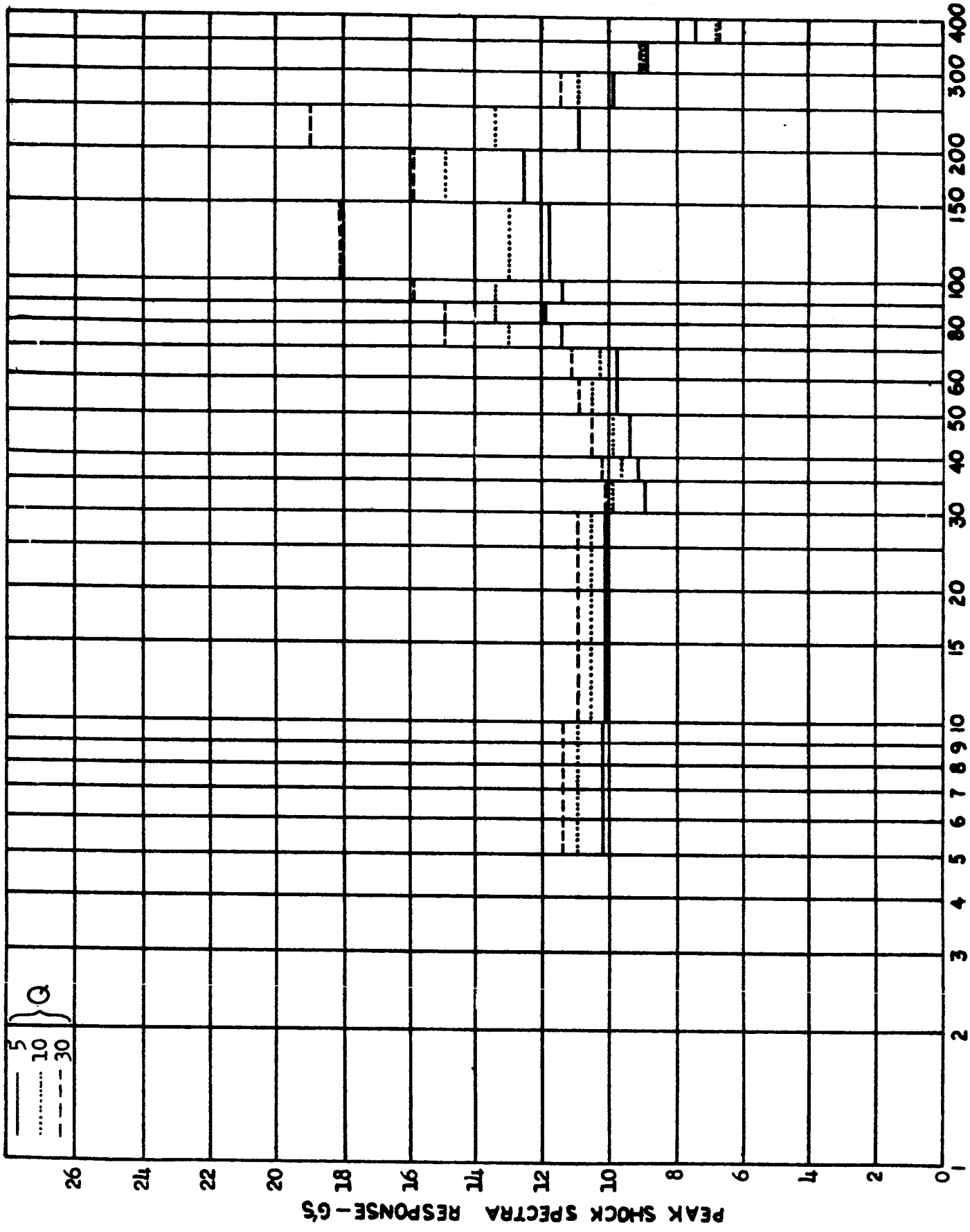

FIGURE 145 - SHOCK SPECTRUM ENVELOPE FOR ACENA SECOND SHUTDOWN AT PS (AXIAL)

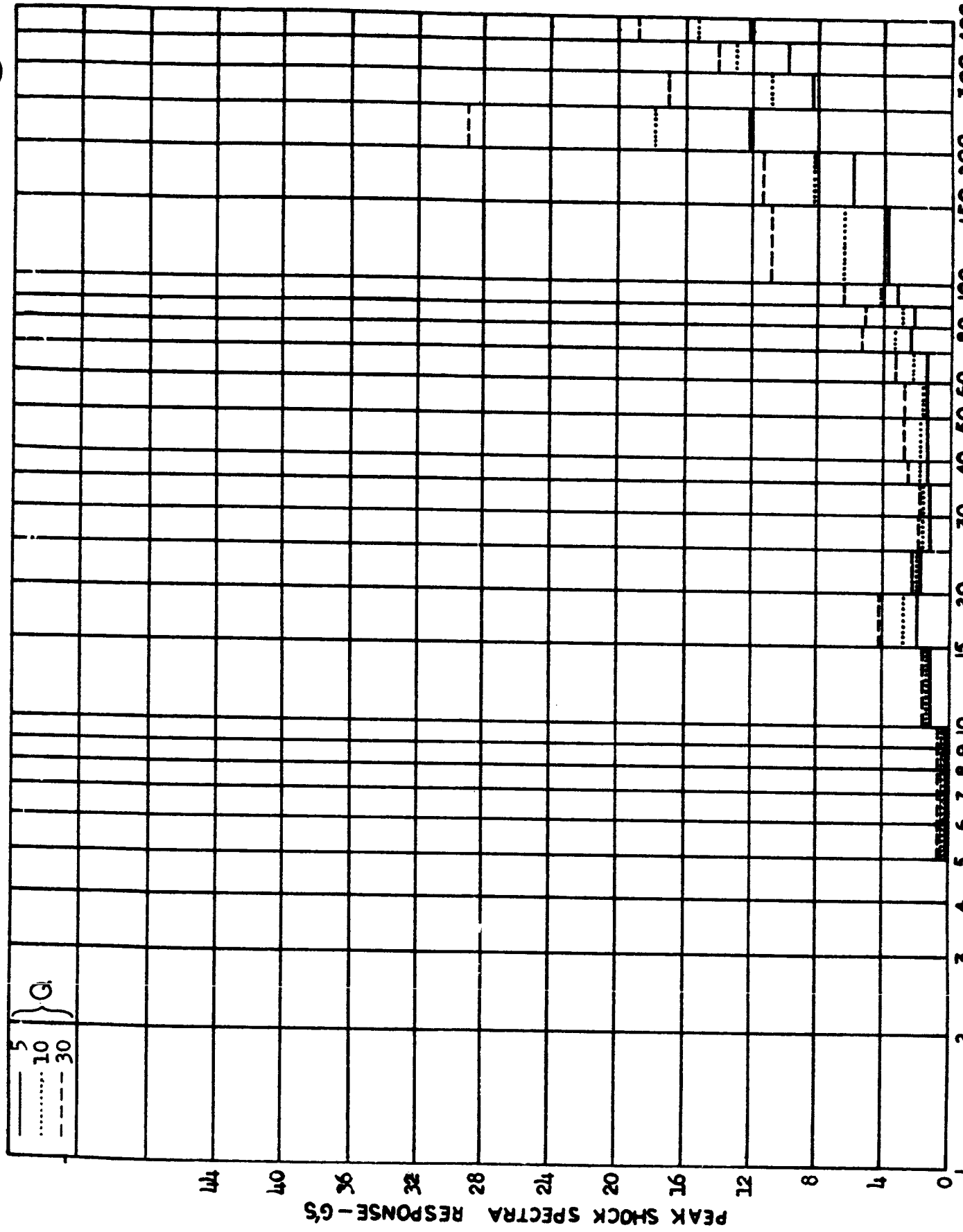

FIGURE 146 - SHOCK SPECTRUM ENVELOPE FOR AGENA SECOND SHUTDOWN AT PS (TRANSVERSE)

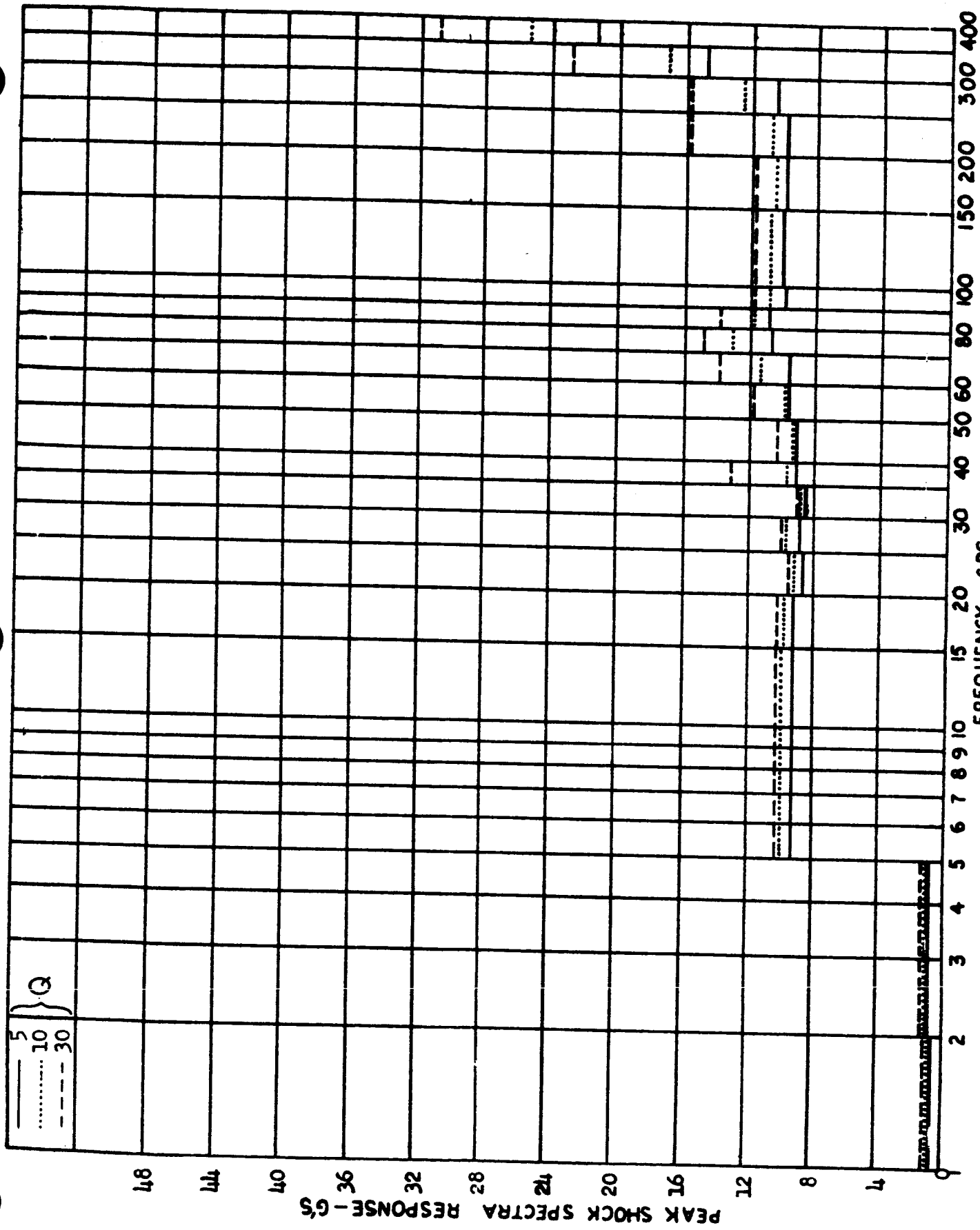

FIGURE 147 - SHOCK SPECTRUM ENVELOPE FOR AGENA SECOND SHUTDOWN AT FER (AXIAL)

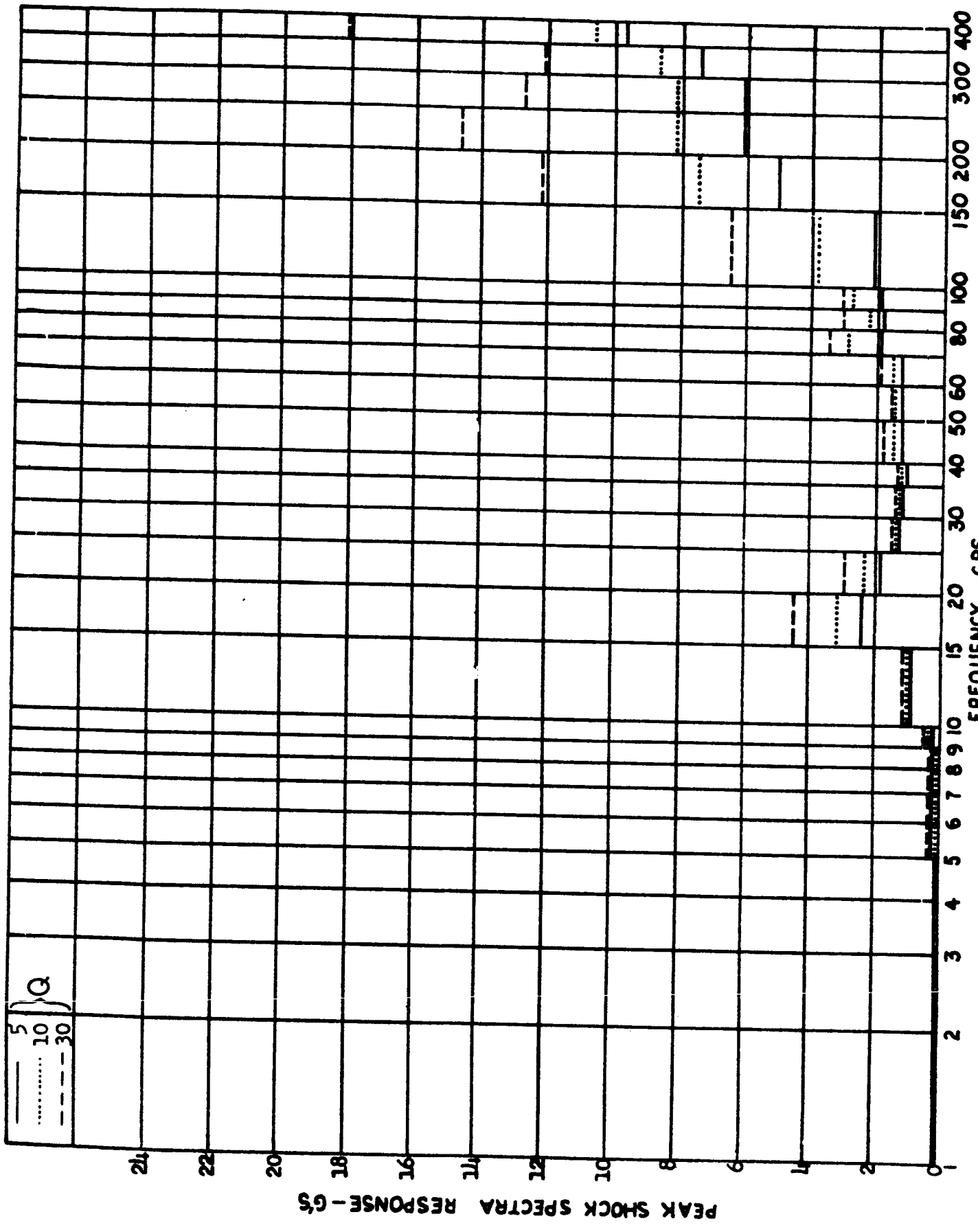

FIGURE 148 - SHOCK SPECTRUM ENVELOPE FOR AGENA SECOND SHUTDOWN AT FER (TRANSVERSE)

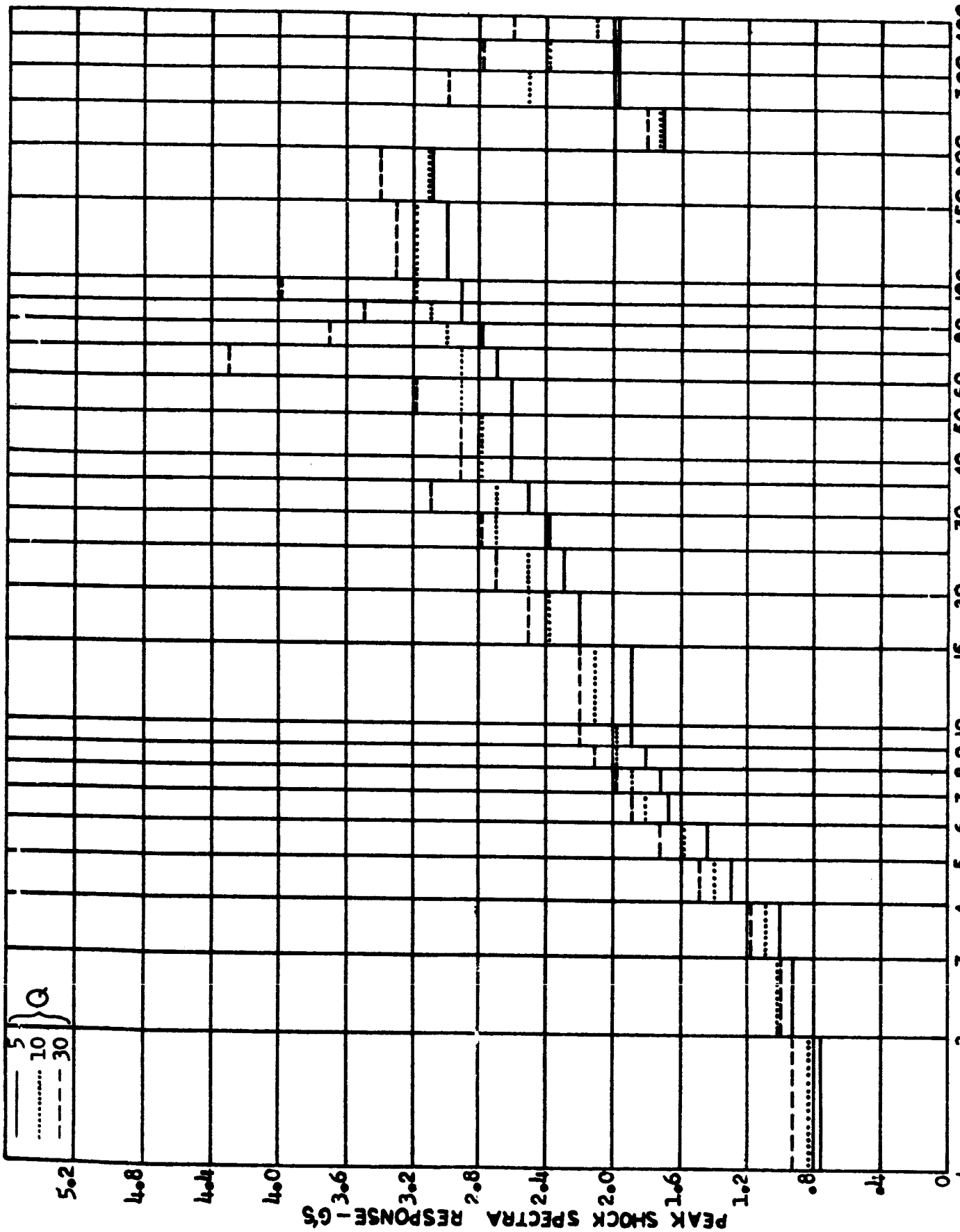

FIGURE 149 - SHOCK SPECTRUM ENVELOPE FOR AGENA SECOND SHUTDOWN AT AER (AXIAL)

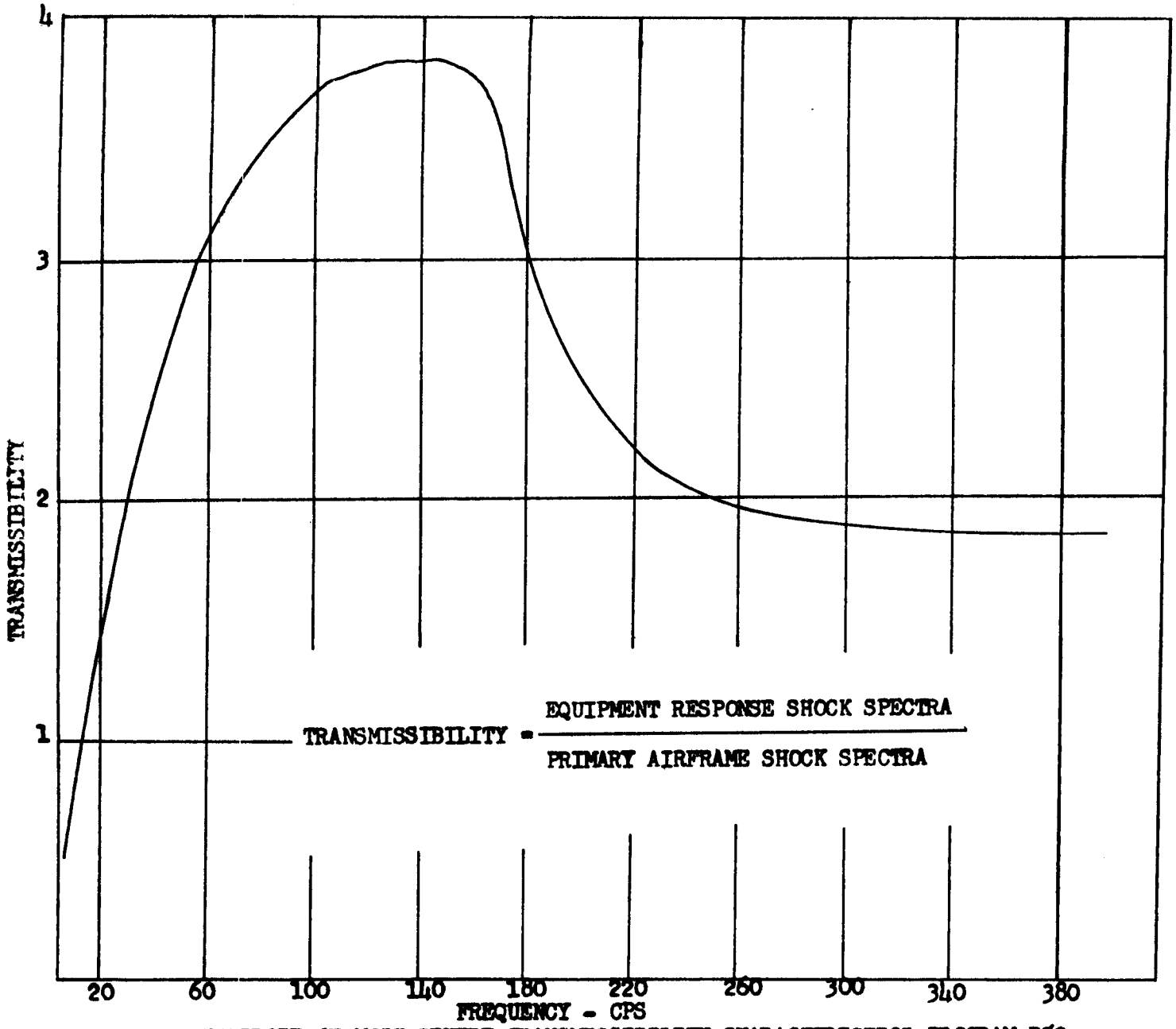

FIGURE 150 - ENVELOPE OF MOST SEVERE TRANSMISSIBILITY CHARACTERISTICS, PROGRAM P50
AFT SECTION EQUIPMENT SUPPORT STRUCTURE

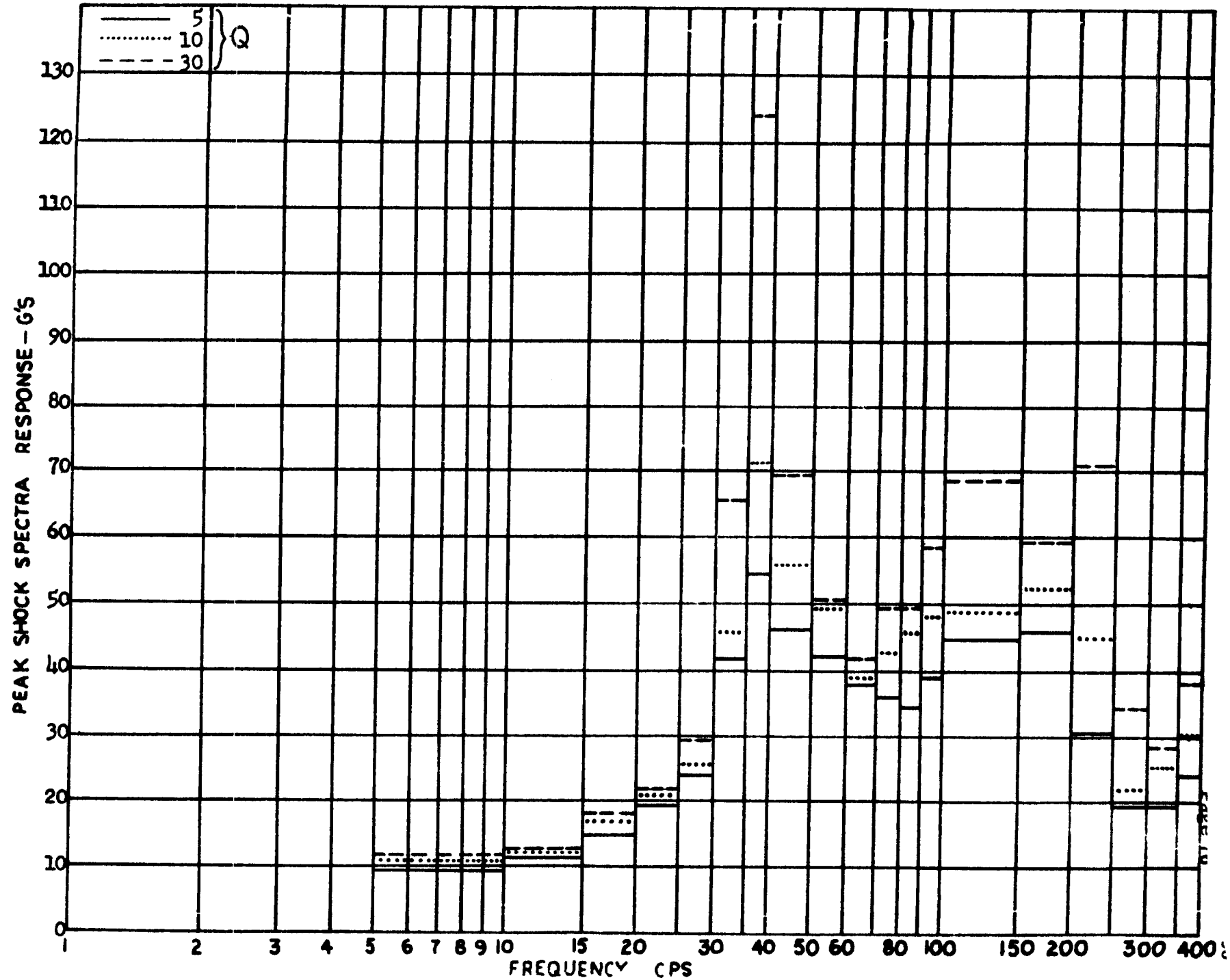

FIGURE 151 - ESTIMATED SHOCK SPECTRA ENVELOPE FOR EQUIPMENT IN PAYLOAD AT AGENA IGNITION AND SHUTDOWN EVENTS

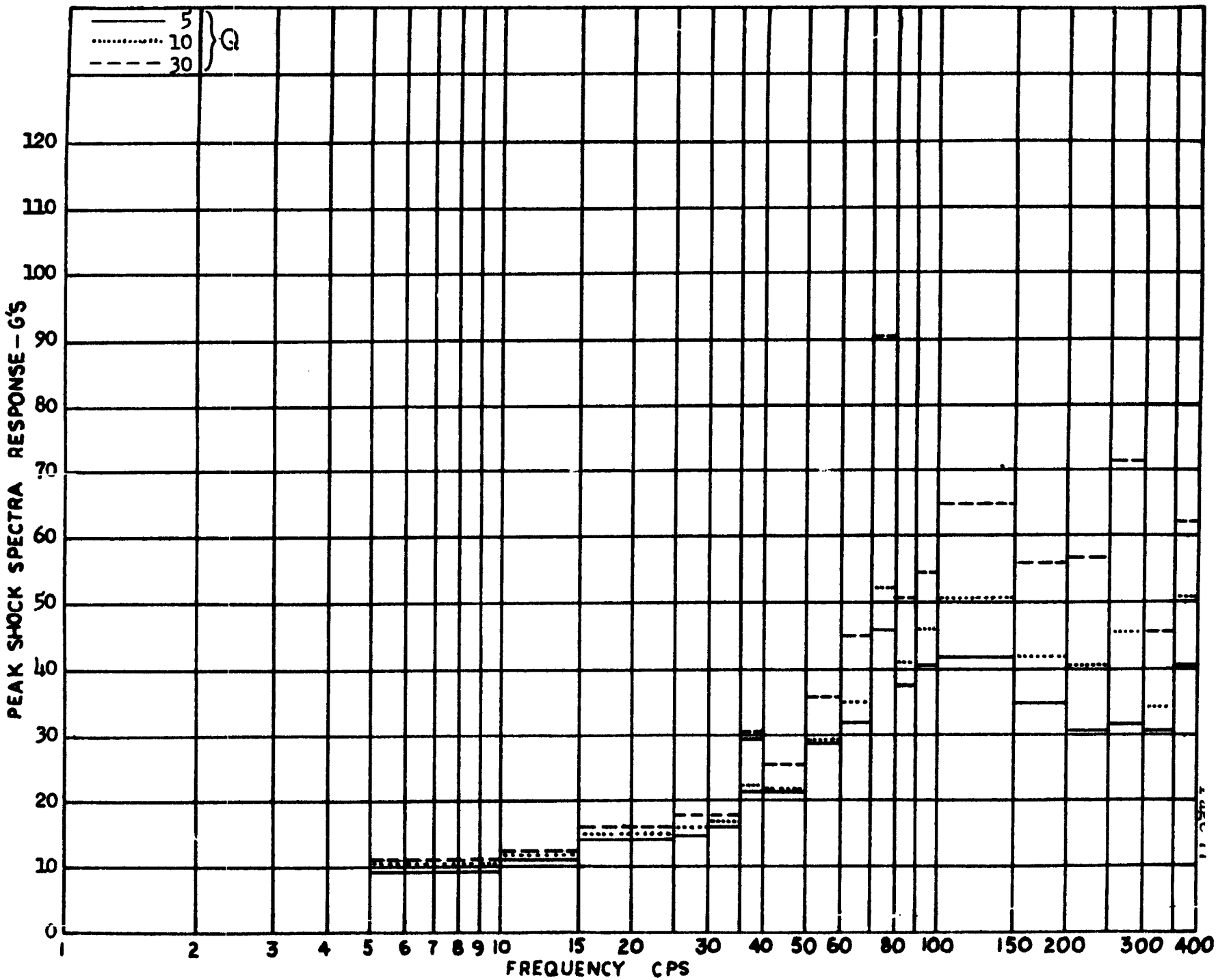

FIGURE 152 - ESTIMATED SHOCK SPECTRA ENVELOPE FOR EQUIPMENT IN FER AT AGENA IGNITION AND SHUTDOWN EVENTS.

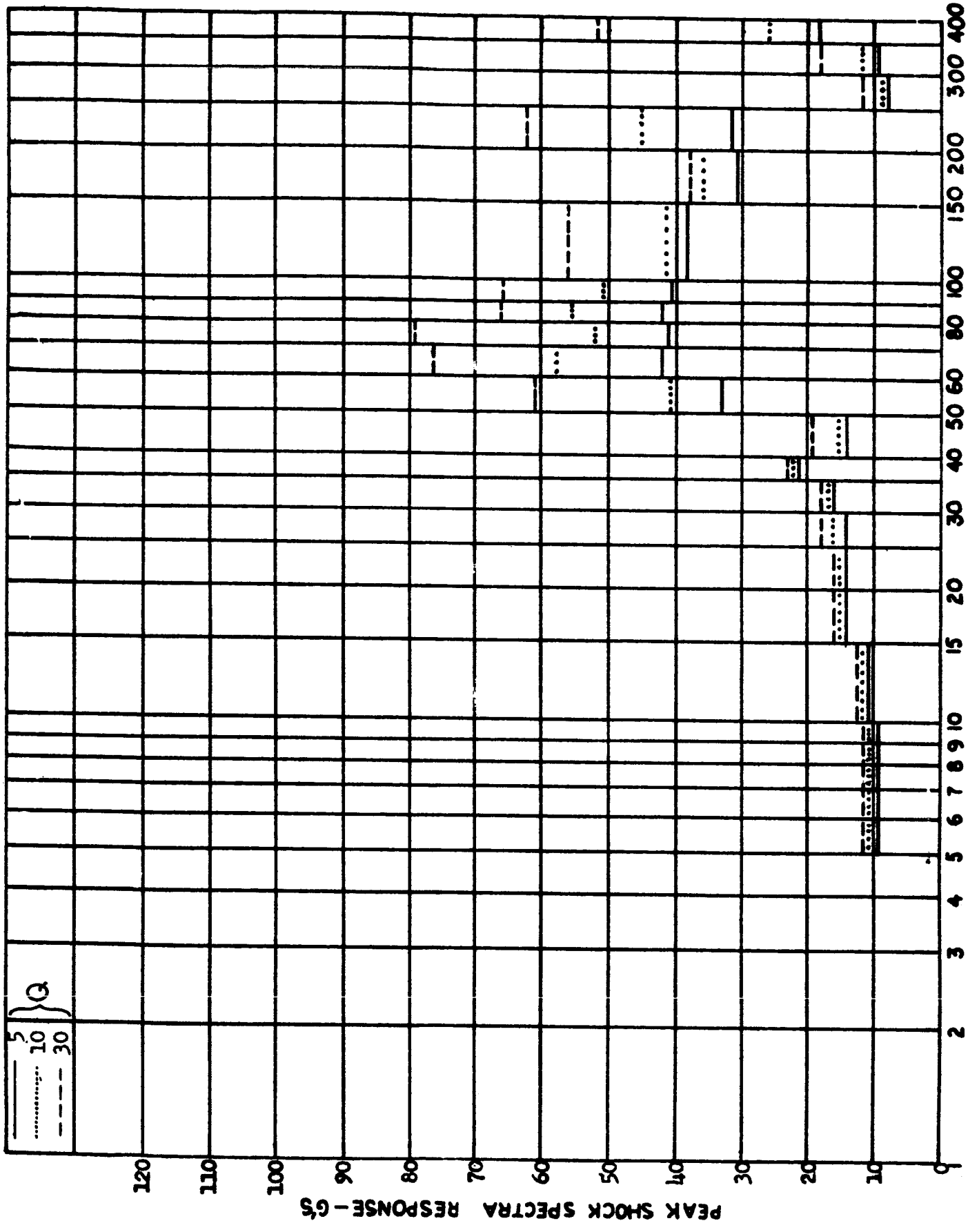

FIGURE 153 - ESTIMATED SHOCK SPECTRA ENVELOPE FOR EQUIPMENT IN AER AT AGENA IGNITION AND SHUTDOWN EVENTS

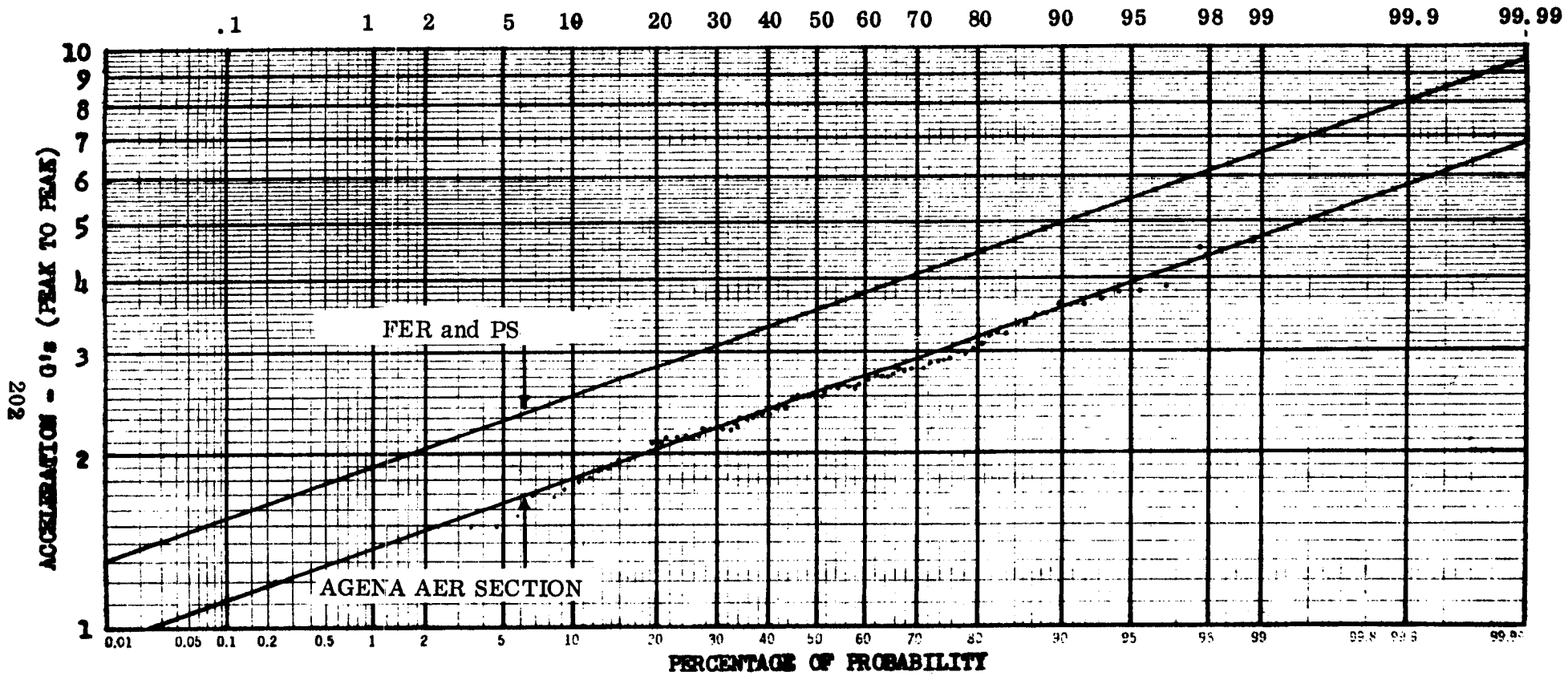

FIGURE 154 - Amplitude of Propulsion System Instability Oscillation versus Probability (Log-normal Distribution) —Thor and TAT Vehicles

Section 4

DYNAMIC CHARACTERISTICS OF THE TRANSDUCER MOUNTING BRACKETS

When analyzing structural vibration measurements consideration must be given to the effect of the added mass and change in stiffness introduced by the transducer mounting brackets. It is important to know approximately at what frequency the motion of the structure will begin to be compromised by these brackets. Step force tests were used to provide this information on the Ranger Block III vehicles. A description of this test and an evaluation of the results are given below.

Step Force Test

A step force test is conducted in the following manner. A wire is attached to a mounting bracket and placed in tension in the direction of the measurement axis of the transducer. The wire is then cut permitting the bracket, and local surrounding structure, to spring back to its normal position. The resulting transient signal generated by the transducer is then recorded.

A schematic illustrating the application of a step force test is shown in Figure 159. The resulting transient motion of the bracket, a damped oscillation of several frequencies, is shown in Figure 160. The influence of the transducer mounting bracket in the measured data can be determined from an analysis of this transient.

Mounting Bracket Correction for Vibration Measurements

The information desired is the motion of point A, Figure 155(A), due to the exciting force F, when the vibration measurement obtained is that of the motion of the mass M as shown in Figure 155(B). Here, the mounting bracket has been idealized as a simple spring-mass system attached to a point on the structure. It is assumed that

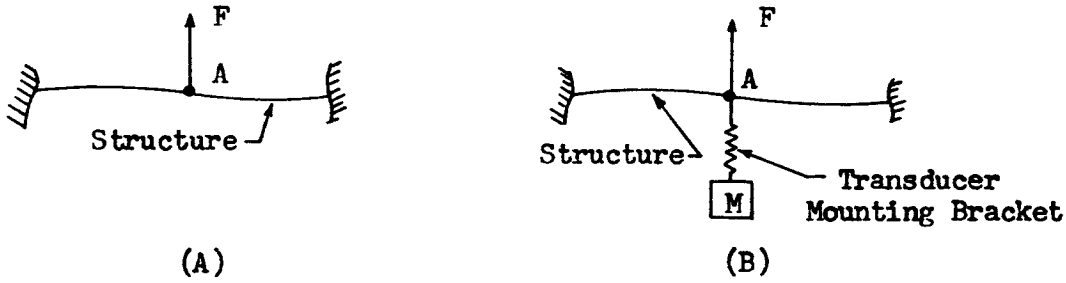

Figure 155 Assumed Measurement Mounting Bracket Arrangement

the vibration transducer itself is part of, and accurately follows the motions of mass M. Clearly, the simple idealized structural model in Figure 155(B) is only a rudimentary approximation for a real structure. However, this model will serve to illustrate the mounting bracket correction procedure.

The measured data under the conditions shown in Figure 155(B) can be corrected to obtain the motion which exists at point A, Figure 155(A), from the results of the previously described step force test. This is shown in the following analysis which was initially documented in Reference (8).

The equation of motion for the bracket under a steady forced excitation at point A (Reference Fig. 156) is:

$$k(y_1 - Z_1) = M\ddot{Z}_1 \tag{1}$$

Substituting for y and Z

$$\frac{k}{\omega^2}(b_1 - a_1)\, e^{i\omega t} = Mb_1\, e^{i\omega t} \tag{2}$$

$$a_1 = b_1\left(1 - \omega^2/\omega_n^2\right) \tag{3}$$

where $k/M = \omega_n^2$.

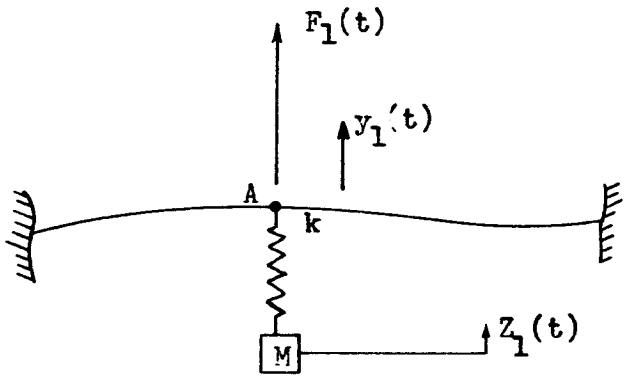

LIST OF SYMBOLS

$F_1(t)$ = $F_o e^{i\omega t}$ complex notation for the force function at point A in lb

$y_1(t)$ = amplitude time history of the point A in inches

$Z_1(t)$ = amplitude time history of the mass M in inches

$\ddot{y}_1(t)$ = $a_1 e^{i\omega t}$ complex notation for the steady forced response of A in inch/sec^2

$\ddot{Z}_1(t)$ = $b_1 e^{i\omega t}$ complex notation for the steady forced response of M in inch/sec^2

k = spring rate in lb/inch

M = mass in lb-sec^2/inch

ω = circular frequency in radian/sec

Figure 156 Description of Terms Used in Analysis of Dynamic Characteristics of Transducer Mount

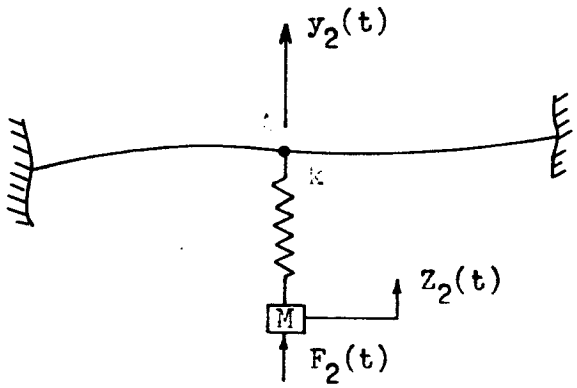

LIST OF SYMBOLS

$F_2(t) = F_2 e^{i\omega t}$ complex notation for the force function at M in lbs

$y_2(t)$ = amplitude time history of the point A in inches

$\ddot{y}_2(t) = a_2 e^{i\omega t}$ complex notation for the steady forced response of A in inch/sec^2

$Z_2(t)$ = amplitude time history of the mass M in inches

$\ddot{Z}_2(t) = b_2 e^{i\omega t}$ complex notation for the steady forced response of M in inch/sec^2

Figure 157 Description of Terms Used in Analysis of Dynamic Characteristics of Transducer Mount

The equation of motion for the bracket under steady forced excitation of the mass M (Reference Figure 157) is:

$$F_2 - k(Z_2 - y_2) = M\ddot{Z}_2 \qquad (4)$$

Substituting for y and Z

$$F_2 - Mb_2 = k/\omega^2(a_2 - b_2) \tag{5}$$

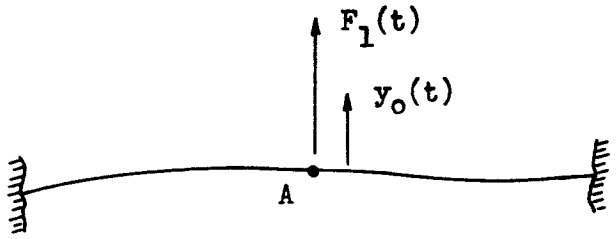

LIST OF SYMBOLS

$F_1(t)$ = $F_o e^{i\omega t}$ complex notation for the force function at point A in lbs. Same force as shown in Figure 156

$y_o(t)$ = amplitude time history of the point A, without the mounting bracket, in inches

$\ddot{y}_o(t)$ = $a_o e^{i\omega t}$ complex notation for the steady forced response of A, without the mounting bracket, in inch/sec^2

Figure 158 Description of Terms Used in Analysis of Dynamic Characteristics of Transducer Mounts

The frequency response functions for the three specific excitation and response combinations shown in Figures 156, 157, and 158 are:

$H_1(\omega)$ = b_1/F_o complex notation for the frequency response function for the response at M and the excitation at A, in inch/lb-sec^2 (6)

$H_2(\omega)$ = b_2/F_2 complex notation for the frequency response function for the response and excitation at M in inch/lb-sec^2 (7)

$H_o(\omega) = a_o / F_o$ complex notation for the frequency response function of the structure without the transducer and its mounting bracket in inch/lb-sec^2 (8)

The frequency response function $H_2(\omega)$ can be obtained, as will be demonstrated further on in this analysis, from the results of the step force test. The relationships that will now be shown are those that exist between b_1, the measured vibration, a_o, the motion of the structure without the transducer-mounting bracket, and $H_2(\omega)$.

The net force on the structure alone for the condition shown in Figure 156 is $F_o - Mb_1$. Therefore

$$H_o(\omega) = a_1 / (F_o - Mb_1) \tag{9}$$

Using equations (9), (3) and (6) the ratio H_o/H_1 is

$$H_o/H_1 = MH_o + \left(1 - \omega^2/\omega_n^2\right) \tag{10}$$

The net force on the structure alone for the condition shown in Figure 157 is $F_2 - Mb_2$. Therefore

$$H_o(\omega) = a_2 / (F_2 - Mb_2) \tag{11}$$

Using equations (11), (5) and (7), the product MH_o can be set equal to

$$MH_o = \omega^2/\omega_n^2 - MH_2/(MH_2 - 1) \tag{12}$$

From equations (10) and (12), and (8) and (6),

$$H_o/H_1 = 1/(1 - MH_2) \tag{13}$$

$$a_o/b_1 = 1/(1 - MH_2) \tag{14}$$

Equation 14 above, is the relationship that exists between the frequency response function (as obtained through the step force tests), the measured vibrations, and the motion at a point on the structure with the mounting bracket removed. The absolute value of the frequency response function $|1/(1 - MH_2)|$, the gain factor, gives the ratio of the absolute value of the response ratio a_o/b_1. The square of the gain factor, $|1/(1 - MH_2)|^2$, will give the ratio between a power spectral density measurements $S_b(\omega)$ and the actual motion $S_o(\omega)$, at a point on the structure. The above relationships are expressed in Equations 15 and 16 below.

$$|a_o| \,/\, |b_1| = |1/(1 - MH_2)| \tag{15}$$

where

$|a_o|$ = the absolute value of a_o in inch/sec^2

$|b_1|$ = the absolute value of b_1 in inch/sec^2

M = the effective mounting bracket and transducer mass in lbs-sec^2/inch

H_2 = step force frequency response function in inch/lb-sec^2

$$S_o(\omega)/S_b(\omega) = |1/(1 - MH_2)|^2 \tag{16}$$

where

$S_b(\omega)$ = measured power spectral density in in.^{2}/sec^3

$S_o(\omega)$ = power spectral density function for a point on the structure with the transducer mounting bracket removed in in.^{2}/sec^3

Step Force Frequency Response Function

The Fourier transform of the step force function applied during a step force test is

$$F_2(f) = \int_{-\infty}^{\infty} \pm P_2 e^{-i2\pi ft}\, dt = \pm iP_2/2\pi f \qquad (17)$$

where

$F_2(f)$ = Fourier transform of the step force function in lbs/cps

$\pm P_2$ = step force function in lbs - plus sign is used when the direction of the applied force is along the positive sensing axis of the transducer; negative sign is used when the applied force is applied in the direction opposite to the positive sensing axis of the transducer

f = frequency in cps

The Fourier transform of the step force response, see Figure 160, is

$$G_2(f) = \int_{-\infty}^{\infty} h(t)e^{-2\pi ft}\, dt \qquad (18)$$

where

$G_2(f)$ = Fourier transform of the step force response in g's/cps

$h(t)$ = step force response in g's

The step force frequency response function $H(f)$, in units of g's/lb, is given by

$$H_g(f) = \frac{G_{2(f)}}{F_2(f)} = \pm i \frac{2\pi f}{P_2} G_2(f) \qquad (19)$$

To reflect the change that has been made in the units, equation 16 becomes

$$G_o(f)/G_b(f) = |\, 1/(1 - WH_g)\,|^2 \qquad (20)$$

where

$G_o(f)$ = measured power spectral density in g^2/cps

$G_b(f)$ = power spectral density function for a point on the structure with the transducer mounting bracket removed in g^2/cps

Figures 161 and 162 present the real and imaginary parts of the Fourier transform $G_2(f)$, of the transient, $h(t)$, shown in Figure 160. Figures 163 and 164 are power spectral density plots corrected, as per equation 20, for a mounting bracket weight of 0.1 pounds. The vibration pickup mounting brackets weighed approximately 0.2 pounds. For the frequency range up to 1400 cps, it can be assumed that the mounting brackets did not compromise the motion of the structure.

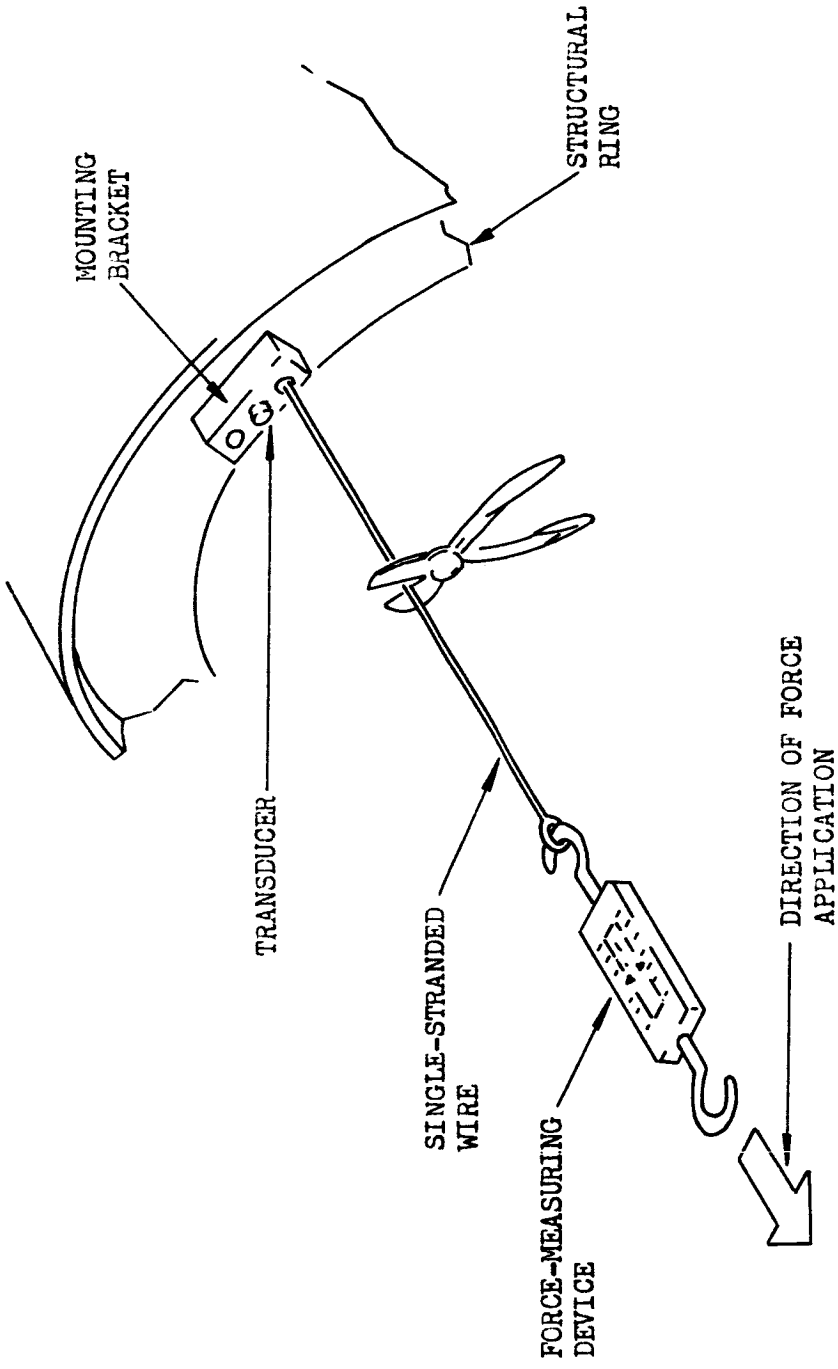

Fig. 159 Schematic Diagram of Step-Force Method of Application.

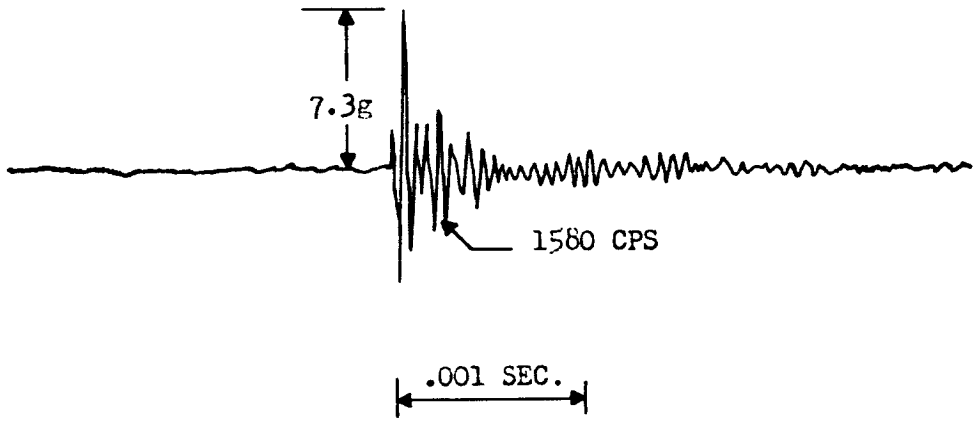

Fig. 160 Transient Response Obtained During Step-Force Test on Ranger Vehicle 6006 Measurement PL 23 (10 pound pull).

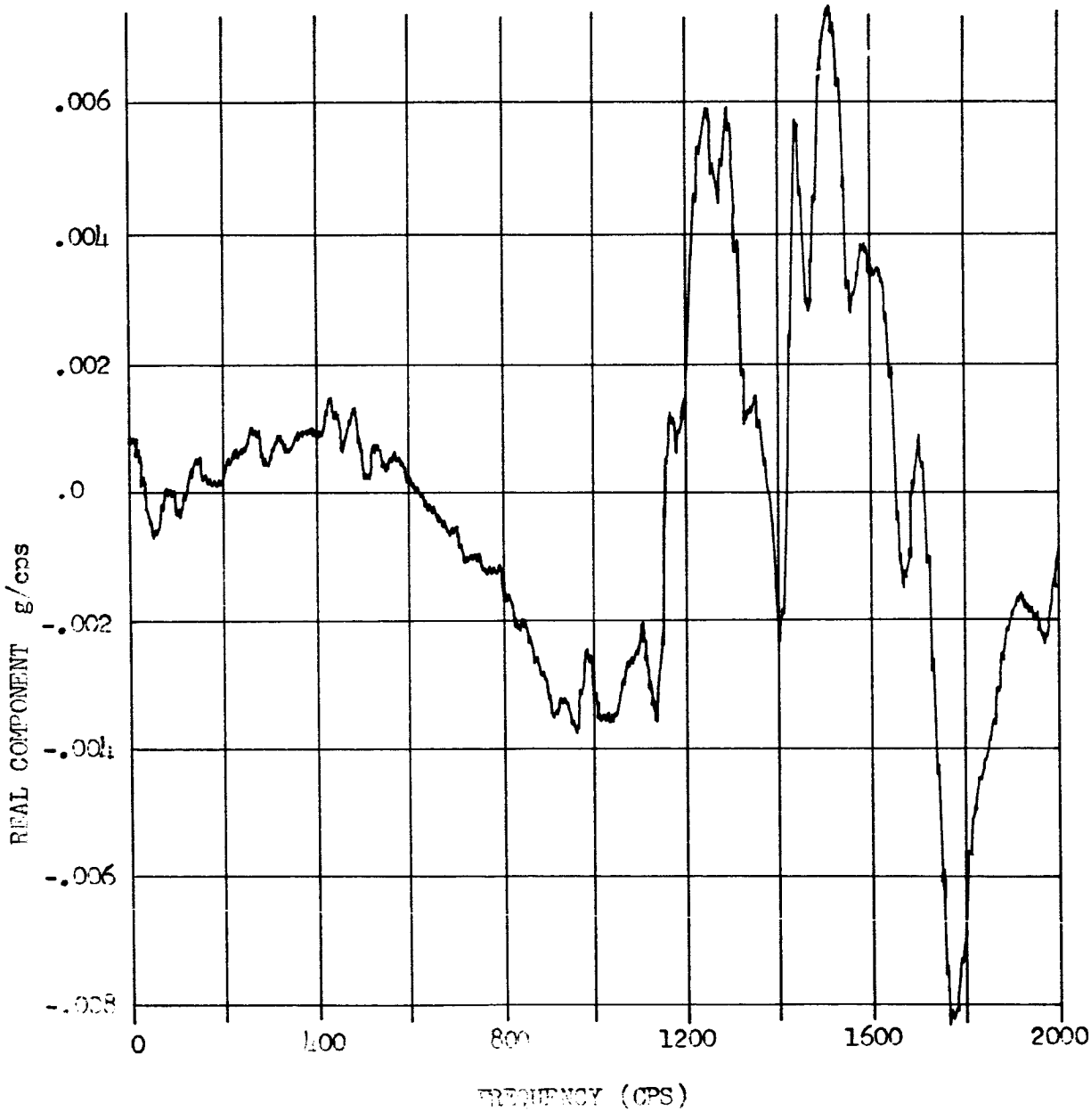

Fig. 161 Fourier Transform (Real Part) of Step Force Transient on Ranger 6006 Measurement PL 23.

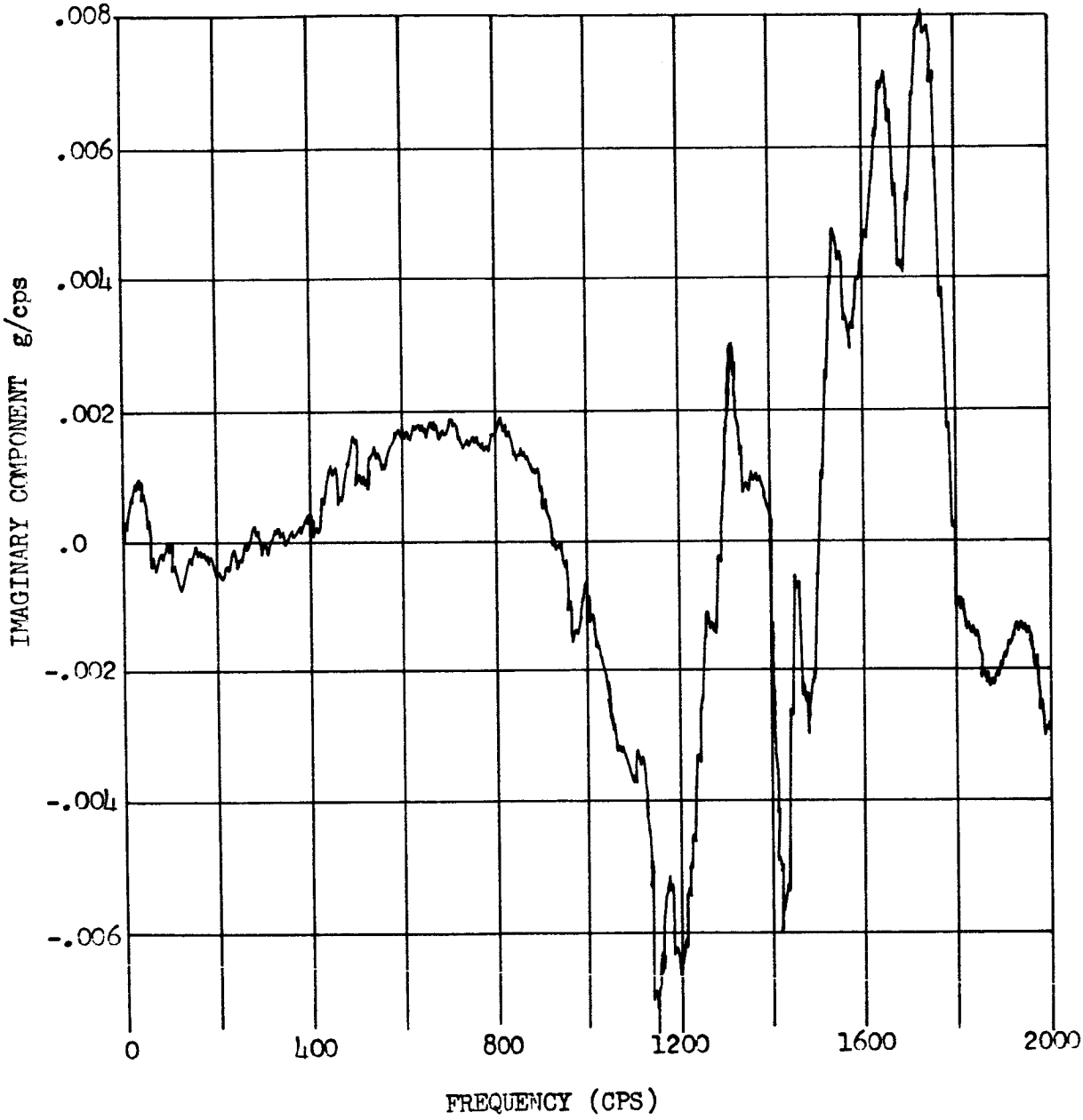

Fig. 162 Fourier Transform (Imaginary Part) of Step Force Test Transient on Ranger 6006 Measurement PL 23.

FREQUENCY	ACCELERATION SPECTRAL DENSITY $g^2/cps \times 10^2$	
	MEASURED	CORRECTED
160	.05	.05
270	.105	.105
292	.315	.315
340	.175	.175
390	.34	.34
400	.29	.29
426	.41	.425
482	.10	.115

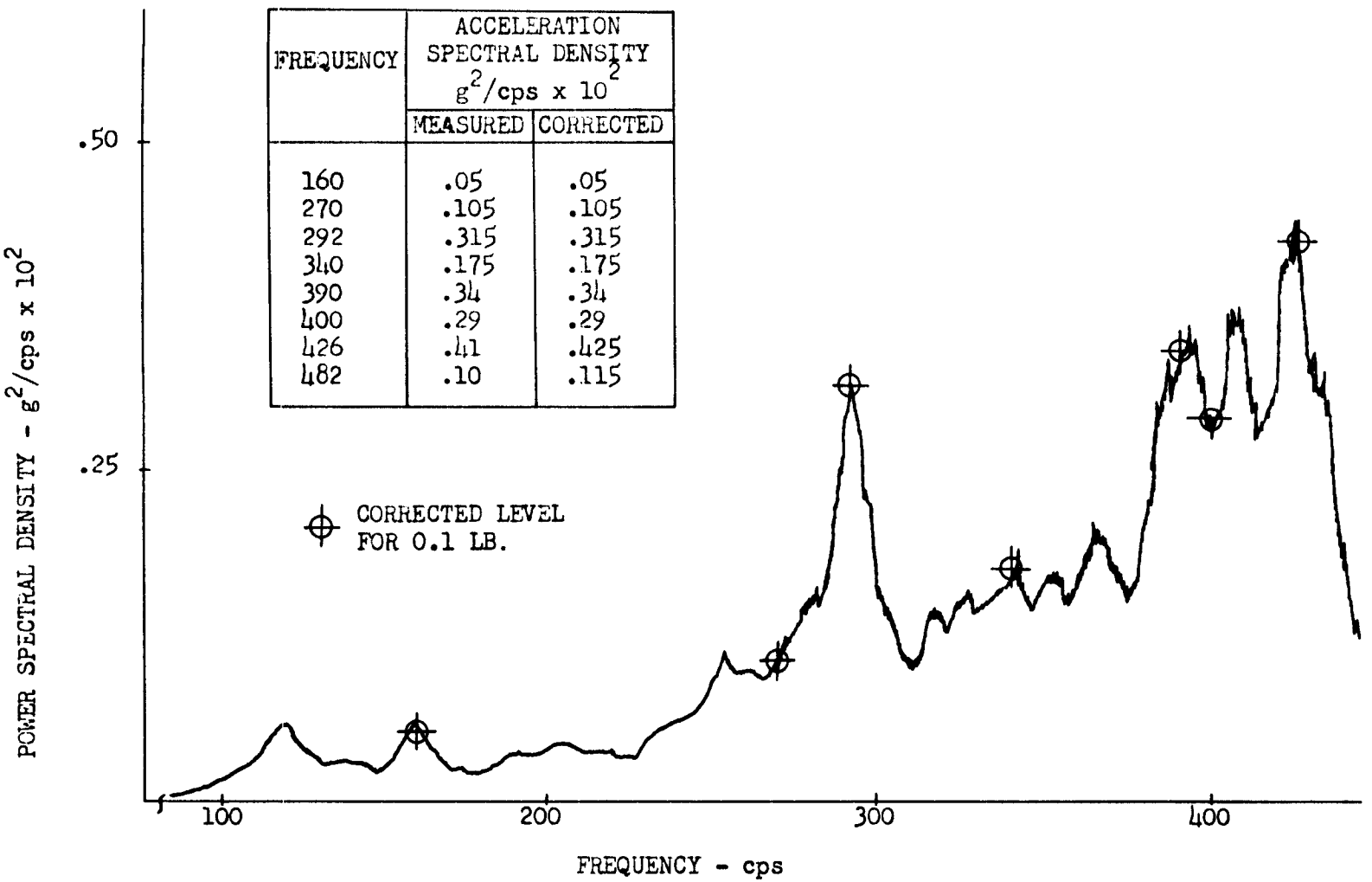

Fig. 163. Corrected Values of Power Spectral Density for Ranger 6006 Measurement on Adapter (Tangential)

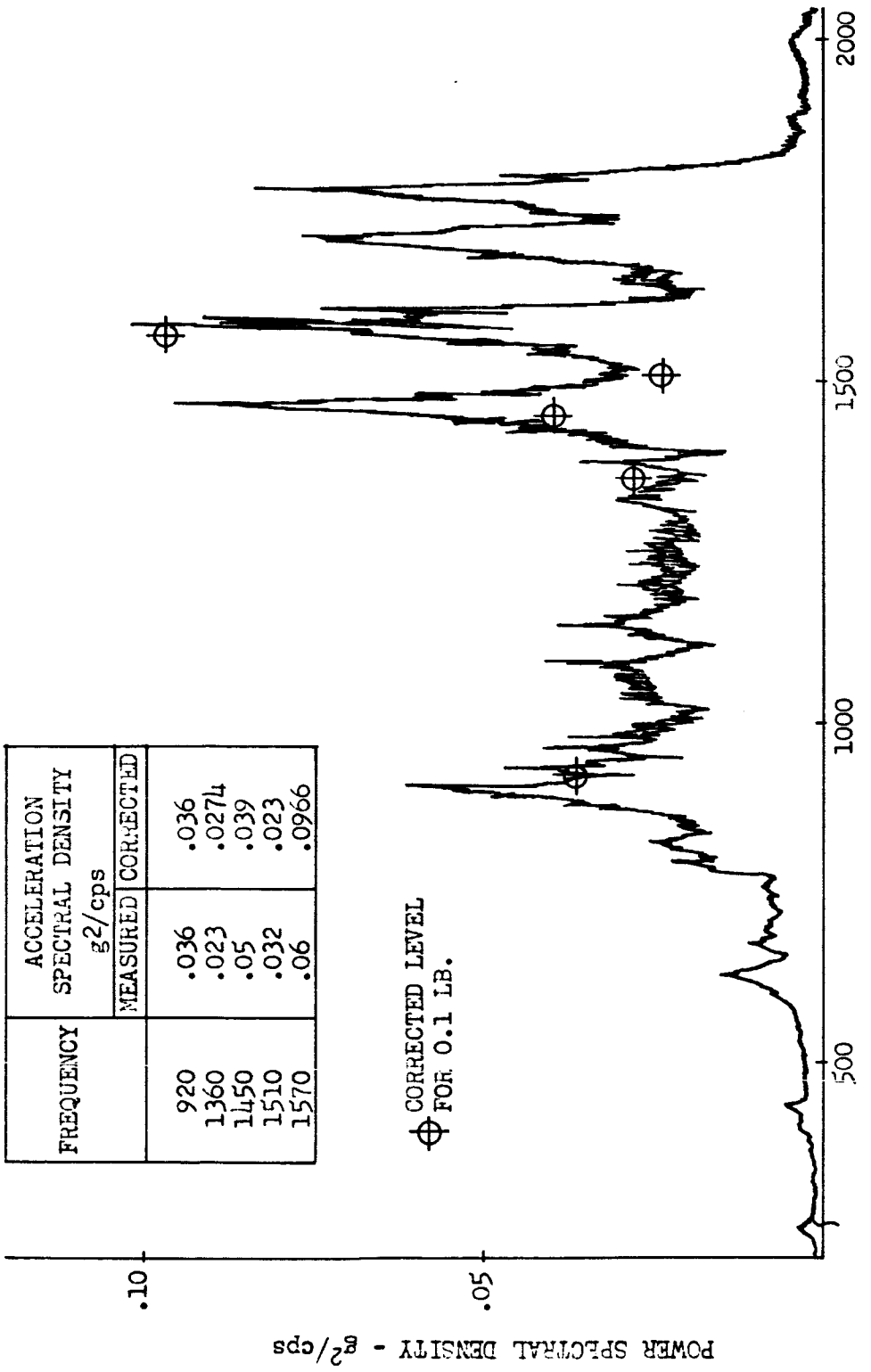

Fig. 164 Corrected Values of Power Spectral Density for Ranger 6006 Measurement on Adapter (radial).

Section 5

INTERPRETATION OF ENVIRONMENTS FOR TEST SPECIFICATIONS

The previous sections have been devoted to descriptions of the methods of analysis employed in determining the acoustic, random vibration, and quasi-periodic environments encountered by the Agena vehicle and associated payload. This section presents a brief dissertation on how these environments, as described, can be interpreted in terms of qualification test specifications. Finally, an example is given for a specific vehicle configuration illustrating the recommended methods of interpretation of the environments into test specifications.

Acoustic Qualification Tests

As discussed previously in this report, both the launch and transonic acoustic environments have been described in terms of launch-field environments. In the case of transonic flight, an "effective" launch-field acoustic environment was found which would produce the structural response effects measured during transonic flight. Prescribing test specifications for this environment presents little difficulty, therefore, since acoustic test facilities such as reverberant chambers expose the test specimen to a similar type of acoustic environment.

LMSC experience, based upon data scatter observed in measurements made in similar acoustic environments, has revealed that a representative scatter band is 5 db in any octave band. Based upon substantial LMSC test experience, the present state-of-the-art in acoustic testing usually precludes control of excitation in any octave band within 5 db. In catering for these limitations, and in order to impose test conditions above expected service conditions (which is desirable when one specimen sample is used), LMSC is of the opinion that acoustic test specifications levels should be 5 db higher than the nominal level shown in Section 1 (see example p. 222)

Random Vibration Testing

Equipment

In general, the available power spectral density (PSD) plots indicate the presence of relatively low background random vibration, extending from low frequencies up to 2000 cps, with superimposed concentrations ("spikes") of energy, approximately 50 cps wide at their base. These "spikes" have relatively high PSD values and account for approximately 80 to 90 percent of the total PSD G_{rms} value.

The random vibration environment for equipment described in Section 2 has been specified in terms of maximum values, 95 percent probability values, and background values of power spectral density. The maximum and the 95 percent PSD plots are essentially envelopes of peak PSD values which could exist during flight within the narrow 50 cps bandwidths but should not be used to estimate the overall G_{rms} levels. The background vibration values, which have been adjusted to the 95 percent probability value of all overall levels measured, are considered to be indicative of the shape of the lower level background random vibration environment.

In the opinion of LMSC, an appropriate test for this environment would be to apply to equipment a background random vibration level, consistent with the values provided, and to superimpose upon this a narrow band "spike" by means of sweeping a 50 cps tracking filter. The energy within the 50 cps bandwidth to be applied should be established from the 95 percent plots by calculating the G_{rms} value associated with the highest energy "spike" in the data being considered. This value should be used to sweep in the ranges where significant concentrations ("spikes") of energy appear. (See example, page 222.)

In the opinion of LMSC, a sufficient degree of overtest above nominal flight level is obtained by testing in this fashion. Since the superimposed "spikes" represent approximately 80 percent of total G_{rms} levels, and background random vibration has been set at the 95 percent probability value of all measured overall values, the overtest is approximately 1.8 times the 95 percent probability overall flight level. (In terms of 99 percent probability values, the test level is approximately 25 percent above flight level).

Large Structural Assemblies

LMSC experience with random vibration testing of large structural assemblies such as payloads, Agena forward racks, and Agena aft racks, has shown that acoustically induced random vibration environments cannot be effectively simulated using large dynamic shaker techniques. The major drawbacks in testing for random vibration in this fashion are:

(1) Large attenuations of the input excitations, applied at the base of a payload for example, are obtained due to the dynamic characteristics of the specimen. Similar inflight attenuations of the level present at the payload/Agena interface would also occur, however, additional random vibration response of the payload is caused by acoustical energy transmitted across the air mass between the shroud and the payload. To produce adequate random vibration levels at regions of the payload remote from the input, it was found necessary to apply unrealistically severe conditions to regions of the specimen near the shaker.

(2) It was found that the dynamic characteristics of the specimen also modified substantially the random vibration frequency spectrum applied at the input location, and different spectrums were produced at various locations. Therefore it is not possible, using this method of test, to produce the desired random vibration spectrum shape at all regions of the specimen.

LMSC has concluded that to qualify structural assemblies for acoustically induced random vibration environment, acoustical excitation should be used. A test in which interface random vibration is simulated by excitation from a series of small electrodynamic shakers while the specimen is exposed to an appropriate acoustic excitation, may provide the best simulation of flight conditions.

The interface random vibration environments have been defined in Section 2 in terms of maximum, 95 percent probability, and mean values, and should be interpreted into test levels in the same manner as previously described for equipment testing.

Equipment and Large Structural Assemblies

Many methods have been adopted in the industry to test for transient quasi-periodic environments such as those which are produced during engine ignition and shutdown events; the most notable of these are the following:

(1) Application of, by means of an electro-dynamic shaker system, steady state sinusoidal excitation sweeps over the frequency range of interest. The test levels in such cases are often evaluated from shock spectra data of the transient being tested for and are determined by evaluating the equivalent steady-state sinusoidal excitation that would produce the same peak response in a single-degree-of-freedom system as would the transient being tested for.

(2) Application, again by means of a shaker system, of decaying transient oscillations similar to those observed during flight. In this case, the magnitude of the applied excitations is measured and controlled by the magnitude of the shock spectra of the applied transient, and also an examination of the wave form of the applied transient with respect to peak value and frequency content. This method utilizes a device called a shock spectra synthesizer which is now available to the industry.

In view of the highly successful experience with the latter mode of testing, as described in Reference (5), it is recommended by LMSC for qualification of structures and equipment for transient environments such as engine ignition and shutdown transients. The method is preferred because it provides for a more realistic representation of the transient environment wave forms and provides better simulation of applied strain rates than does the sinusoidal sweep test. Each event should be tested separately using the appropriate shock spectra data provided.

Since the present shock spectra synthesizer available has a lowest filter center frequency of 16 cps, events which have significant excitation at frequencies lower than

this value should be tested for using the equivalent sinusoidal sweep technique. Also, "Pogo" environments should be tested for using sinusoidal sweeps.

In the opinion of LMSC, the levels established from the data contained in this report should, for the purposes of qualifications testing for quasi-periodic environments, be increased by 25 percent, since only one test sample is usually available. It was established in Reference (9) that a constant octave sweep rate of 3 minutes per octave was sufficient to produce steady state conditions in a viscously damped single-degree-of-freedom system. This sweep rate is recommended for tests in which the equivalent sinusoidal technique is being employed. In cases where test specifications for payloads having weights greater than 3000 pounds are required it is recommended that transient test criteria be developed from theoretical analysis of the vehicle configuration being considered. This would be accomplished by compiling dynamic models of the booster/payload combination and applying thrust build-up or thrust decay profiles to these systems as required. LMSC adopts digital computer techniques in this analysis which yield acceleration-time histories at the location of the vehicle of interest, from which shock spectra analyses are evaluated for use as the transient test control media.

Example of Test Specification

The following is a qualification test specification for an Agena payload, having a weight of 2000 lb and a cone-cylinder shroud configuration (see Figure 165) which is to be launched from a "dry" launch pad using the TAT booster system. It will be assumed that a preliminary resonance survey of the specimen has yielded a minimum resonant amplification of equipment of 5.0.

Acoustic Test

Referring to Figures 9 and 13, which respectively describe the launch and transonic acoustic environments for this shroud and booster combination launched from a "dry" pad, the combined envelope of the two environments (which has been increased by 5 db)

is as shown in Figure 166. The combined external environment is described by Figure 166(A) while the combined internal environment is denoted by Figure 166 (B). The Figure 166(A) levels should be used when acoustic testing of the payload is conducted with its shroud, while the Figure 166(B) level apply in the case where testing is conducted without the shroud.

Random Vibration

For payload assemblies as stated earlier in this section, LMSC does not recommend random vibration testing using large electro-dynamic shaker techniques to simulate this acoustically induced environment in large structures. It may be realistic however, to simulate acoustically induced random vibration environment which is introduced to the payload across the payload/Agena interface using a series of small shakers attached to the interface, while the acoustic excitation is being applied. This method of combining acoustic excitation with mechanically simulated vibration would only be used if an acoustic facility was not available which was large enough to accommodate an Agena forward section, assembled to the payload specimen. If it is desired to mechanically reproduce the random vibration levels at the interface, the environmental data presented for internal structure in Figures 49, 51, 79, and 81, apply. The random vibration occuring during transonic is the most severe for this configuration and therefore should be used. Background random vibration shaped as shown in Figure 81 (having overall level of 19 G_{rms}) should be applied. Superimposed upon this should be a narrow band random vibration applied by means of a tracking filter in the frequency range 400−2000 cps.

The G_{rms} value of the narrow band random to be applied is obtained by assuming a triangular shape for the spike having the maximum 95 percent PSD value (Figure 79), so that the G_{rms} value in the narrow band is given by:

$$G_{rms} = \sqrt{0.5\ (3.0\ g^2/cps)\ (50\ cps)} = 8.7\ G_{rms}$$

Equipment

The equipment environments for the launch and transonic phases are obtained from Figures 37,38,82, and 84. The transonic condition is the more severe and therefore should be used. The background random vibration level should be shaped as shown in Figure 84 and have an overall level of 16.8 G_{rms}, while the narrow band level to be applied using the tracking filter should be:

$$G_{rms} = \sqrt{0.5\ (0.5\ g^2/cps)\ (50\ cps)}$$

$$= 3.5\ G_{rms}$$

Quasi-Periodic Environment

Payload Assembly

The environments to be tested for are ignition and shutdown of the TAT engines, "Pogo" oscillations and transient oscillations resulting from ignition and shutdown of the Agena main engine. Comparing Figures 108 and 113, it can be seen that of the two booster ignition and shutdown events the former is the most severe; yielding an equivalent sinusoidal level of 2.6 divided by 5 = 0.52 G (0 to peak). However, the 99 percentile "Pogo" oscillation values is 3.25 G (0 to peak) and is the governing environment in the 15 to 20 cps frequency range. The test level recommended for this frequency range is 3.25 (1.25) $\simeq$ 4.0 G using a constant octave sweep rate of 3 minutes per octave.

The most severe Agena transient event, according to the data shown in Figures 128, 134,140, and 145 occurs at Agena first shutdown (Figure 134). This shock spectra analysis should therefore be used as the control criteria for transient testing of this payload specimen. The control accelerometer should be attached to the payload primary structure in the region(s) where it is desired to apply the appropriate

excitation (i.e., where significant or sensitive payload equipments are located). The test is conducted by means of an electro-dynamic shaker system to which the specimen is attached, and the shock synthesizer unit. A series of pulses are to be applied to the specimen until, by means of adjustment of the bank of filters which are within the synthesizer, the shock spectra of the transient output of the control accelerometer matches to desired shock spectra. LMSC recommends, for qualification purposes, that the Figure 134 results be increased by 25 percent to compensate for the fact that only one sample is generally tested.

Payload Equipment

The shock synthesizer technique should also be used for transient testing of equipment. The appropriate criteria, in this case, would be Figure 151 increased again by 25 percent.

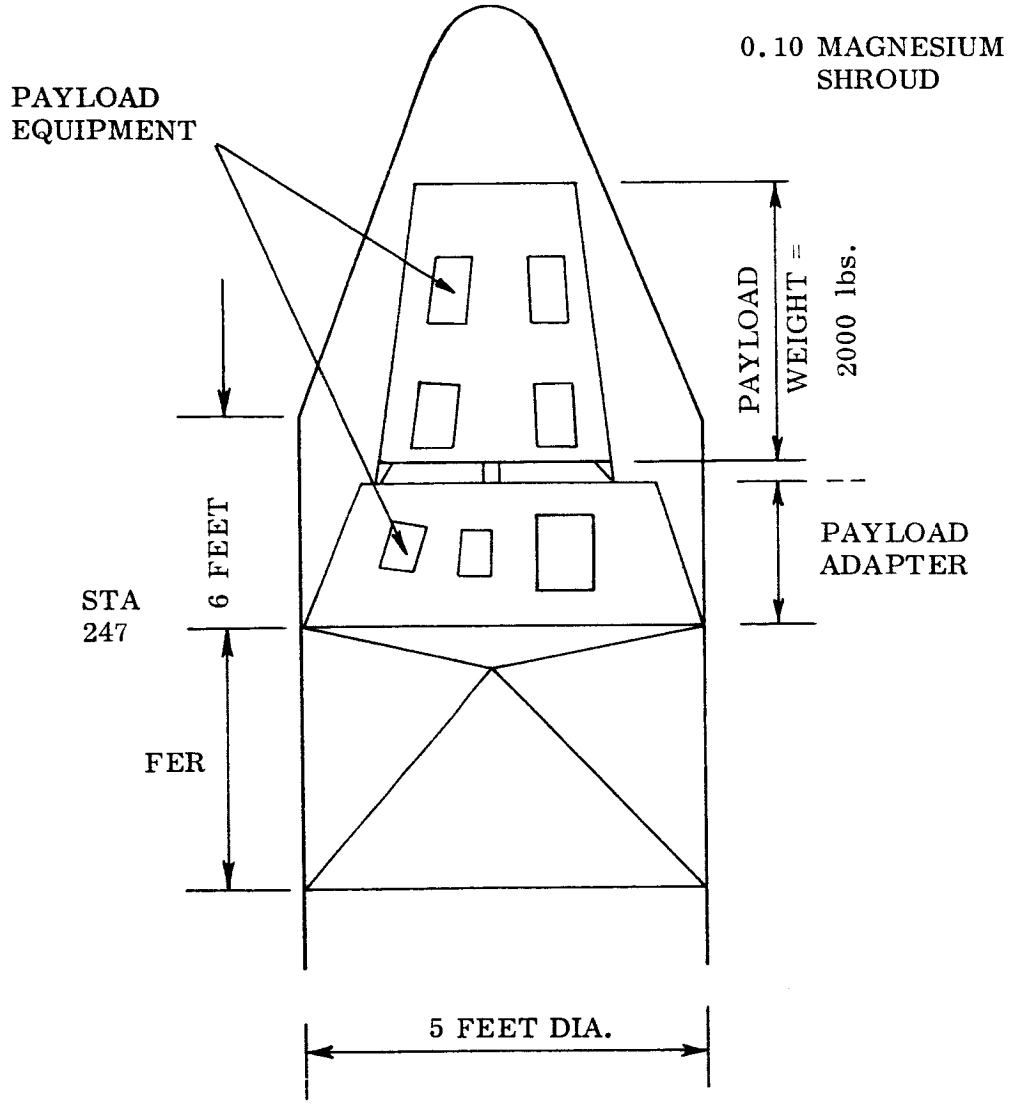

Fig. 165 Vehicle Configuration for Illustrative Example of Test Specification.

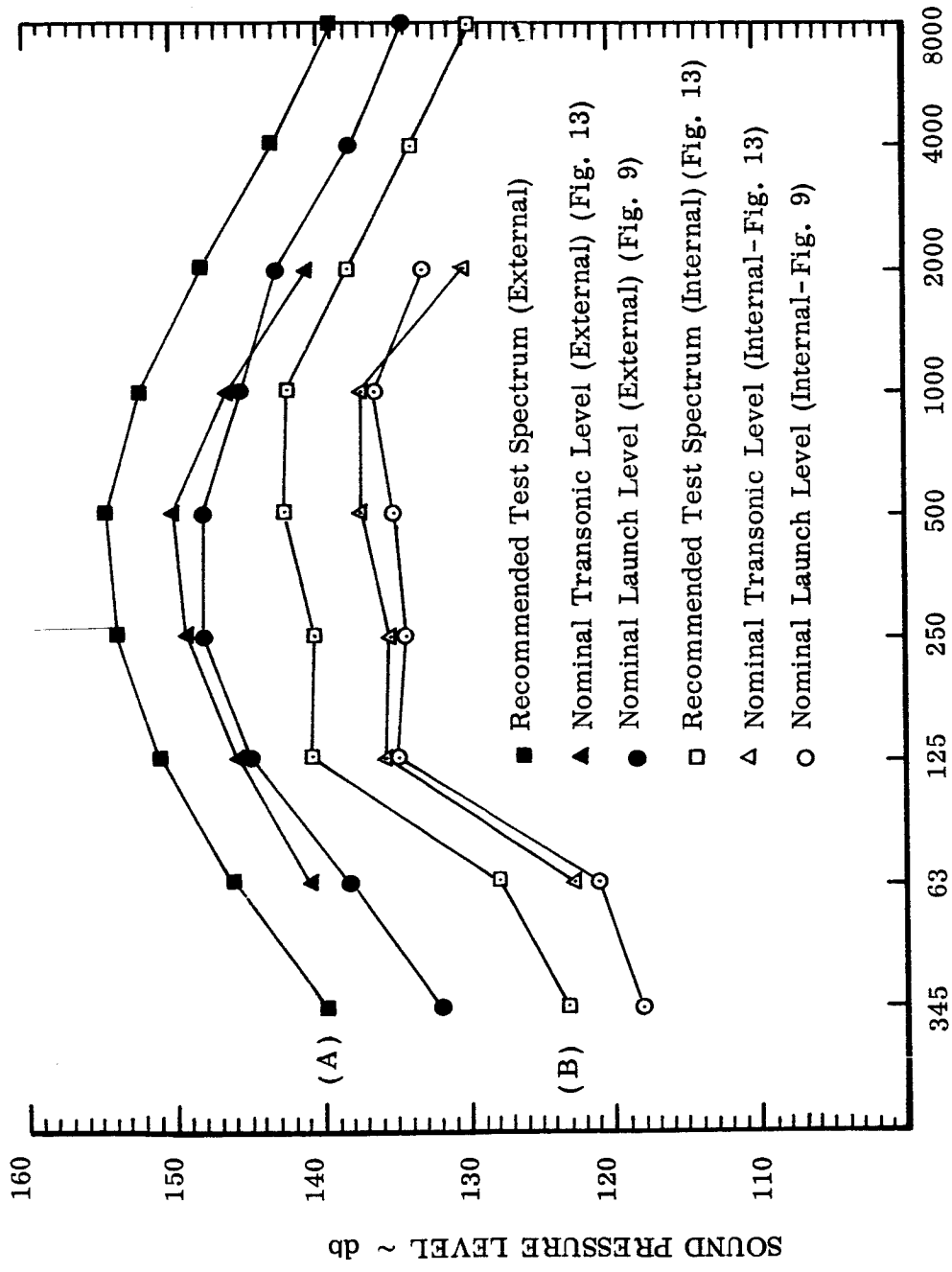

Fig. 166 Acoustic Test Levels for Illustrative Example

CONCLUSIONS

The acoustic, random vibration and quasi-periodic environments encountered by the Agena vehicle, during a variety of mission configurations, have been defined in the foregoing sections of this report. The form of the acoustically induced random vibration environment in the vehicle is such that it can be best simulated by means of the application of low level background random vibration with a superimposed narrow band high energy random vibration which sweeps over a wide range of frequency. On the basis of successful LMSC experience with simulation of engine shutdown transients using the shock spectra synthesizer, LMSC recommends that this method of test be considered and investigated for future qualification programs of large structures and equipment. In estimating certain random vibration environments corresponding to high acoustic excitations (157 db), it was conservatively assumed that observed correlations between random vibration and low levels acoustic excitation (up to 153 db) prevailed at the higher levels. It is recommended that the levels provided be used until appropriate flight measurements be made to verify the environments. The presence of significant random vibration levels in the aft section (Station 409) during the entire Agena burn period indicates the need for additional flight measurements to determine the distribution of this environment throughout the aft section.

REFERENCES

(1) LMSC/636953, SS/747/5351, "S-01B Dynamic Qualification Summary Report", 6 March, 1964

(2) LMSC/A778347, SS/1066/5522, Structures Study, "Qualification Test Requirement for Booster Adapter-Mounted Equipment", dated 16 December, 1965, M. Wherry and A. Houston.

(3) LMSC/72065 "Gemini ATV Forward Section and Auxiliary Rack Acoustical Test."

(4) Gemini Vehicle 5001 Static Firing Data Pack, Published by LMSC Organization 59-33.

(5) LMSC/A775401, Structures Study SS/1055/5522; "Qualification of Program P-50 Vehicle for Anticipated Vibration Environment", A. Houston, dated 19 November, 1965.

(6) LMSC Document, Structures Study SS/277/5522, "Estimated Advent Load Response to Random Pressure Fields", R. Bieser, dated Jul, 1961.

(7) LMSC Document, Structures Study SS/113/5351, "Transient Loads in Non-Uniform Beams Resulting From Lateral, Longitudinal or Torsional Vibrations", G. H. Moore.

(8) LMSC Document, Structures Study SS/964/5522, "Flight Correction Measurement Techniques for Defining Vibration Environments, Y. Morimoto (Dept. 55-22)

(9) LMSC Document, Structures Study SS/352/5318, "Response of a Single Degree of Freedom System to Exponential Sweep Rates, II; P. Hawkes, dated May 8, 1962.

APPENDIX A –

SUMMARY OF VEHICLES EXAMINED IN ANALYSIS OF ENGINE IGNITION AND SHUTDOWN TRANSIENTS

(1)	(2)	(3)	(4)	(5) "Flat" Freq. Resp. of Telemetry Syatem (cps)	EVENTS ANALYZED (6)	(7)	(8)	(9)	(10)	(11)	(12)
Vehicle	Booster	Location	Meas.		Lift-off	MECO	SECO	Agena 1st Ignition	Agena 1st Shutdown	Agena 2nd Ignition	Agena 2nd Shutdown
1162	TAT	FER	D7	100	S	S		S	S		
1163	TAT	FER	D7 (A)	100	P, D	P,D		-			
			A531 (T)	200	-	-		S	S		
			A529 (T)	200	-	-		S	S		
		AER	A532 (T)	200	-	-		S	S		
			A530 (T)	200	-	-		S,P	S		
			A528 (A)	200	-	-		S,P	S		
			A527 (A)	200	-	-		S,P	S		
		FER	D7 (A)	100	P, D	P,D		P,D	P,D		
1164	TAT	PS	A522 (T)	50	S	-		P	-		
		AER	A523 (T)	60	S	-		P,S	-		
1165	TAT	FER	D7 (A)	100	P,D,S	S		P,D,S	S		
		FER	D7 (A)	100	P,D			-	P,D		
1166	TAT	BTL Unit(PS)		450	-			P,S	P,D		
		AER	A523 (T)	60	-			P,S	P,S		
		FER	D7 (A)	100	P,D,S	S		S	P,D,S		
1167	TAT	FER	A536 (A)	1000	-	-		-	P,D		
		PS	A522 (T)	50	-	-		P	P,S		
		BTL Unit(PS)		450	-	-		P,S	P		
		AER	A523 (T)	60	-	-		P,S	P,S		
1168	TAT	FER	D7 (A)	100	P,D				-		
		FER	A522 (T)	50	-				P,D		
		AER	A523	60	-				P,S		
1169	Thor	FER	D7 (A)	100	P,D,S	S		S	P,D,S		

D = ANALYSIS OF TRANSIENT DAMPING

P = ANALYSIS OF TRANSIENT PEAKS

S = SHOCK SPECTRA ANALYSIS

(1) Vehicle	(2) Booster	(3) Location	(4) Meas.	(5) "Flat" Freq. Resp. of Telemetry System (cps)	EVENTS ANALYZED (6) Lift-off	(7) MECO	(8) SECO	(9) Agena 1st Ignition	(10) Agena 1st Shutdown	(11) Agena 2nd Ignition	(12) Agena 2nd Shutdown
1172	Thor	AER	A520 (A)	100				S			
1175	TAT	FER	D7 (A)	100	P,D						
1401	Thor	FER	D7 (A)	100	P,D						
1411	Thor	FER	D7 (A)	100	P,D						
1412	Thor	FER	D7 (A)	100	P,D				P,D		
2314	TAT	PS	A3 (T)	160	P,D,S	-			P		
			A4 (T)	110	P,D,S	-			-		
			A9 (A)	450	P,D,S	P,D			P,S	•	
2313	Thor	PS	A004	110	P,D						
			A003	160	P,D						
			A009	450	P,D						
2353	Thor	FER	D7 (A)	100	S	S		S			
2301	Thor	FER	A3 (A)	160	P,D						
			A9 (T)	450	P,D						
6501	Atlas	FER	PL 30 (A)	40		S		S	S	S	S
		FER	PL 31 (T)	110		S		S	S	S	S
		FER	PL 33 (T)	160		S		S	-	S	S
		P/L PS	PL 20 (A)	1000		S		-	S	S	S
		P/L PS	PL 21 (T)	800		S		S	S	S	S
6301	Thor	FER	A004 (A)	100				S			
			A002 (T)	160				S			
			A006 (T)	800				S			
			A005 (A)	1000				S			

(1)	(2)	(3)	(4)	(5) "Flat" Freq. Resp. of Telemetry System (cps)	EVENTS ANALYZED (6) Lift-off	(7) MECO	(8) SECO	(9) Agena 1st Ignition	(10) Agena 1st Shutdown	(11) Agena 2nd Ignition	(12) Agena 2nd Shutdown
Vehicle	Booster	Location	Meas.								
6008	Atlas	PS	PL31	110		P,D,S	S		S	-	-
			PL32	100		-	S		P,D,S	P,D	P,D
			PL33	160		P,D,S	S		S	-	-
			PL23	800		-	S		-	-	-
6009	Atlas	PS	PL20	800	-		S	-	-	-	S
			PL34	60	-		-	S	-	P	P
			PL31	110	P,D	P,D,S	-	S	-	-	-
			PL33	160	-	S	-	S	S	P	SP
			PL32	100	P,D	P,D	-	P,D,S	S	P,D	P,D
6101	Thor	PS (A)	AD007	100	S	-	-	-	-	-	-
		PS (T)		110	-	-	-	-	-	P	P,S
		FER (T)		220	-	-	-	-	-	P	P,S
		FER (A)		450	-	-	-	-	-	P	P,S
		FER (A)	AA014	450	-	-	-	P,S	P,S	P,S	P,S
		FER (T)		220	-	-	-	-	-	P,S	P,S
		PS (T)	Loc. 2	110	-	-	-	-	P,S	-	-
		PS (T)	Loc. 6	160	-	-	-	-	P,S	-	-
		PS (T)	Loc. 5	220	-	-	-	-	P,S	-	-
		PS (A)	Loc. 9	600	-	-	-	-	P,S	-	-
		FER (T)	AA018	160	S	-	-	-	-	-	-

(1)	(2)	(3)	(4)	(5) "Flat" Freq. Resp. of Telemetry System (cps)	EVENTS ANALYZED (6) Lift-off	(7) MECO	(8) SECO	(9) Agena 1st Ignition	(10) Agena 1st Shutdown	(11) Agena 2nd Ignition	(12) Agena 2nd Shutdown
Vehicle	Booster	Location	Meas.								
1203	Atlas	AER	A190 (T)	2000	-	S					
			A009 (T)	150	-	P,D					
			A003 (A)	250	P,D	P,D					
2402	Atlas	AER	A009	800	-	P,D					
		AER	A003	50	-	P,D					
2404	Atlas	AER	A009	800		P,D					
7001	Atlas	~~PAL~~ PS	A10 (A)	750		S		S		S	
			A11 (T)	750		S		S		S	
			A12 (T)	750		S		S		S	
			AI86 (A)	500		S		S		S	
			AI87 (T)	500		S		S		S	
			AI88 (T)	500		S		S		S	
6001	Atlas	PS	RA005	800	S	-					
			RA006	1000	S	-					
			RA001	100	P,D	-					
			RA002	110	P,D	-					
			RA003	160	P,D	S					
6002	Atlas	PS	RA001	100	P,D	-					
			RA003	160	P,D	S					
6003	Atlas	PS	RA001	100	P,D						
			RA003	160	P,D						
6004	Atlas	PS	RA001	100	F,D,S	P,D			P,D		
			RA003	160	S	P,D					
6005	Atlas	PS	PL33	1000	P,D	P,S					
			PL32	800		P					
			PL31	160		S					

(1)	(2)	(3)	(4)	(5) "Flat" Freq. Resp. of Telemetry System (cps)	EVENTS ANALYZED (6)	(7)	(8)	(9)	(10)	(11)	(12)
Vehicle	Booster	Location	Meas.		Lift-off	MECO	SECO	Agena 1st Ignition	Agena 1st Shutdown	Agena 2nd Ignition	Agena 2nd Shutdown
		~~PAL~~ PS	A006 (T)	1000	S	S		S			
			PL 32(T)	100	S	S		S			
			PL 36(T)	110	S	S		S			
			PL 34(A)	160	S	S		S			
6201	Thor	FER	A5	30	S	S		S	S	S	S
			A3	50	S	S		S	S	-	-
			A4	60	S	S		S	-	S	S
		AER	A9 (A)	20	S	S		S	S	S	S
			A8 (A)	800	S	S		S	-	-	-
4701	Atlas	FER	D7 (A)	100	S	S			S		
			P2 (T)	800	S	-			S		
			P1 (A)	1000	S	-			S		
4702	Atlas	FER	D7 (A)	100	S				S		
			P1 (A)	1000	S				S		
4703	Atlas	FER	D7 (A)	100	S	S			S,P,D		
			P2 (T)	800	S	-			S		
			P1 (A)	1000	S	-			S		
6932	Atlas	~~PAL~~ PS	PL 37	100	-	-	S		P,S		P,S
			PL 31	160	S	S	S		P,S		P,S
			PL 33	220	S	S	S		P,S		-
			PL 25	800	-	-	-		P,S		-
2701	Thor	FER PCU tray		1000					P,S		
2203	Atlas	PS	PA037	330		P,D					
2204	Atlas	AER	A003	60	P,D	P,D	P,D	P,D	P,D		
		AER	A004	100	-	P,D	P,D	P,D	-		
		AER	A009	160	-	P,D	P,D	-	-		
		PS	PA039	1000	-	P,D	-	-	-		

APPENDIX B –
SUMMARY OF VEHICLE WIND GUST AND BUFFET RESPONSES

TABLE A - SUMMARY OF AGENA FORWARD SECTION WIND GUST AND BUFFET LATERAL RESPONSES (ATLAS-BOOSTED VEHICLES)

Vehicle	Axis	Flight Time of Maximum Response (Seconds)	Approx. Mach Number at Max. Response	Max. Response G's (zero to peak)	Frequency cps	Vehicle Bending Mode
1801	Y	52	1.15	.06	2.5	1
		50	1.0	.15	9.1	3
	Z	52	1.15	.06	2.5	1
		50	1.0	.06	9.1	3
1803	Y	59	1.5	.06	8.5	2
		48	0.9	.09	10	3
	Z	59	1.5	.08	8.5	2
		48	0.9	.09	10	3
2204	Y	50	1.0	.10	7	2
	Z	50	1.0	.05	7	2
2401	Y	21	0.3	.10	6.2	2
	Z	45	0.8	.07	6.2	2
4701	Y	32	0.5	.07	2.1	1
		48	0.9	.22	20	Prob. P/L mode
	Z	32	0.5	.05	2.1	1
		22	0.4	.09	20	Prob. P/L mode
4702	Y	39	0.6	.08	2.4	1
		46	0.8	.18	19.7	Prob. P/L mode
	Z	46	0.8	.08	19.7	

FORM LMSC 5787-1

Vehicle	Axis	Flight Time of Maximum Response	Mach Number at Max. Response	Maximum Response	Frequency	Mode
4703	Y	45	0.8	.26	20	Probable Payload Mode
4805	Y	37	0.60	.22	19.7	" "
		47	0.85	.16	19.7	" "
	Z	37	0.60	.07	19.7	" "
		47	0.85	.07	19.7	" "
4814	Y	51	1.1	.04	2.1	1
		43	0.7	.13	19.4	P/L Mode
	Z	43	0.7	.04	2.1	1
		43	0.7	.06	19.4	P/L Mode
4815	Y	37	0.6	.16	19	P/L Mode
		43	0.7	.13	19	" "
	Z	41	0.6	.07	19	" "
		52	1.15	.07	19	" "
4816	Y	31	0.5	.10	19.2	" "
		44	0.7	.12	19.2	" "
	Z	44	0.7	.05	19.2	" "
		59	1.5	.06	19.2	" "
4817	Y	39	0.6	.11	19.1	" "
	Z	39	0.6	.06	19.1	" "
4818	Y	42	0.65	.12	19.1	" "
	Z	46	0.8	.05	19.1	" "
4819	Y	43	0.7	.14	19.7	" "
	Z	43	0.7	.05	19.7	" "
6004	Y	45	0.7	.10	2.7	1
		45	0.7	.13	9	3
	Z	45	0.7	.16	2.7	1
		20	0.3	.20	20	Unknown

FORM LMSC 0787-1

Vehicle	Axis	Flight Time	M	Max. Response	Frequency	Mode
6005	Tang.	67	1.9	.06	2.8	1
		67	1.9	.12	9.1	3
	Rad.	67	1.9	.06	2.8	1
	Tang.	67	1.9	.06	2.8	1
		67	1.9	.12	9.1	3
6009	Rad.	37	0.6	.16	2.7	1
		50	1.0	.17	8.0	3
7001	Y	48	0.9	.06	2.9	1
		48	0.9	.10	6.7	2
		48	0.9	.08	10	3
		48	0.9	.11	19	P/L Mode
	Z	48	0.9	.10	2.9	1
		32	0.5	.12	6.7	2
		48	0.9	.10	10	3
		48	0.9	.09	19	P/L Mode
4821	Y	15	0.2	.18	19.2	Probable P/L Mode
	Z	15	0.2	.05	19.2	Probable P/L Mode

FORM LMSC 5787-1

TABLE B - SUMMARY OF AGENA FORWARD SECTION WIND GUST AND BUFFET LATERAL RESPONSES (TAT-BOOSTED VEHICLES)

Vehicle	Axis	Flight Time of Maximum Response	Mach Number	Maximum Response G's (zero to peak)	Frequency cps	Mode
2355	Y	24	1.1	.08	3.5	1
		24	1.1	.06	8.1	2
	Z	17	0.7	.07	12.4	3
1159	Y	26	1.2	.06	3.3	1
	Z	26	1.2	.06	3.3	1
1161	Z	24	1.1	.05	3.4	1
1165	Z	40	1.7	.05	3.4	1
1166	Z	25	1.15	.05	3.3	1
		34	1.5	.05	8.8	2
1167	Z	40	1.8	.05	6.7	2
		50	2.0			
		63	2.6			
1168	Z	24	1.1	.06	3.3	1
1618	Z	36	1.6	.04	3.7	1
		23	1.0	.04	9.1	2

FORM LMSC 0701-1

TABLE C - SUMMARY OF AGENA FORWARD SECTION WIND GUST AND BUFFET LATERAL RESPONSES (THOR-BOOSTED VEHICLES)

Vehicle	Axis	Flight Time of Maximum Response	Approx. Mach Number	Maximum Response G's (zero to peak)	Frequency cps	Vehicle Bending Mode
2303	Y	36	0.5	.08	4.4	1
		48	0.85	.18	13	3
	Z	36	0.5	.08	4.4	1
		48	0.85	.12	13	3
2304	Y	48	0.85	.12	14.4	3
	Z	47	0.8	.10	4.5	1
		48	0.85	.11	18.5	3
2701	Y	47	0.8	.09	4.2	1
		47	0.8	.09	13.3	3
	Z	27		.04	4.2	1
		47	0.8	.12	13.3	3
1151	Z	48	0.85	.08	11	2
1152	Z	45	0.75	.05	4.2	1
		30		.07	11.9	2
1155	Z	39	0.65	.08	10.7	2
1157	Z	45	0.75	.05	4.2	1
1160	Z	30	0.4	.07	4.0	1
		30	0.4	.10	11.2	2
1602		None				
1110	Y	53	1.2	.34	13	3
	Z	53	1.2	.24	13	3
1115		None				

FORM LMSC 0707-1

TABLE D - SUMMARY OF AGENA PAYLOAD SECTION WIND GUST AND BUFFET LATERAL RESPONSES (THOR-BOOSTED VEHICLES)

Vehicle	Axis	Flight Time	Approx. Mach Number	Max. Response G's (zero to peak)	Frequency	Mode
	Radial	47	0.80	.74	2.9	1
6101		54	1.25	1.06	9	2
	Lateral	43	0.65	.15	4.3	2
		43	0.65	.30	14.7	Probable Payload Mode
6201	Y	46	0.78	.18	4.2	1
		46	0.78	.18	10	2
	Z	38	0.60	.13	10	2

FORM LMSC 0909-1